Prepared for:

National Institute for Coastal and Marine Management (RIKZ)

# Effects of low-frequency waves on wave growth in SWAN

Validation and verification of an extended whitecapping formulation

September, 1999

H3529

WL | delft hydraulics

# Effects of low-frequency waves on wave growth in SWAN

Validation and verification of an extended whitecapping formulation

R.C. Ris and E. Cecchi (WL | DELFT HYDRAULICS)
L.H. Holthuijsen and N. Booij (Delft University of Technology)

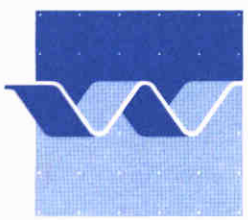

WL | delft hydraulics

WL | delft hydraulics

CLIENT: National Institute for Coastal and Marine Management (RIKZ)

TITLE: Effects of low frequency waves on wave growth in SWAN: 'Validation and verification of an extended whitecapping formulation'


ABSTRACT:

The objective of the present study is to improve the SWAN performance in situations in which a local wind sea is generated in presence of low frequency waves. In such situations SWAN tends to overestimate the significant wave height and to underestimate the mean wave period of the local wind sea considerably.

From field and laboratory cases it is known that low frequency waves affect the evolution and growth of a local wind sea. It has been observed from various experiments that the growth rate of a local wind sea in presence of low frequency waves (propagating in the same direction) is suppressed and that the energy of the low frequency waves increases. In this study, the performance of the SWAN model has been analysed and it has been found that the model behaviour is contrary to what has been observed in e.g. the flume experiment of Donelan (1987). At present the default whitecapping formulation in SWAN is the Komen et al. (1984) expression. This formulation is such that in presence of low frequency waves whitecapping dissipation rate is greatly reduced, resulting in enhanced growth of locally generated waves.

To improve the model performance, alternative formulations have been proposed and evaluated. Two of that have been implemented in SWAN version 40.00: (1) redefinition of integral and local wave steepness and (2) extended Komen et al. (1984) expression. Both options have been tested in fetch-limited wave growth situations. The redefinition of integral and local steepness cannot (at present) be applied in practical applications of SWAN. With the extended Komen et al. (1984) expression, however, it has been shown that the wave growth can accurately be described in situations with and without low frequency waves. In a laboratory case of Donelan (1987) and in a number of field cases the extended formulation improves the model performance. This makes the extended Komen et al. (1984) expression suitable for SWAN. However more research is required to investigate the validity of the extended formulations in other situations (i.e. crossing wind-seas, swell opposing wind-sea, etc.), then described in this study.


REFERENCES: Letters:
1) RIKZ/OSF/995426 (dated March 15, 1999) of ir J.J.W. Seijffert
2) order 22990767 (dated March 26, 1999) of drs A.T. Kamsteeg

| REV. | ORIGINATOR | | DATE | REMARKS | REVIEW | | APPROVED BY | |
|---|---|---|---|---|---|---|---|---|
| 0 | E. Cecchi | | August 1999 | | R.C. Ris | | W.M.K. Tilmans | |
| 1 | E. Cecchi | | September 1999 | | L.H. Holthuijsen | | W.M.K. Tilmans | |
| | | | | | | | | |
| | | | | | | | | |
| | | | | | | | | |

| KEYWORDS | CONTENTS | | STATUS |
|---|---|---|---|
| SWAN wave model, low frequency waves, wave growth, whitecapping formulation, validation, verification | TEXT PAGES: | 66 | ☐ PRELIMINARY |
| | TABLES: | 3 | ☐ DRAFT |
| | FIGURES: | 200 | ☒ FINAL |
| | APPENDICES: | 8 | |
| | PROJECT IDENTIFICATION: H3529 | | |

# Contents

# List of Figures

# List of Tables

# List of Symbols

**Roman letters**

| | |
|---|---|
| $C$ | tuneable coefficient |
| $E$ | wave energy |
| $E_{tot}$ | total wave energy |
| $E_{hf}(\sigma)$ | total energy frequency dependent |
| $E^*$ | non-dimensional wave energy |
| $f$ | frequency |
| $f_m$ | mean frequency |
| $f_m^*$ | non-dimensional mean frequency |
| $f_p$ | peak frequency |
| $f_p^*$ | non-dimensional peak frequency |
| $f_{low}, f_{min}$ | lowest discrete frequency in SWAN in Hz |
| $f_{high}, f_{max}$ | highest discrete frequency in SWAN in Hz |
| $F$ | filter function |
| $g$ | acceleration of gravity |
| $H_S$ | significant wave height (defined as $H_s=4\sqrt{m_0}$) |
| $k$ | wave number |
| $\tilde{k}$ | mean wave number cf. WAM (Komen et al., 1994) |
| $\tilde{k}(\sigma)$ | frequency dependent mean wave number |
| $m, n$ | tuneable coefficients |
| $m_0, m_1$ | zero-order moment and first order moment of the energy density spectrum |
| $T_{m01}$ | mean wave period |
| $T_p$ | peak period |
| $U_{10}$ | wind speed at 10 m height |
| $U_*$ | friction velocity |
| $x,y$ | $x$-, $y$- co-ordinate |
| $X$ | fetch |
| $X^*$ | non-dimensional fetch |

**Greek symbols**

| | |
|---|---|
| $\hat{\alpha}$ | overall wave steepness |
| $\hat{\alpha}(\sigma)$ | adapted steepness at frequency $\sigma$ |
| $\hat{\alpha}_L$ | local wave steepness |
| $\hat{\alpha}_I$ | integral wave steepness |
| $\beta$ | straining parameter |
| $\sigma$ | radian frequency |
| $\sigma_\theta$ | standard deviation in directional-space |
| $\sigma_\sigma$ | standard deviation in frequency-space |
| $\sigma_{low}$, $\sigma_{min}$ | lowest discrete frequency in SWAN in radians |
| $\sigma_{high}$, $\sigma_{max}$ | highest discrete frequency in SWAN in radians |
| $\tilde{\sigma}$ | mean frequency cf. WAM (Komen et al., 1994) |
| $\sigma_{PM}$ | Pierson-Moskowitz frequency for fully developed spectra |
| $\sigma_{PM}^*$ | non-dimensional Pierson-Moskowitz frequency for fully developed spectra |
| $\gamma_o$ | peak enhancement factor |
| $\theta$ | mean wave direction (Cartesian convention) |
| $\theta_w$ | mean wind direction (Cartesian convention) |
| $\theta_o$ | incident mean wave direction (Cartesian convention) at up-wave boundary |
| $\Delta x$,$\Delta y$ | increment in x- and y-direction, respectively |
| $\Delta f$,$\Delta\theta$ | increment in frequency- and directional-space, respectively |

# 1 Introduction

## 1.1 General

The numerical wave model SWAN has been developed to compute waves in coastal areas, lakes and estuaries from given wind, bottom and current conditions (see e.g. Holthuijsen et al., 1993; Booij et al., 1999). Although the SWAN model performs fairly well in many complex field cases for which it has been developed, it has been observed that the model tends to overestimate the significant wave height and underestimate the mean wave period of a local wind sea particularly in presence of low frequency waves (see e.g. Ris et al., 1999 and Alkyon, 1999).

It has recently been found that the overestimation in of the significant wave height of a local wind sea in presence of low frequency waves may be ascribed to the whitecapping dissipation as it is formulated in SWAN (see e.g. Ris et al., 1999 and Alkyon, 1999). The whitecapping formulation that is presently implemented is that of Komen et al. (1984). It has been formulated in such a way that it accurately describes the dissipation rate for a single peaked JONSWAP type spectrum and that fetch-limited wave growth can accurately be simulated. However, it seems that in the presence of low frequency waves (i.e. multimodal wave spectrum) the formulation is not adequate to reproduce the whitecapping dissipation for the local wind sea (and the low frequency waves). In such cases, with multimodal sea waves, it greatly underestimates the dissipation rate of the wind sea and the model thus overestimates the significant wave height of the local wind sea.

It is noted that this observed model behaviour is contrary to what has been observed in many laboratory and field cases. From such observations it has been shown that the growth of a local wind sea is suppressed in presence of low frequency waves.

## 1.2 Objective of the study

To improve the model performance of SWAN in cases in which a local wind sea is generated in presence of low frequency waves, the present whitecapping source term in SWAN (version 40.00) should be adapted or replaced by an alternative formulation. Therefore, the

Dutch Ministry of Public Works and Coastal Management (hereafter to be called RIKZ), commissioned WL | DELFT HYDRAULICS to carry out a study to analyse the observed model behaviour in idealised cases and to investigate possible alternative formulations for the whitecapping source term. Such alternative source term should be such that it can be applied in SWAN in practical applications (it should therefore be robust and accurate).

In order to achieve the above mentioned objective, the following activities have been proposed:

- Literature survey on the effect of low frequency waves on the dissipation of a wind sea.
- Analysis of the observed model behaviour with respect to the whitecapping of a local wind sea in presence of low frequency waves in idealised conditions.
- Implementation of possible alternative solutions or adapted formulations for whitecapping dissipation in SWAN 40.00.
- Validation of such whitecapping formulations in an experimental version of SWAN 40.00 in idealised cases.
- Verification of such whitecapping formulations in a number of field cases.
- Analysis and reporting of model results.

## 1.3 Outline of the report

The present report is organised as follows: In Chapter 2 some observed effects in a situation of a local wind sea generated on low frequency waves are described. The observed model behaviour of SWAN 40.00 is investigated and demonstrated. In Chapter 3 a number of alternative expressions for whitecapping dissipation, which may be appropriate for SWAN, are described. The implementation of two alternative formulations in SWAN, is described in Chapter 4. In Chapter 5 the validation of two alternative whitecapping formulations is investigated in the idealised situation of fetch-limited wave growth without and with swell. In Chapter 6 the selected whitecapping expression is validated using the data of the laboratory flume experiment of Donelan (1987). In Chapter 7 the expression is verified in a number of complex field cases (i.e. Lake George, Haringvliet estuary, Norderneyer Seagate and Westerschelde estuary). A discussion with conclusion and recommendations is given in Chapter 8.

This project was carried out between April 1 and September 31, 1999 at WL | DELFT HYDRAULICS as project H3529. The modifications to the source code are made to **SWAN CYCLE 2, version 40.00**.

# 2 Interaction between wind sea and low frequency waves

## 2.1 Introduction

From field and laboratory cases it is known that the presence of low frequency waves may effect the evolution and growth of a local wind sea (e.g., Mitsuyasu, 1966; Phillips and Banner, 1975; Donelan, 1987). Generally, it has been observed from these experiments that if low frequency waves are added to a wind sea (and they propagate in the same direction) that:

(a) The growth rate of the local wind sea is suppressed;
(b) the energy of the low frequency waves increase;
(c) the total energy (of the low frequency waves and the wind sea) decreases.

An illustrative observation of this phenomena is shown in Fig. 2.1 (Donelan, 1987).

The theory of the interaction between wind sea and low frequency waves, that has been described in literature, is the point of concern in Section 2.2. A brief literature survey has been carried out.

As described in Chapter 1, it seems that the present whitecapping formulation in third-generation models such as WAM and SWAN is not adequate in describing the dissipation of the wind sea in presence of low frequency waves. In Section 2.3 the model behaviour of SWAN has been analysed for a wind sea situation with and without low frequency waves.

## 2.2 Some observed effects in field and laboratory condition

From several laboratory studies and observations in field cases it has been found that when a train of long waves propagate in the same direction as in which the wind is blowing, the total energy (wind sea and low frequency waves) and the energy of the wind generated waves decrease and the steepness of the long waves increase (Mitsuyasu, 1966).

Donelan (1987) has found that the total energy of the wind induced waves was reduced by a factor of about 2.5 in presence of low frequency waves and that the energy density of low frequency waves increase in response to the wind (see Fig. 2.1). The reason for this observed behaviour is not completely clear. Donelan proposed that a possible mechanism for the reduction in the wind sea induced by paddle waves is the detuning of resonant non-linear wave-wave interactions.

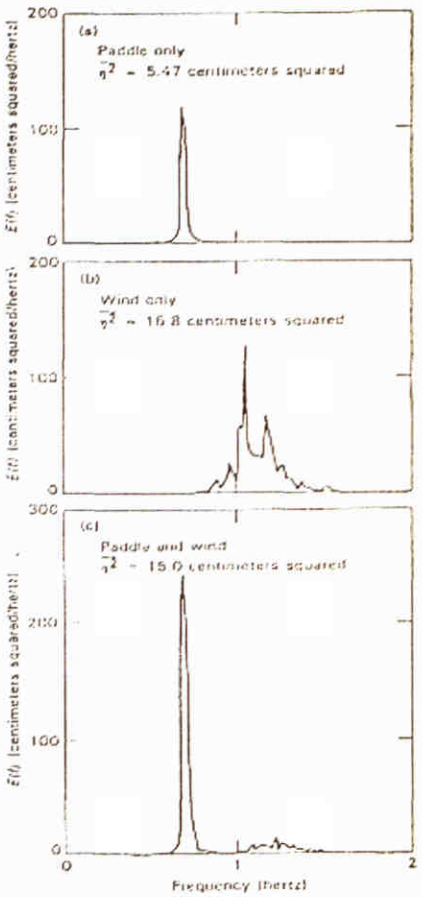


Figure 2.1 Wave spectra at 50 meters fetch in a laboratory wind-wave tank. (a) The spectrum of the low frequency waves 0.707 Hz paddle-generated waves of steepness ak = 0.067. (b) The spectrum of a wind sea (measured wind speed of 11 m/s at 26 cm height). (c) The wave spectrum with wind and paddle exited together as in (a) and (b). Figure from Donelan (1987).

A limitation of the Donelan experiment is the small scale in which it has been carried out and that it is not known if this effect can be scaled to an ocean scale. However, in the context of ocean wave models, this effect of swell on the growth of a wind sea may be important, it is therefore that this effect should be accounted for in a model such as SWAN.

All three mechanism of generation by wind, quadruplet wave-wave interaction and dissipation by whitecapping have been used to explain the observed reduction of local wave

growth in the presence of low frequency waves. Phillips and Banner (1974) attributed this phenomena to enhanced wave breaking. According to this idea, the wind-driven drift current is modulated by the long waves, which enhances the breaking of short wind waves at the crest of the wave. However, Wright (1976) has shown that the Phillips-Banner mechanism is too weak at higher wind speeds and does not have the correct variation with wind speed.

Masson (1993) suggested that non-linear wave-wave interactions might be responsible for the reduction of the growth of the wind sea in presence of low frequency waves. Masson (1993) showed no quantitative comparisons with data, but the results of calculations show that the non-linear energy transfer between a long wave and wind waves decreases rapidly with the ratio of the peak frequency. The energy transfer between the low frequency and wind sea was not present for ratios $f_{p,\ wind\ sea}/f_{p,\ swell}$ greater than about 1.6. Since in the Donelan experiment the ratio is greater than 1.6, this explanation does not seem viable.

Chen and Belcher (1999) suggested that the suppression of wind waves by a long wave is due to direct coupling of the long wave with the wind. They follow an idea suggested by Makin et al. (1995) and more recently developed by Makin and Kudryatsev (1999). In their model of the drag of the sea surface, they assume that the long wave exerts a drag on the air flow, which reduces the turbulent stress in the air flow that is available to generate wind waves. They assume that the total turbulent wind stress at the sea surface (which generates the waves) is insensitive to the presence of swell. Since the swell would absorb some of that stress, the stress available to the wind sea would be reduced and the growth of the wind sea would consequently diminish.

In conclusion, the mechanism that controls the reduction of the growth of the wind sea in presence of low frequency waves and the enhancement of the swell peak it self, is still open to discussion.

## 2.3 Whitecapping in presence of low frequencies waves in SWAN

In third-generation models (at least in WAM and SWAN) for deep water, the whitecapping formulation is based on the pulse-based model of Hasselmann (1974). In this pulse-based model it is assumed that the dissipation rate is quasi-linear in the spectral density and that it depends on an average wave steepness. For the development of the WAM model,

Komen et al. (1984) proposed a definition of wave steepness which has been used in the WAM model. However, this definition is such formulated that in the presence of low frequency waves, the whitecapping dissipation rate is resulting in enhanced (net) growth of a local wind sea. Since the Komen et al. (1984) formulation is the default option in SWAN, some problems are to be expected in presence of low frequency waves.

The SWAN model computes the energy dissipation source term due to whitecapping according to Komen et al. (1984):

$$S_{wc}(\sigma,\theta) = -C\tilde{\sigma}\frac{k}{\tilde{k}}\left(\frac{\hat{\alpha}}{\hat{\alpha}_{PM}}\right)^{m} E(\sigma,\theta) \tag{2.1}$$

where $\tilde{\sigma}$ and $\tilde{k}$ denote the mean frequency and the mean wave number respectively, $\hat{\alpha}$ is an overall wave steepness, $\hat{\alpha}_{PM}$ is the value of $\hat{\alpha}$ for the Pierson-Moskowitz (1964) spectrum ( $\hat{\alpha}_{PM} = 3.02 \times 10^{-3}$ ), so that $\hat{\alpha} / \hat{\alpha}_{PM}$ is a normalised overall steepness. The values of the tuneable coefficients $C$ and the exponent $m$ in this model have been obtained by closing the energy balance of the waves in idealised wave growth conditions (JONSWAP-type spectra) for deep water. The values are $C = 2.36 \times 10^{-5}$ and $m = 2$.

The mean frequency $\tilde{\sigma}$ and the mean wave number $\tilde{k}$ are defined as (cf. WAMDI group, 1988):

$$\tilde{\sigma} = \left[ E_{tot}^{-1} \int_0^{2\pi} \int_0^{\infty} \frac{1}{\sigma} E(\sigma,\theta) d\sigma d\theta \right]^{-1} \tag{2.2}$$

$$\tilde{k} = \left[ E_{tot}^{-1} \int_0^{2\pi} \int_0^{\infty} \frac{1}{\sqrt{k}} E(\sigma,\theta) d\sigma d\theta \right]^{-2} \tag{2.3}$$

$E_{tot}$ is the total wave energy:

$$E_{tot} = \int_0^{2\pi} \int_0^{\infty} E(\sigma,\theta) d\sigma d\theta \tag{2.4}$$

The overall wave steepness $\hat{\alpha}$ is defined as:

$$\hat{\alpha} = \tilde{k}^2 E_{tot} \tag{2.5}$$

To show the whitecapping source term as expressed in Eq. 2.1 for a JONSWAP type frequency spectrum ( $H_s$ = 1 m and $T_p$ = 5 s), the spectral shape and the source term $S_{wc}$ have been plotted as function of frequency (see Fig. 2.2).

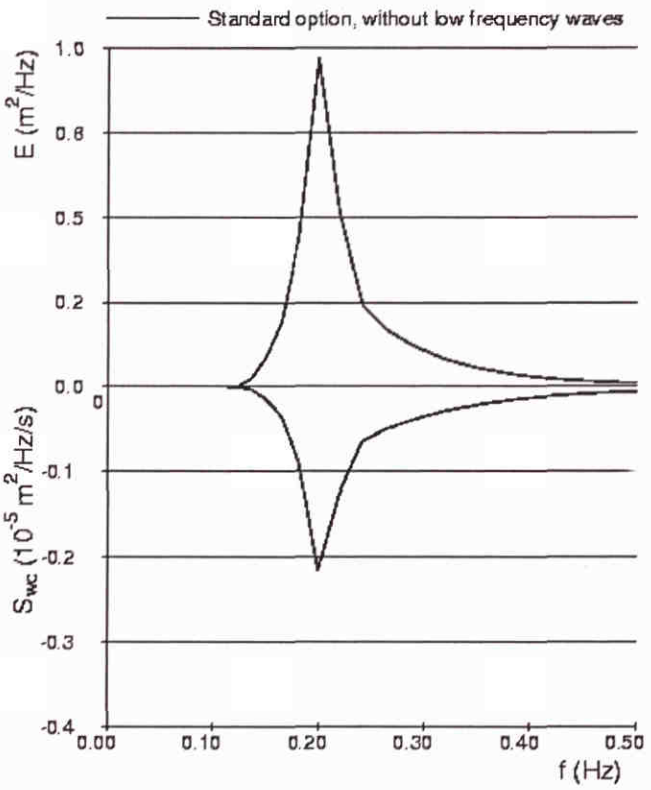


Figure 2.2 Whitecapping dissipation for a wind sea spectrum $H_s$ = 1 m, $T_p$ = 5 s.

By adding some low frequency waves to the spectrum, it can be easily shown that the present formulation for whitecapping (see Eq. 2.1 to Eq. 2.5) is not adequate to represent the dissipation rate of the local wind sea. To this end, low frequency waves (with $H_s$ = 0.5 m and $T_p$ = 15 s) have been added to the wave spectrum as presented in Fig. 2.2. The spectral shape and the source term $S_{wc}$ have been plotted as function of frequency in Fig. 2.3. It is clearly visible that with the swell added, the whitecapping source term is significantly reduced for the wind sea, as is evident from the bottom panel. This is obviously not in agreement with field and laboratory observations where it is seen that (at least) whitecapping should be enhanced (i.e., reducing the growth of the wind sea) in the presence of swell.

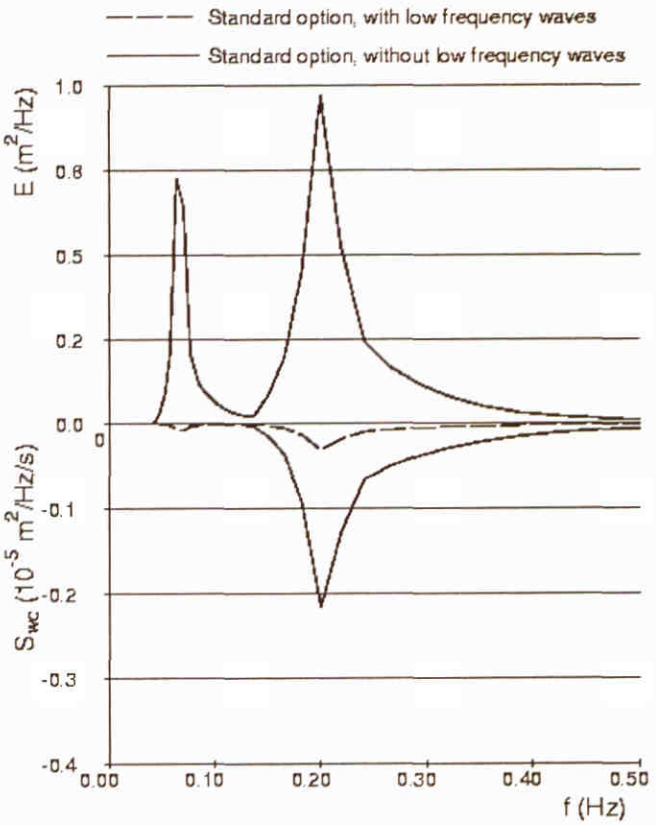


Figure 2.3 Whitecapping dissipation for a wind sea spectrum in presence of a low frequency peak with $H_s$ = 0.5 m, $T_p$ = 15 s.

The reason for this behaviour in SWAN is that the low frequency waves affect the mean frequency and the mean wave number $\tilde{k}$. Due to the presence of the swell waves, the mean frequency and mean wave number shift to the lower values. This significantly affects the wave steepness $\hat{\alpha}$, (see Eq. 2.5) since it is proportional to $\tilde{k}^2 (\approx \tilde{\sigma}^4)$. The situation is aggravated since the source term $S_{wc}$ is proportional to $\hat{\alpha}^2$ (see Eq. 2.1; $m$ = 2). It may be concluded that the whitecapping source term is rather sensitive, through the wave steepness $\hat{\alpha}$ to low frequency waves ($S_{wc}$ is actually proportional to $\tilde{k}^4 \approx \tilde{\sigma}^8$). The result is that the whitecapping dissipation source term of the wind sea is reduced significantly and the net wave growth of the wind sea is increased.

# 3 Alternative formulations for whitecapping

## 3.1 Introduction

To remedy the shortcomings of the present whitecapping formulation, an alternative formulation should be implemented. This can be achieved by treating the dissipation of swell different than from the wind waves. The first intuitive ideas is to split low frequency waves from the wind sea in two different sea systems as proposed by Tolman and Chalikov (1996). One other alternative is to redefine the wave steepness $\hat{\alpha}$ to take into account the effect of swell on the dissipation of the wind sea.

It is noted that the adapted whitecapping formulations should (a) reproduce (at least) the growth curves, (b) increase the whitecapping dissipation for the wind sea part of the spectra in presence of low frequency waves, and (c) should not be effective on the low frequency waves.

Some of the possible literature solutions for a modified whitecapping formulation in SWAN in view of swell - sea interaction are proposed in this section.

## 3.2 Decoupling of wind sea and low frequency waves

Tolman and Chalikov (1996) have recently proposed a new dissipation source term based on the consideration that the dissipation process for frequencies around and below the spectral peak are fundamentally different from those in the equilibrium range of the spectrum. In the low frequency region it has been assumed that the dissipation source term can be described using an analogy with dissipation of wave energy due to oceanic turbulence. For the high-frequency waves a diagnostic parameterisation for the dissipation function has been obtained by assuming a quasi steady balance of source terms. The total dissipation source term has been defined as a linear combination of the above high and low frequency constituents. Tolman and Chalikov (1996) use the wind speed to separate the wind sea part from the swell peak.

The above mentioned procedure to split the spectrum in a wind sea part and a swell part may encounter some difficulties if the peak of the wind sea and swell are too close to each other (see WL | DELFT HYDRAULICS, 1999a). Such conditions are often present in coastal areas where a local wind sea is superimposed on swell waves. To split the spectrum in such situations may be difficult. For this reason the above mentioned procedure has not been considered in the remainder of this study.

## 3.3 Redefinition of wave steepness

### 3.3.1 Redefinition of integral and local wave steepness

One formulation, that may not be sensitive to the presence of the low frequency waves has been obtained by introducing the concept of a wave steepness that is based on an integral steepness $\hat{\alpha}_I$ and a local steepness $\hat{\alpha}_L$ (personal communication with N. Booij, 1999). The idea is that the dissipation of a certain spectral bin does not depend on the overall steepness of the wave field, which is the usual assumption, but on the steepness of lower frequency waves only. As described in Chapter 2, the presence of low frequency waves intensifies the dissipation of waves of higher frequencies. On the other hand it is assumed that high-frequency waves, hardly affect the dissipation of the low frequency waves.

The integral steepness $\hat{\alpha}_I$ is computed per frequency as steepness of all wave components with frequencies lower than that frequency. The integral steepness parameter can also be computed by adding a filter function $F$, which allows for numerical integration over all frequencies. The integral wave steepness is given by:

$$\hat{\alpha}_I(\sigma_0) = \int_0^{2\pi}\int_0^{\infty} F(\sigma/\sigma_0)k^2 E(\sigma,\theta)d\sigma d\theta \tag{3.1}$$

where $F$ is a smooth filter function (equal 1 for values of the argument considerably smaller than 1 and 0 for values much larger than 1). The filter function reads:

$$F = \frac{z}{z+1/z}, \quad where \quad z = e^{n\left(\frac{1-\sigma}{\sigma_0}\right)} \tag{3.2}$$

Here $n$ is a tuneable coefficient in a range between 2 and 10. It controls the slope of the filter function.

The local steepness $\hat{\alpha}_L$ (frequency and direction dependent) is:

$$\hat{\alpha}_L(\sigma,\theta) = C_L k^2 \sigma E(\sigma,\theta) \tag{3.3}$$

The formulation for the whitecapping source term, assuming that the total steepness parameter $\hat{\alpha}$ can be considered as the product of the two steepness parameters $\hat{\alpha}_I$ and $\hat{\alpha}_L$, then becomes:

$$S_{wc}(\sigma,\theta) = C\sigma\hat{\alpha}_L \hat{\alpha}_I{}^m E(\sigma,\theta) \tag{3.4}$$

Where $C$ and $m$ are tuneable coefficients. This expression has been implemented in SWAN. The coefficients $C$ and $m$ have been tuned for wave growth in fetch-limited situations.

### 3.3.2 Extended Komen et al. (1984) expression

For locally generated waves the overall steepness as defined in SWAN may be replaced by the steepness of the high-frequency waves as these steepnesses are nearly equal. The extended source term is computed in analogy with the Komen et al. (1984) source term, but the wave steepness $\hat{\alpha}$ is frequency dependent. The extended formulation of the source term is:

$$S_{wc}(\sigma,\theta) = -C\beta^n \tilde{\sigma} \frac{k}{\tilde{k}} \left( \frac{\hat{\alpha}(\sigma)}{\hat{\alpha}_{PM}} \right)^m E(\sigma,\theta) \tag{3.5}$$

Where $C$, $m$ and $n$ are tuneable coefficients (default values are $C = 2.36 \times 10^{-5}$ and $m = 2$), $\hat{\alpha}(\sigma)$ is the adapted steepness at frequency $\sigma$ where only the contributions of frequencies higher than $\sigma$ are accounted for (see Fig. 3.1). The steepness $\hat{\alpha}(\sigma)$ can be expressed (analogously to Komen et al., 1984) as:

$$\hat{\alpha}(\sigma) = \tilde{k}^2(\sigma) E_{hf}(\sigma) \tag{3.6}$$

Where the mean wave number $\tilde{k}(\sigma)$ and the frequency dependent total energy $E_{hf}(\sigma)$ can be expressed as:

$$\tilde{k}(\sigma)=\left[E_{hf}^{-1}(\sigma)\int_{0}^{2\pi}\int_{\sigma}^{\infty}\frac{1}{\sqrt{k}}E(\sigma,\theta)d\sigma d\theta\right]^{-2} \tag{3.7}$$

and

$$E_{hf}(\sigma)=\int_{0}^{2\pi}\int_{\sigma}^{\infty}E(\theta,\sigma)d\sigma d\theta \tag{3.8}$$

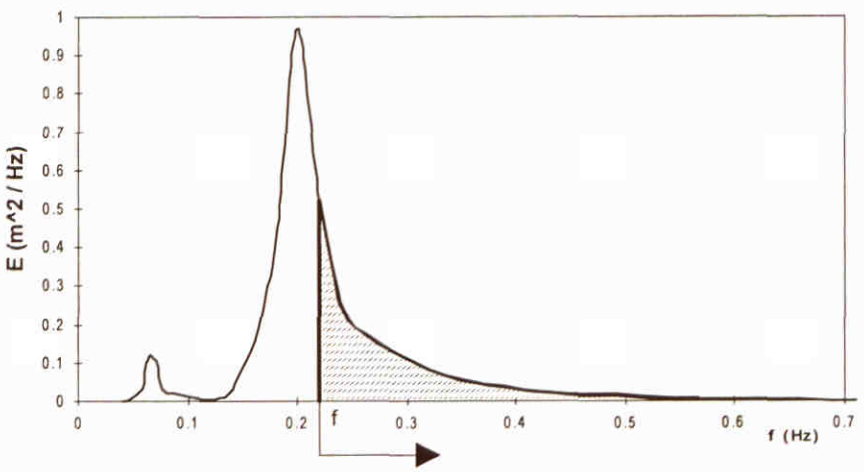


Figure 3.1 Part of energy spectrum that is accounted for the steepness $\hat{\alpha}(\sigma)$ at frequency $\sigma$

To represent the observed effect of the suppression of the growth of the wind waves when they are generated on low frequency waves that are propagating in the same direction in which the wind is blowing, a straining parameter $\beta$ is introduced. The parameter $\beta$ *is* defined as the ratio of the steepness of the high-frequency part of the spectrum (see Eq. 3.6) and overall steepness (see Eq. 2.5) and is:

$$\beta=\frac{\hat{\alpha}(\sigma)}{\hat{\alpha}}=\frac{\tilde{k}^{2}(\sigma)E_{hf}(\sigma)}{\tilde{k}^{2}E_{tot}} \tag{3.9}$$

Where $\tilde{k}$ and $E_{tot}$ are integrated over all frequencies according to Komen et al. (1984) (see Eq. 2.3 and Eq. 2.4). The exponent $n$ of $\beta$(see Eq. 3.5) is a tuneable coefficient that controls the ratio of the reduced net growth of wind and the enhancement of the low frequency peak. This coefficient should be tuned.

# 4 Implementation of alternative formulations

## 4.1 Introduction

In this section, the required modifications to the source code of SWAN 40.00 in order to activate the alternative formulations are described. In addition the commands that have been added to SWAN 40.00 are described. At each modified or new source code line (except for the new developed subroutine) the string '32.10' has been added in column 75. The modifications are made according to the 'SWAN 30.75 *programming protocol'* (see for further information the internet home page of SWAN: http://swan.ct.tudelft.nl). The new subroutines that have been developed, are stored in a file called SWANWL.FOR.

## 4.2 Implementation of new source code

In order to perform computations with the alternative formulations, modifications have been made to the FORTRAN 77 source code in a number of subroutines of SWAN. These modifications concern subroutines of the pre-processing module and the computational module of SWAN. The modifications to the source code that have been made, can simply be found by searching for the text string 32.10 (string located in column 75). In this section a brief description of the modifications per file and a listing of modified source code of SWAN is given. A listing of the code of the new subroutines that have been developed, i.e. the integral and local steepness and for the source code of the extended Komen et al. (1984) expression, are given in Appendices A and B, respectively.

**SWANWL.FOR:**

The new subroutine WCAP6 that has been developed and implemented is listed in App. B.

**SWANPRE1.FOR:**

Subroutine SWREAD: the code has been modified to include for the extended dissipation source term **WCAP EKOM** and the following lines have been added:

```
C     |                                                    |          32.10
C     |   EKOM      [pown] [cds3]                          |          32.10


      ELSE IF ( KEYWIS ('EKOM')) THEN                                 32.10
        IWCAP = 6                                                     32.10
        CALL INREAL ('POWN' , PWCAP(12), 'UNC', 0.)                   32.10
        CALL INREAL ('CDS3' , PWCAP(13), 'UNC', 0.)                   32.10
      ELSE                                                            32.10
```

**SWANMAIN.FOR:**

Subroutine SWINIT: the following coefficients have been added to the array for the whitecapping coefficient:

```
C     *** Initialisation of variables ***                           32.10
      PWCAP(12) = 0.5                                               32.10
      PWCAP(13) = 1.                                                32.10
```

**SWANCOM1.FOR:**

Subroutine SOURCE: to activate the extended Komen et al. (1984) whitecapping expression, the following ' call ' has been added:

```
      ELSE IF ( IWCAP .EQ. 6 ) THEN                                 32.10
C                                                                   32.10
C       *** extended whitecapping formulation: option 6 ***         32.10
C                                                                   32.10
        CALL SWCAP6 (MDC     ,MSC     ,MWCAP   ,ETOT    ,IMATDA  ,  32.10
     &               KWAVE   ,ICMAX   ,PWCAP   ,KMESPC  ,SMESPC  ,  32.10
     &               IDCMIN  ,IDCMAX  ,PLWCAP  ,ISSTOP  ,DISSC1  ,  32.10
     &               AC2     ,KCGRD   ,MCGRD   ,SPCSIG  ,DDIR    ,  32.10
     &               PWTAIL                                    )    32.10
C                                                                   32.10
      END IF                                                        32.10
C                                                                   32.10
```

To validate that the modifications and the new source code have correctly been implemented, computations have been carried out in fetch-limited wave growth conditions. Additional output has been requested to check the values of coefficients and parameters. Moreover, the expressions have been verified in the flume experiment of Donelan (1987) and in a number of field cases (see Chapters 6 and 7).

# 5 Fetch-limited wave growth

## 5.1 Introduction

To investigate the validity of the alternative formulations, deep water fetch-limited wave growth has been considered. Computations have been carried out with the following formulations:

1. Standard whitecapping formulation (cf. Komen et al., 1984);
2. redefinition of integral and local wave steepness;
3. extended Komen et al. (1984) expression.

A comparison has been carried out in fetch-limited wave growth conditions without and with incident low frequency waves. The reason for considering fetch-limited wave growth firstly is that the alternative formulations (i.e. redefinition of integral and local wave steepness and the extended Komen et al. (1984) expression) should at least reproduce the growth curves as computed with the present SWAN model in a situation of a wind sea. If necessary, coefficients may be tuned with respect to the observations, in terms of non dimensional energy and peak frequency, by Kahma and Calkoen (1992), Wilson (1965) and Pierson-Moskowitz (1964) limits.

## 5.2 Description of tests cases

Deep water wave evolution is computed in an idealised case of a constant uniform wind blowing normally off a long and straight coastline in wind sea conditions (following the SWAMP II test case; the SWAMP group, 1985). The computations have been carried out with the one-dimensional mode of SWAN.

To demonstrate the performance of SWAN, the model results have been made dimensionless using the friction velocity $U_*$ according to Wu (1982), the following dimensionless variables have been introduced:

$$X^* = \frac{g\,X}{U_*^2} \quad , \quad E^* = \frac{g^2\,E_{tot}}{U_*^4} \quad , \quad f_p^* = \frac{f_p\,U_*}{g} \quad , \quad f_m^* = \frac{f_m\,U_*}{g} \qquad (5.1)$$

in which $X^*$ is the dimensionless fetch, $X$ is the fetch (the distance from the coast in upwind direction), $U_*$ is the friction velocity, $E^*$ is the dimensionless total energy, $E_{tot}$ is the total energy (where $E_{tot} = H_s^2 / 16$, with $H_s$ the significant wave height), $f_p^*$ is the dimensionless peak frequency, $f_m$ is a mean frequency defined as $(T_{m01})^{-1}$ and $f_m^*$ is the dimensionless mean frequency.

Figure 5.1 shows the locations of the non dimensional fetch $X^*$ where spectral output has been plotted: the top, middle and bottom panel correspond respectively to a wind speed of $U_{10}$ = 10 m/s, 20 m/s, 30 m/s.

The model results are presented in a collection of figures indicated with indices *a* to *e* for each computation (see e.g. Fig. 5.2.*a* to 5.2.*e*). The non-dimensional wave growth curves are shown in e.g. Fig. 5.2.*a* and should be interpreted as follows: the top left panel and the top right panel in the growth curves figures show the computed non-dimensional wave energy $E^*$ and the non-dimensional peak frequency $f_p^*$ as a function of non-dimensional fetch $X^*$. The bottom left panel shows the computed non-dimensional mean frequency $f_m^*$ as a function of $X^*$. These results are compared with the observations compiled by Kahma and Calkoen (1992), Wilson (1965) and Pierson-Moskowitz (1964). Note that in the bottom left panel the SWAN results are in terms of mean frequency $f_m^*$ whereas the data of the observations are in terms of peak frequency $f_p^*$ (since no information is available of the observed mean frequency). In the bottom right panel the computed directional width $\sigma_\theta$ of the wave energy is plotted as a function of non dimensional fetch $X^*$.

In figures with indices 5.2.*b*, 5.2.*c* and 5.2.*d*, the wave spectrum has been plotted for $U_{10}$ = 10 m/s, 20 m/s and 30 m/s, respectively at the locations shown in Fig. 5.1. Figure 5.2.*e* shows on a logarithmic scale the comparison of the computed spectral shape with a $f^{-4}$ and $f^{-5}$ power law.

## 5.3 Model results: wave growth in absence of low frequency waves

### 5.3.1 Standard formulation (WAM Cycle 3: Komen et al., 1984)

The model results using the default formulations in SWAN are presented in Figures 5.2.*a* to 5.2.*e*. The agreement between the model results and the data of Kahma and Calkoen (1992), Wilson (1965) and Pierson-Moskowitz (1964) is good, however, it is seen that the average directional spreading is relatively large (about 37°) compared to observations (see e.g. Forristall and Ewans, 1997). The wave spectra look reasonable although some small oscillations are visible at large fetches (see bottom right panel of Fig 5.2.c).

### 5.3.2 Redefinition of integral and local wave steepness

The first alternative formulation that has been validated in the idealised case of fetch-limited wave growth is that with the adapted integral and local wave steepness (see Eq. 3.1 to Eq. 3.4). In the present study, the tuneable coefficients $C$ and $m$ have been varied in order to investigate the effect on the model results and to obtain the best possible agreement between the observations. Various computations have been performed with different values of the coefficient: $C = 10, 15, 20, 10^3, 5\ 10^3, 10^4$ and $m = 1, 1.5, 2, 4$ with a default value for $n = 2$ (coefficients defined in Eq. 3.2), results are shown here for $C = 15$ and $m = 1$ only. It is seen from Fig. 5.3.*a* that the results are not in good agreement with the observations, the peak frequency is oscillating considerably and the directional spreading is too large (> 45°). The wave spectra show some unwanted low frequency peaks (see Fig. 5.3.*b*, 5.3.*c*, 5.3.*d*). The observed oscillations were present in all results. In order to explain this model behaviour, two-dimensional wave spectra have been plotted at $X^* = 26\times10^5$, $13\times10^6$, $30\times10^7$, respectively (see Fig. 5.4, Fig. 5.5 and Fig. 5.6). As it is visible, instabilities grow in the low frequency part of the spectra. The energy pumped to lower frequencies (at widely varying spectral directions) by non-linear wave-wave interactions is not sufficiently dissipated and such they may grow unbounded.

To avoid the growth of low frequency waves (at large angles with respect to the mean wave direction) only the wave directions that are inside the 80° sector with respect to the wind (and mean wave propagation) direction have been taken into account. Computations have been carried out with the 'SECTOR' option in SWAN activated ( sector -80° to +80). The

results of these computations are shown in Fig. 5.7. It is seen that the agreement between the model and the observation of Kahma and Calkoen (1992) is now reasonable but that it is poor for fully developed conditions. The significant wave height continues to increase with increasing fetch. The directional spreading of the waves is too large. Since the use of sector is not convenient in practical applications of SWAN, the formulation with the integral and local steepness will not be considered in the remainder of this study.

### 5.3.3 Extended Komen et al. (1984) expression

The extended Komen expression has been implemented in SWAN in agreement with the formulations of Section 3.3.2. To observe the behaviour of the implemented expression in a wind sea condition, computations have been performed for different values of the exponent $n = 0, 0.5, 1, 2$ of the coefficient $\beta$ (see Eq. 3.5).

Figures 5.8 to Fig. 5.11, show the growth curves of the wind sea for each value of the exponent $n$. The agreement between the SWAN results with the extended whitecapping formulation implemented, and the expressions of Kahma and Calkoen (1992) is reasonable, both for the total energy and the peak frequency. The computed growth of the wind sea is hardly affected by the choice of the exponent $n$, however, for fully developed situations the significant wave height is smaller for larger values of $n$.

The Figures 5.8.*b, c, d* tot 5.11.*b, c, d* shown the wave spectra, compared with the standard formulation of Komen et al. (1984). It can be seen that the peak frequency shifts toward the lower frequencies and that more energy is dissipated at the high-frequency part of the spectrum. The mean frequency has also slightly decreased.

| | $U_{10}$ = 10 m/s | | $U_{10}$ = 20 m/s | | $U_{10}$ = 30 m/s | |
|---|---|---|---|---|---|---|
| | $H_s$ [m] | $T_p$ [s] | $H_s$ [m] | $T_p$ [s] | $H_s$ [m] | $T_p$ [s] |
| P.M. (1964) | 1.95 | 6.94 | 11.4 | 16.94 | 33.3 | 28.65 |
| Komen et al. (1984) | 1.9 | 6.5 | 11 | 15 | 32 | 27 |
| $\beta^n$; $n = 0$ | 1.8 | 7.8 | 11 | 22 | 31 | 29 |
| $\beta^n$; $n = 0.5$ | 1.6 | 7.8 | 10 | 22 | 29 | 36 |
| $\beta^n$; $n = 1$ | 1.3 | 10 | 10 | 22 | 28 | 36 |
| $\beta^n$; $n = 2$ | 0.79 | 14 | 8.6 | 20 | 25 | 36 |

Table 5.1 Values of the computed significant wave height and the peak period for the fully developed conditions

The significant wave heights and the peak periods for the long fetches ($X^* > 1.2\times10^8$), computed with the new version of the model are in Table 5.1. The data presented is compared with that of the Pierson-Moskowitz limits and with the value obtained with the standard expression (i.e. Komen et al., 1984).

The reason for the underestimation of the significant wave height at fully developed conditions may be explained as follows: for a $f^{-5}$ spectrum it can be shown analytically that $\hat{\alpha}(\sigma) = \hat{\alpha}$ in a condition of only wind sea without incident low frequency waves. For a JONSWAP spectrum (Hasselmann et al., 1973) this is true but for a spectrum as computed by SWAN this is only approximately true. The approximation that $\hat{\alpha}(\sigma) \approx \hat{\alpha}$ implies that for spectra of wind sea, the proposed extended whitecapping dissipation reduces to the whitecapping dissipation as suggested by Komen et al. (1984), but not for the long fetches where the spectrum is a Pierson-Moskowitz type ($f^{-4}$) and the approximation $\hat{\alpha}(\sigma) \approx \hat{\alpha}$ is not valid anymore.

To reproduce the Pierson-Moskowitz (1964) limits, in terms of non dimensional energy and peak frequency, the coefficient $C$ should be tuned. To that end, computations with the coefficient $C$ reduced with 10% and 20% have been carried out. The results of computations with SWAN with a reduction of 20%, which gave the best agreement with the values of Pierson-Moskowitz (1964), have been plotted in Fig. 5.12 and Fig. 5.13, respectively for value of $n = 0.5$ and 1. From the figures it is seen that there is an improvement for fully developed conditions. It is seen that changing the coefficient $C$, in order to obtain the Pierson-Moskowitz (1964) limits, affects the wave parameters in wave growth conditions (in the range of Kahma and Calkoen (1992); $5\times10^4 < X^* < 4\times10^6$), as is evident from Fig. 5.13. Decreasing the value of the coefficient $C$ (and thus decreasing the dissipation rate) resulted in a slightly more curved behaviour of the growth curve.

## 5.4 Model results: wave growth in presence of low frequency waves

The investigation proceeds by adding low frequency waves to the above wind sea situation. The low frequency waves have been imposed as boundary condition in such a way that the wind sea is separated from the swell at initial wave growth condition ($X = 0$ m) and almost completely absorbed by the wind sea for fully developed conditions. The peak frequency of the swell has been assumed to be equal to 75% of the peak frequency of the Pierson-

Moskowitz limit $f_{p,PM}$, and the incident significant wave height of the swell has been obtained by $H_{s,\,swell} = 4\,(\,0.05\,E_{tot,\,PM})^{1/2}$ (i.e. the energy of the low frequency peak is equal to 5% of the energy of Pierson-Moskowitz limit). The directional width of the incident swell has been chosen equal to $cos^{15}(\theta)$. The incident wave conditions are presented in Table 5.2.

| $U_{10}$ [m/s] | $H_{s,\,PM}$ | $f_{p,\,PM}$ [Hz] | $H_s$ [m] $E_{tot,swell} = 5\%\ E_{tot,\,PM}$ | $f_p$ [Hz] $f_{p,swell} = 0.75\,f_{p,PM}$ |
|---|---|---|---|---|
| 10 | 1.95 | 0.144 | 0.436 | 0.108 |
| 20 | 11.44 | 0.059 | 2.55 | 0.04425 |
| 30 | 33.33 | 0.0349 | 7.45 | 0.026 |

Table 5.2 Values of significant wave height and peak frequency of the Pierson-Moskowitz observed data and for the incident low frequency waves

It is noted that the model resolutions in spectral space have been adapted in order to accurately describe the (long-crested) low frequency waves. The directional resolution has been increased from MDC = 36 to MDC = 72. The frequency range has been adapted to ensure that the low frequency peaks are inside the range.

### 5.4.1 Standard SWAN (WAM Cycle 3: Komen et al, 1984)

Figures 5.14.*a* to 5.14.*d* show the model results using the standard option in SWAN (i.e. GEN3). It is seen that the SWAN model does not properly simulate the observed suppression of the local wind sea in presence of low frequency waves but it shows the opposite effect of what has been observed by Donelan (1987) (see Section 2.2): the significant wave height for $X^* < 10^6$ is significantly larger of the data of Kahma and Calkoen (1992).

### 5.4.2 Extended Komen et al. (1984) expression

Activating the extended expression of Komen et al. (1984) resulted in a reduction in the growth of the wind sea with respect to the standard option, as is evident from Figures 5.15.*b*, 5.15.*c* and 5.15.*d* where results have been plotted for $\beta^0$. It is now clearly seen that, with $n = 0$, the local wind sea is suppressed in presence of low frequency waves in wave growth conditions. For fully developed conditions (where the low frequency peak is absorbed by the local wind sea), the wave spectra reduce to those as computed in the situation without incident swell. The model results with increasing values of $n$ ($n = 0.5$, and $n = 1$) are shown in Fig. 5.16 and 5.17. For these values the local wind sea is

even more suppressed by the presence of the swell and the value of the total energy for the fully developed conditions is slightly smaller than those in the absence of low frequency waves.

With these new formulations SWAN performs in such way that if in a wind sea, low frequency waves are present, the overall steepness $\hat{\alpha} = \tilde{k}^2 E_{tot}$ decreases whereas the high-frequency steepness $\hat{\alpha}(\sigma) = \tilde{k}^2(\sigma) E_{hf}(\sigma)$ is hardly affected by the low frequency waves. By this the whitecapping dissipation of the wind sea is enhanced by the swell as represented by the increased value of $\beta$.

## 5.5 Whitecapping formulations using point model

To demonstrate the distribution of the dissipation rate of the standard and the adapted whitecapping formulations for a local wind sea (with and without low frequency waves) computations with SWAN have been carried out. In order to obtain the whitecapping source term as output of SWAN, the physical processes of quadruplets and wind have been deactivated. To avoid that the whitecapping term actually affects the spectral shape of the spectrum, it is required that the computed source term $S_{wc}(\sigma,\theta)$ is not applied to the spectrum (i.e. stored in the matrix with the propagation coefficients). This has been activated by modifying the source code of SWAN (these modifications have not been described here).

Computations have been carried out for a wind sea of $H_s$ = 1 m and $T_p$ = 5 s and with different low frequency waves. The low frequency waves conditions considered are presented in Table 5.3.

| | $H_s$ [m] | $T_p$ [s] |
|---|---|---|
| Top left panel | wind sea | |
| Top right panel | 0.1 | 15 |
| Bottom left panel | 0.2 | 15 |
| Bottom right panel | 0.5 | 15 |

Table 5.3 Values of significant wave height and peak frequency of the incident low frequency waves

The results have been plotted from Fig. 5.18 to Fig. 5.21. The figures may be interpreted as follow: the top left panel represents a situation of a wind sea with $H_s$ = 1 m and $T_p$ = 5 s,

the top right panel a combination of wind sea and a swell system (swell $H_s = 0.1$ m and $T_p = 15$ s); the bottom left panel the swell have a $H_s = 0.2$ m and $T_p = 15$ s and the bottom right panel $H_s = 0.5$ m and $T_p = 15$ s.

Figure 5.18 shows the frequency spectra and the whitecapping source term for the standard formulation (i.e. Komen et al., 1984). The effect of swell on the whitecapping dissipation of the wind sea part of the spectrum is clearly visible. Figure 5.19 shows a comparison between the computed $S_{wc}$ with the extended Komen expression implemented for a value of $n = 0$ and the standard formulation. The results clearly show that with the extended formulation the dissipation rate for the wind sea is roughly identical for the cases with and without swell. Increasing the value of $n$ ($n = 0.5$ and 1) results in enhanced whitecapping, as is evident from the Figures 5.20 and 5.21.

# 6 Wave flume experiment (Donelan, 1987)

## 6.1 Introduction

To verify the extended Komen et al. (1984) formulation in SWAN, the flume experiment of Donelan (1987) is used. The observations by Donelan (1987) show that a wind sea generated in a flume change significantly if low frequency waves are imposed (see Fig 2.1).

## 6.2 Description of the flume test case

The experiment of Donelan (1987) were carried out in wave flume (100 m long, 4.57 m wide). The water depth was equal to 1.20 m. The waves are generated by a piston-type paddle and dissipated on a beach of fibrous matting with a slope of 1:8 at 100 m. For more details of the flume experiment reference is made to Donelan (1987).

In the present study only one case of Donelan is considered. In this case, the variance of the generated swell at 50 m fetch was 5.47 $cm^2$, concentrated at a peak frequency of 0.707 Hz in the absence of wind (see top panel Fig 2.1). (It is noted here that this peak frequency, does not correspond to the peak frequency of the spectrum as it is plotted in the top panel of Fig. 2.1 (i.e. the observed spectrum by Donelan). In the remainder of this study the wave spectrum as plotted in the top panel is therefore used in the SWAN computations.) The variance of the young sea state was 16.8 $cm^2$ with a peak frequency of about 0.11 Hz in the absence of low frequency waves (see middle panel of Fig. 2.1). When the waves were generated simultaneously, the swell roughly doubled its variance (to about 11 $cm^2$) and retained its frequency whereas the wind sea was greatly reduced (to about 4 $cm^2$ variance) and shifted to higher frequencies (see Fig. 2.1).

## 6.3 Model schematisation for the SWAN test cases

The SWAN computations have been carried out using the one-dimensional mode. The spatial resolution that has been used in the computations was $\Delta x = 2$m, $\Delta\sigma/\sigma = 0.0245$ and $\Delta\theta = 1°$. The maximum discrete frequency $f_{max}$ has been taken equal to 2 Hz and $f_{min}$ equal to 0.35 Hz. To obtain fully convergence of the model, 50 iterations have applied.

The incident low frequency waves in SWAN have been simulated by imposing the observed swell by Donelan (1987; the data of Fig. 2.1 has been digitised to that end).

The wind speed as measured at 26 cm above the mean water level should be adapted to a wind speed at 10 m height $U_{10}$ for SWAN. This can be achieved by using a boundary layer theory, however, for the present study it has been decided to chose the wind speed such that the observed significant wave height of the wind sea at $x$ = 50 m corresponds to the significant wave height of the wind sea as computed by SWAN. It was found that with a wind speed of 27.5 m/s the agreement between the significant wave height as computed by SWAN and the observation is reasonable (see middle panel of Fig. 6.1.*b*). This wind speed has been applied in the computations to reproduce the wind sea conditions with SWAN.

Fig. 6.1.*a* shows the $H_s$, $T_{m01}$, *Dir* and the directional spreading of the wind sea as computed by SWAN using the standard option of SWAN (GEN3) and the extended Komen et al. (1984) expression (with $n = 0, 0.5, 1, 2$). It is seen that at $x$ = 50 m (where spectra have been measured) the significant wave height is roughly identical for all computations. The mean wave period $T_{m01}$ computed with the standard option is slightly smaller than those as computed with the extended Komen et al. (1984) expression. This is as expected since it was shown from the idealised wave growth curves that the wave spectra with the extended Komen et al. (1984) expression is more peaked and contain less energy at the high frequencies. The spectra at $x = 0$ m, 50 m and 100 m and source terms at $x$ = 50 m are plotted in Fig. 6.1.*b* and 6.1.*c*, respectively. In the middle panel of Fig 6.1.*b* the computed spectra have been compared with the one as observed by Donelan (1987).

## 6.4 Model results

The model results using the standard option of SWAN (GEN3) and with incident low frequency waves imposed on the growing wind sea are shown in Fig. 6.2. Although it seems that the model performs well, in terms of integral wave parameters. It is clearly seen that the wave spectra and source terms show large oscillations. An analysis has shown that this unexpected model behaviour is due to the Discrete Interaction Approximation (DIA). The reason for this is that for nearly long crested low frequency waves the DIA is not accurate to simulate the transfer due to non-linear interactions. The interaction coefficient for these nearly long-crested low frequency waves should nearly be equal to zero in theory, however, in the DIA it is not. From this, the DIA is pumping energy from the peak of the low

frequency waves towards the lower and higher frequencies at spectral directions different than the mean wave direction..

Since the interactions are nearly zero for the long crested waves it has been decided to deactivated the $S_{nl4}$ for the low frequency waves only. By this the interactions are only computed for the wind sea part. To achieve this, the source code of the SWSNL2 subroutine has slightly been changed such that the swell is not accounted for when computing $S_{nl4}$. The results of comparisons with these modifications added (see Fig. 6.3), clearly show that the spurious oscillations have disappeared, the swell and wind sea are well reproduced by SWAN (for reference, the model results of the standard SWAN have also been plotted: dashed line).

Figure 6.4 shows the model results (using the standard option GEN3) with and without low frequency waves. It is seen that with the standard option (GEN3), the local wind sea increases in presence of low frequency waves. This is not in agreement with the laboratory observations.

The results of the SWAN computations with the extended Komen et al. (1984) expression for different values of the power $n$ = 0, 0.5, 1, 2 have been plotted in Fig. 6.5 to Fig. 6.8, respectively. It has been found that with the extended formulation the growth of the wind sea in Donelan (1987) flume experiment can be suppressed but that the enhancement of the energy density of the low frequency peak could not be reproduced. The reason for this is presumably that the non-linear transfer from the wind sea to the low frequency waves has been neglected (for reasons given above). It has been found that the coefficient $n$ should be taken about 2 to simulate the suppression of the wind sea as observed by Donelan. This value, however, is too large to accurately simulate the fetch-limited wave growth curves. Since the results with $n$ = 0, 0.5 and 1 are reasonable, these coefficients are considered in the next Chapter.

# 7 Field cases

## 7.1 Introduction

It has been shown that the results obtained with the extended Komen et al. (1984) formulation are fairly reasonable in the fetch-limited wave growth situations and in the Donelan (1987) flume experiment. In this Chapter the extended formulation is verified in four field cases (with increasing complexity). They are:

1. Lake George (Australia);
2. The Haringvliet estuary (the Netherlands);
3. The Norderneyer Seagate (Germany);
4. Westerschelde estuary (The Netherlands).

The selected cases (i.e. model resolution, wave boundary conditions, etc.) are identical to those of the bench mark tests for SWAN (WL | DELFT HYDRAULICS, 1999b). A brief description of each test case with respect to the model schematisation, resolution, boundary conditions etc., has been given in the Appendices (Lake George, see App. D; The Haringvliet estuary, see App. E; The Norderneyer Seagate, see App. F; Westerschelde estuary, see App. G).

The figures presented here are directly taken from the bench mark tests. It is noted that in the present study 30 iterations have been performed to ensure full model convergence. Computations have been performed with values of $n = 0$, 0.5 and 1.

It is mentioned here that the model results of the version 40.00 of SWAN are identical to those obtained with the previous version 30.75 except for the complex field cases of the Haringvliet estuary and the Norderneyer Seagat. In these cases some small differences have been found at locations where triad wave interactions are dominant (since the coefficients of triads have slightly been adapted in version 40.00).

### 7.1.1 Lake George (Australia)

The results of the SWAN computations with activated the extended Komen et al. (1984) expression, for value of $n$ = 0, 0.5, 1 have been plotted in Figures 7.1, 7.2, 7.3, respectively. It is seen that the differences in the results of the three computations (i.e. $n$ = 0, 0.5, 1) are not significant, as expected, since low frequency waves are absent. The computed spectra are more peaked and the high frequency peak of the spectrum contains less energy. This is in better agreement with the observations (particularly for the high wind speeds). The value of the mean and peak period have slightly increased whereas the significant wave height has not changed significantly (see e.g. Figures 7.1.*b*, 7.1.*d* and 7.1.*f* for $n$ = 0).

### 7.1.2 The Haringvliet estuary (the Netherlands)

The model results for different values of $n$ have been plotted in Figures 7.4, 7.5, 7.6, respectively. In this case, where a low frequency peak is present, it is visible that the computed results with the extended Komen et al. (1984) expression show a suppression of the growth of the local wind sea at station 8 and a slightly enhancement of the low frequency peak at all stations. The agreement between SWAN and the observations has improved compared to the model results of version 30.75. It is also seen, that with the extended expression the low frequency peak is still poorly predicted by the model.

### 7.1.3 The Norderneyer Seegat (Germany)

The results of computation with SWAN for value of $n$ = 0, 0.5, 1 have been presented in Figures 7.7, 7.8, 7.9, respectively. In this complex case it is clearly visible from the figures that there are significant differences between the results obtained with different values of $n$ and SWAN 30.75. The growth of the wind sea is significantly suppressed proportionally to the power $n$ of the straining parameter $\beta$. The agreement between SWAN and the observations has improved particularly for the mean wave period and the significant wave height. The reason that the extended expression is effective in the Norderneyer Seegat is because low frequency waves (with frequencies of about 0.08 - 0.12 Hz) are present. It can be concluded that the best agreement between SWAN and the observation is obtained with $n$ about 0.5.

### 7.1.4 Westerschelde estuary (The Netherlands)

In the case of the Westerschelde estuary, the model performance improved considerably for different values of $n$. It seems, as in the Norderneyer Seegat case, that the coefficient $n$ should be taken about 0 or 0.5 to have the best possible agreement between the SWAN model results and observations. The effect of the extended formulation on the growth of the local wind sea is significant at stations in the inner area (stations W0V3 to W0V6). From Figures 7.10, 7.11, 7.12, it is clearly seen that the prediction of the local wind sea is now in better agreement with the observations.

# 8 Conclusions and recommendations

## 8.1 Conclusions

In the present study the effect of low frequency waves on wave growth in SWAN has been investigated. From the study the following conclusion can be drawn:

### Fetch-limited wave growth

- It has been shown that the growth of a local wind sea in presence of low frequency, using the default formulations in SWAN, is enhanced compared to the results without low frequency waves. This is contrary to observations (see e.g. Donelan, 1987; Mitsuyasu, 1966; Phillips and Banner, 1974).

- It was found that an alternative expression, in which the wave steepness has been defined in terms of an integral and a local steepness of the waves have been adapted, is not appropriate for the third-generation wave model SWAN in practical applications. It appeared that the dissipation rate for the low frequencies is too low. From this, wave energy of these low frequency components may grow unbound, resulting in unrealistic model results.

- The expression of Komen et al. (1984) has been extended in this study such that:
  1. the wave steepness $\hat{\alpha}$ has been made frequency dependent $\hat{\alpha}(\sigma)$ (but not directional dependent) accounting for contributions of frequencies higher than the frequency $\sigma$ only.
  2. the dissipation rate for a local wind sea in presence of low frequency waves is enhanced (whereas the dissipation rate at the low frequency waves is slightly reduced). This has been achieved by scaling the whitecapping source term with the straining parameter $\beta$.

- The extended formulation has been implemented (and coefficients have been tuned) and verified in SWAN. From the verification in idealised fetch-limited wave growth, it was found that wave growth could properly be reproduced with the extended formulations

(at least for values of $n$ equal 0 and 0.5). It was shown that with the extended formulation the wave spectra were slightly more peaked (with slightly lower peak and mean frequencies) and that the high frequency tail of the spectrum contains less energy. The mean wave periods have, therefore, increased with the extended formulation. The significant wave height and peak frequency, however were slightly underestimated for fully developed conditions as compared to the value of Pierson-Moskowitz (1964). This obviously needs some retuning of coefficients.

- On the basis of the figures in which an $f^{-4}$ and an $f^{-5}$ tail and the spectra have been plotted, it has been found that the high frequency part of the spectrum as computed by SWAN is in better agreement with an $f^{-5}$ tail than with an $f^{-4}$ tail.

- With the extended formulation, it was possible to suppress the growth of a local wind sea in presence of low frequency waves compared to the situation in which no incident low frequency waves were present (see Figures 5.15, 5.16, 5.17). The dissipation rate at the higher frequencies is controlled by the coefficient $\beta^n$.

### Donelan (1987) flume experiment

- The discrete interaction approximation (DIA) is not adequate in reproducing the non-linear transfer for long-crested waves in the simulations of the Donelan (1987) flume experiment. To get around with this problem it was required to deactivate the DIA for the (long-crested) low frequency waves in Donelan experiment.

- The results obtained with the extended formulation indicate that the suppression of the wind sea can be simulated with SWAN. The coefficient $n$ should be chosen about 2 to simulate the suppression of the wind sea as observed by Donelan. It should be noted here, however, that the conditions of the Donelan flume experiment are rather extreme (with respect to the wind speed (27.5 m/s), the length of the flume (100 m) and the location at which observations are available (x = 50 m); non-dimensional fetch $X^*$ is only 250). The results should therefore be considered with some care and only indicate that with the formulation it is possible to suppress the growth of the local wind sea and that the value of the coefficient $n$ should be of the order 1.

### Field Cases

- The results with the extended expression of Komen et al. (1984) with different values of the tuneable coefficient $n$ ($n$ = 0, 0.5 and 1) have shown that the agreement with the field observations has improved (in particular for the mean wave period). The wave spectra are more peaked and the high frequency peak of the spectrum contains less energy (which is in better agreement with the observations). The values of the mean and peak period have increased whereas the significant wave height has not changed significantly.

- On the basis of the model results for all the field cases considered, it may be concluded that the best agreement between the extended Komen et al. (1984) expression and the observations, is obtained for values of $n$ between 0 and 0.5. Choosing a larger value for $n$ (i.e. $n > 0.5$) has the disadvantage that fetch-limited wave growth at fully developed conditions can only be reproduced with SWAN with retuning of the coefficient $C$ of the whitecapping source term.

## 8.2 Recommendations

- It has to be noted that the extended Komen et al. (1984) expression is directional independent. That means that the direction of incidence of the low frequency waves has not been considered. However, it has to be noted that works of Mitsuyasu and Yoshida (1989), Mitsuyasu (1997) mention the fact that swell propagating against the wind intensifies the growth of the wind sea. The mechanism of interaction between swell and wind sea is poorly understood and it may be expected to depend on the propagation direction of the low frequency waves itself relative to the wind direction. Therefore an additional implementation of the directional dependence in the extended Komen et al. (1984) expression is recommended.
- Further tuning procedures for the coefficient $C$ and $n$ may be necessary if the directional dependence of the extended expression is taken into account. Additional tests are recommended in other (complex) field situations with different low frequency conditions (e.g. swell opposing a wind sea).
- It should be investigated whether the present $f^{-4}$ tail that is applied (at frequencies higher than the maximum discrete frequency) should be adapted to a $f^{-5}$ tail since it has been

found that the high frequency part of the spectrum as computed by SWAN is in better agreement with a $f^{-5}$ tail.

- To determine to what extent the SWAN model performance has improved with the extended formulation, it is recommended to analyse the model results using statistical parameters (e.g. bias, rms, etc.).

# References


Alkyon, 1999: Source term investigation SWAN. G. van Vledder, Report A162, the Netherlands

Booij N., R.C. Ris and L.H. Holthuijsen, 1999: A third-generation wave model for coastal regions. Part I: Model description and validation, *J. Geoph. Research*, Vol. 104, No. C4, 7649-7666

Chen, G., and S.E. Belcher, 1999 : The suppression of long waves on wind-generated waves. Manuscript to be published

Donelan, M.A., 1987 : The effect of swell on the growth of wind waves. John Hopkins APL Tech. Digest 8, 18-23

Forristall, G. Z., and K.C. Ewans, 1997: Worldwide measurements of directional wave spreding. *J. Atmosoheric Oceanic Technology*, Vol. 9, 440-469

Gerling, T.W., 1992: Partitioning sequences and arrays of directional ocean wave spectra into component wave systems. *J. Atmosphere Oceanic Technology*, Vol. 9, 444-458

Hasselmann, K., T.P. Barnett, E. Bouws, H. Carlson, D.E. Cartwright, K. Enke, J.A. Olbers, K. Richter, W. Sell and H. Walden, 1973: Measurements of wind-wave growth and swell decay during the Joint North Sea Wave Project (JONSWAP), *Dtsch. Hydrogr. Z.* Suppl., 122, A8

Hasselmann, K., 1974: On the spectral dissipation of ocean waves due to whitecapping. *Bound.-layer Meteor.*, 6 No. 1-2, 107-127

Hasselmann,K., 1992: Proposal for a wind-sea swell separation scheme as part of a general wave-spectrum spectral partitioning scheme. Letter to the WAM development group. July 30, 1992, Max Plank Institute fur Meteorology

Holthuijsen L.H., N. Booij and R.C. Ris, 1993: A spectral wave model for the coastal zone, *2nd Int. Symposium Ocean measurement and Analysis*, pp. 630-641, New Orleans

Kahma, K.K. and C.J. Calkoen, 1992: Reconciling discrepancies in the observed growth of wind-generated waves. *J. Phys. Oceanogr.*, 22, 1389-1405

Komen, G. J., S. Hasselmann, and K. Hasselmann, 1984: On the existence of a fully developed wind-sea spectrum, *J. Phys. Oceanogr.*, 14, 1271-1285

Komen, G.J., Cavaleri, L., Donelan, M., Hasselmann, K., Hasselmann, S. and P.A.E.M. Janssen, 1994: *Dynamics and Modelling of Ocean Waves*, Cambridge University Press, 532 p

Makin, V. K., V. M. Kudryatsev and C. Mastenbroek, 1995: Drag of the sea surface. *Boundary-Layer Meteorol.*, 73, 159-182

Makin, V. K. and V. M. Kudryatsev, 1999: Coupled sea surface-atmosphere model. Part I. Wind over waves coupling. *J. Geophys. Res.* in press

Masson, D.,1993 : On the nonlinear coupling between swell and wind waves, Note and correspondence, June 1993, 1249-1257

Mitsuyasu, H., 1966: Interactions between water waves and wind (1). Rep. Inst. Appl. Mech. Kyushu Univ., 14, 67-88

Mitsuyasu, H. and Y. Yoshida, 1989: Air-Sea interactions under the existence of swell propagation against the wind, Bull. Res. Inst. Appl. Mech. Kyushu Univ., No. 63, 47-71.

Mitsuyasu, H., 1997: On the contribution of swell to sea surface phenomena. Int. J, off. and Polar Eng., Vol. 7, No. 4, 141-245.

Phillips, O.M. and Banner, M.L.,1975: Wave breaking in the presence of wind drift and swell, *J. Fluid Mech*, vol.66, part 4, pp. 625-640

Pierson, W.J. and L. Moskowitz, 1964: A proposed spectral form for fully developed wind seas based on the similarity theory of S.A.. Kitaigorodskii. *J. Geophys. Res.*, 69, No. 24, 5181-5190

Ris, R.C., 1997: Spectral modelling of wind waves in coastal areas, Ph.D.-dissertation, Delft University of Technology, Department of Civil Engineering, The Netherlands

Ris, R.C., N. Booij and L.H. Holthuijsen, 1999: A third-generation wave model for coastal regions. Part II: Verification, *J. Geoph. Research*, Vol. 104, No. C4, 7667-7682

SWAMP group, 1985: Ocean wave modelling, Plenum Press, New York and London

Tolman, H.L., and D.V. Chalikov, 1996: Source terms in a third-generation wind wave model, *J. Phys. Oceanogr.*, 26, No. 11, 2497-2518

WAMDI group, 1988: The WAM model - a third-generation ocean wave prediction model, *J. Phys. Oceanogr.*, 18, 1775-1810

Wilson, B.W., 1965: Numerical prediction of ocean waves in the North Atlantic for December 1959, *Deutsch. Hydrogr. Z.*, 18, No. 3, p. 114-130

WL | DELFT HYDRAULICS, 1999a: Effects of a self scaling cut-off frequency on wave growth. R.C. Ris and K.J. Bos, Report H3396, the Netherlands

WL | DELFT HYDRAULICS, 1999b: Standard bench mark tests for the shallow water wave model. R.C. Ris and C.M.G. Somers, Report H3515, the Netherlands

Wright, J. W., 1976: The wind drift and wave breaking. *J. Phys. Oceanogra.*, 6, 402-405

Wu, J., 1982: Wind-stress coefficients over surface from breeze to hurricane, *J. Geophys. Res.*, 87, C12, 9704-9706

# Acknowledgements

We thank IJ. Haagsma of Delft University of Technology for providing us with the beta-release of SWAN 40.00. We thank dr G. Ph. Van Vledder from Alkyon for additional information on the redefinition of integral and local wave steepness and for his comments on the draft report. Thanks also to J.H. Andorka Gal, J.G. De Ronde, A.T. Kamsteeg and Mrs. D. Abeysirigunawardena of the Dutch Ministry of Public Works and Coastal Management (RIKZ) for providing us with the data of the Westerschelde estuary case and for additional information on this complex field case. For providing us with the data of Lake George, Australia, we want to express our gratitude to I.R. Young, University of New South Wales, Canberra, Australia. We would like to thank Hans Niemeyer and Ralf Kaiser for providing us with the original field data of the Norderneyer Seegat.

# Figures

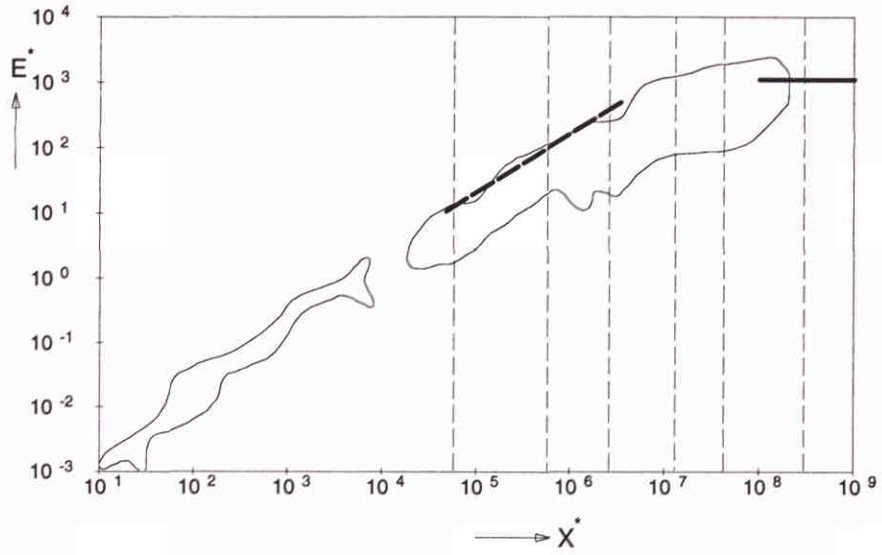


$U_{10}$=10 m/s

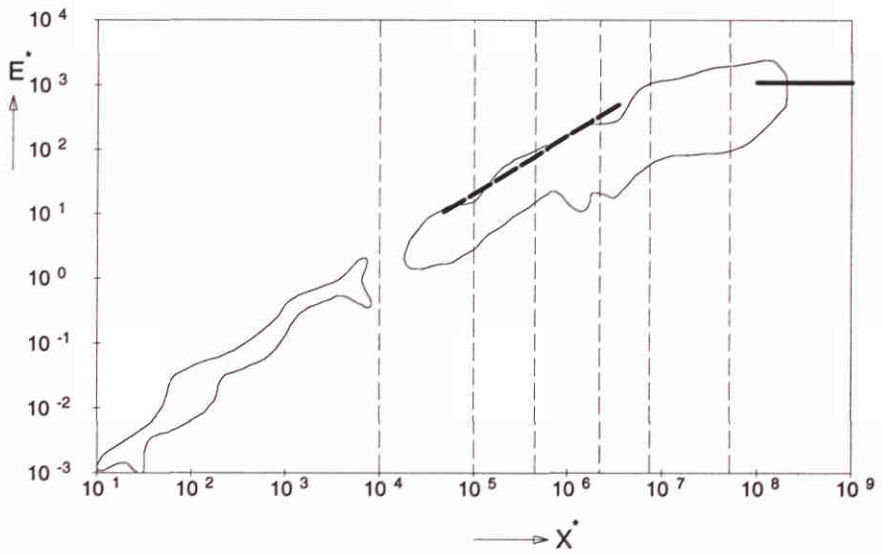


$U_{10}$=20 m/s

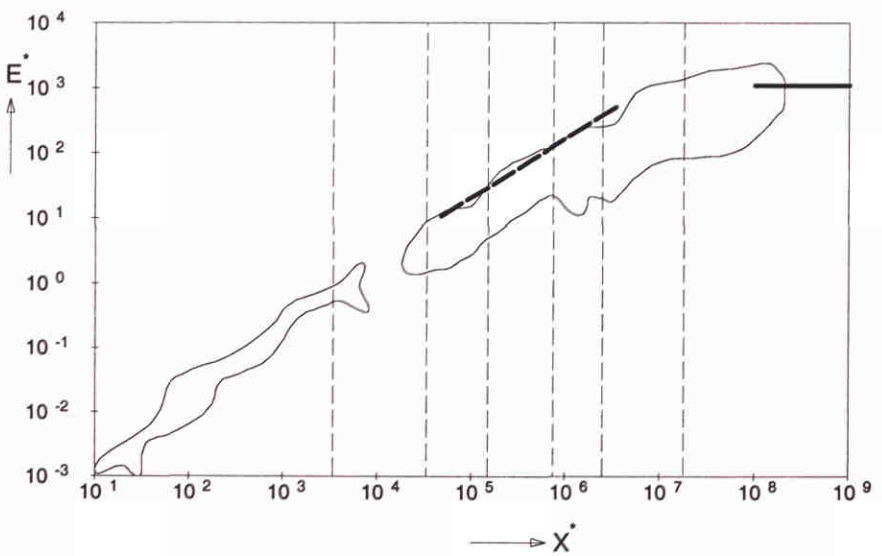


$U_{10}$=30 m/s

Fetch limited wave growth (deep water)

Locations (in terms of dimensionless fetch) at which spectral output is generated.

SWAN 40.00

WL | delft hydraulics

H3529

Fig. 5.1

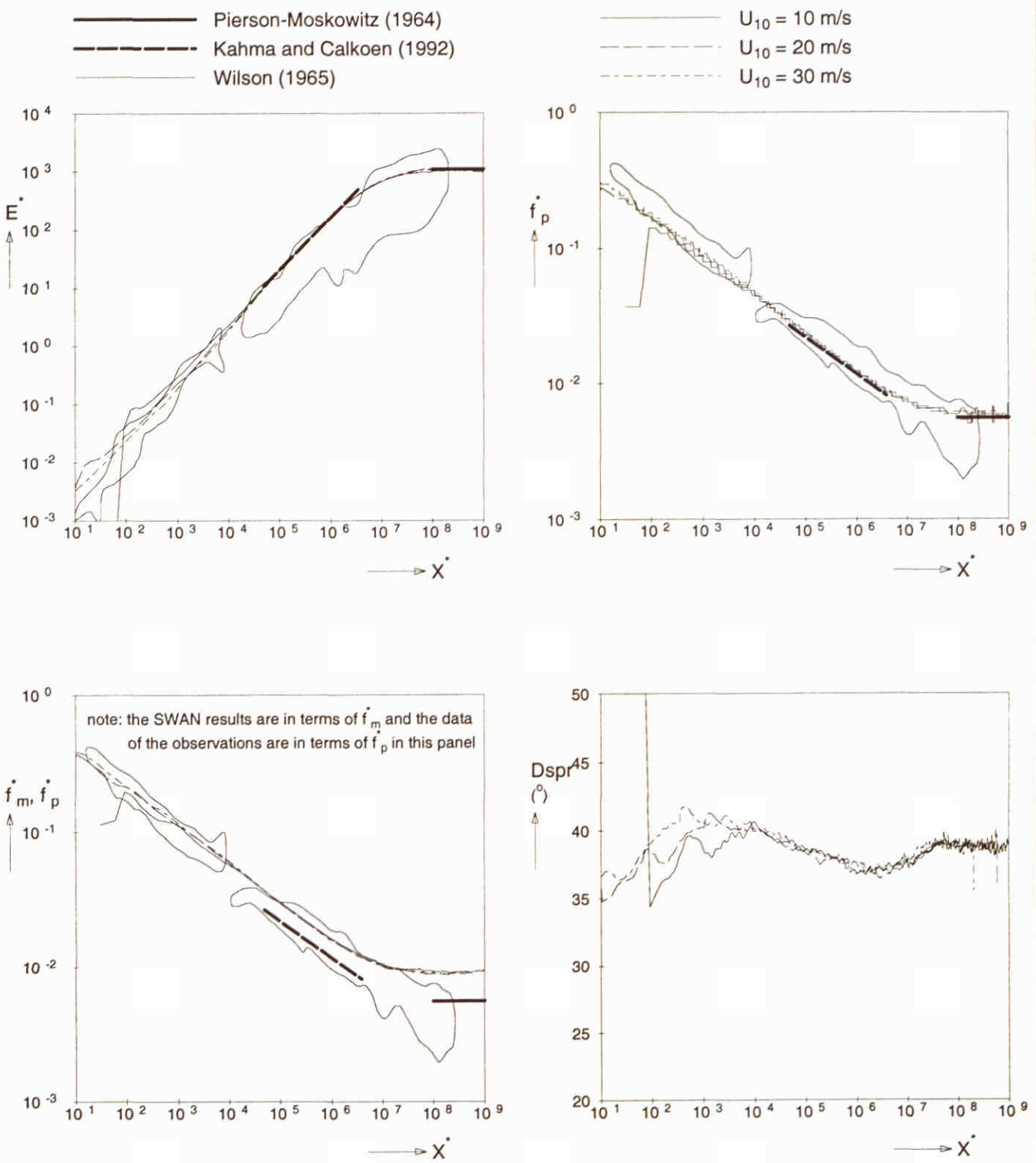


Fetch limited wave growth (deep water)
Third-generation formulations (standard option: GEN3)

SWAN 40.00

WL | delft hydraulics

H3529

Fig. 5.2.a

Standard option: GEN3

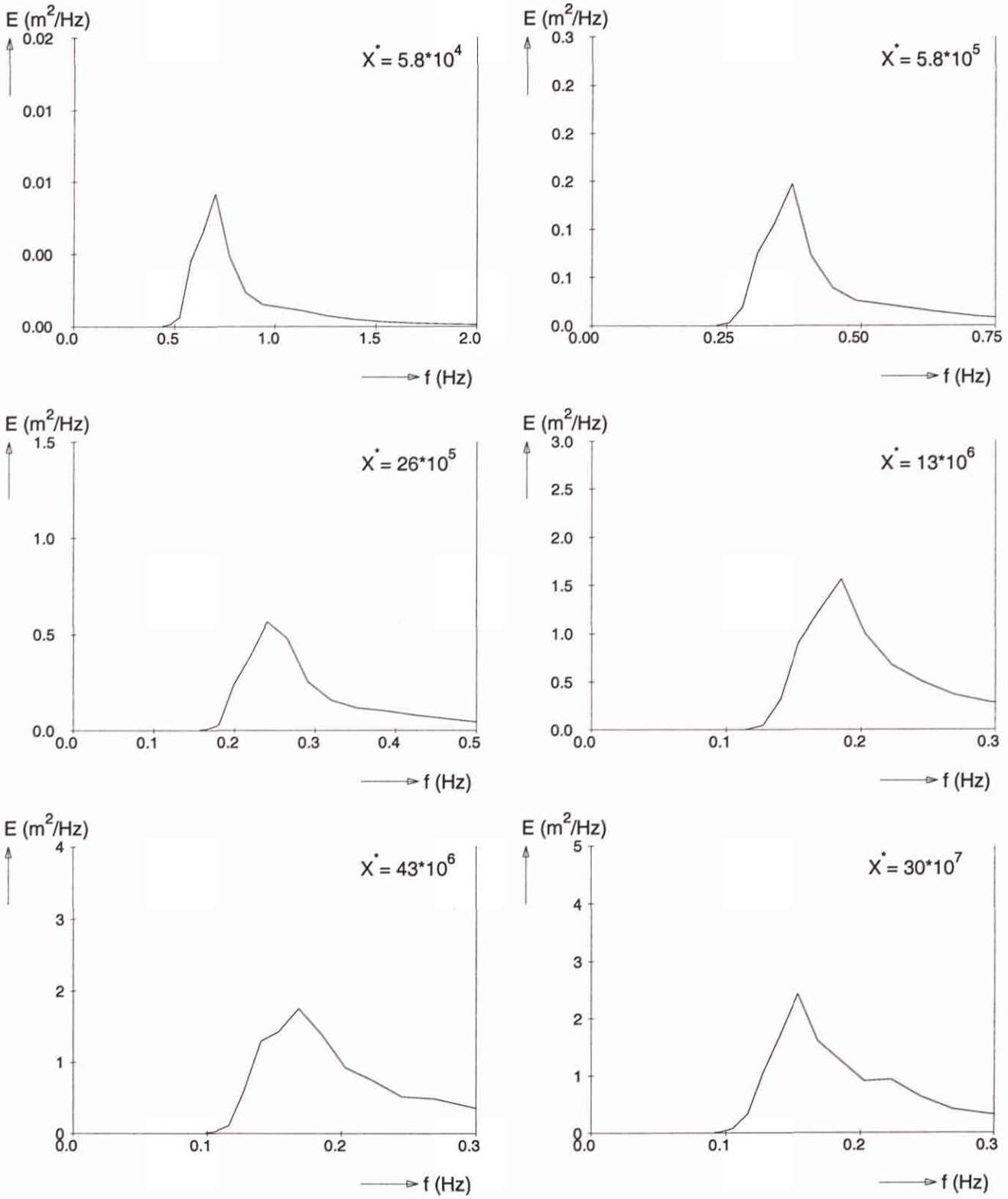


| | | |
|---|---|---|
| Frequency spectra at different locations ($U_{10}$ = 10 m/s) | SWAN 40.00 | |
| | | |
| WL \| delft hydraulics | H3529 | Fig. 5.2.b |

Standard option: GEN3

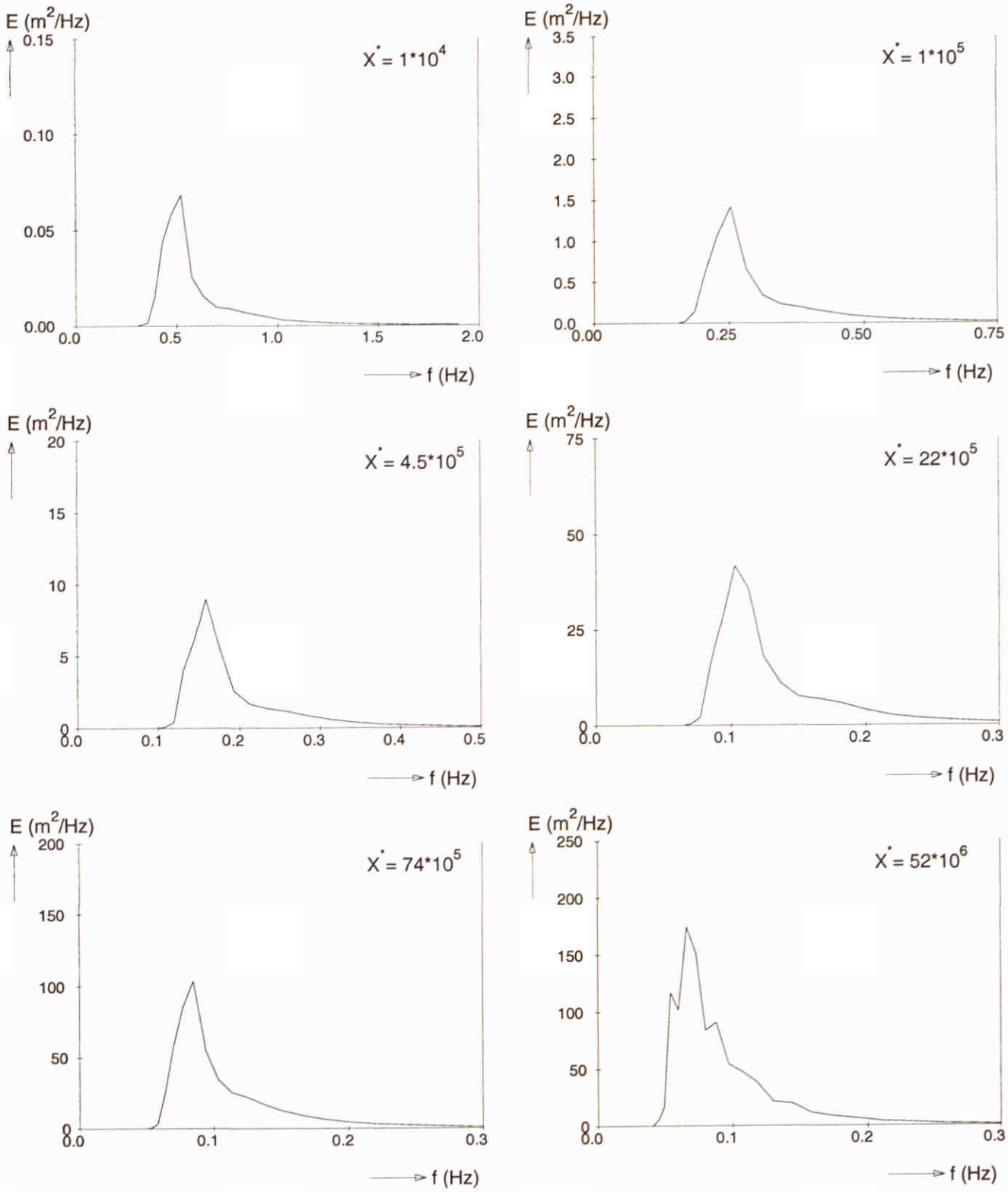


Frequency spectra at different locations ($U_{10}$ = 20 m/s)

SWAN 40.00

WL | delft hydraulics

H3529

Fig. 5.2.c

Standard option: GEN3

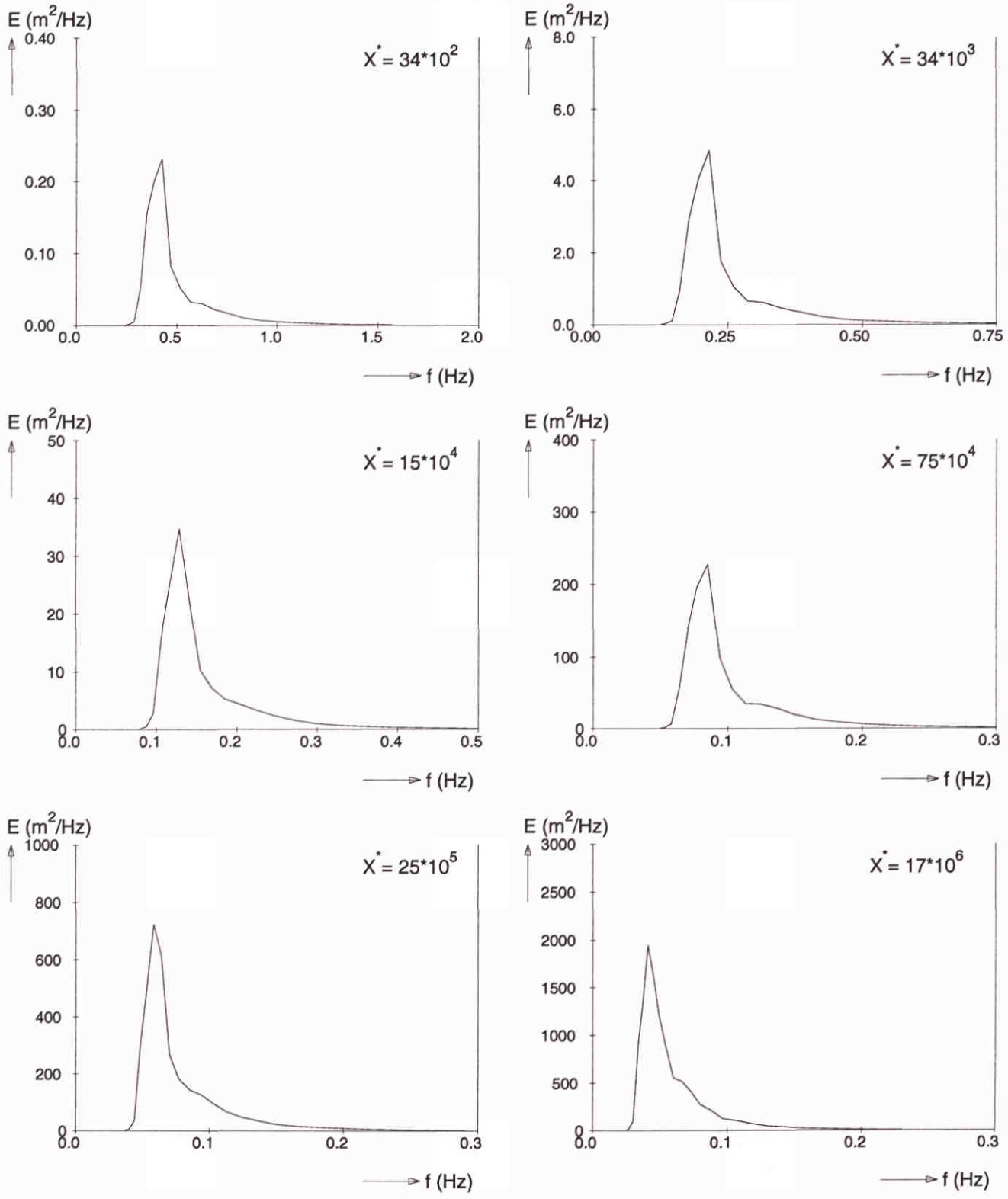


Frequency spectra at different locations ($U_{10}$ = 30 m/s)

SWAN 40.00

WL | delft hydraulics

H3529

Fig. 5.2.d

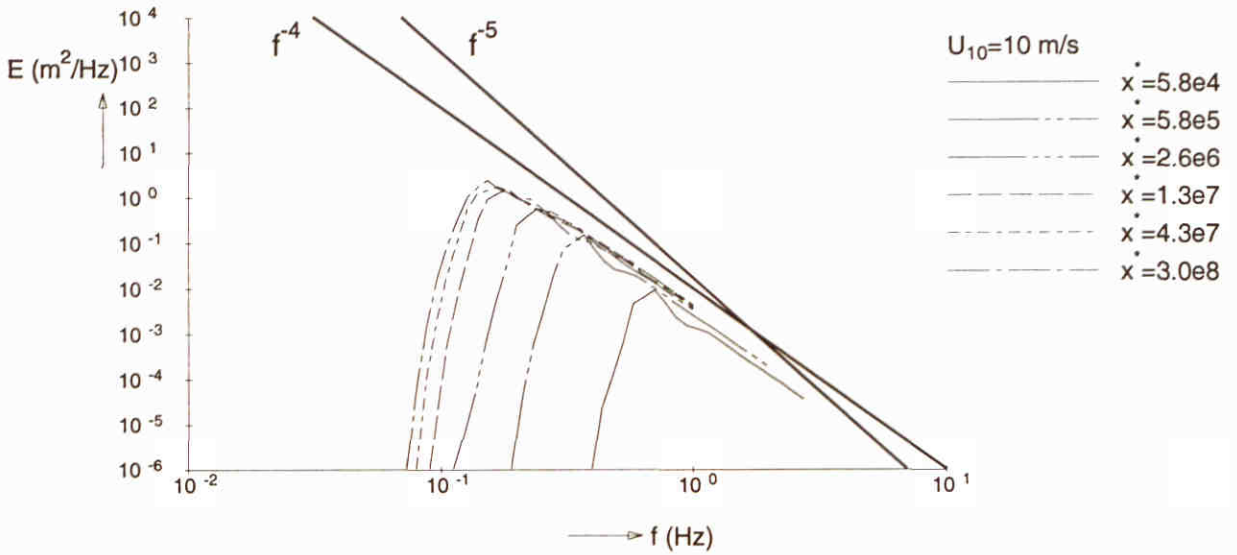


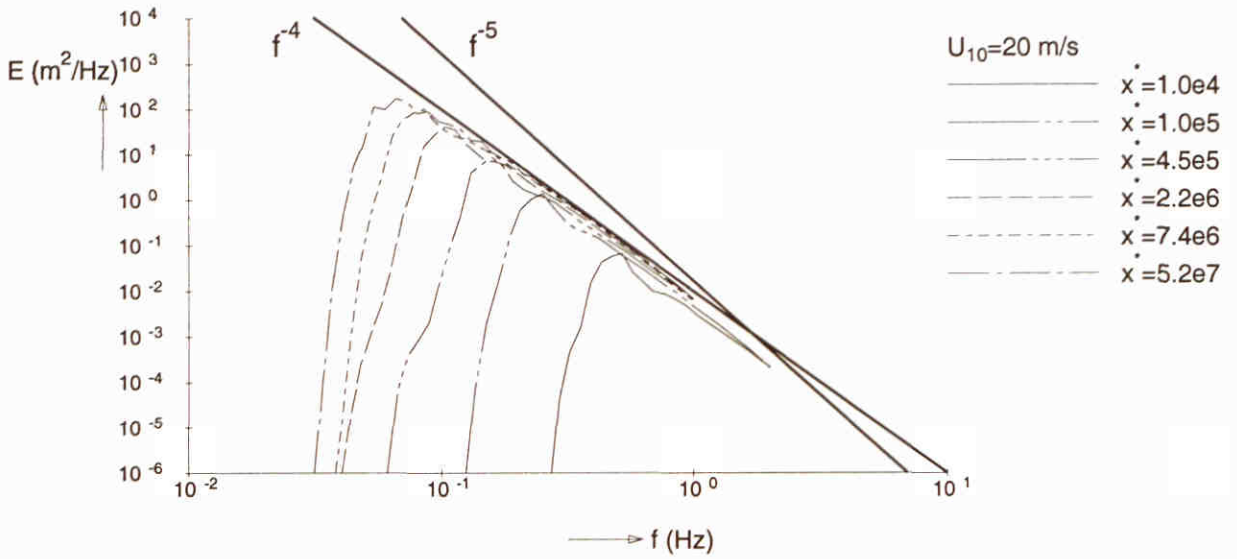


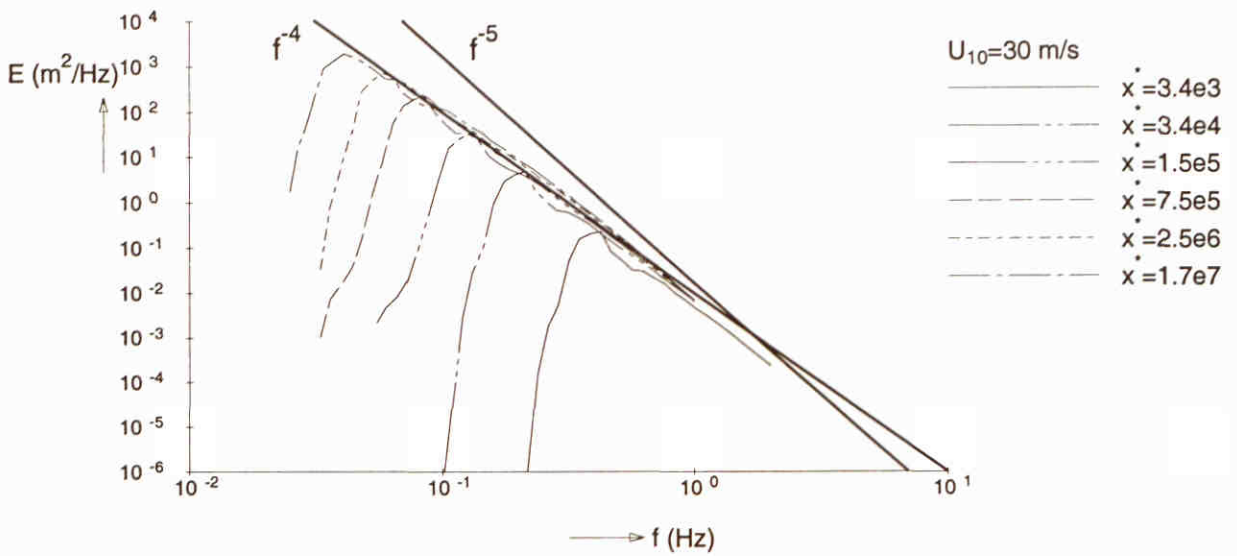


Wave spectra at different fetches
Standard option: GEN3

SWAN 40.00

WL | delft hydraulics

H3529

Fig. 5.2.e

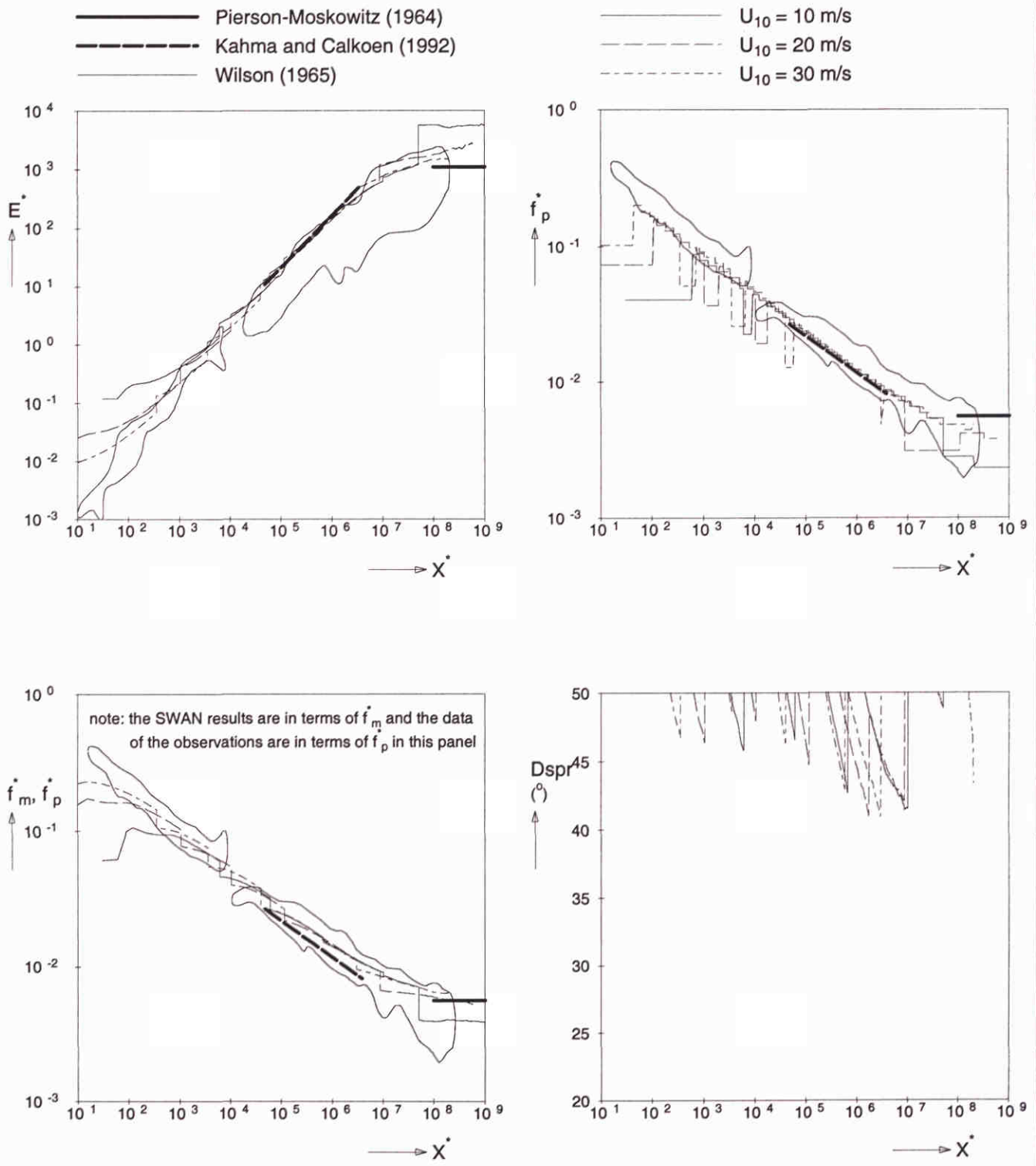


Fetch limited wave growth (deep water)
Third-generation formulations
Redefinition of integral and local wave steepness

SWAN 40.00

WL | delft hydraulics

H3529

Fig. 5.3.a

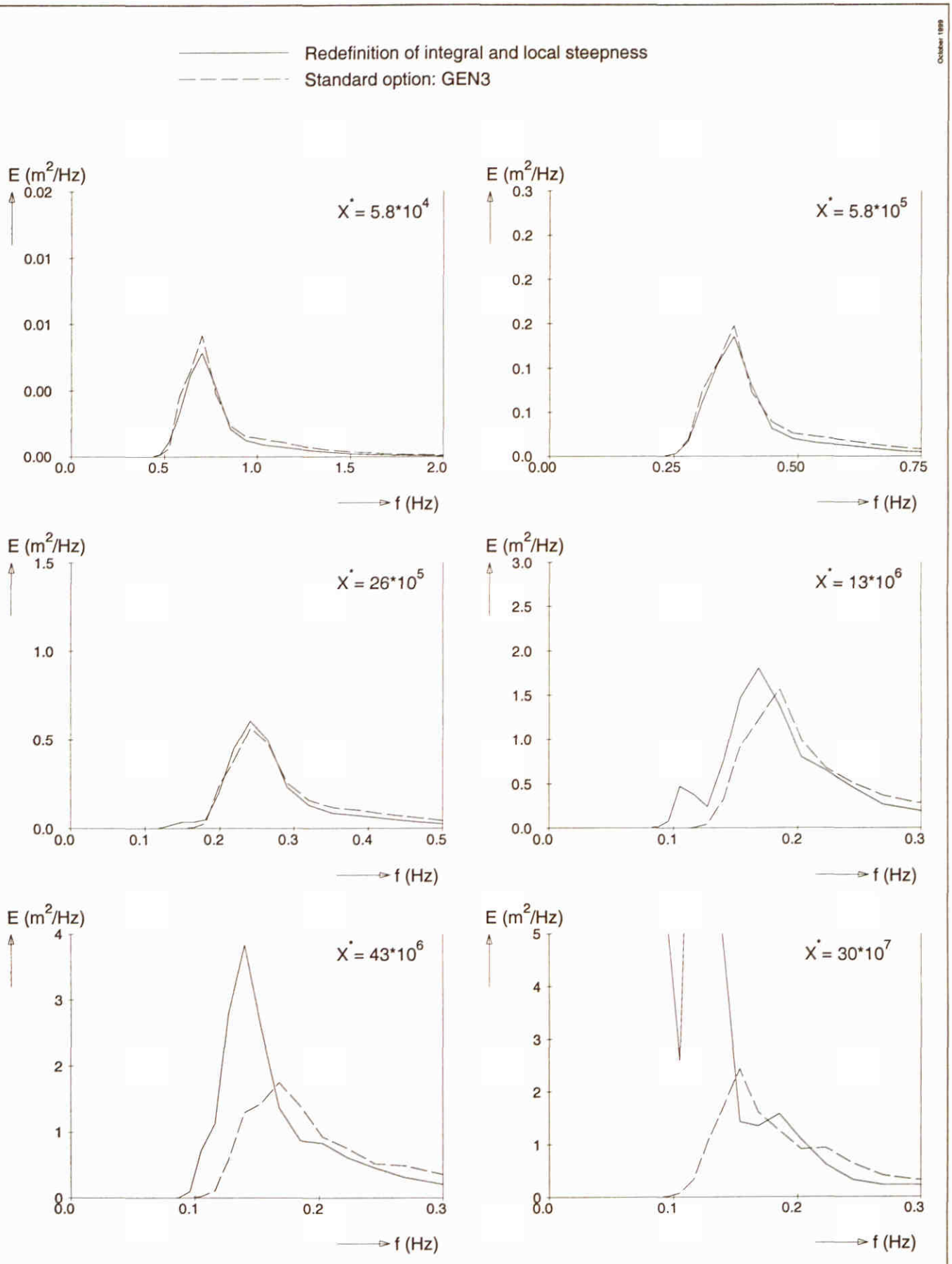


Frequency spectra at different locations ($U_{10}$ = 10 m/s)

SWAN 40.00

WL | delft hydraulics

H3529

Fig. 5.3.b

Redefinition of integral and local steepness
Standard option: GEN3

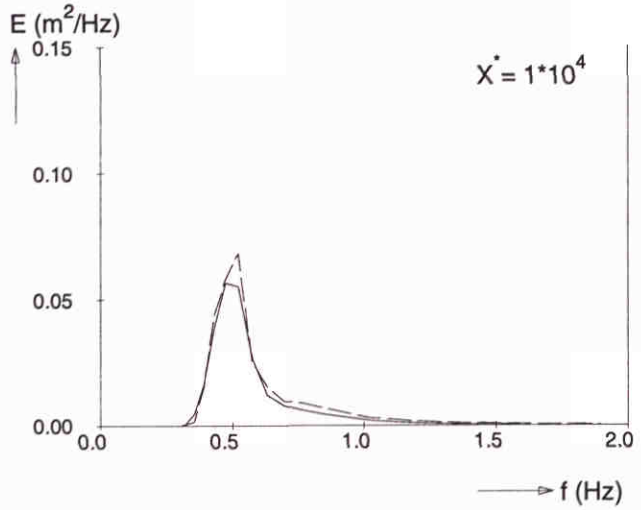


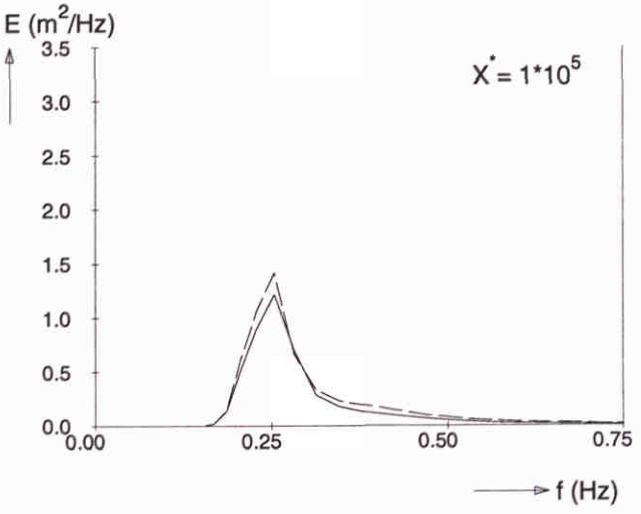


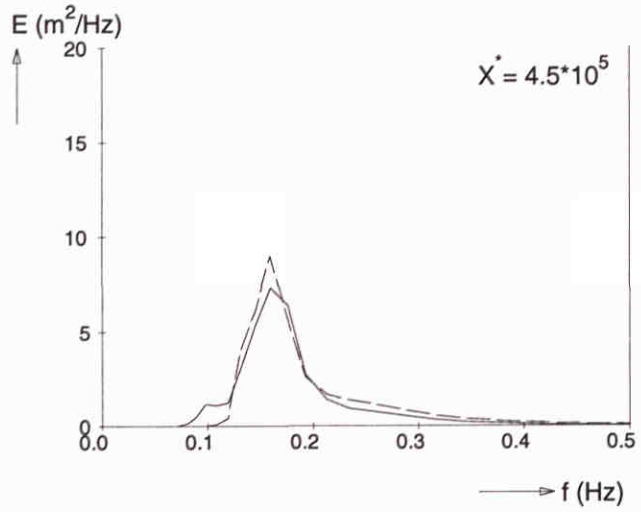


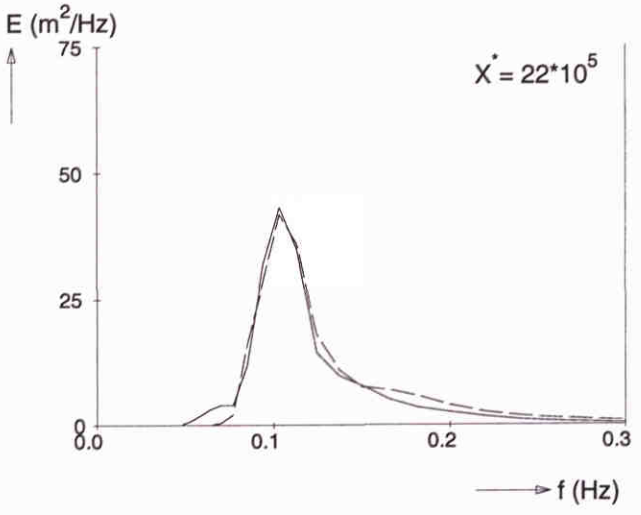


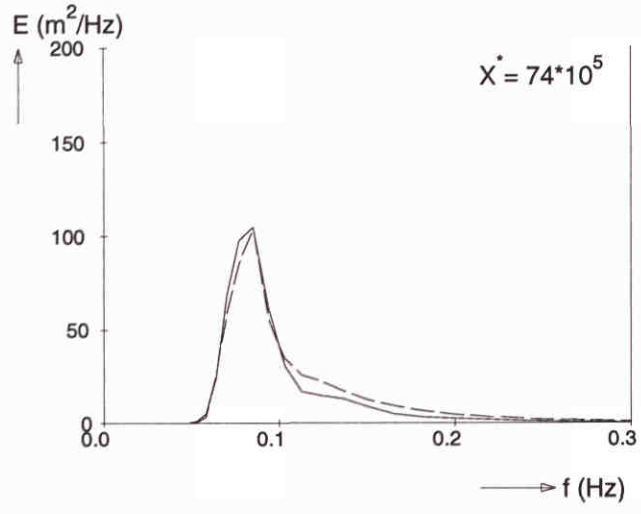


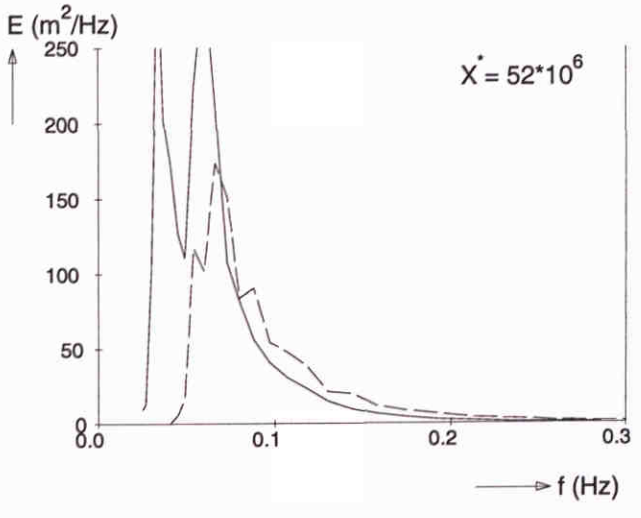


| | | |
|---|---|---|
| Frequency spectra at different locations ($U_{10}$ = 20 m/s) | SWAN 40.00 | |
| | | |
| WL \| delft hydraulics | H3529 | Fig. 5.3.c |

Redefinition of integral and local steepness
Standard option: GEN3

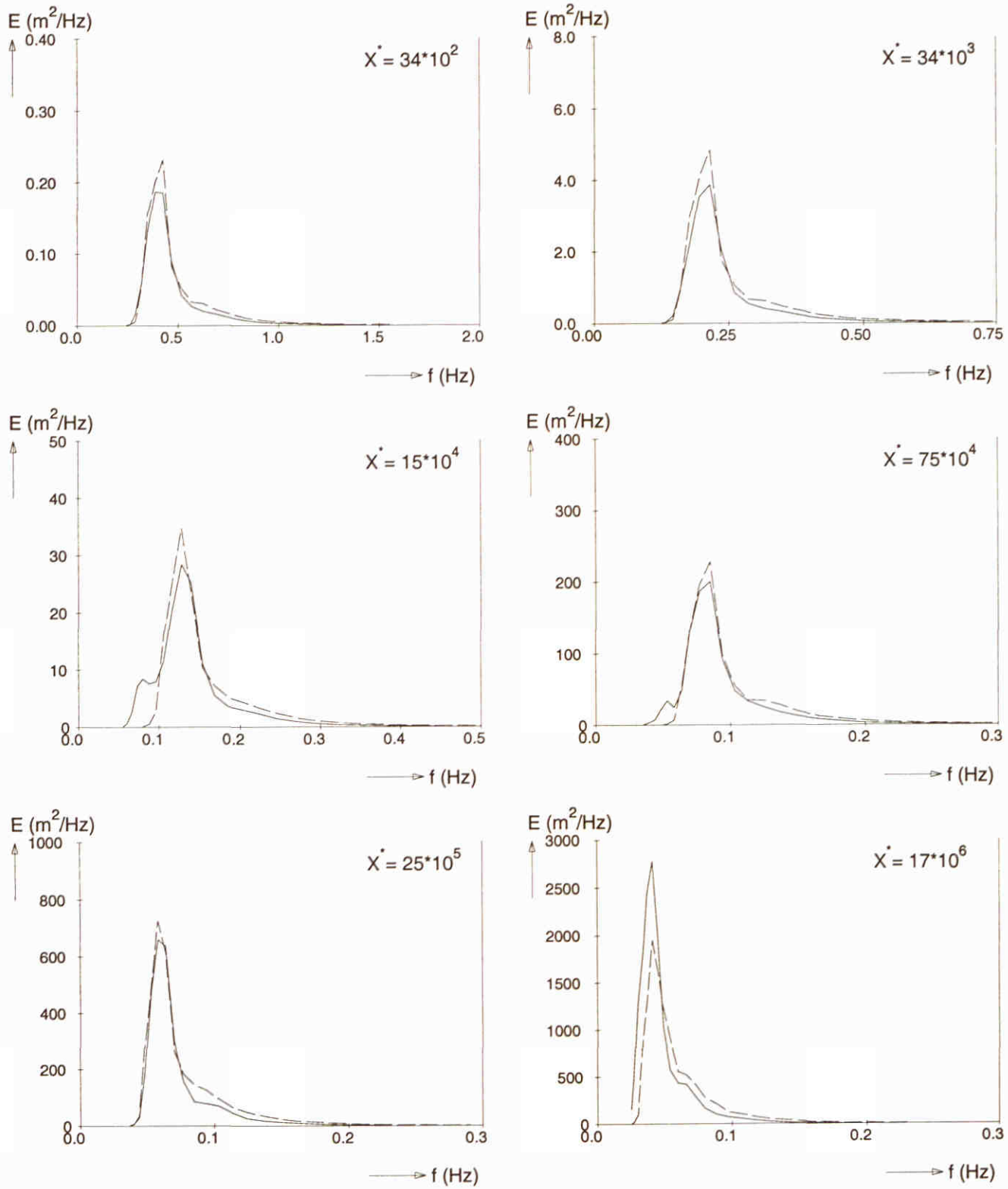


| | | |
|---|---|---|
| Frequency spectra at different locations ($U_{10}$ = 30 m/s) | SWAN 40.00 | |
| WL \| delft hydraulics | H3529 | Fig. 5.3.d |

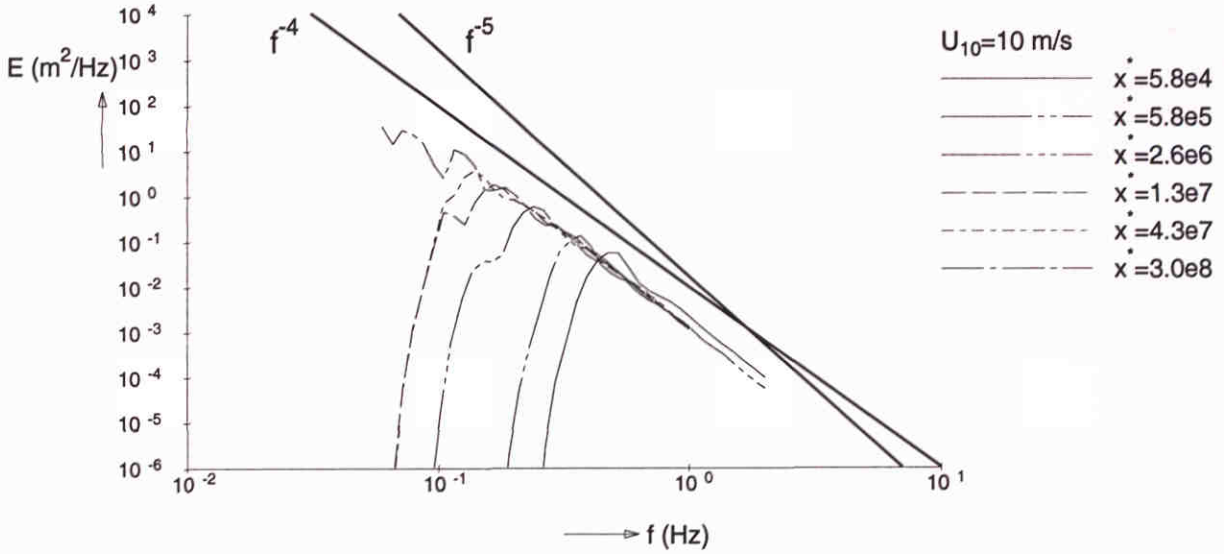


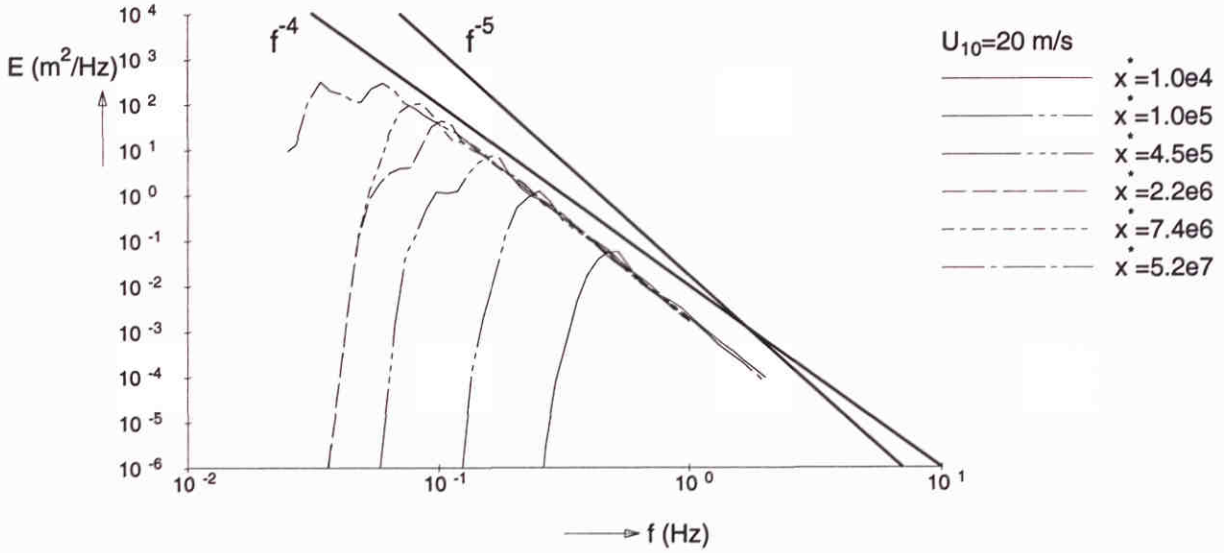


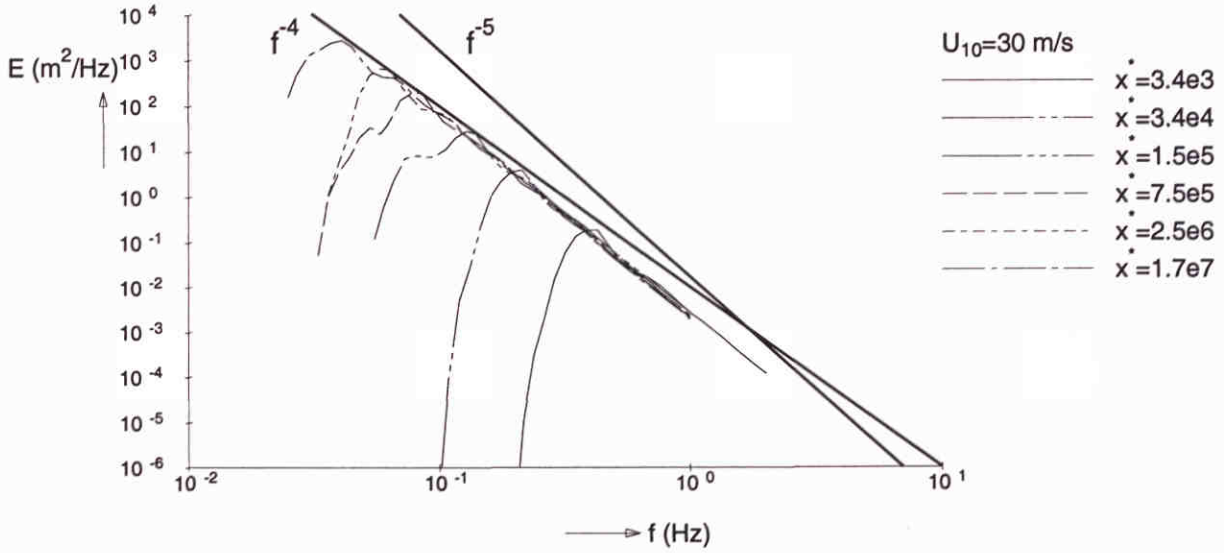


Wave spectra at different fetches

Redefinition of integral and local wave steepness

SWAN 40.00

WL | delft hydraulics

H3529

Fig. 5.3.e

Location: spc 2

2-D SPECTRUM E(f,θ)

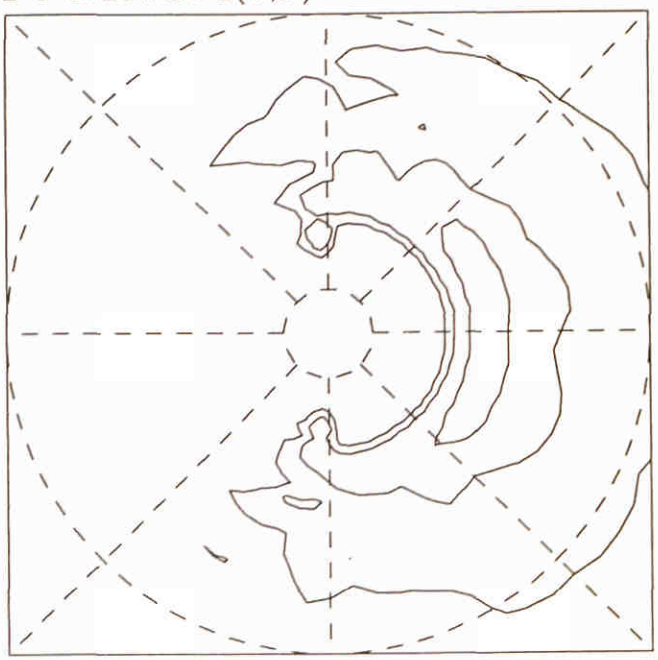

Contour levels :

0.500 $E_{max}$
0.100 $E_{max}$
0.020 $E_{max}$

Freq. scales :

0.070 Hz
0.500 Hz

Wind :

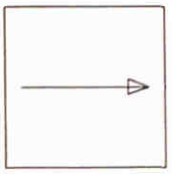

10.0 m/s

North :

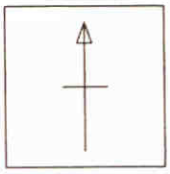

1-D SPECTRUM E(f)

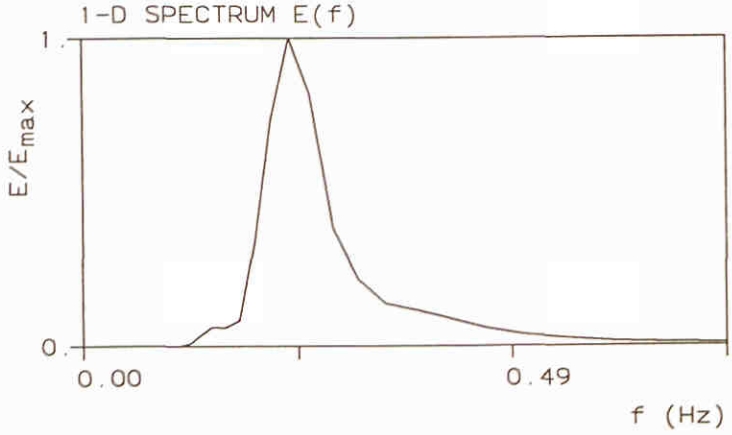


parameters :

$H_s$ = 1.02 m
$f_p$ = 0.241 Hz
$\bar{f}$ = 0.299 Hz
$\bar{\theta}$ = 358.8 °
$\bar{\sigma}_\theta$ = 46.2 °

wave growth 3

Redefinition of integral and local wave steepness
Two- and one-dimensional wave spectrum
Location: $X^{\cdot} = 26 * 10^5$

SWAN 40.00

WL | delft hydraulics

H3529

Fig. 5.4

Location: spc 1

2-D SPECTRUM E(f,θ)

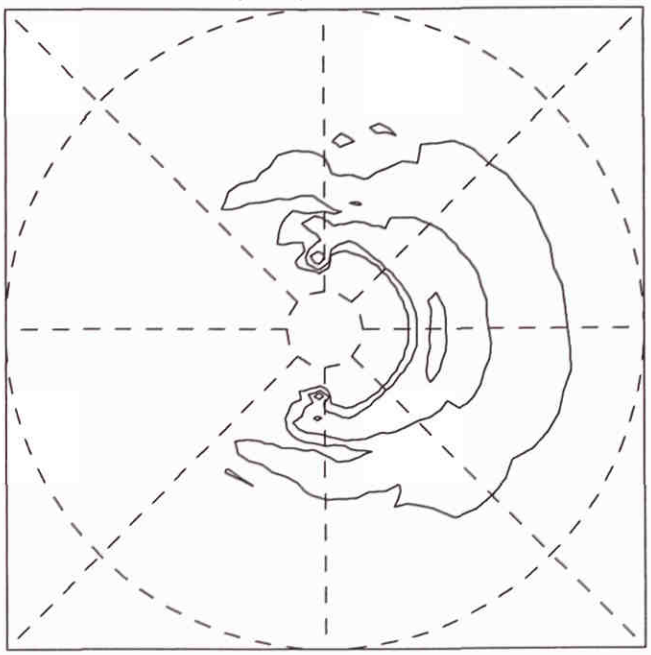

Contour levels :

0.500 $E_{max}$
0.100 $E_{max}$
0.020 $E_{max}$

Freq. scales :

0.060 Hz
0.500 Hz

Wind :

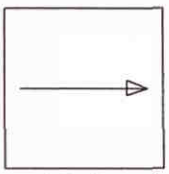

10.0 m/s

North :

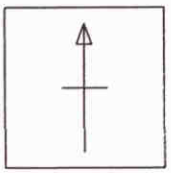

1-D SPECTRUM E(f)

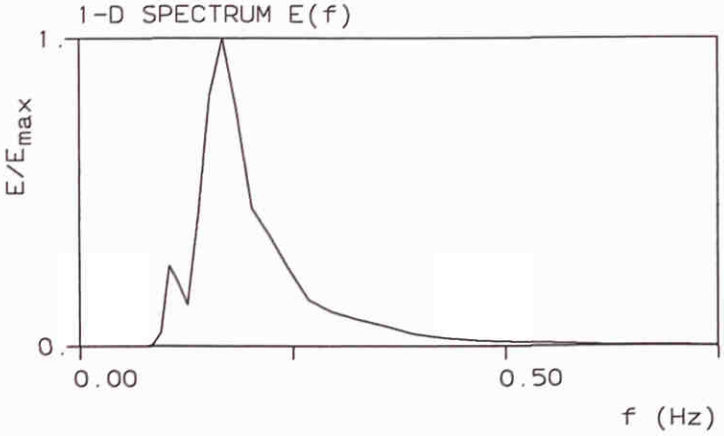


parameters :

$H_s$ = 1.63 m
$f_p$ = 0.168 Hz
$\overline{f}$ = 0.215 Hz
$\overline{\theta}$ = 359.6 °
$\overline{\sigma}_\theta$ = 51.3 °

wave growth 4

Redefinition of integral and local wave steepness
Two- and one-dimensional wave spectrum
Location: $X^{\bullet} = 13 * 10^6$

SWAN 40.00

WL | delft hydraulics

H3529

Fig. 5.5

Location: spc 2

2-D SPECTRUM E(f,θ)

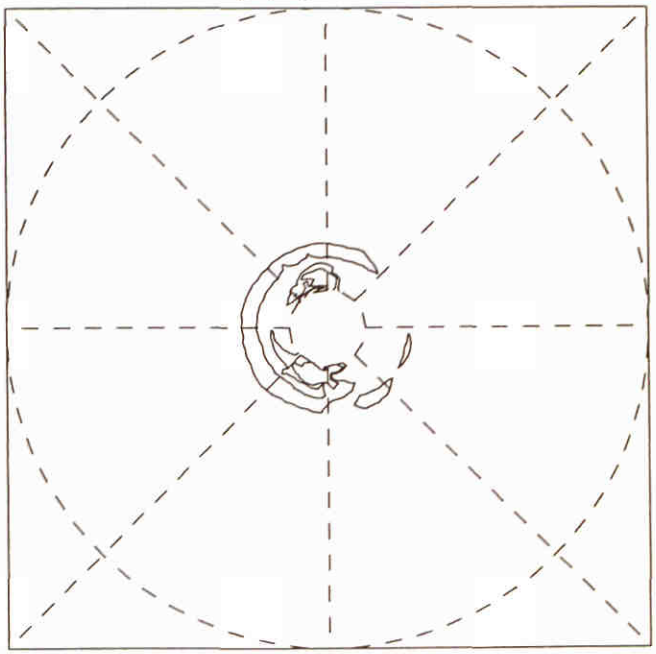

Contour levels :

0.500 $E_{max}$
0.100 $E_{max}$
0.020 $E_{max}$

Freq. scales :

0.060 Hz
0.500 Hz

Wind :

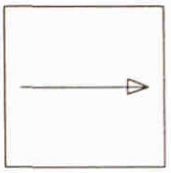

10.0 m/s

North :

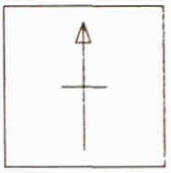

1-D SPECTRUM E(f)

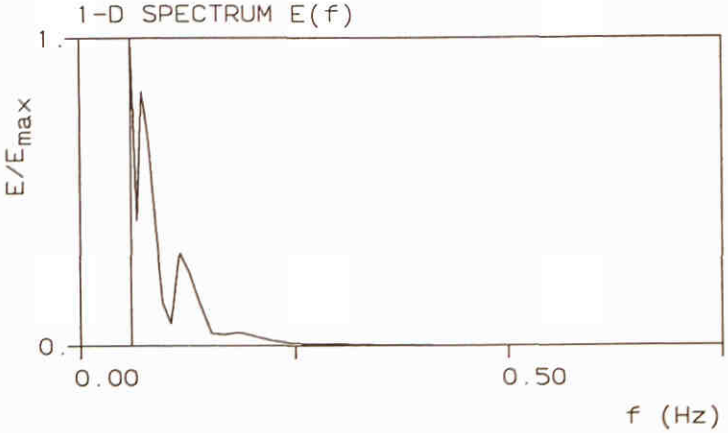


parameters :

$H_s$ = 4.37 m
$f_p$ = 0.060 Hz
$\overline{f}$ = 0.102 Hz
$\overline{\theta}$ = 209.4 °
$\overline{\sigma}_\theta$ = 73.6 °

wave growth 5

Redefinition of integral and local wave steepness
Two- and one-dimensional wave spectrum
Location: $X^{\bullet} = 30 * 10^7$

SWAN 40.00

WL | delft hydraulics

H3529

Fig. 5.6

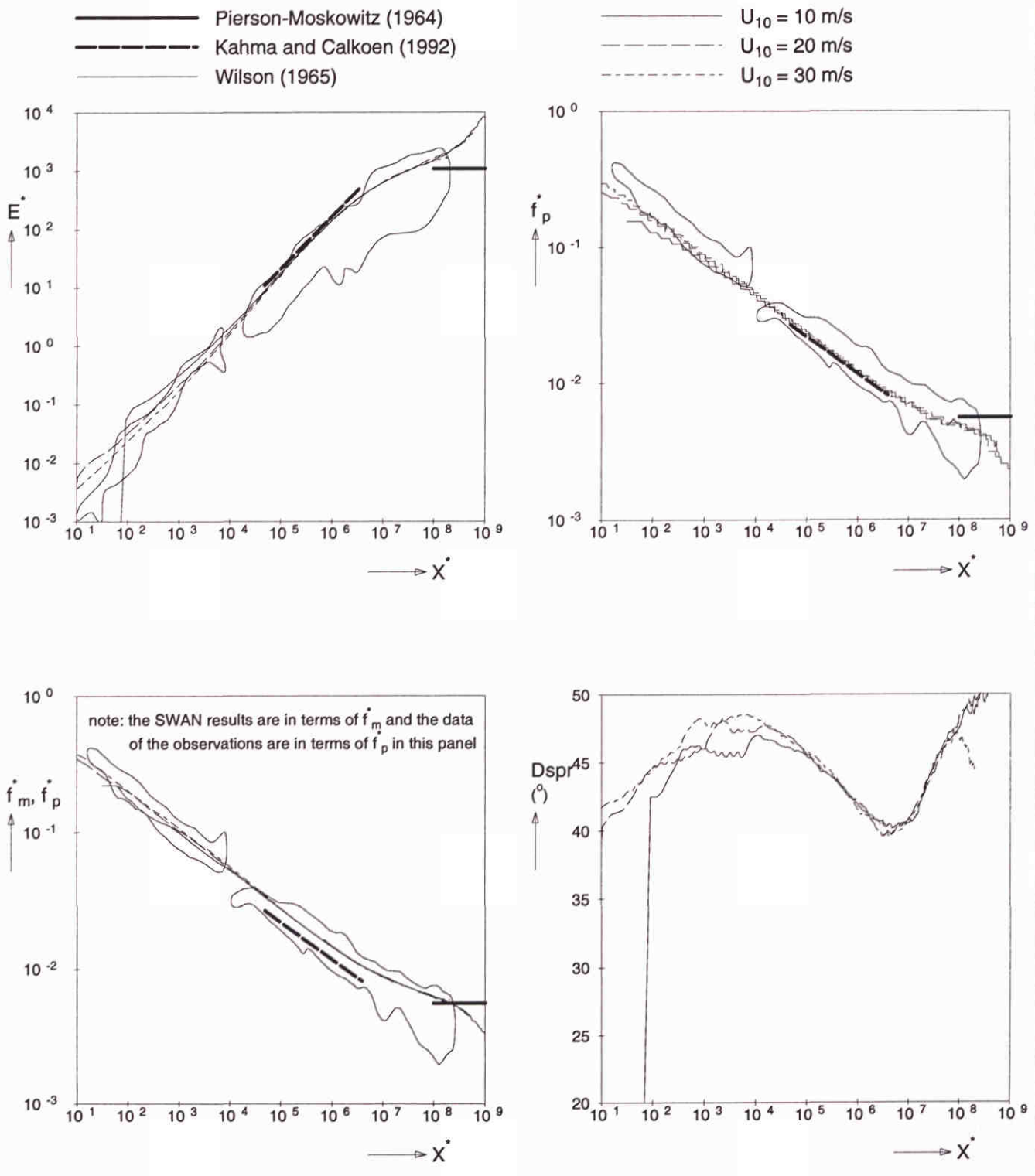


Fetch limited wave growth (deep water)
Third-generation formulations. Redefinition
of integral and local wave steepness: SECTOR (-80°, +80°)

SWAN 40.00

WL | delft hydraulics

H3529

Fig. 5.7.a

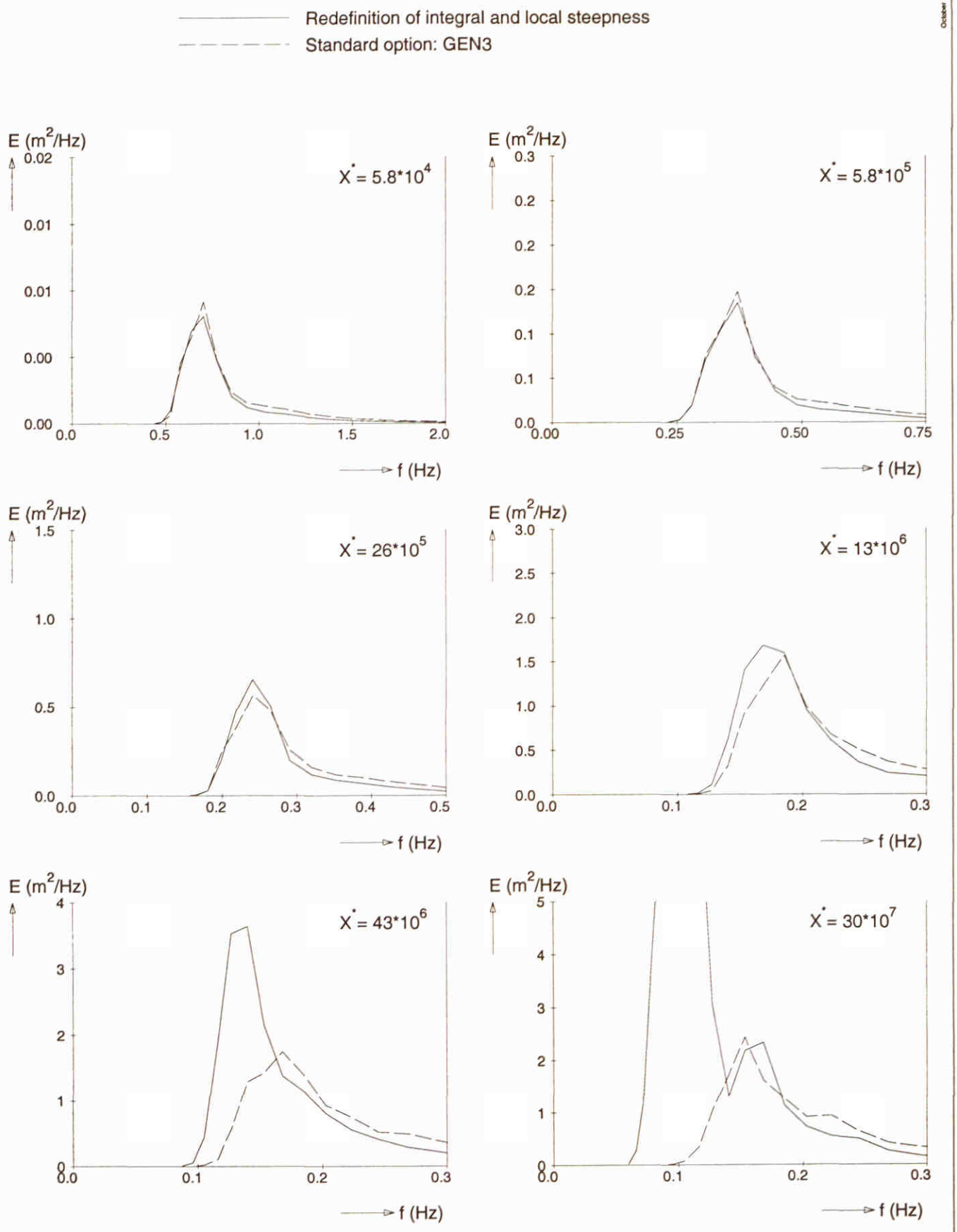


Frequency spectra at different locations ($U_{10}$ = 10 m/s)
SECTOR (-80°, +80°)

SWAN 40.00

WL | delft hydraulics

H3529

Fig. 5.7.b

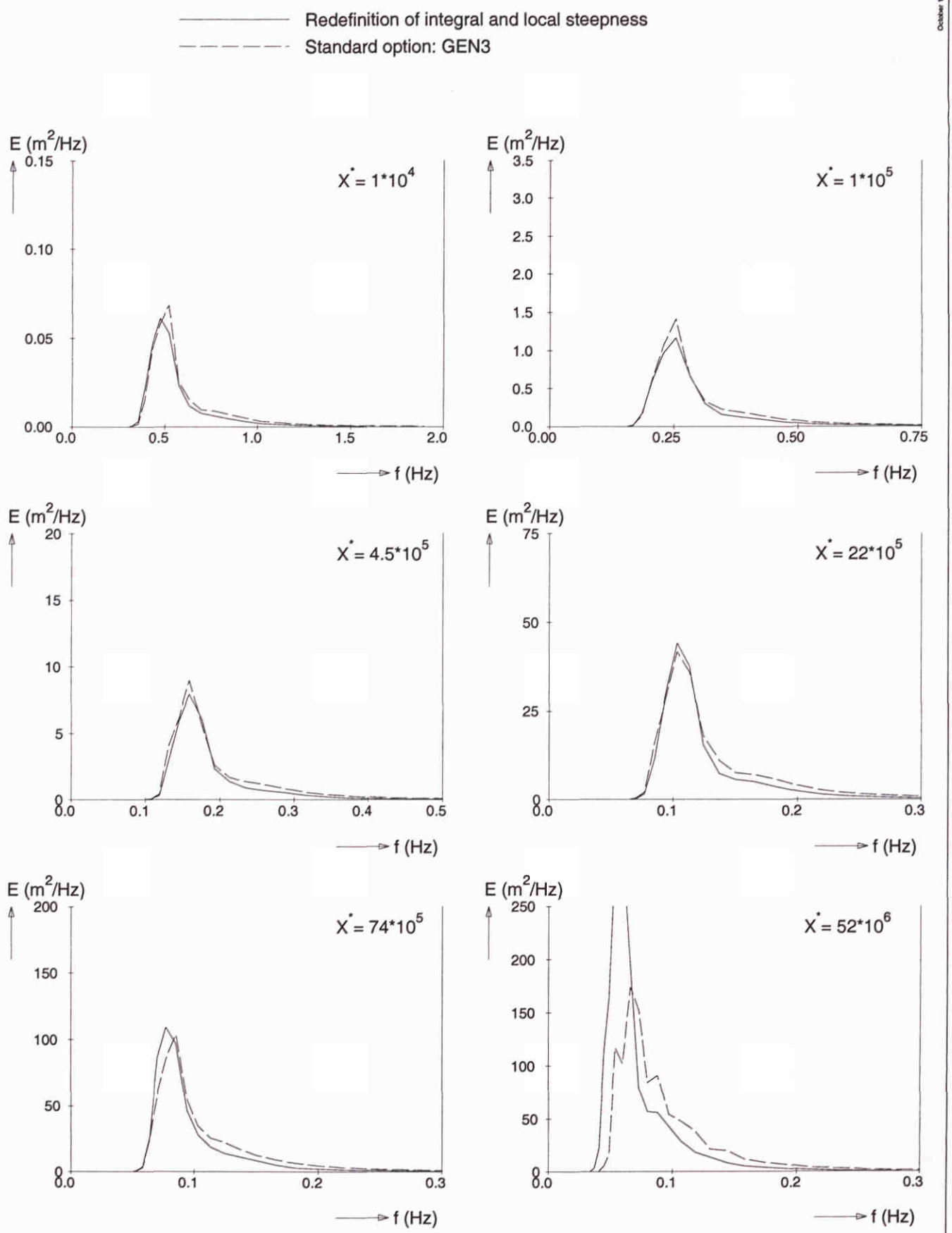


| | | |
|---|---|---|
| Frequency spectra at different locations ($U_{10}$ = 20 m/s)<br>SECTOR (-80°, +80°) | SWAN 40.00 | |
| WL \| delft hydraulics | H3529 | Fig. 5.7.c |

Redefinition of integral and local steepness
Standard option: GEN3

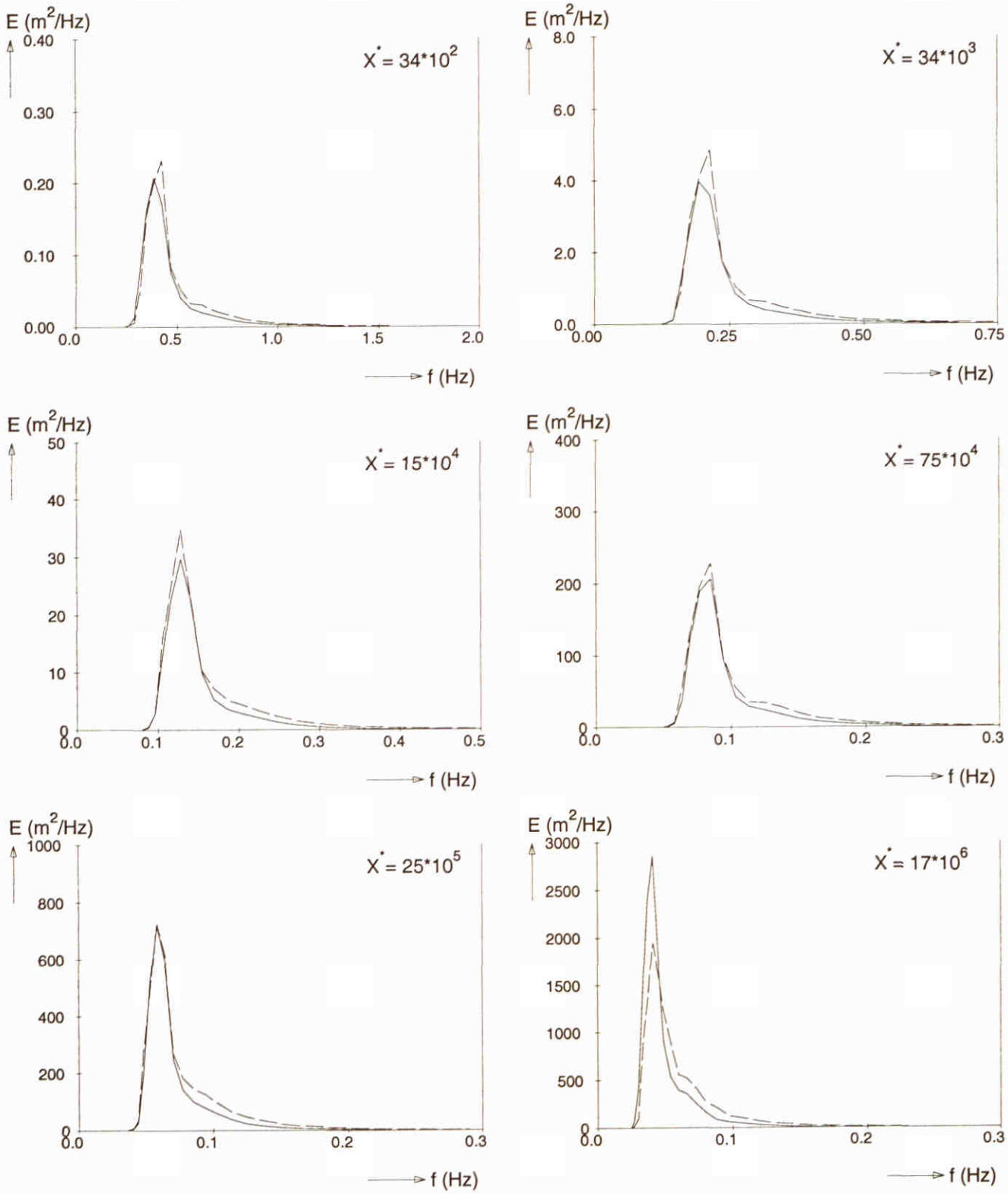


Frequency spectra at different locations ($U_{10}$ = 30 m/s)
SECTOR (-80°, +80°)

SWAN 40.00

WL | delft hydraulics

H3529

Fig. 5.7.d

October 1999

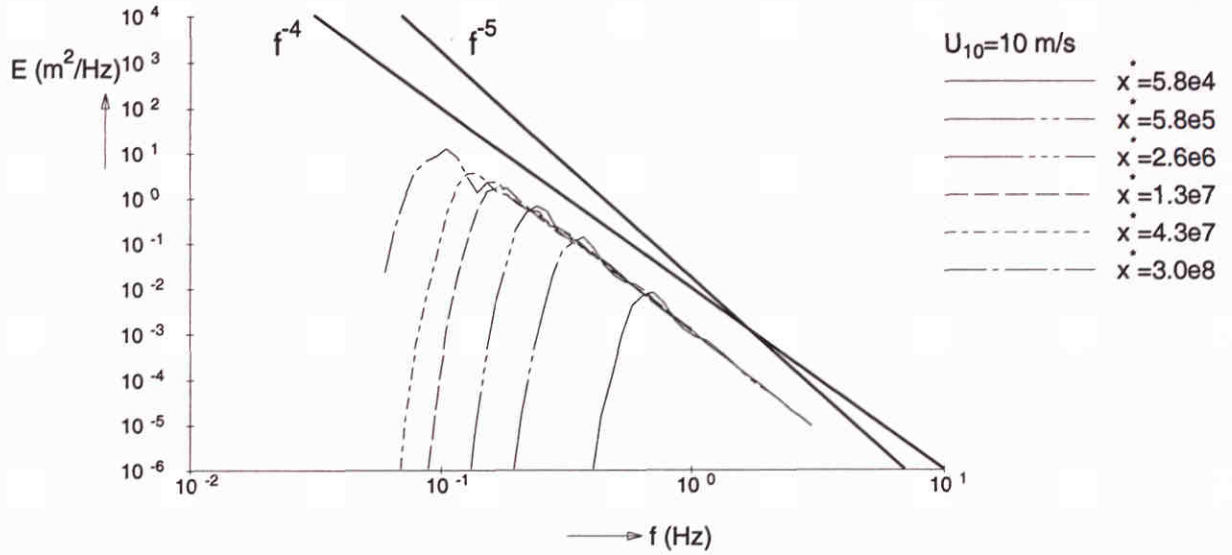


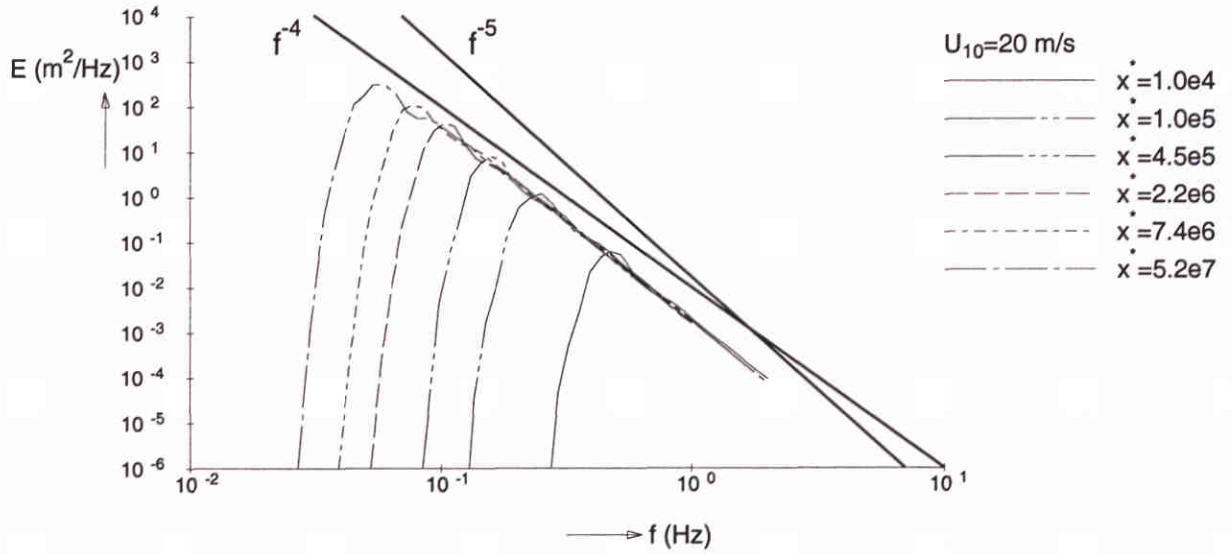


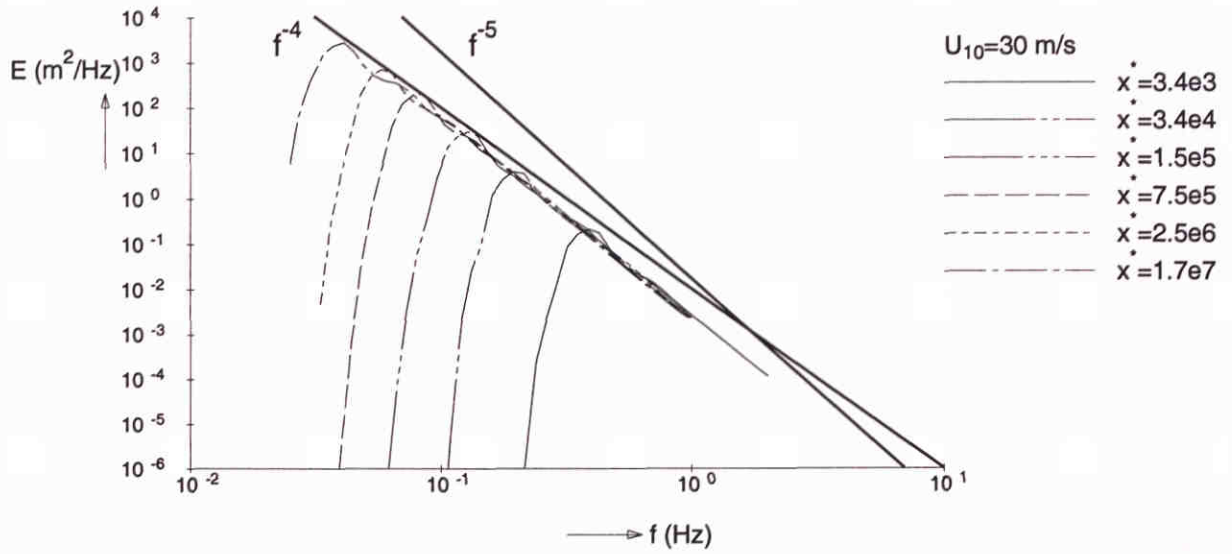


Wave spectra at different fetches

Redefinition of integral and local wave steepness

SWAN 40.00

WL | delft hydraulics

H3529

Fig. 5.7.e

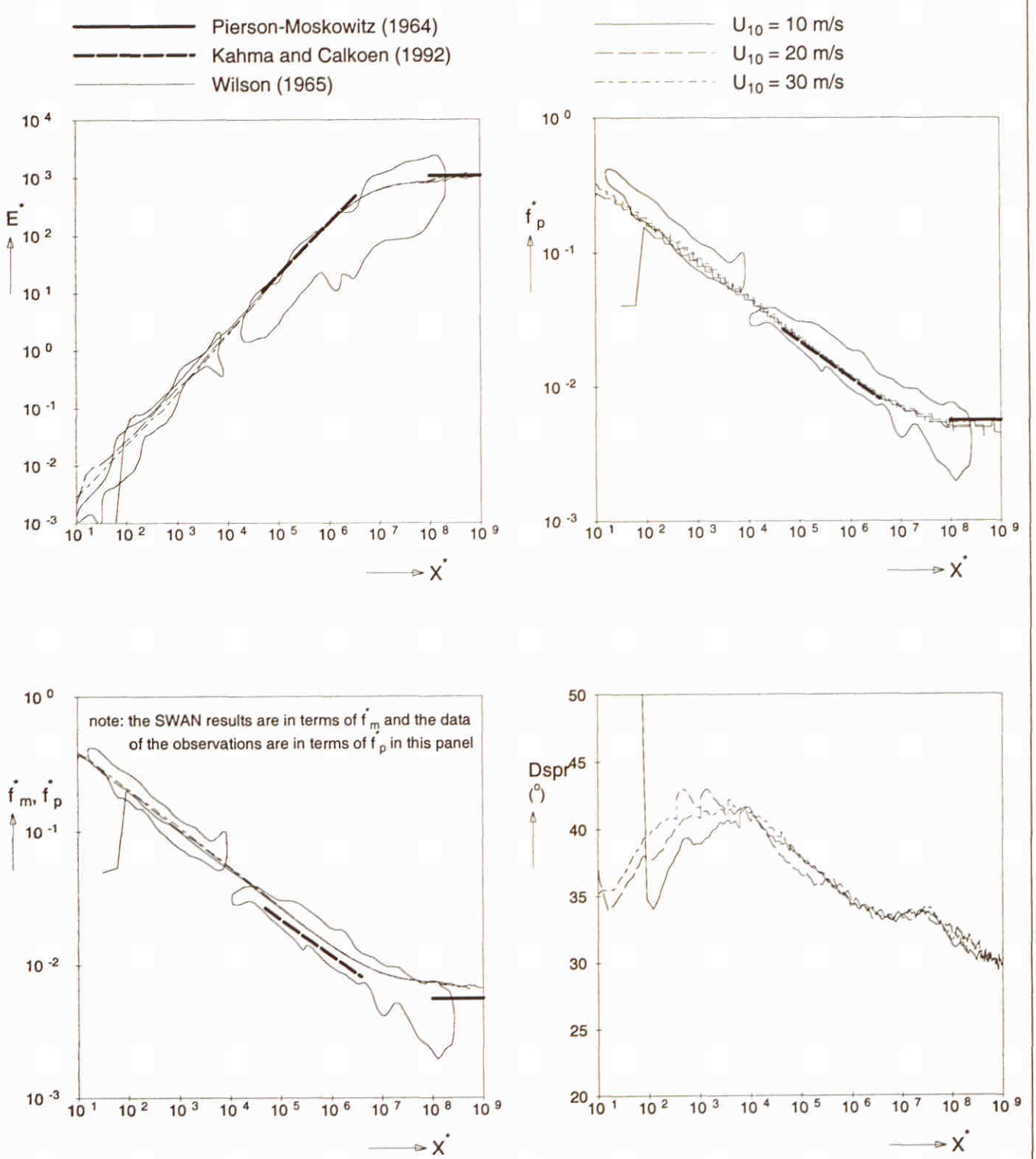


| | | |
|---|---|---|
| Fetch limited wave growth (deep water)<br>Third-generation formulations<br>Extended Komen et al. (1984) expression with $\beta^0$ | SWAN 40.00 | |
| WL \| delft hydraulics | H3529 | Fig. 5.8.a |

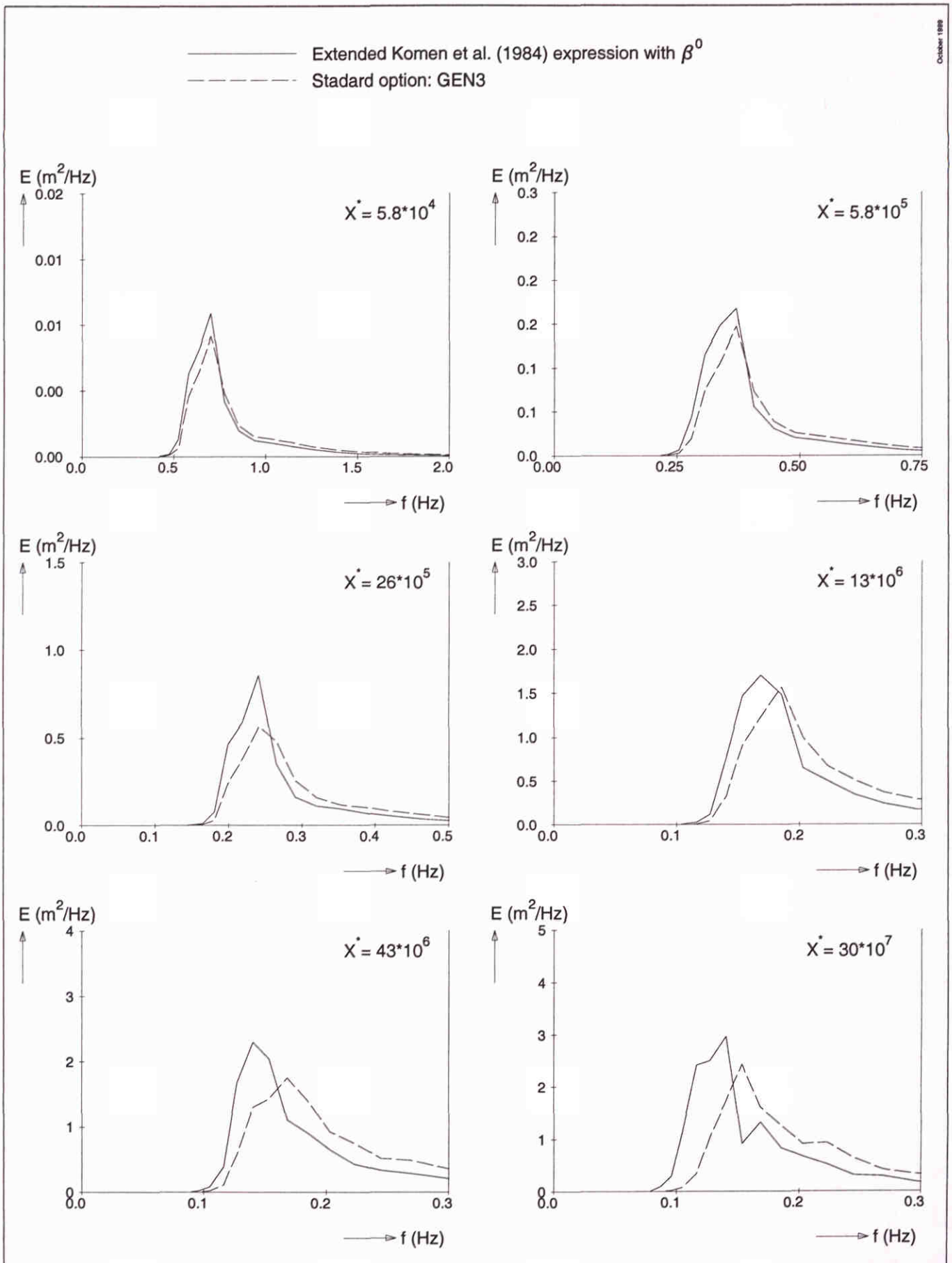


| | | |
|---|---|---|
| Frequency spectra at different locations ($U_{10}$ = 10 m/s) | SWAN 40.00 | |
| | | |
| WL \| delft hydraulics | H3529 | Fig. 5.8.b |

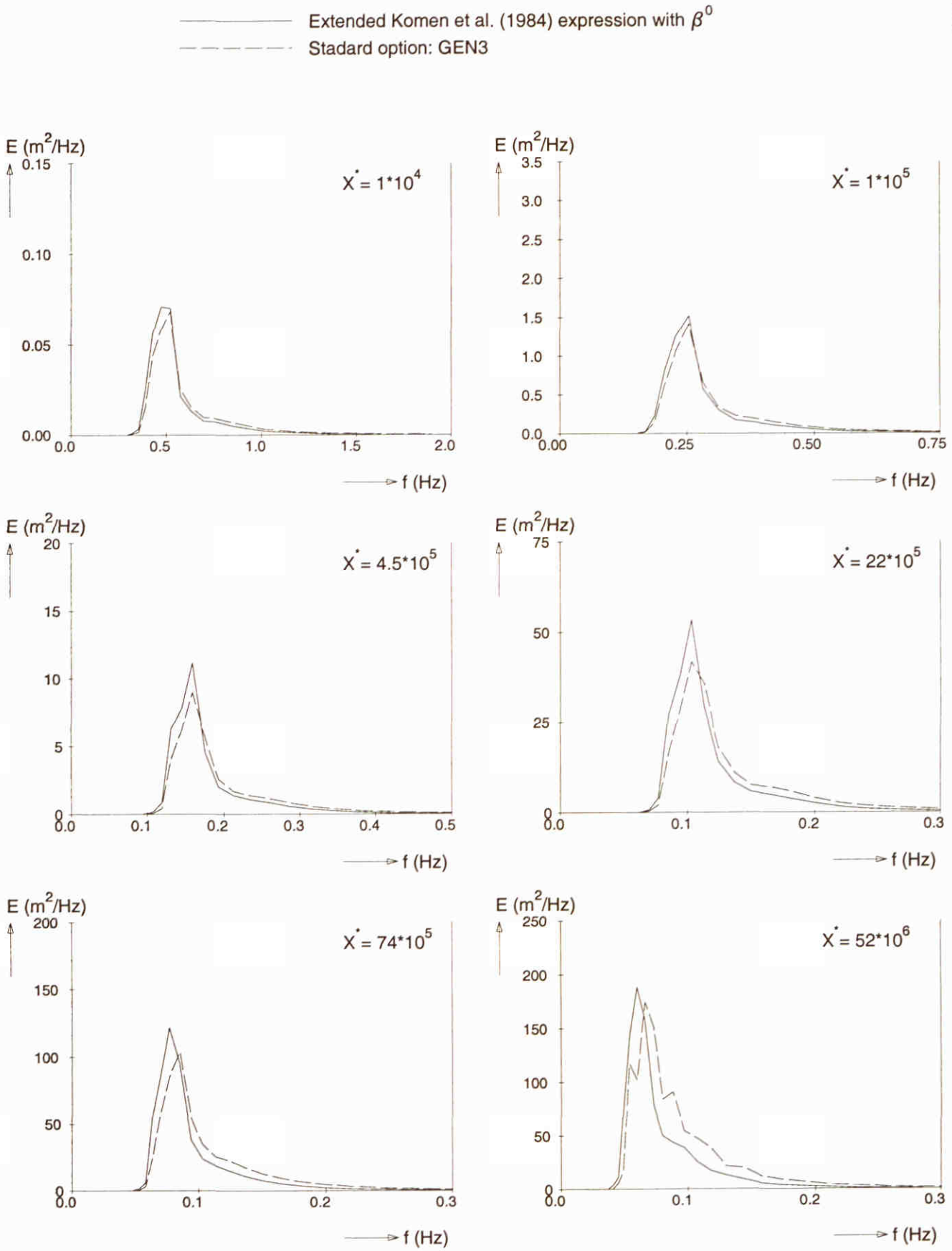


Frequency spectra at different locations ($U_{10}$ = 20 m/s)

SWAN 40.00

WL | delft hydraulics

H3529

Fig. 5.8.c

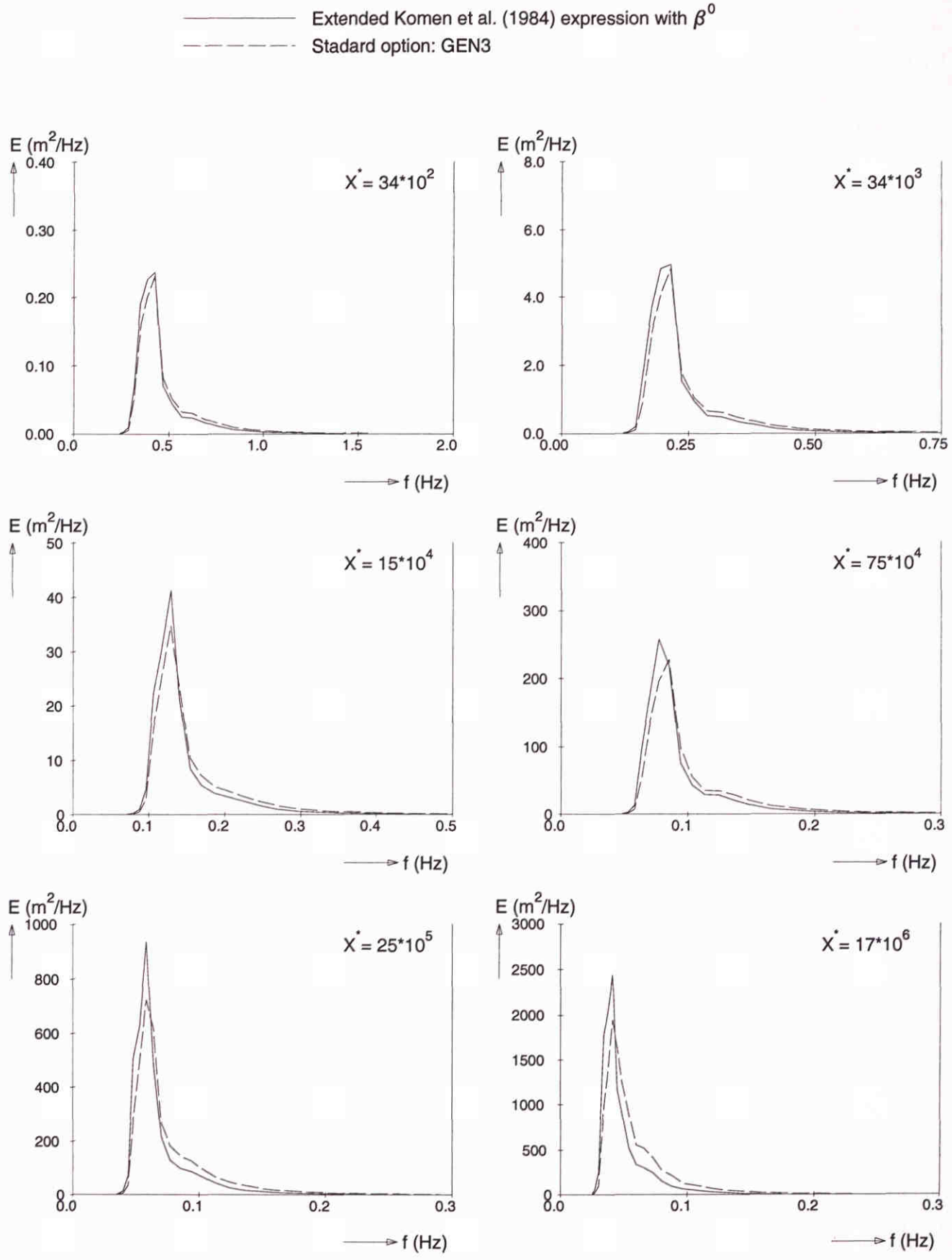


Frequency spectra at different locations ($U_{10}$ = 30 m/s)

SWAN 40.00

WL | delft hydraulics

H3529

Fig. 5.8.d

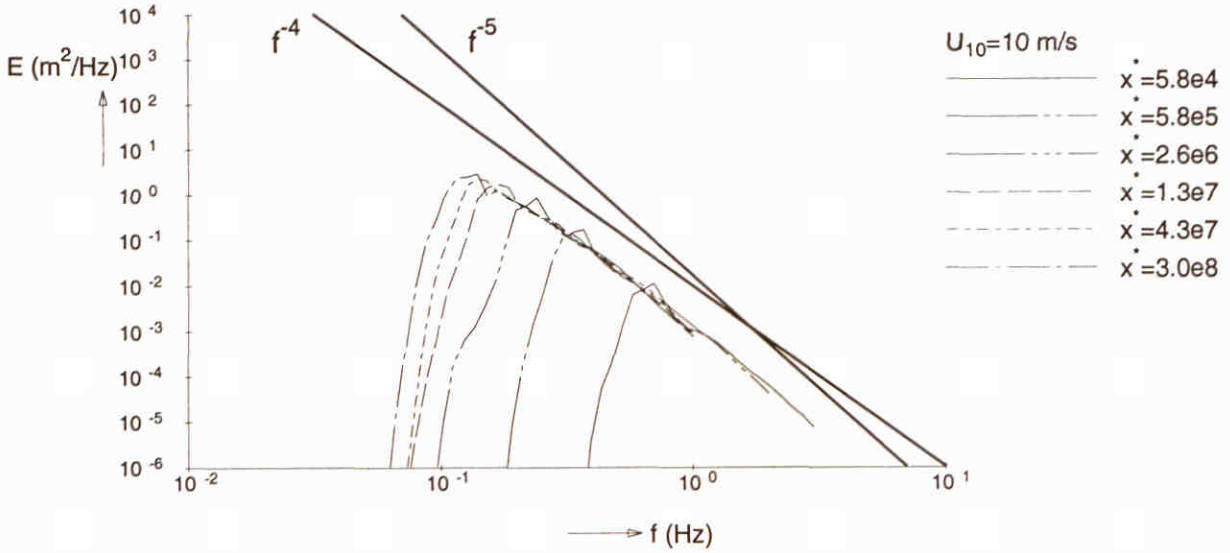


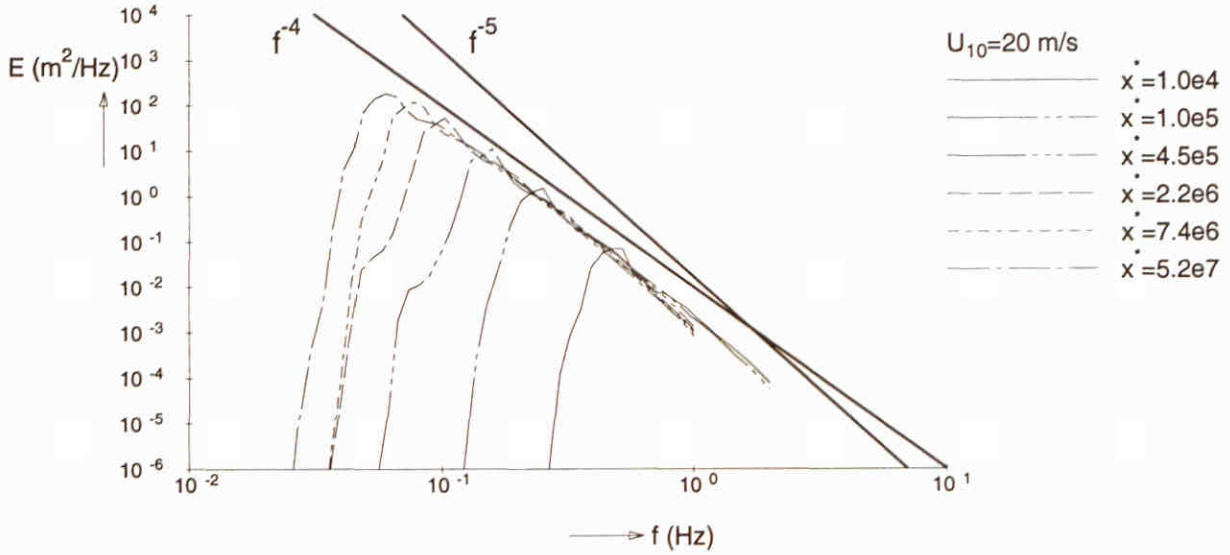


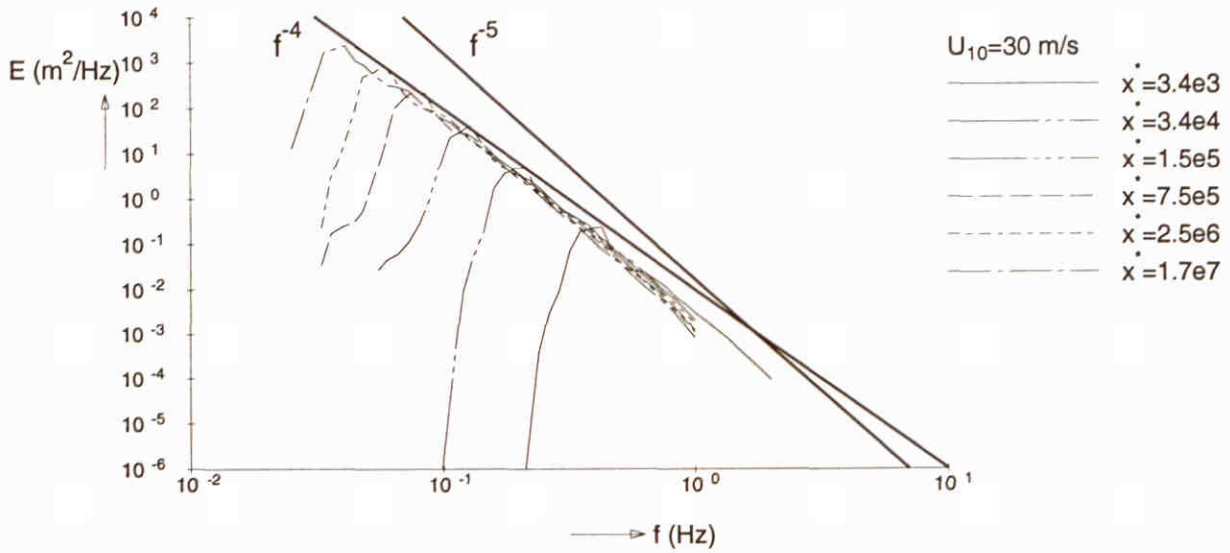


| | | |
|---|---|---|
| Wave spectra at different fetches<br>Extended Komen et al. (1984) expression with $\beta^0$ | SWAN 40.00 | |
| WL \| delft hydraulics | H3529 | Fig. 5.8.e |

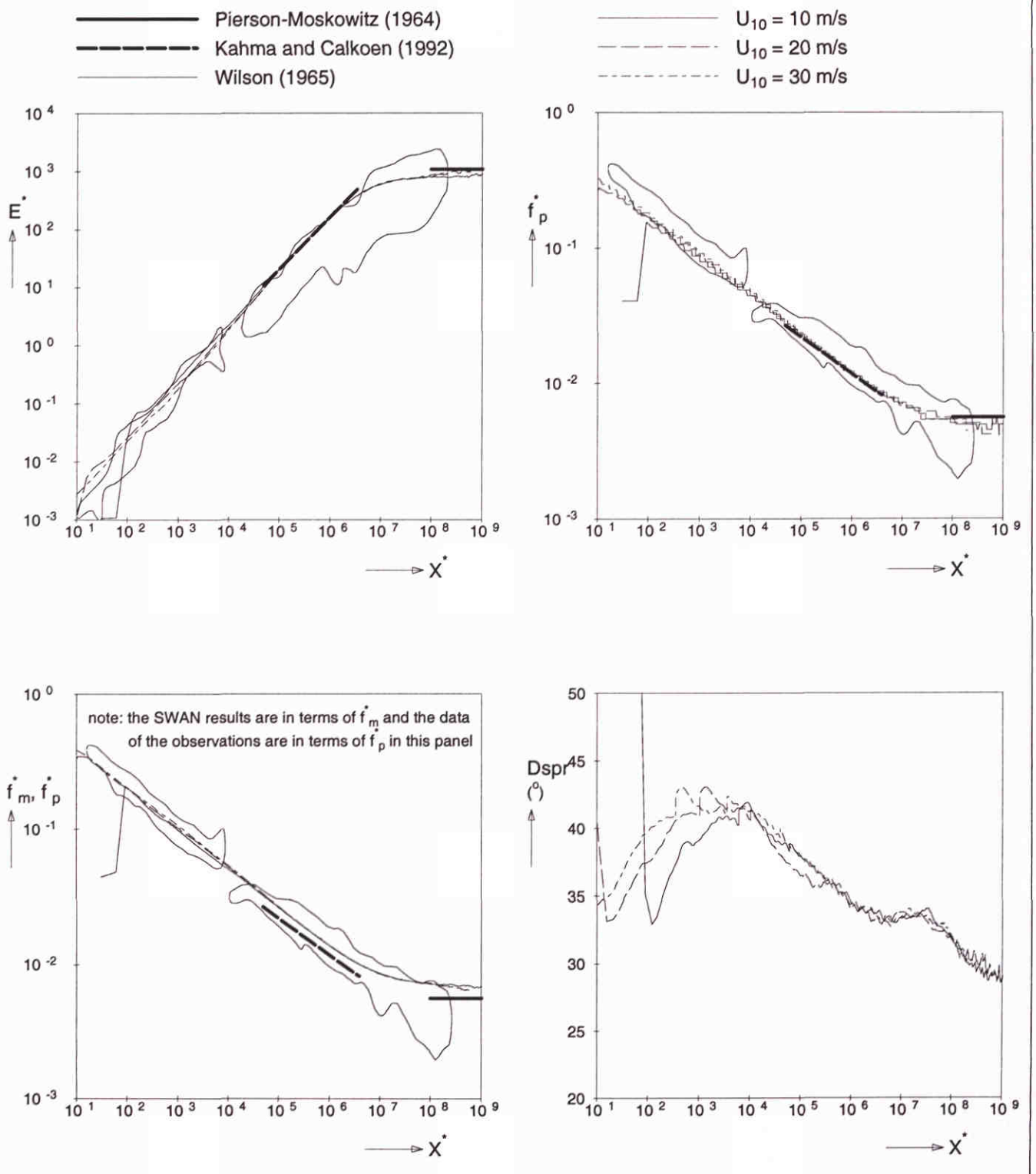


| | | |
|---|---|---|
| Fetch limited wave growth (deep water)<br>Third-generation formulations<br>Extended Komen et al. (1984) expression with $\beta^{0.5}$ | SWAN 40.00 | |
| WL \| delft hydraulics | H3529 | Fig. 5.9.a |

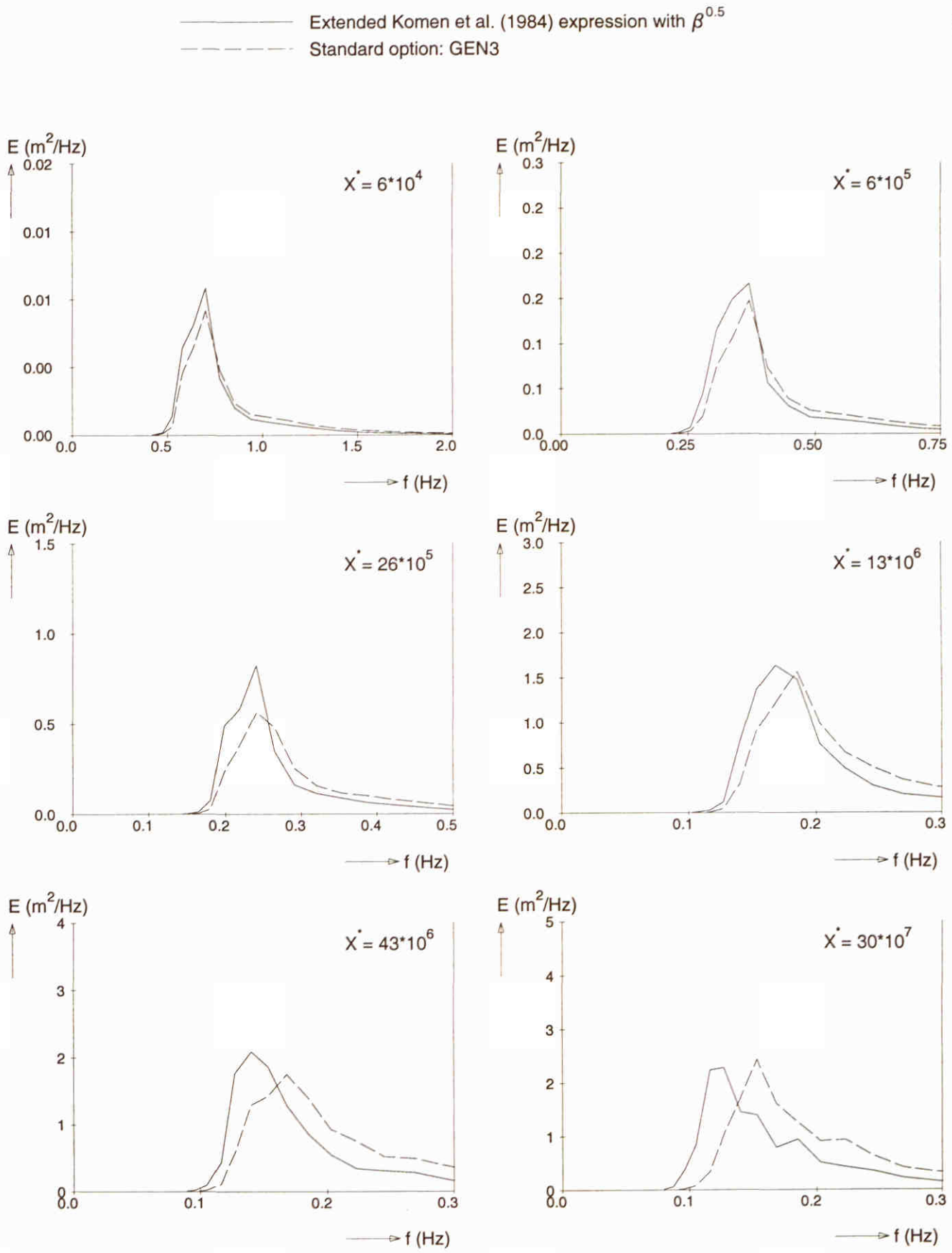


Frequency spectra at different locations ($U_{10}$ = 10 m/s)

SWAN 40.00

WL | delft hydraulics

H3529

Fig. 5.9.b

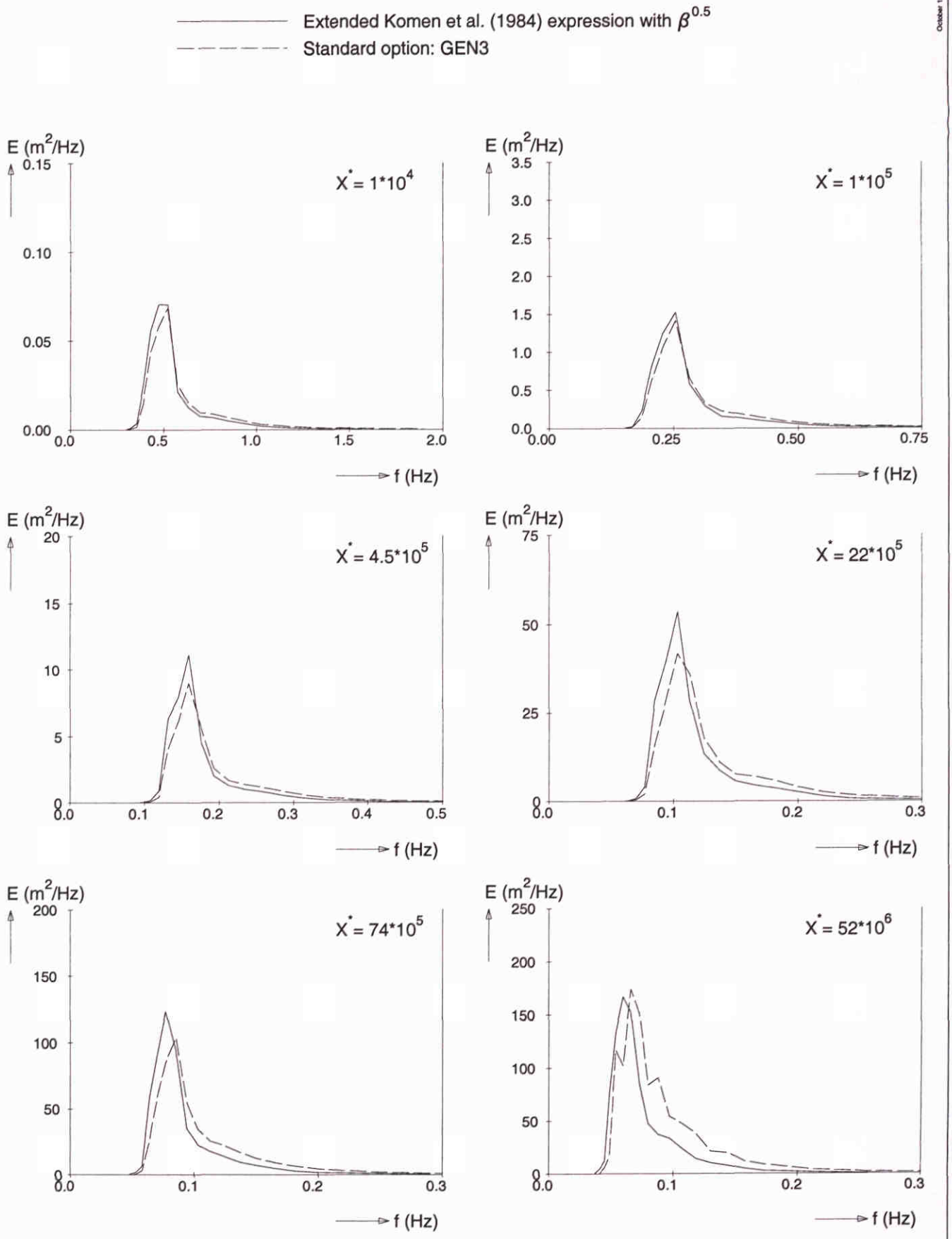


Frequency spectra at different locations ($U_{10}$ = 20 m/s)

SWAN 40.00

WL | delft hydraulics

H3529

Fig. 5.9.c

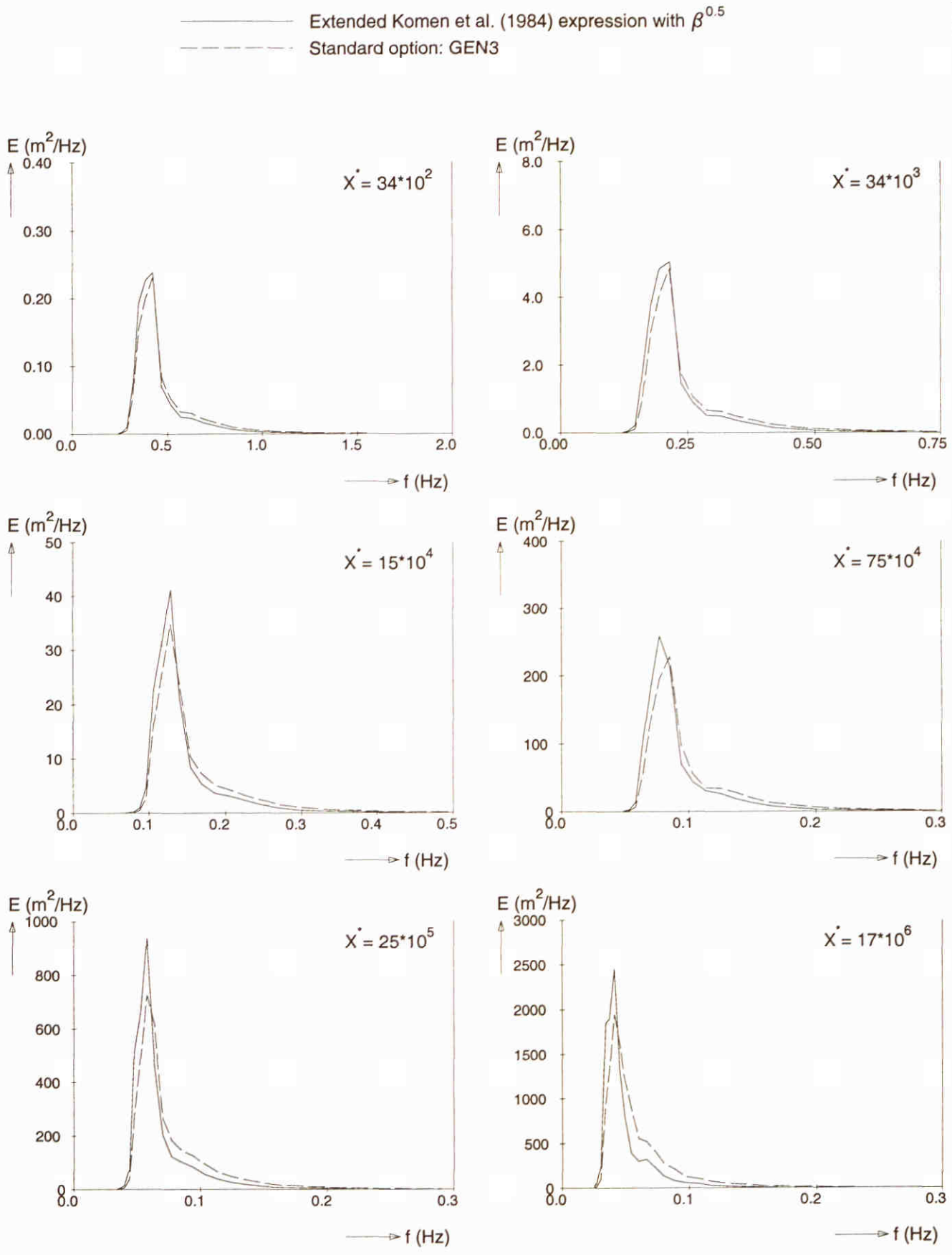


Frequency spectra at different locations ($U_{10}$ = 30 m/s)

SWAN 40.00

WL | delft hydraulics

H3529

Fig. 5.9.d

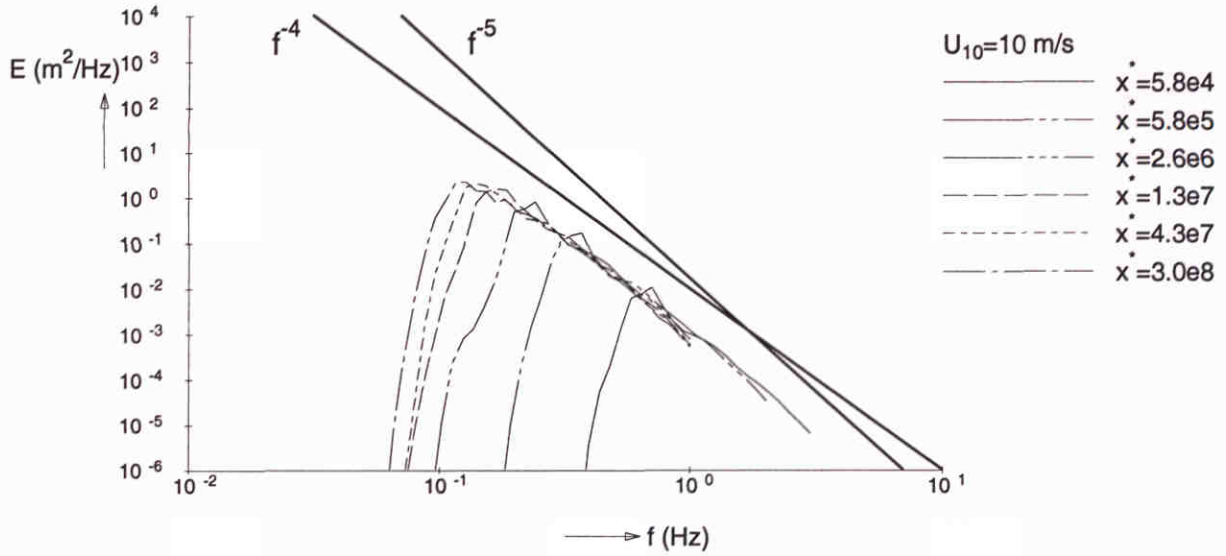


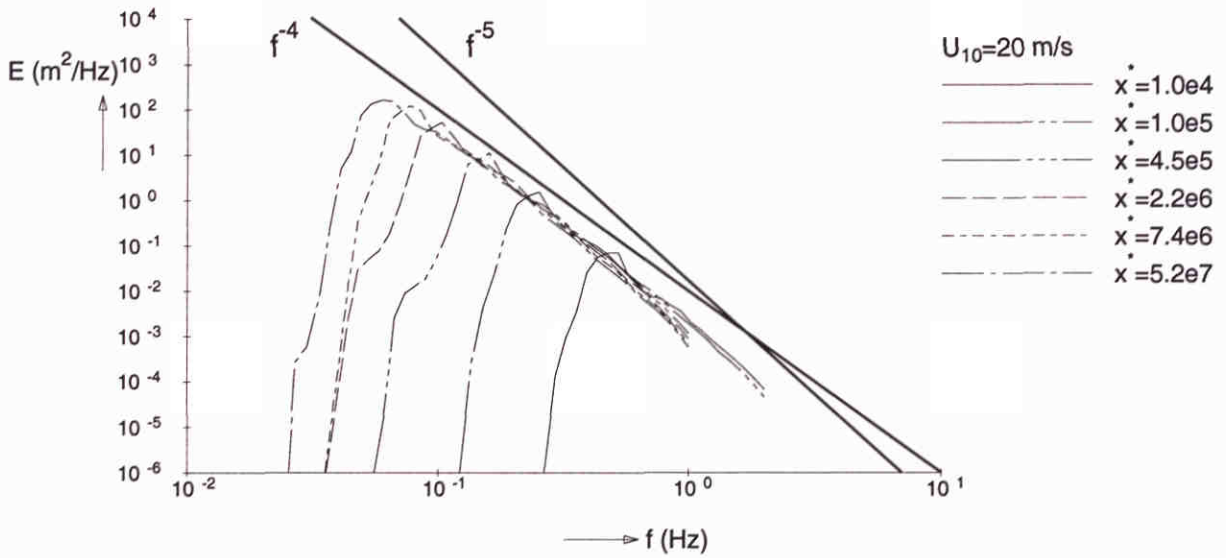


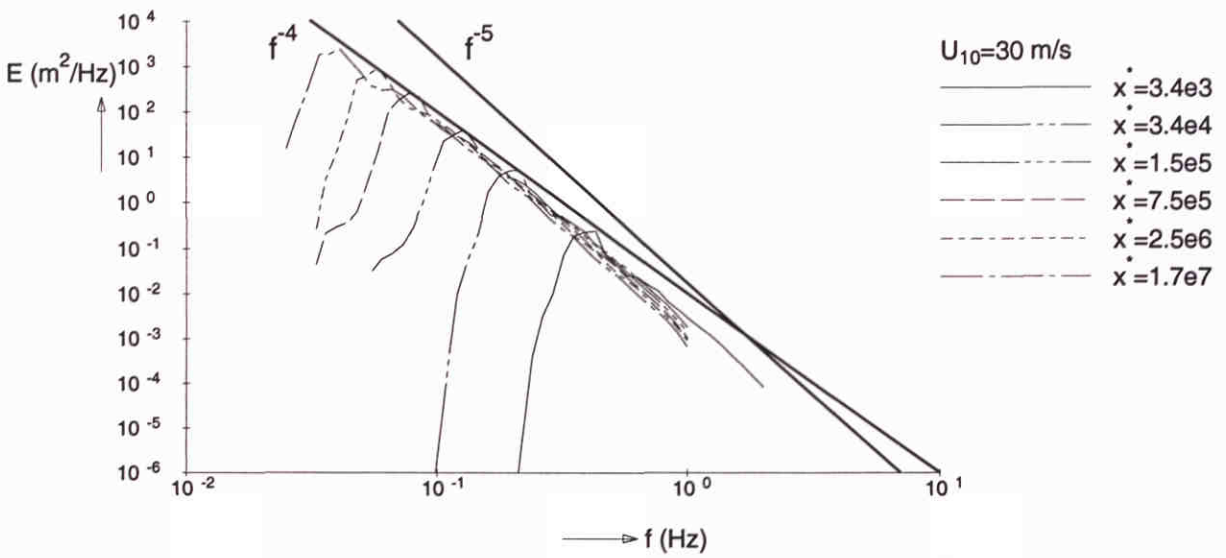


Wave spectra at different fetches

Extended Komen et al. (1984) expression with $\beta^{0.5}$

SWAN 40.00

WL | delft hydraulics

H3529

Fig. 5.9.e

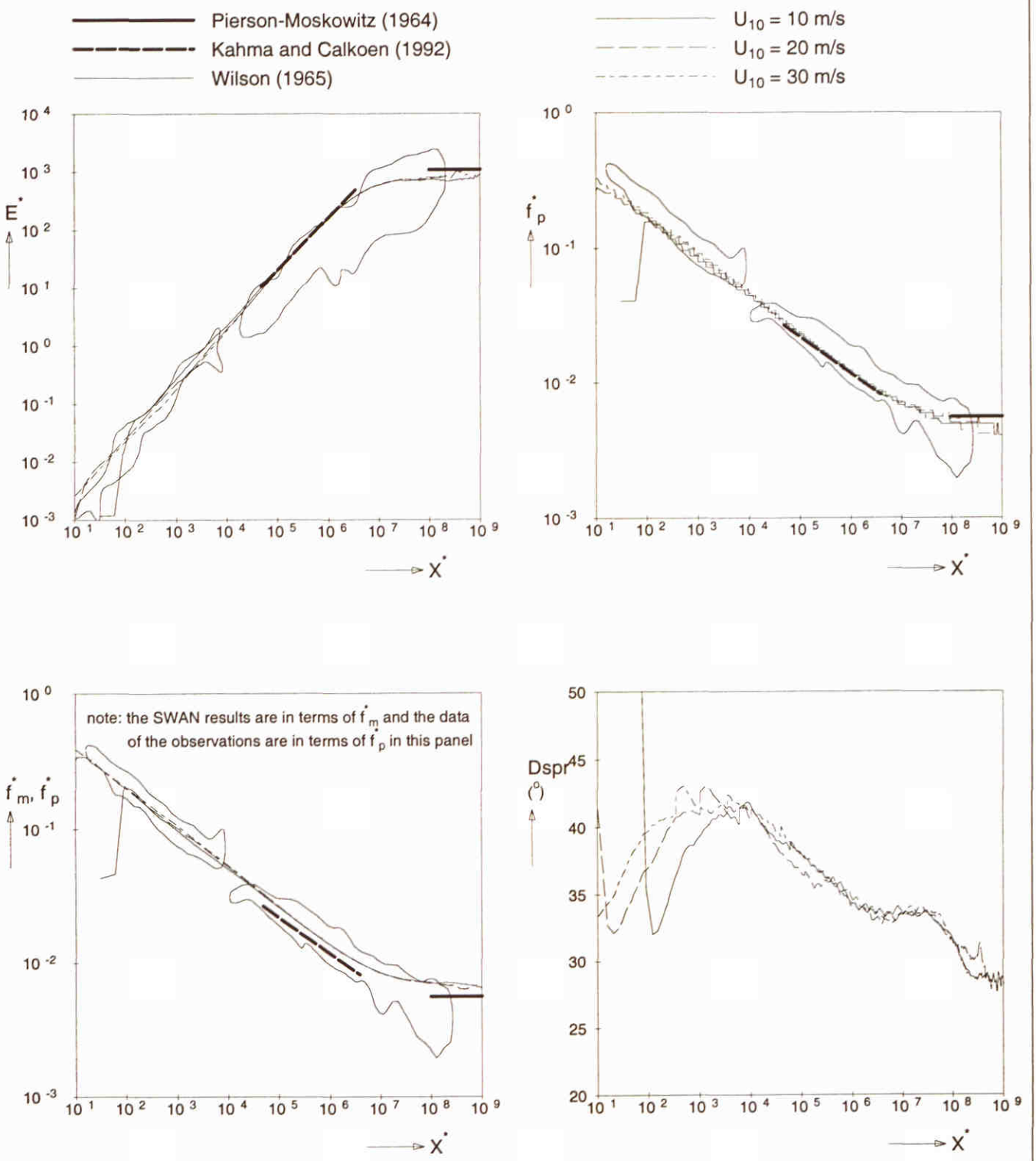


Fetch limited wave growth (deep water)
Third-generation formulations
Extended Komen et al. (1984) expression with $\beta^1$

SWAN 40.00

WL | delft hydraulics

H3529

Fig. 5.10.a

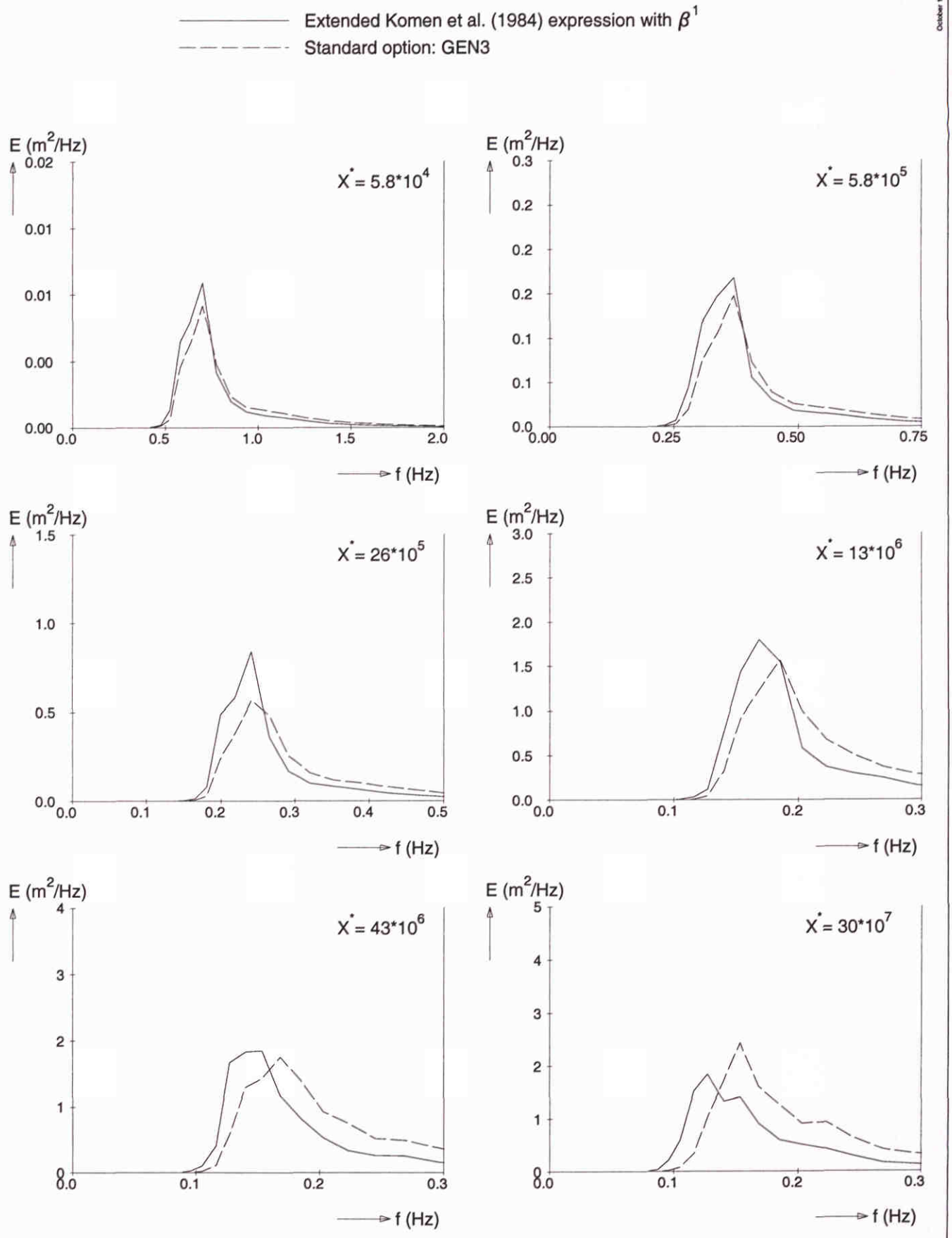


| | | |
|---|---|---|
| Frequency spectra at different locations ($U_{10}$ = 10 m/s) | SWAN 40.00 | |
| | | |
| WL \| delft hydraulics | H3529 | Fig. 5.10.b |

Extended Komen et al. (1984) expression with $\beta^1$

Standard option: GEN3

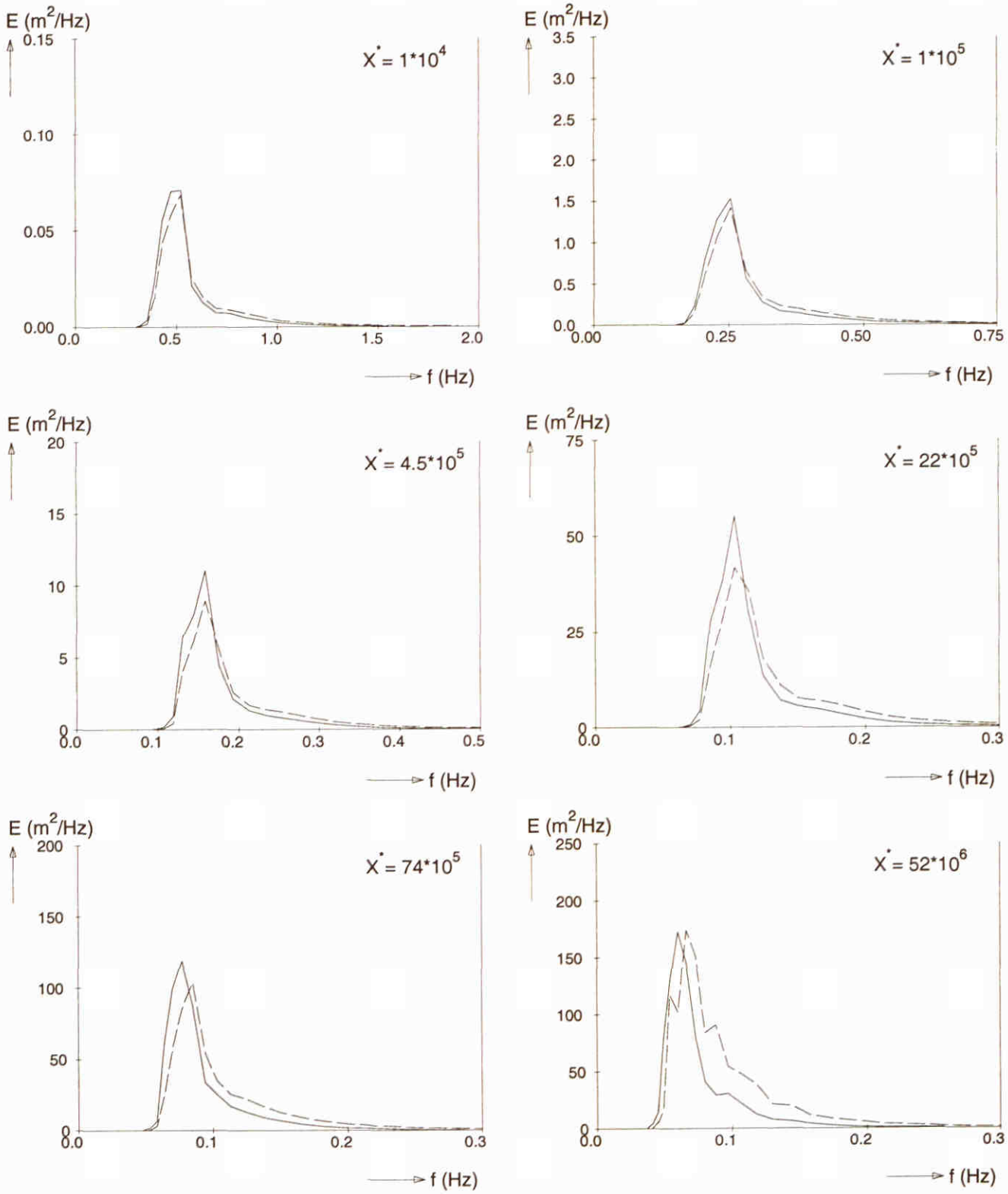


| | | |
|---|---|---|
| Frequency spectra at different locations ($U_{10}$ = 20 m/s) | SWAN 40.00 | |
| | | |
| WL \| delft hydraulics | H3529 | Fig. 5.10.c |

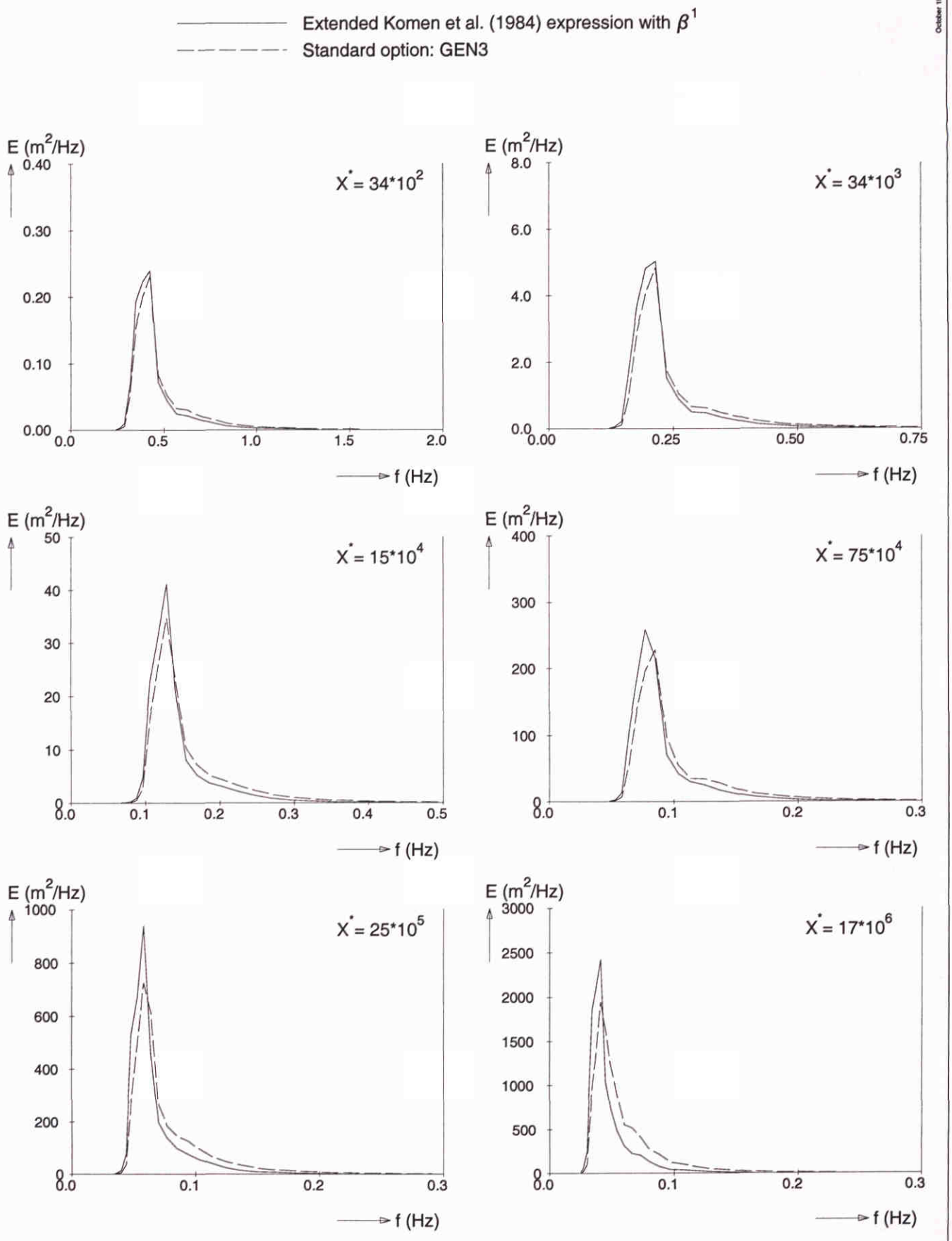


Frequency spectra at different locations ($U_{10}$ = 30 m/s)

SWAN 40.00

WL | delft hydraulics

H3529

Fig. 5.10.d

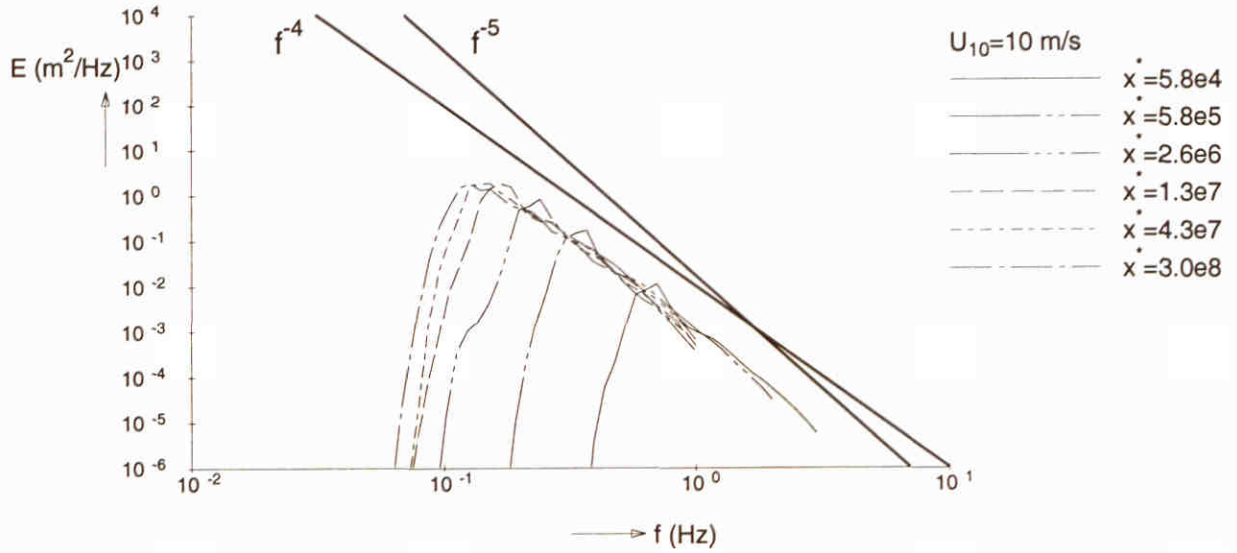


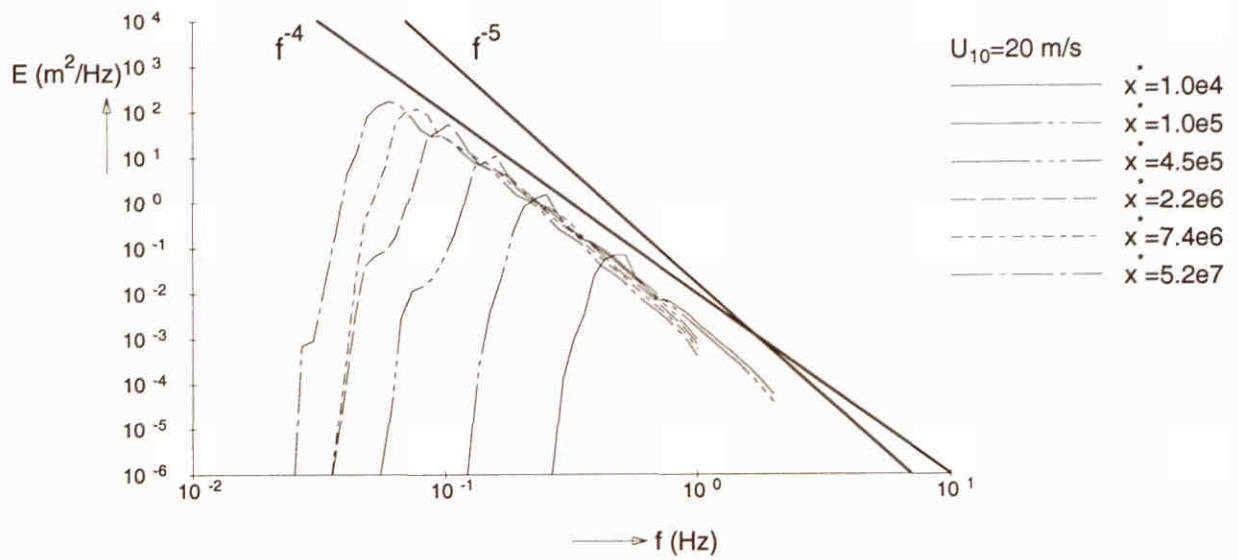


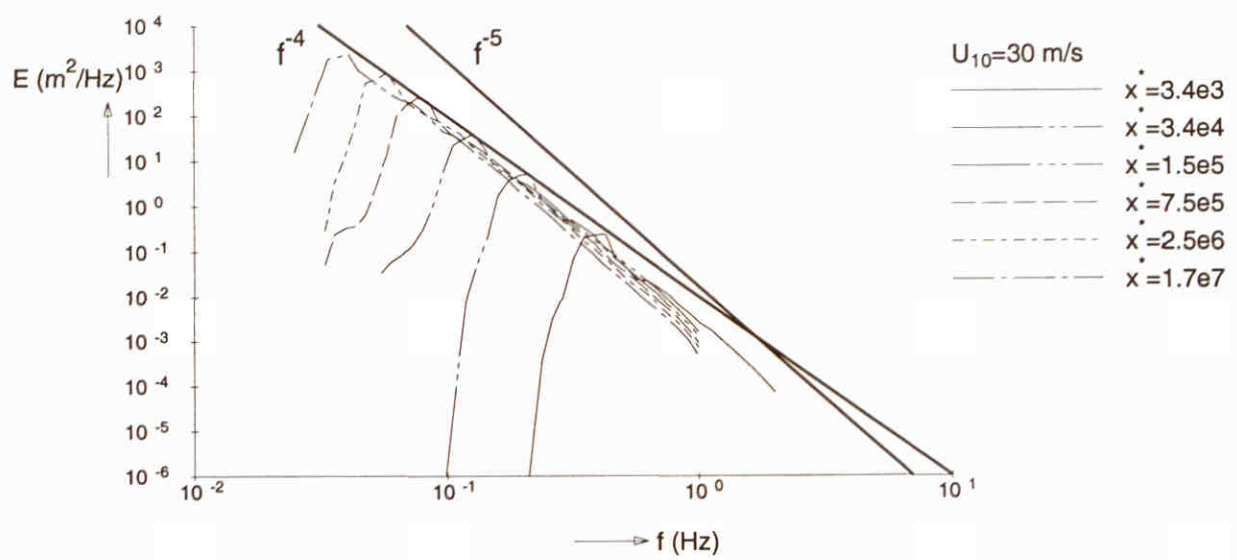


Wave spectra at different fetches

Extended Komen et al. (1984) expression with $\beta^1$

SWAN 40.00

WL | delft hydraulics

H3529

Fig. 5.10.e

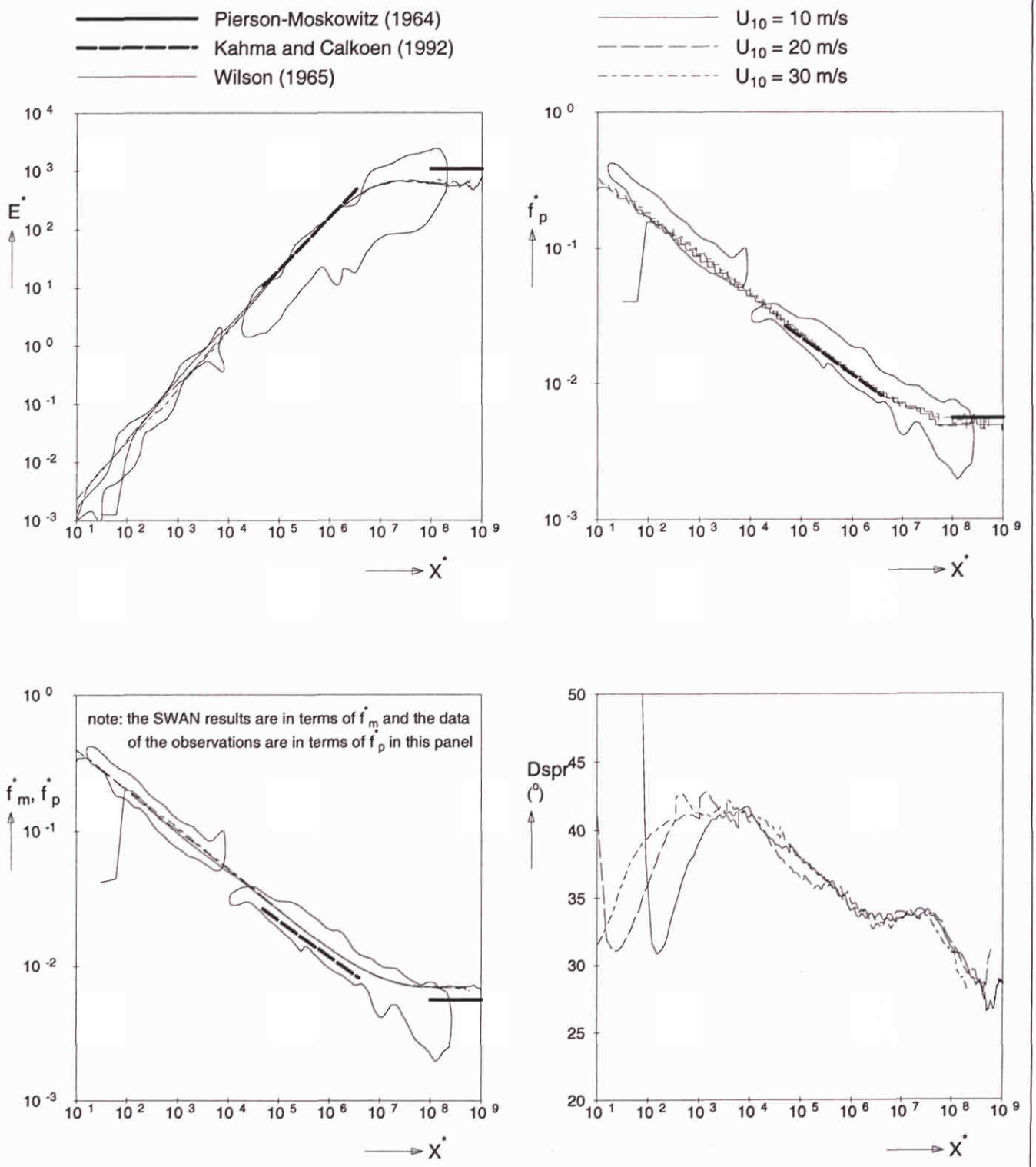


| | | |
|---|---|---|
| Fetch limited wave growth (deep water)<br>Third-generation formulations<br>Extended Komen et al. (1984) expression with $\beta^2$ | SWAN 40.00 | |
| WL \| delft hydraulics | H3529 | Fig. 5.11.a |

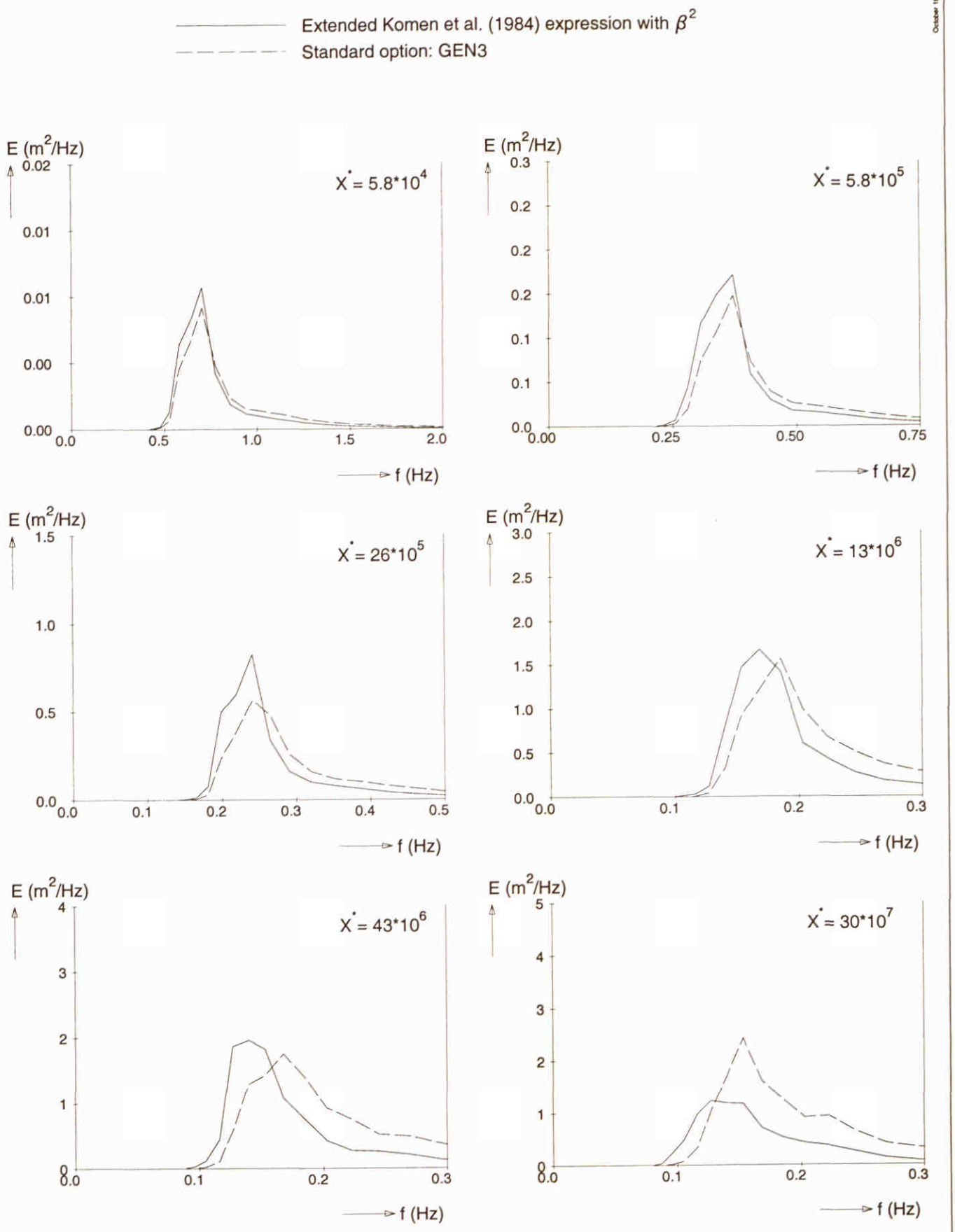


Frequency spectra at different locations ($U_{10}$ = 10 m/s)

SWAN 40.00

WL | delft hydraulics

H3529

Fig. 5.11.b

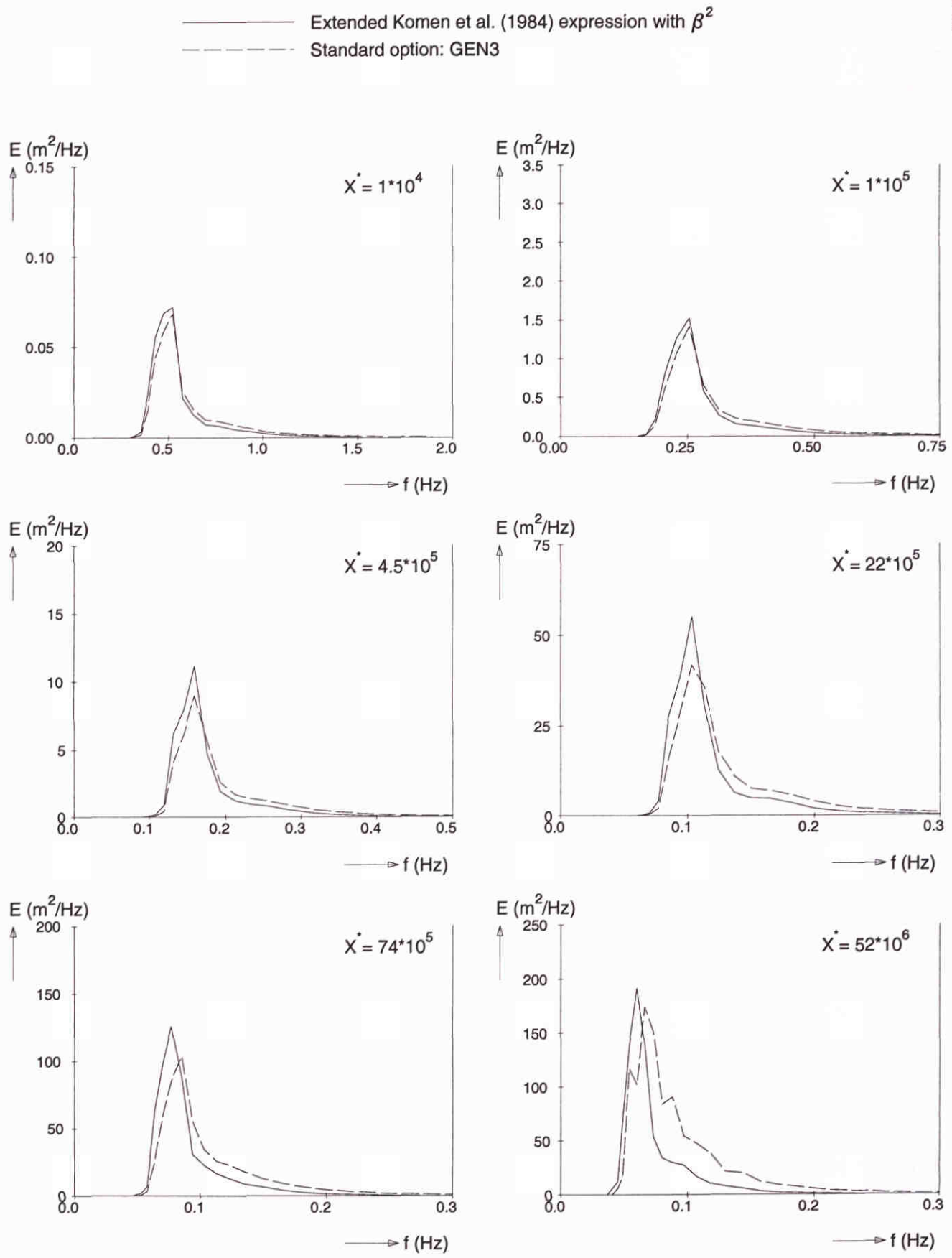


Frequency spectra at different locations ($U_{10}$ = 20 m/s)

SWAN 40.00

WL | delft hydraulics

H3529

Fig. 5.11.c

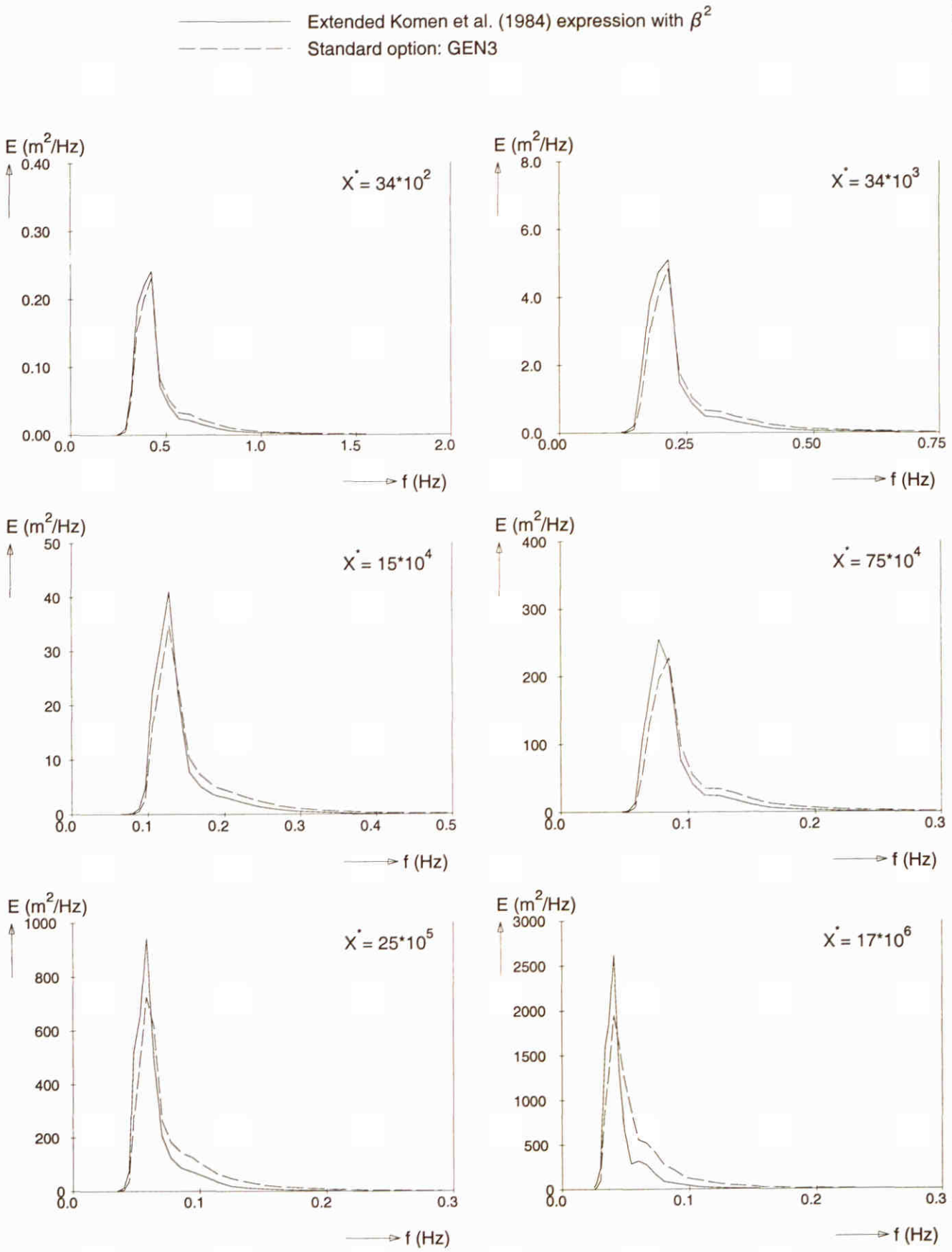


Frequency spectra at different locations ($U_{10}$ = 30 m/s)

SWAN 40.00

WL | delft hydraulics

H3529

Fig. 5.11.d

October 1999

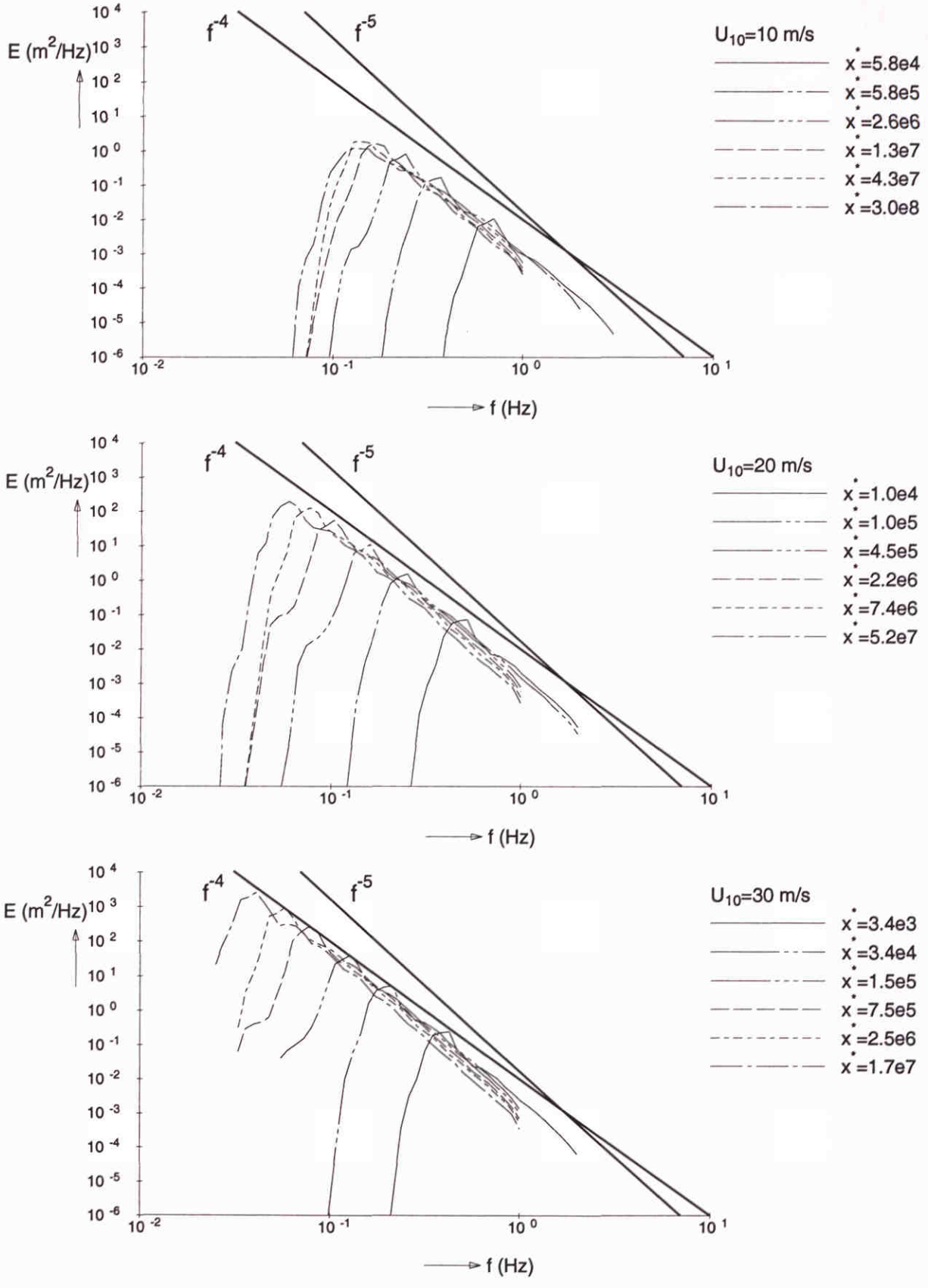


Wave spectra at different fetches

Extended Komen et al. (1984) expression with $\beta^2$

SWAN 40.00

WL | delft hydraulics

H3529

Fig. 5.11.e

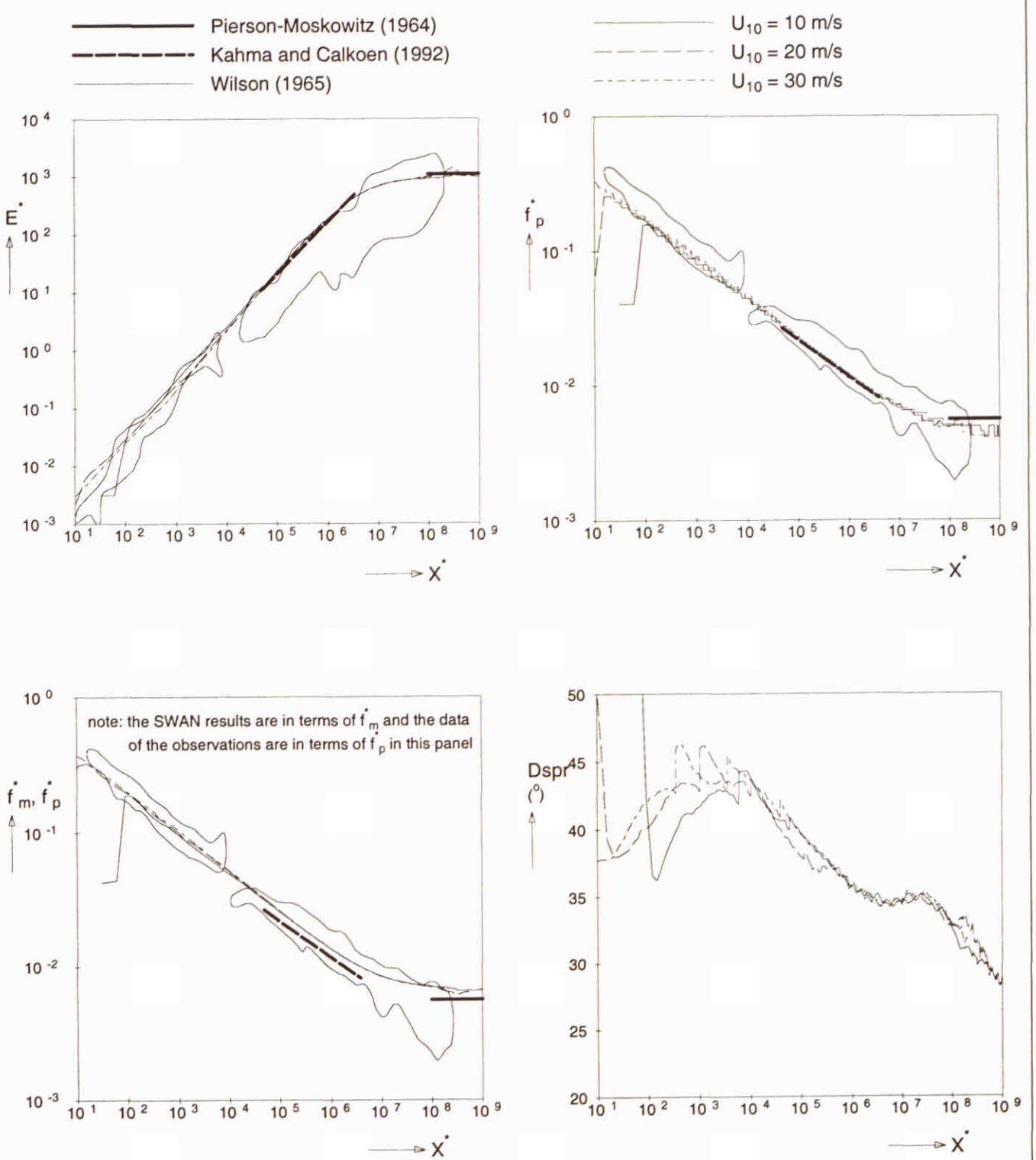


Fetch limited wave growth (deep water)
Extended Komen et al. (1984) expression with $\beta^{0.5}$
Modified coefficient $C_{new}$ = 0.8 C

SWAN 40.00

WL | delft hydraulics

H3529

Fig. 5.12.a

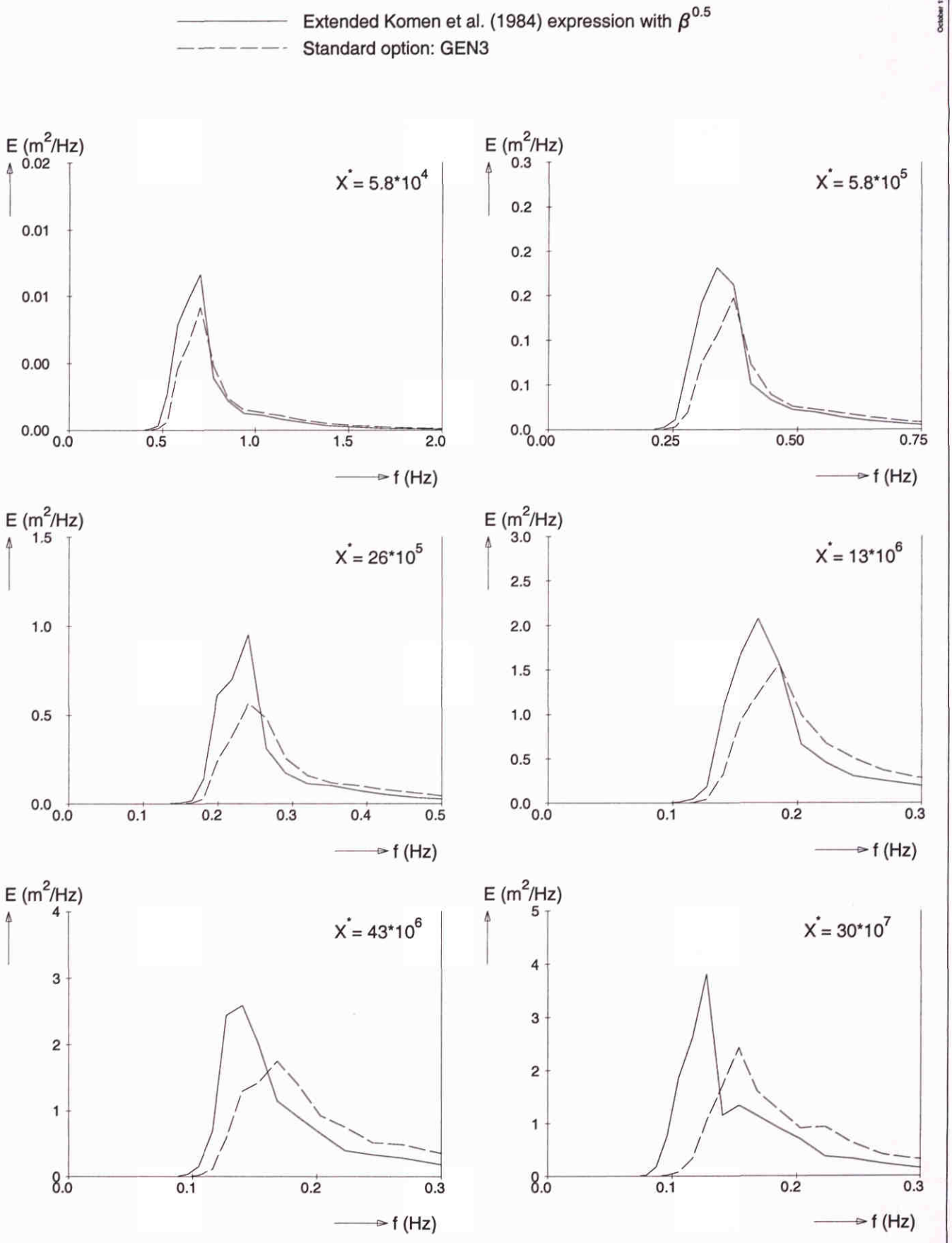


Frequency spectra at different locations ($U_{10}$ = 10 m/s)
Modified coefficient $C_{new}$ = 0.8 C

SWAN 40.00

WL | delft hydraulics

H3529

Fig. 5.12.b

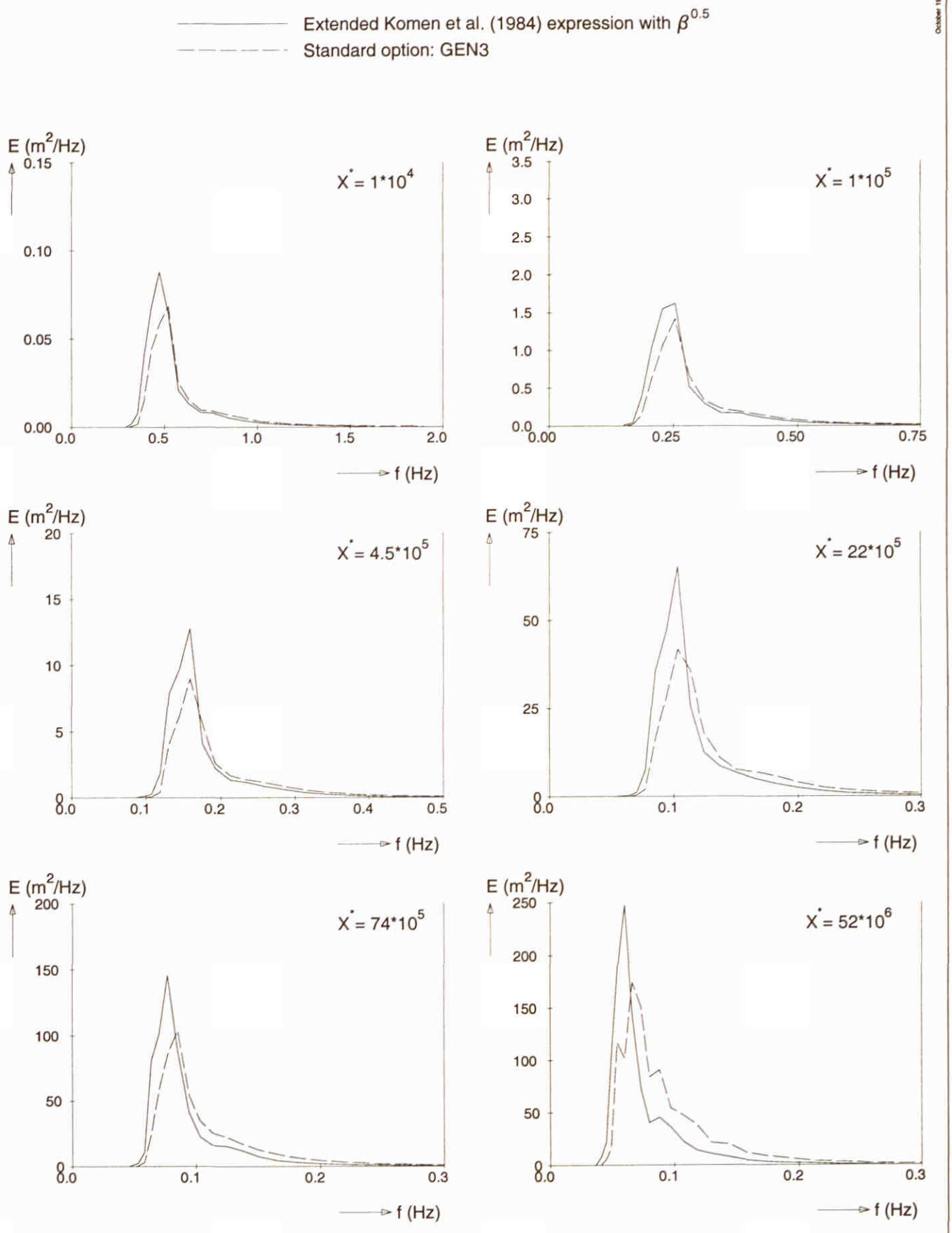


Frequency spectra at different locations ($U_{10}$ = 20 m/s)
Modified coefficient $C_{new}$ = 0.8 C

SWAN 40.00

WL | delft hydraulics

H3529

Fig. 5.12.c

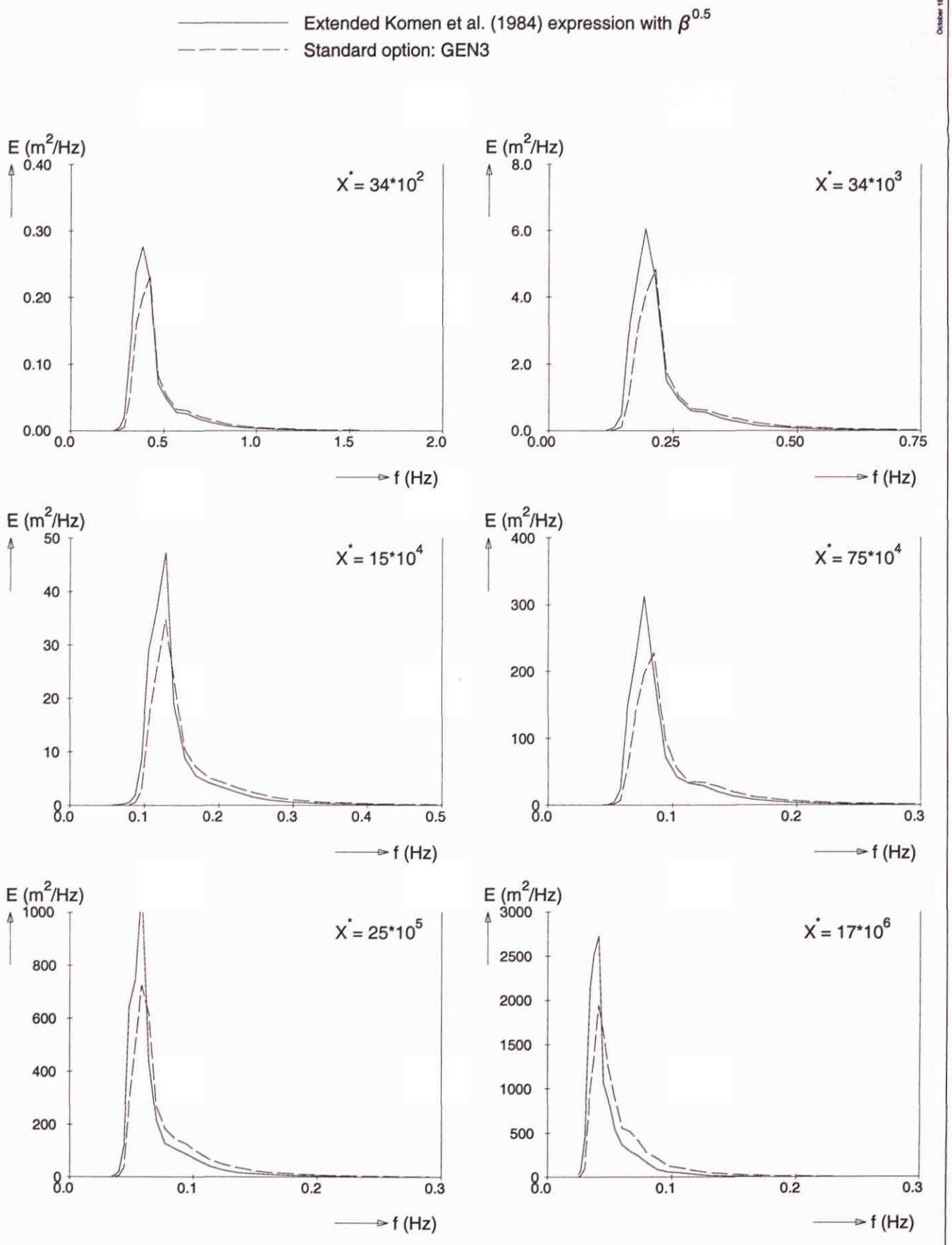


Frequency spectra at different locations ($U_{10}$ = 30 m/s)
Modified coefficient $C_{new}$ = 0.8 C

SWAN 40.00

WL | delft hydraulics

H3529

Fig. 5.12.d

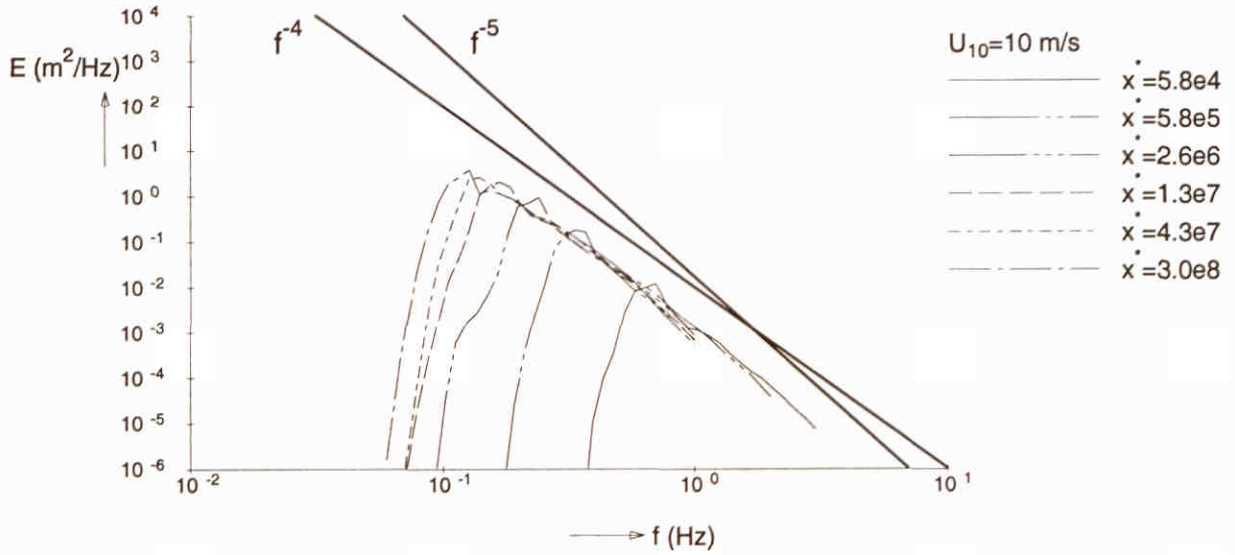


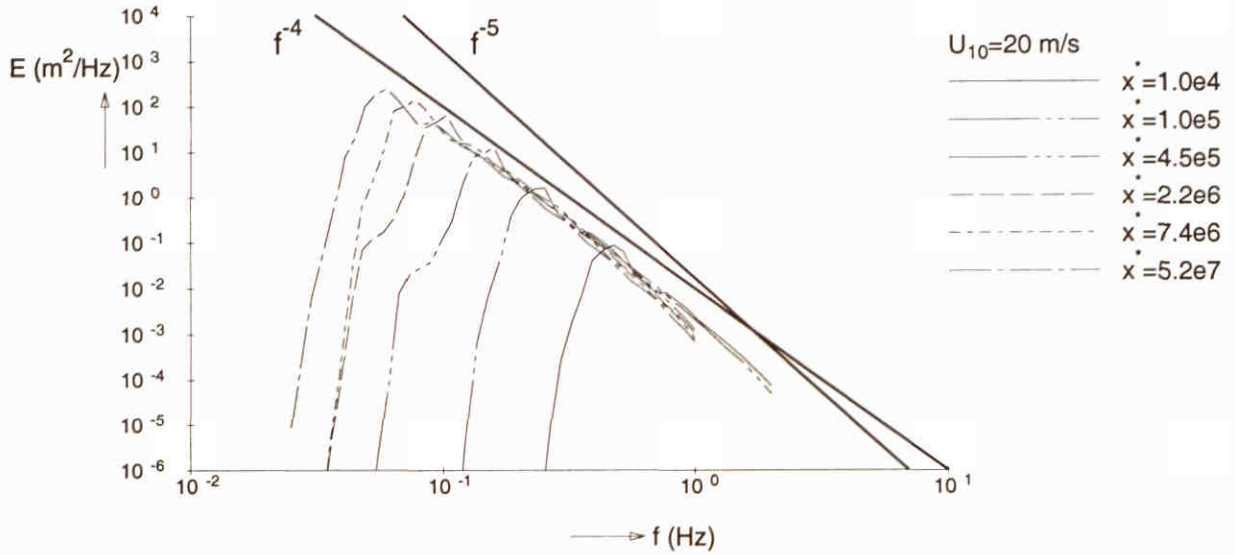


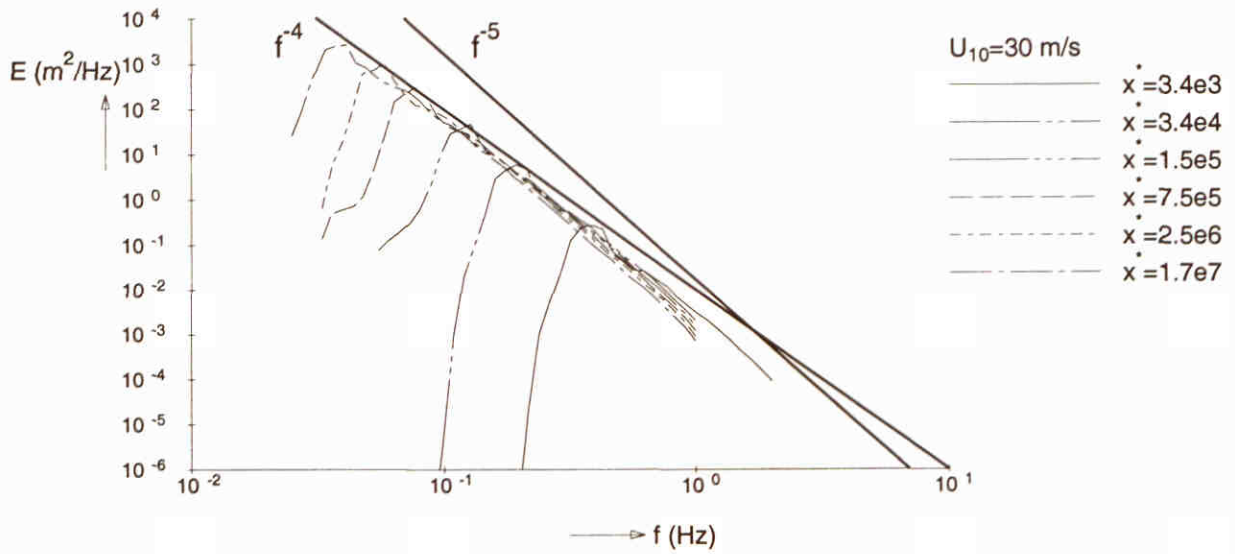


| | | |
|---|---|---|
| Wave spectra at different fetches<br>Extended Komen et al. (1984) expression with $\beta^{0.5}$<br>Modified coefficient $C_{new}$ = 0.8 C | SWAN 40.00 | |
| WL \| delft hydraulics | H3529 | Fig. 5.12.e |

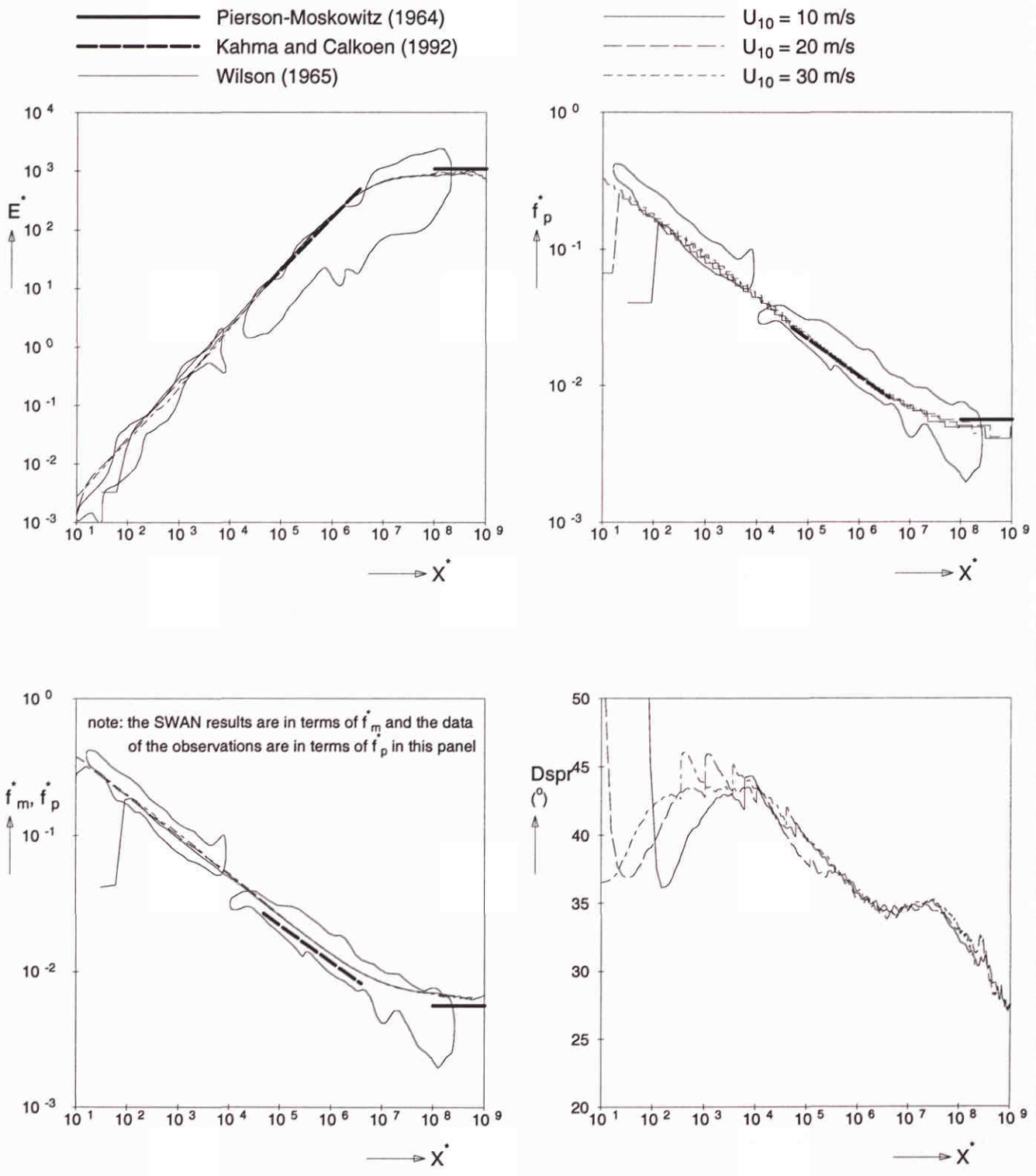


Fetch limited wave growth (deep water)
Extended Komen et al. (1984) expression with $\beta^1$
Modified coefficient $C_{new}$ = 0.8 C

SWAN 40.00

WL | delft hydraulics

H3529

Fig. 5.13.a

Extended Komen et al. (1984) expression with $\beta^1$

Standard option: GEN3

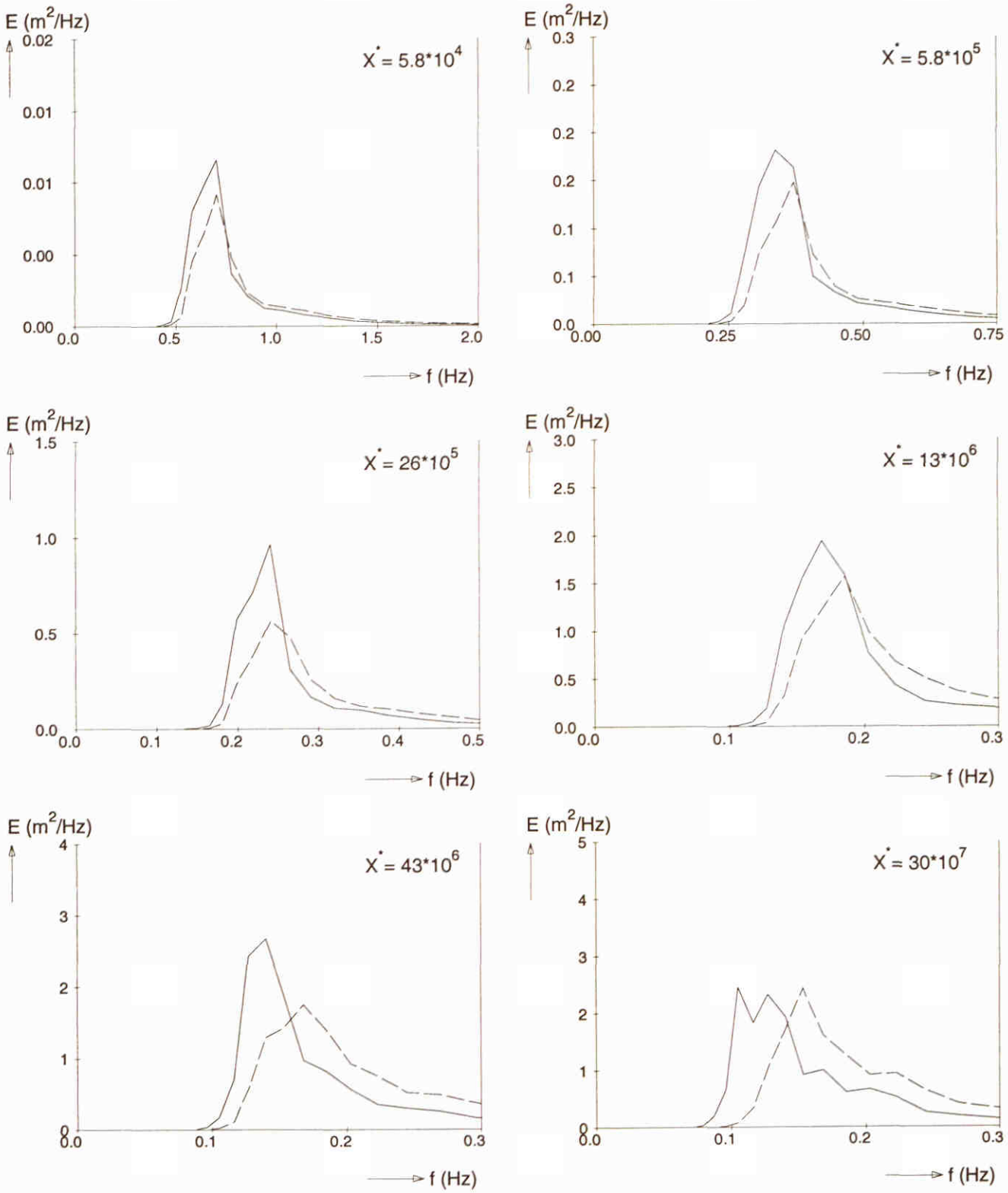


Frequency spectra at different locations ($U_{10}$ = 10 m/s)

Modified coefficient $C_{new}$ = 0.8 C

SWAN 40.00

WL | delft hydraulics

H3529

Fig. 5.13.b

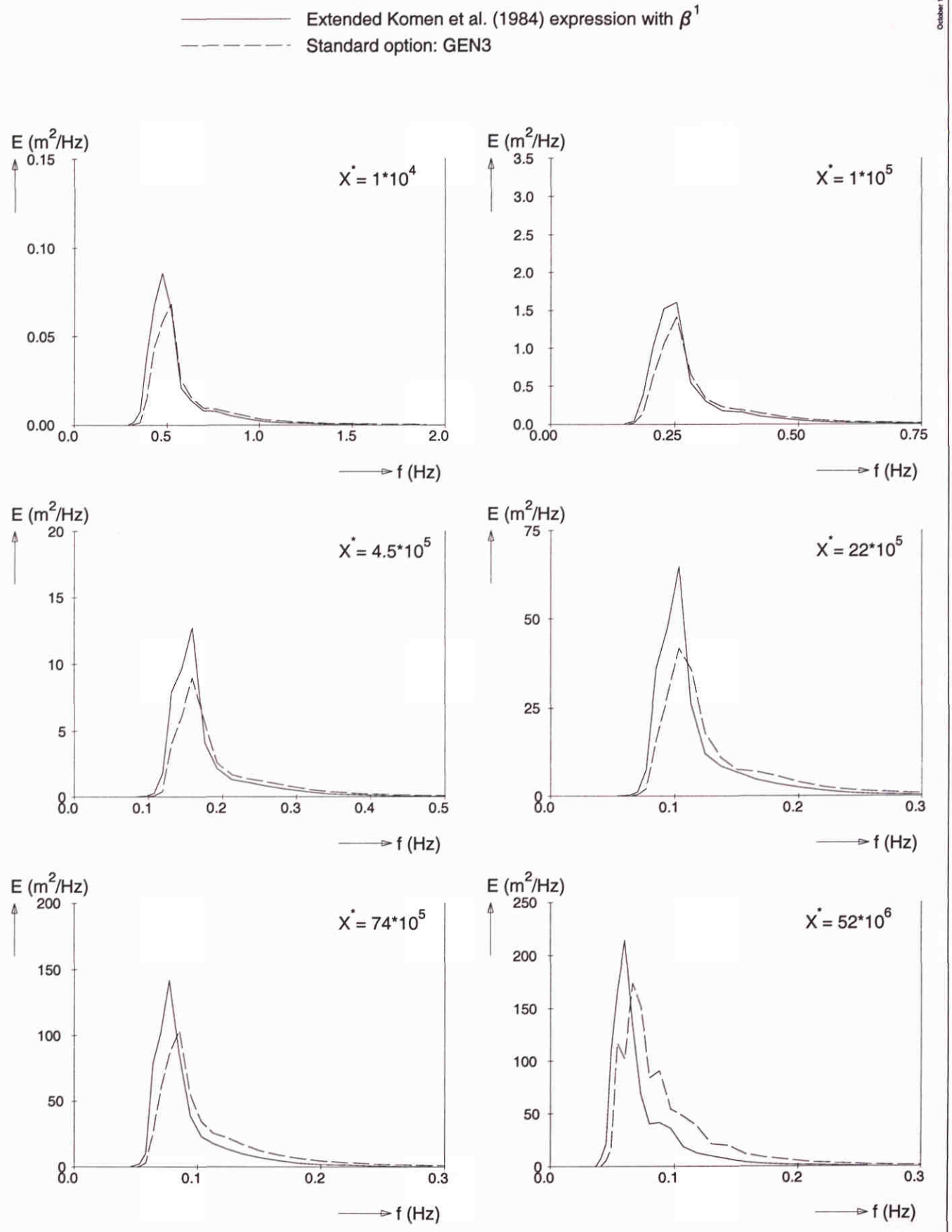


Frequency spectra at different locations ($U_{10}$ = 20 m/s)
Modified coefficient $C_{new}$ = 0.8 C

SWAN 40.00

WL | delft hydraulics

H3529

Fig. 5.13.c

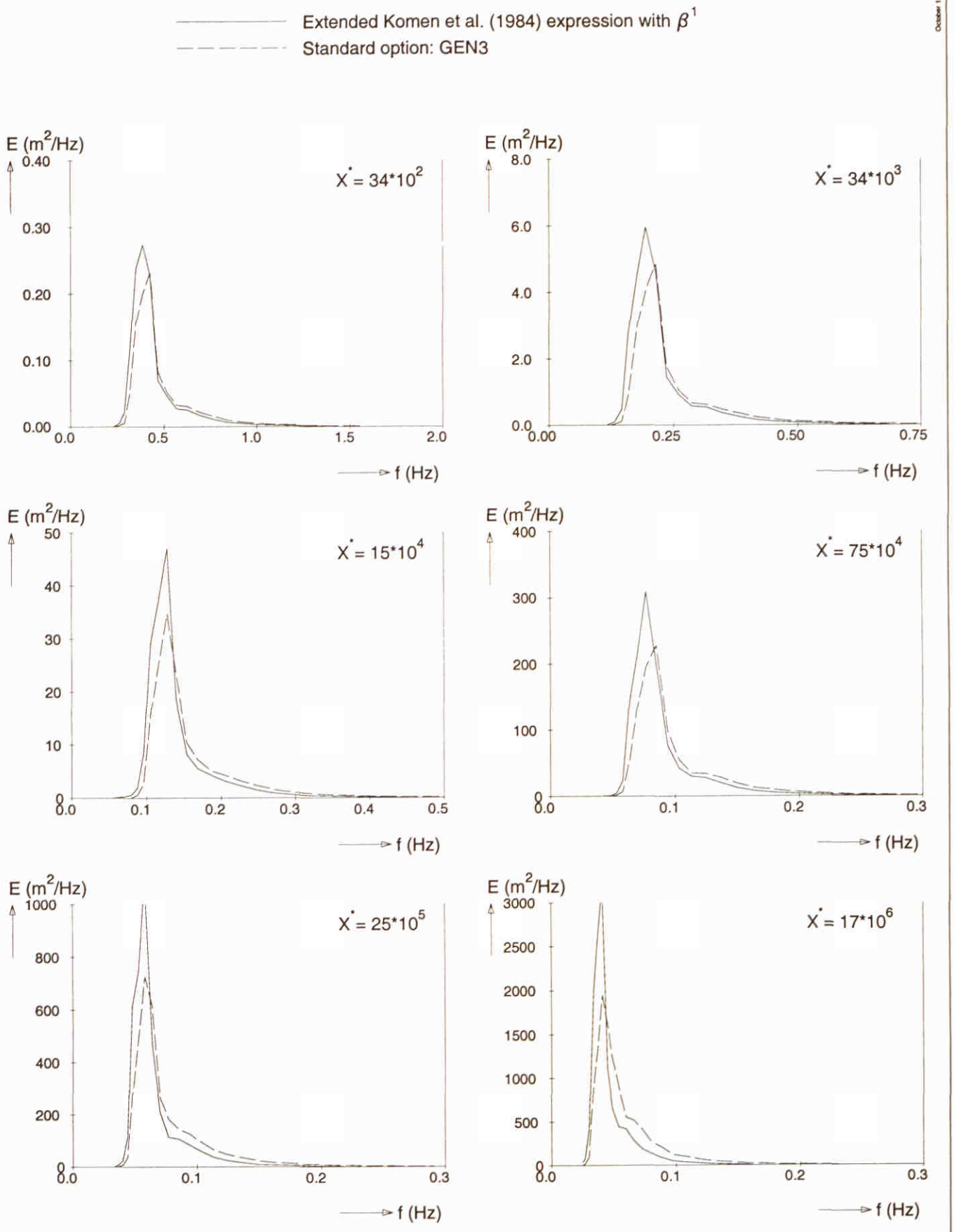


Frequency spectra at different locations ($U_{10}$ = 30 m/s)
Modified coefficient $C_{new}$ = 0.8 C

SWAN 40.00

WL | delft hydraulics

H3529

Fig. 5.13.d

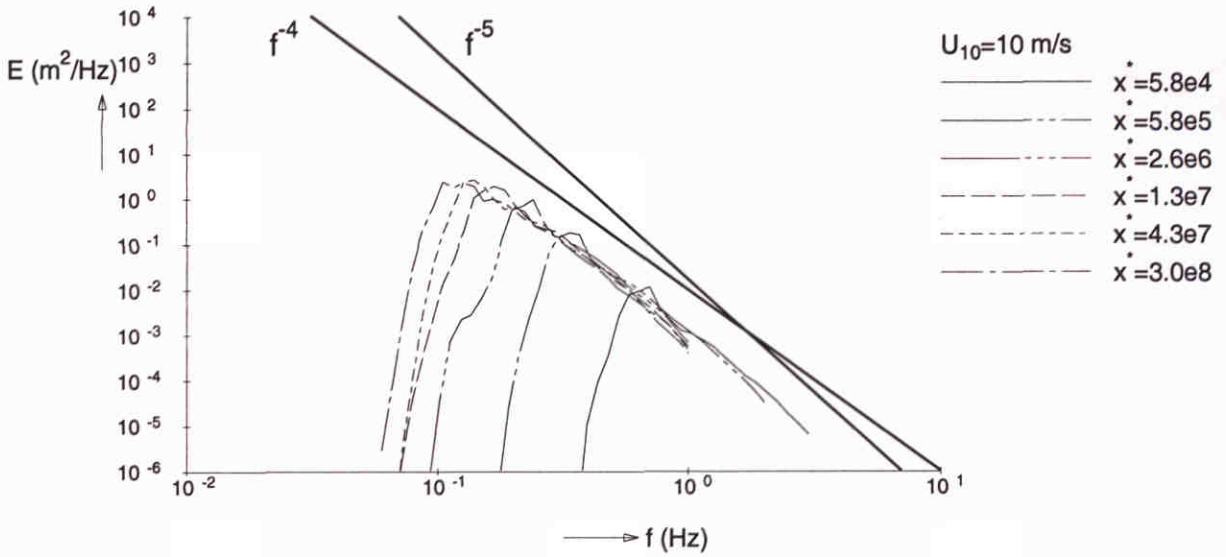


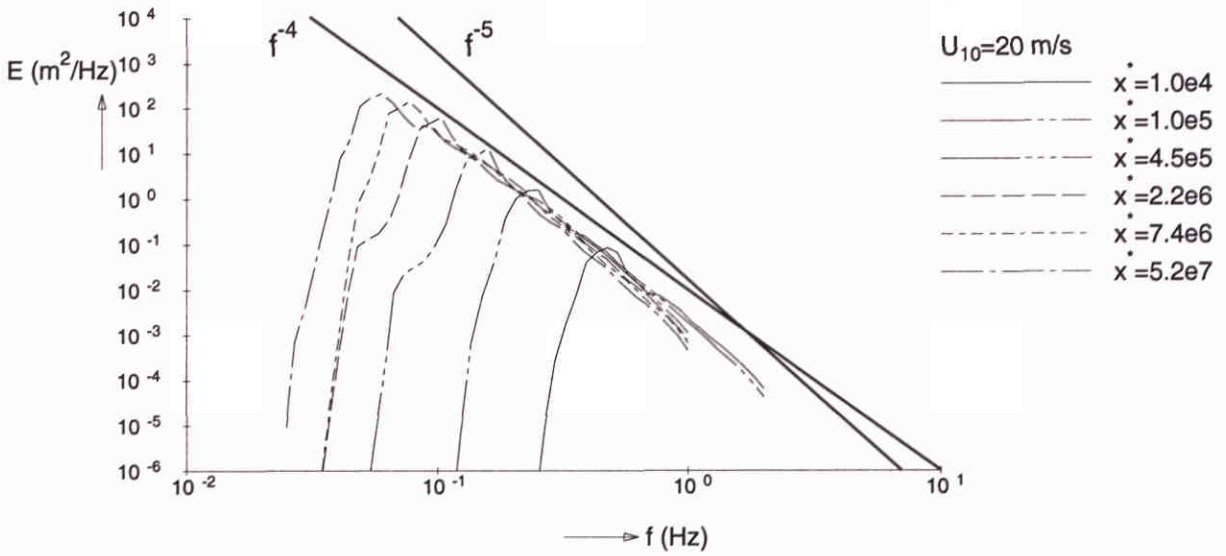


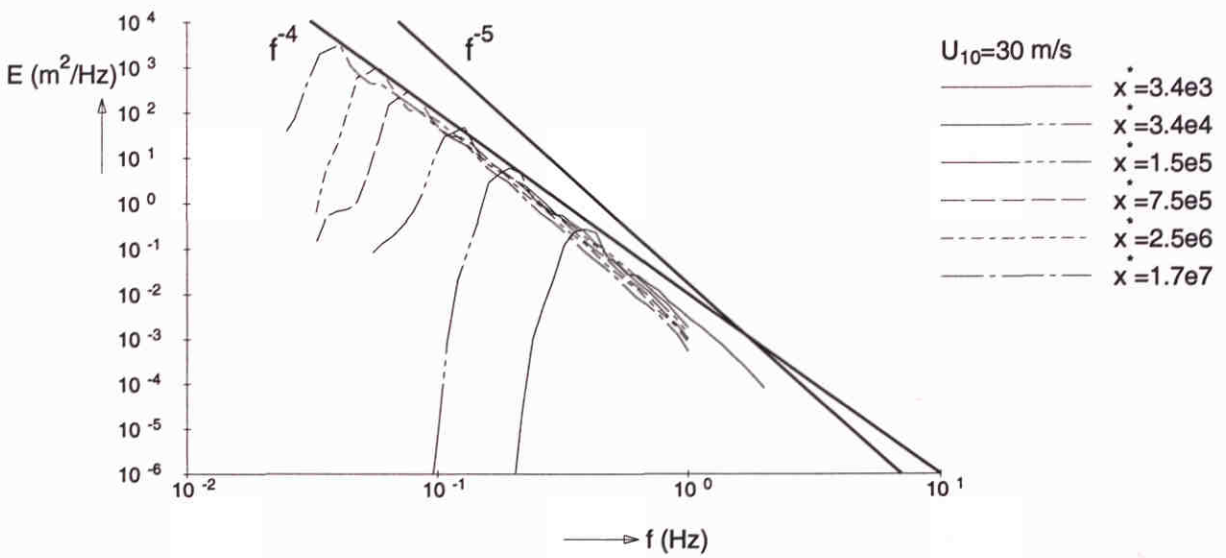


Wave spectra at different fetches
Extended Komen et al. (1984) expression with $\beta^1$
Modified coefficient $C_{new}$ = 0.8 C

SWAN 40.00

WL | delft hydraulics

H3529

Fig. 5.13.e

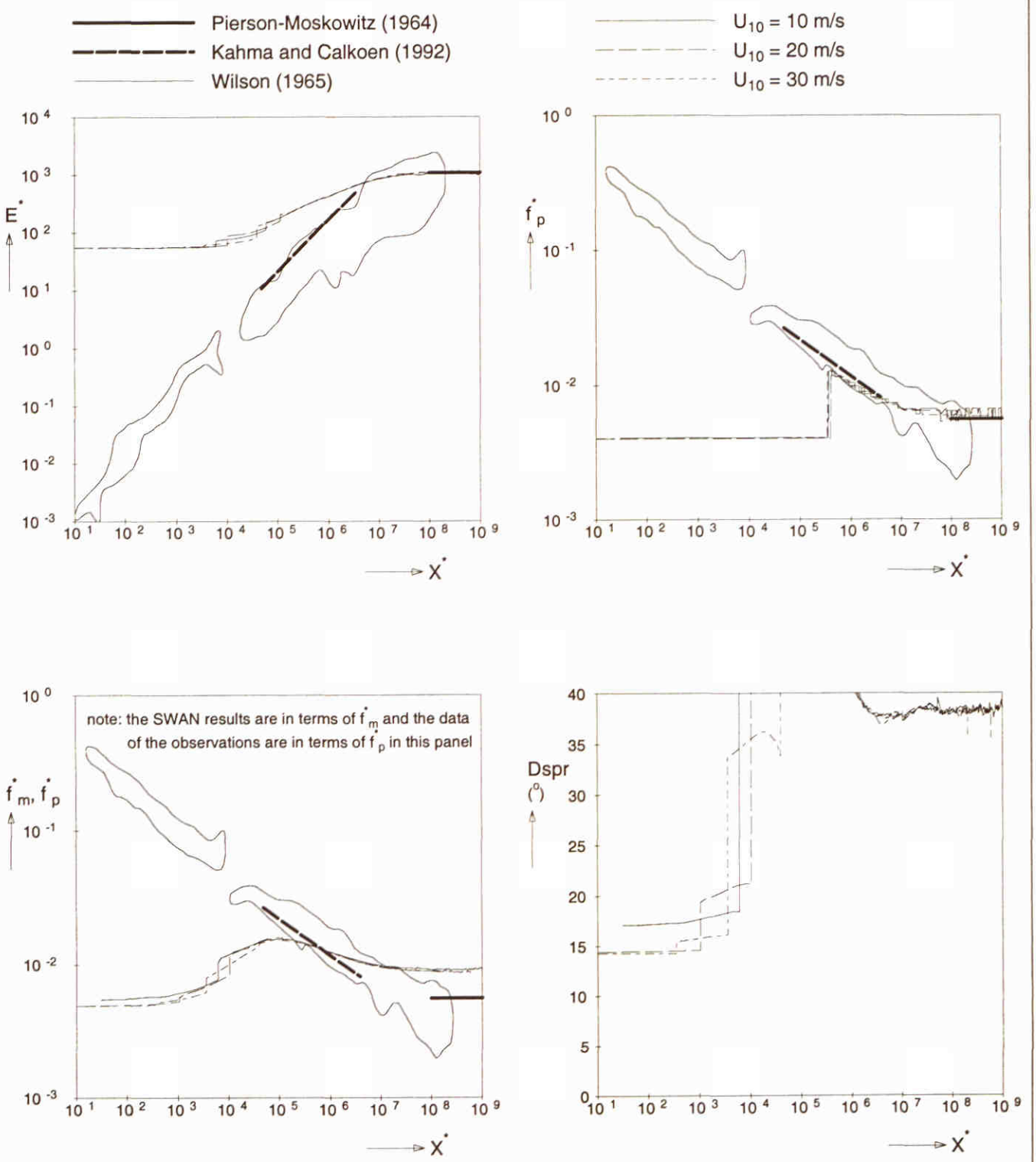


| | | |
|---|---|---|
| Fetch limited wave growth (deep water)<br>Third-generation formulations (standard option: GEN3)<br>With incident low frequency waves | SWAN 40.00 | |
| WL \| delft hydraulics | H3529 | Fig. 5.14.a |

October 1999

Standard option: GEN3, with incident low frequency waves

Standard option: GEN3, without incident low frequency waves

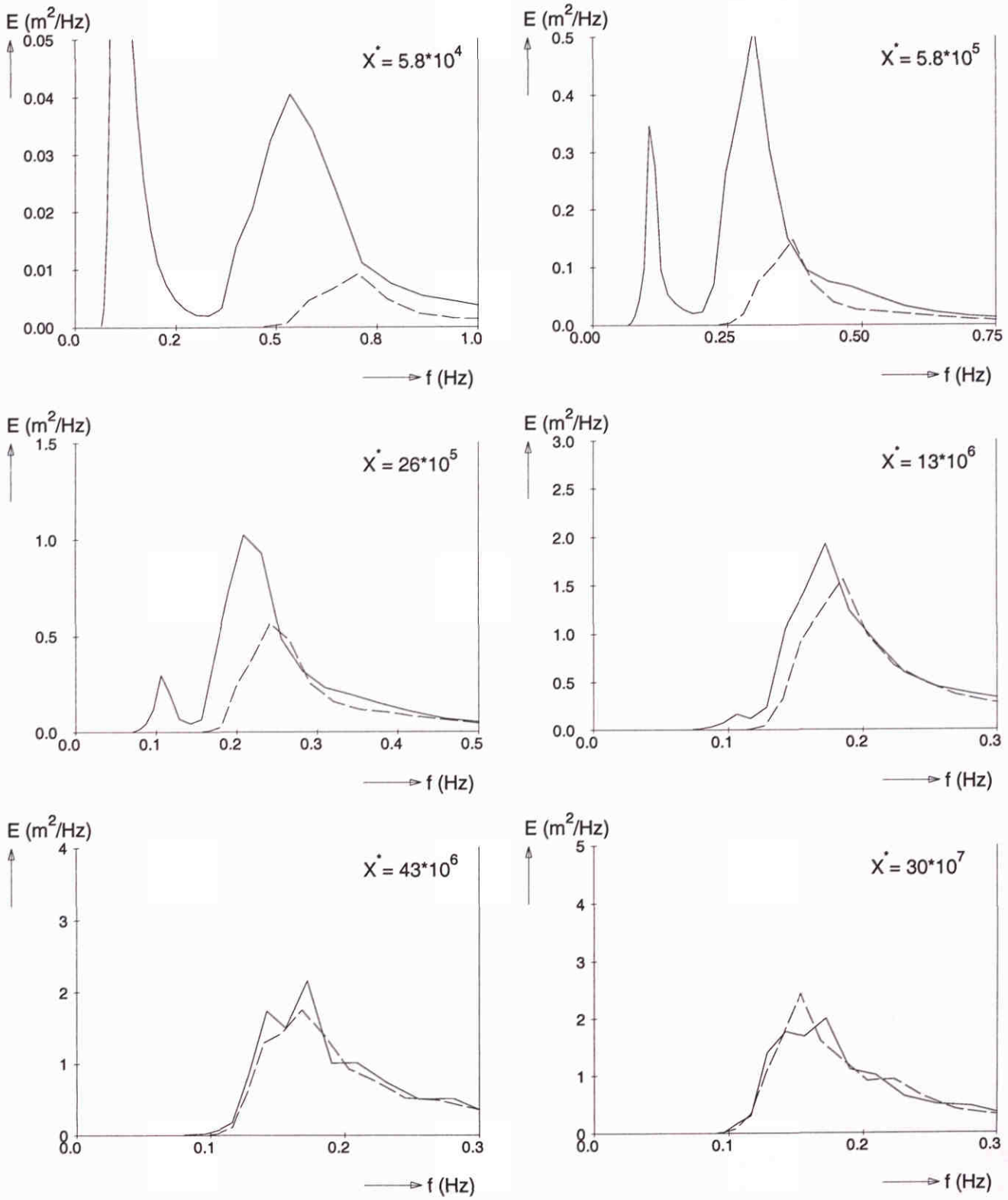


Frequency spectra at different locations ($U_{10}$ = 10 m/s)

With incident low frequency waves

SWAN 40.00

WL | delft hydraulics

H3529

Fig. 5.14.b

Standard option: GEN3, with incident low frequency waves

Standard option: GEN3, without incident low frequency waves

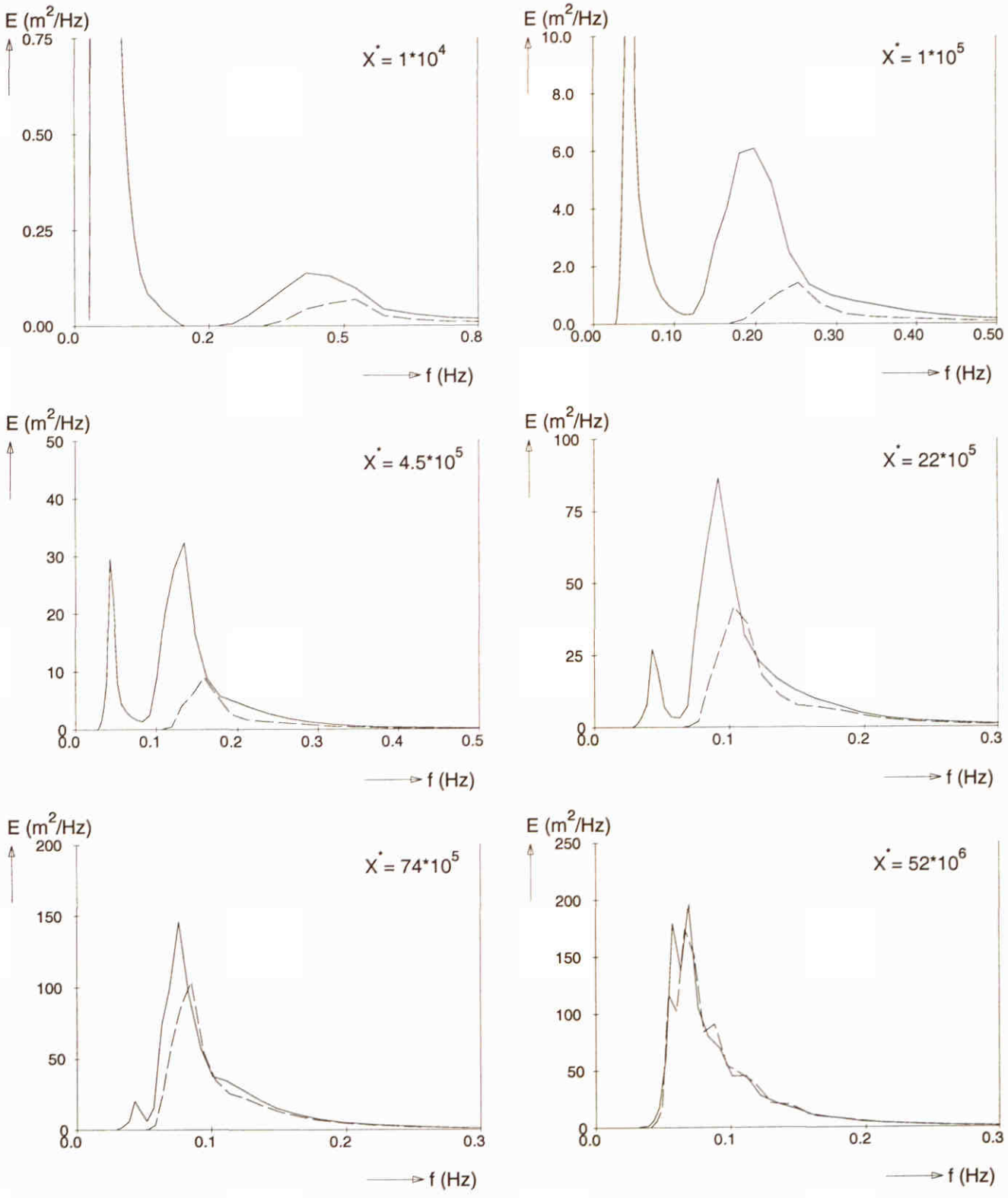


Frequency spectra at different locations ($U_{10}$ = 20 m/s)

With incident low frequency waves

SWAN 40.00

WL | delft hydraulics

H3529

Fig. 5.14.c

Standard option: GEN3, with incident low frequency waves

Standard option: GEN3, without incident low frequency waves

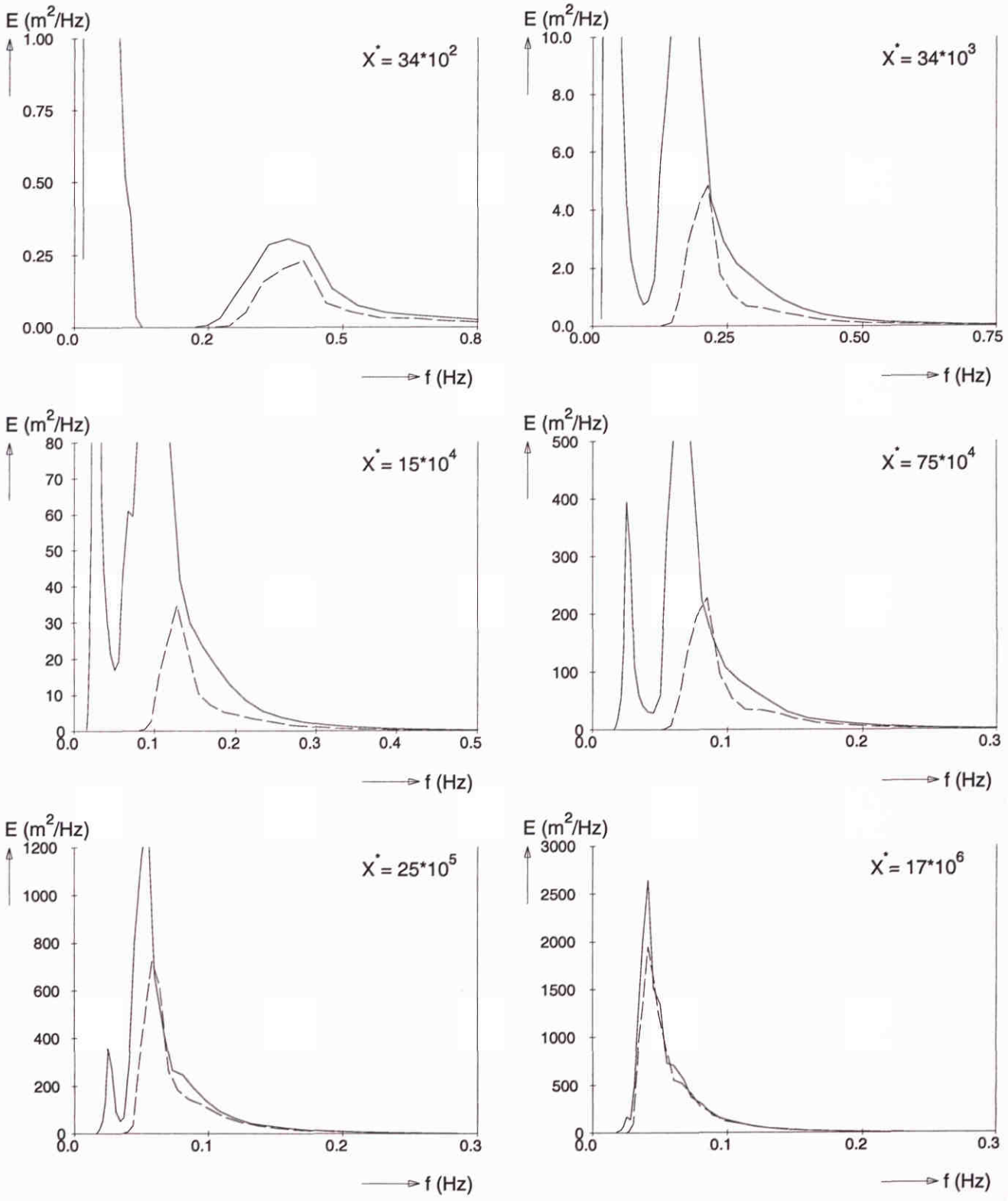


Frequency spectra at different locations ($U_{10}$ = 30 m/s)

With incident low frequency waves

SWAN 40.00

WL | delft hydraulics

H3529

Fig. 5.14.d

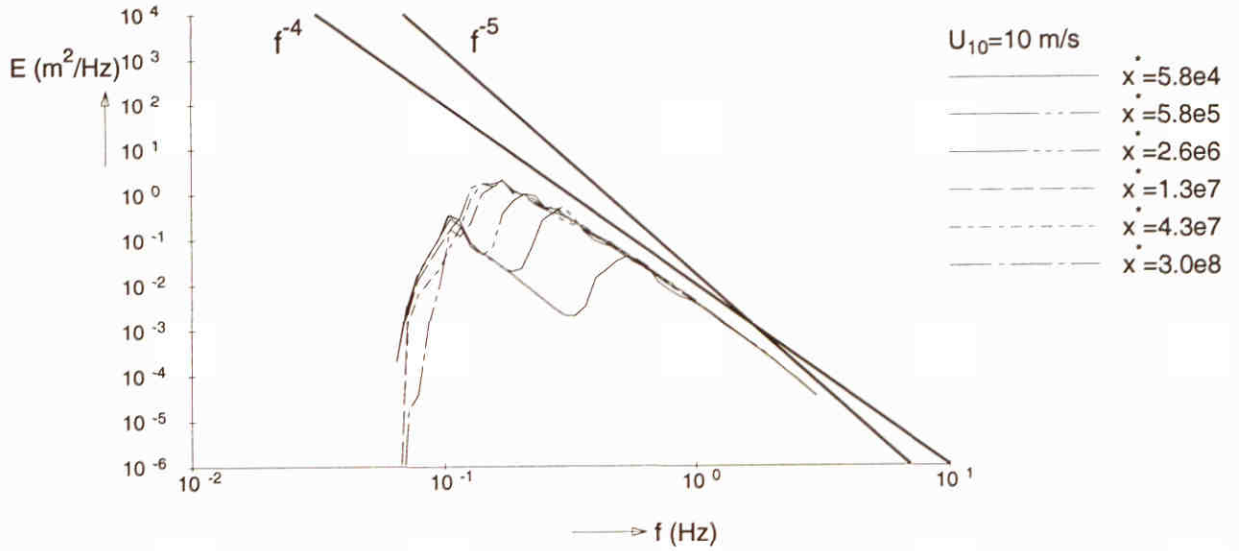


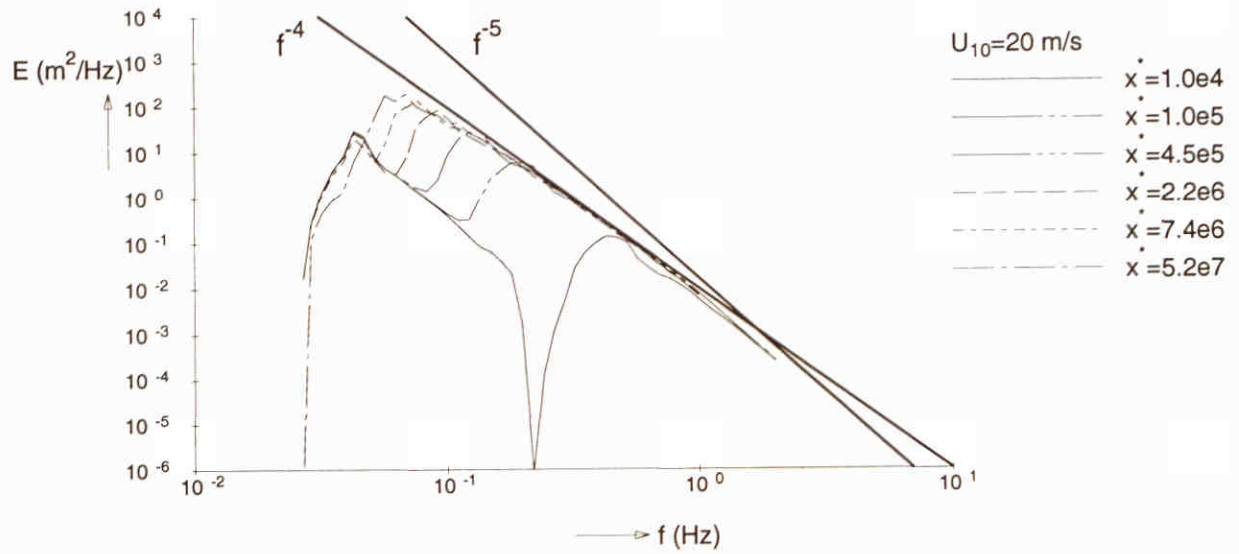


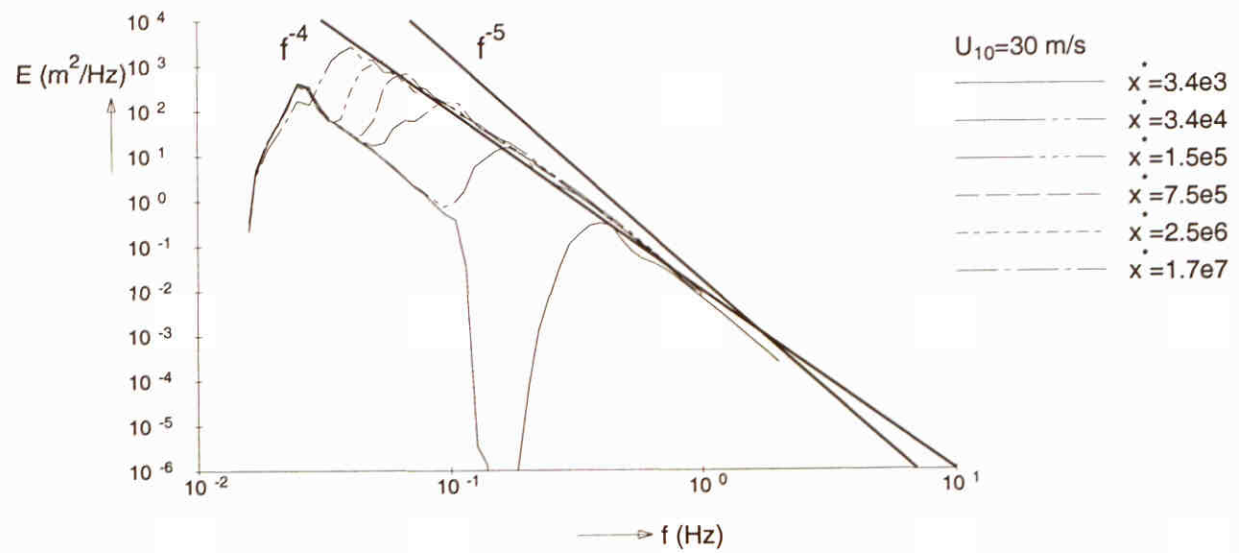


Wave spectra at different fetches
Standard option: GEN3
With incident low frequency waves

SWAN 40.00

WL | delft hydraulics

H3529

Fig. 5.14.e

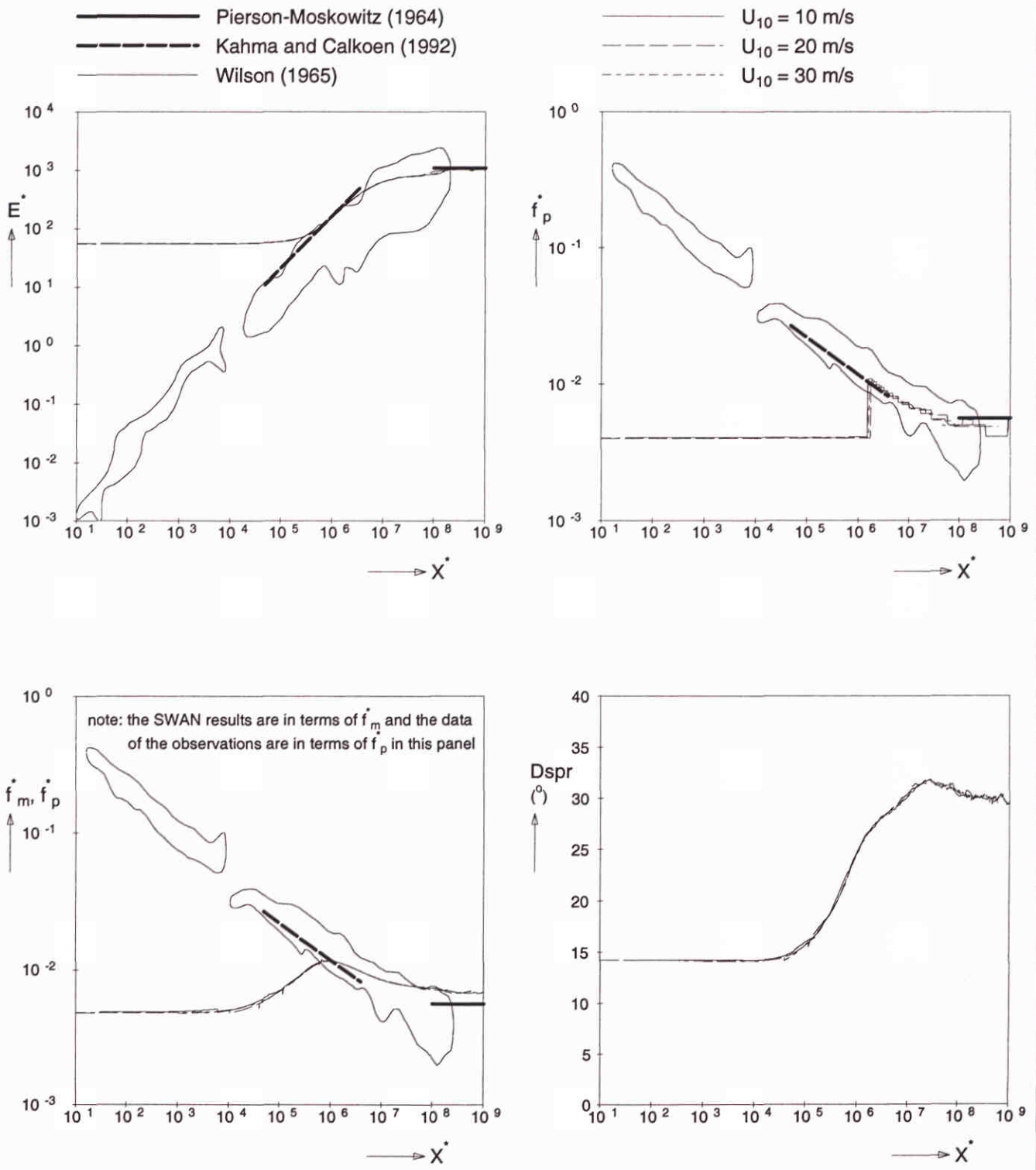


| | | |
|---|---|---|
| Fetch limited wave growth (deep water)<br>Extended Komen et al. (1984) expression with $\beta^0$<br>With incident low frequency waves | SWAN 40.00 | |
| WL \| delft hydraulics | H3529 | Fig. 5.15.a |

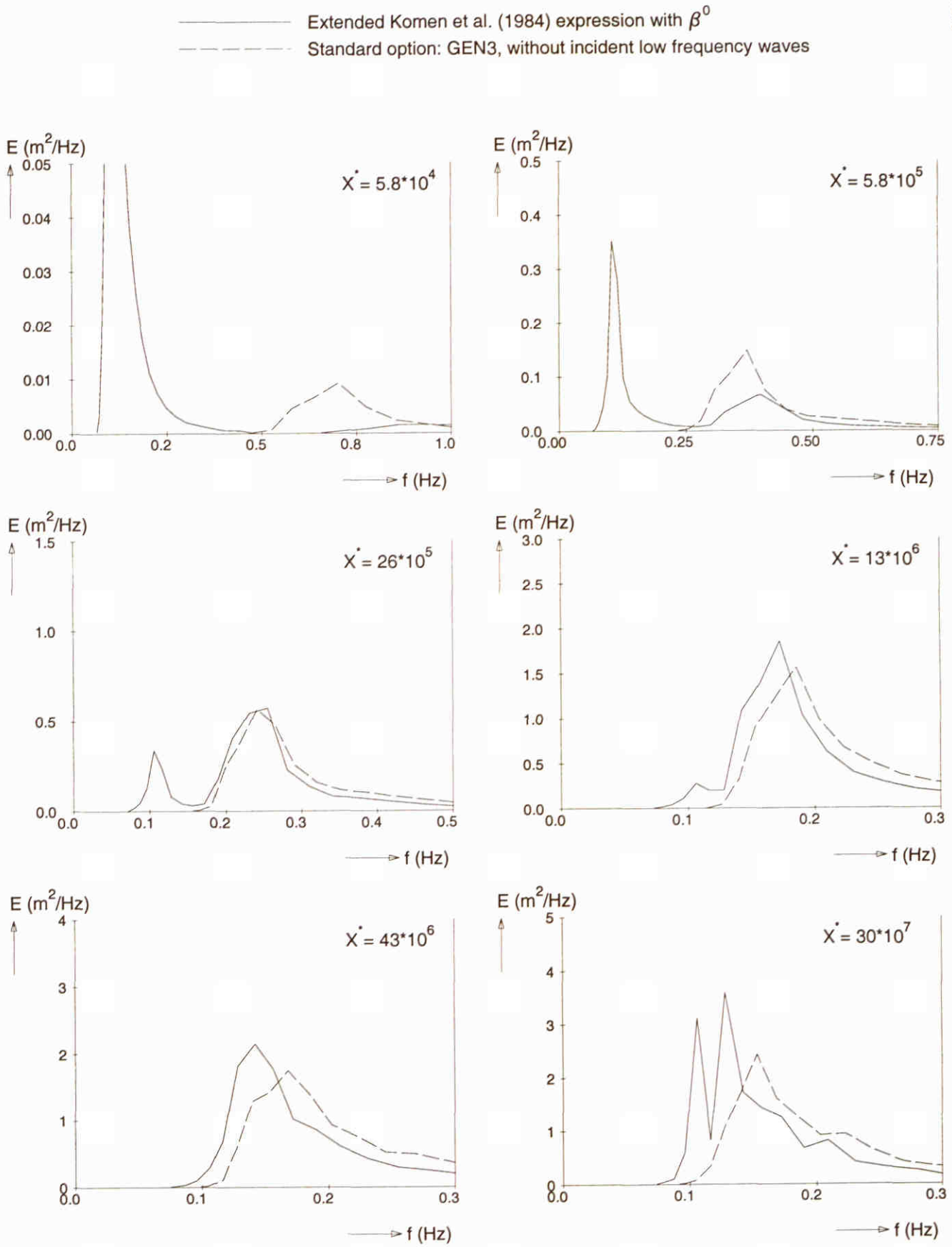


Frequency spectra at different locations ($U_{10}$ = 10 m/s)
With incident low frequency waves

SWAN 40.00

WL | delft hydraulics

H3529

Fig. 5.15.b

Extended Komen et al. (1984) expression with $\beta^0$

Standard option: GEN3, without incident low frequency waves

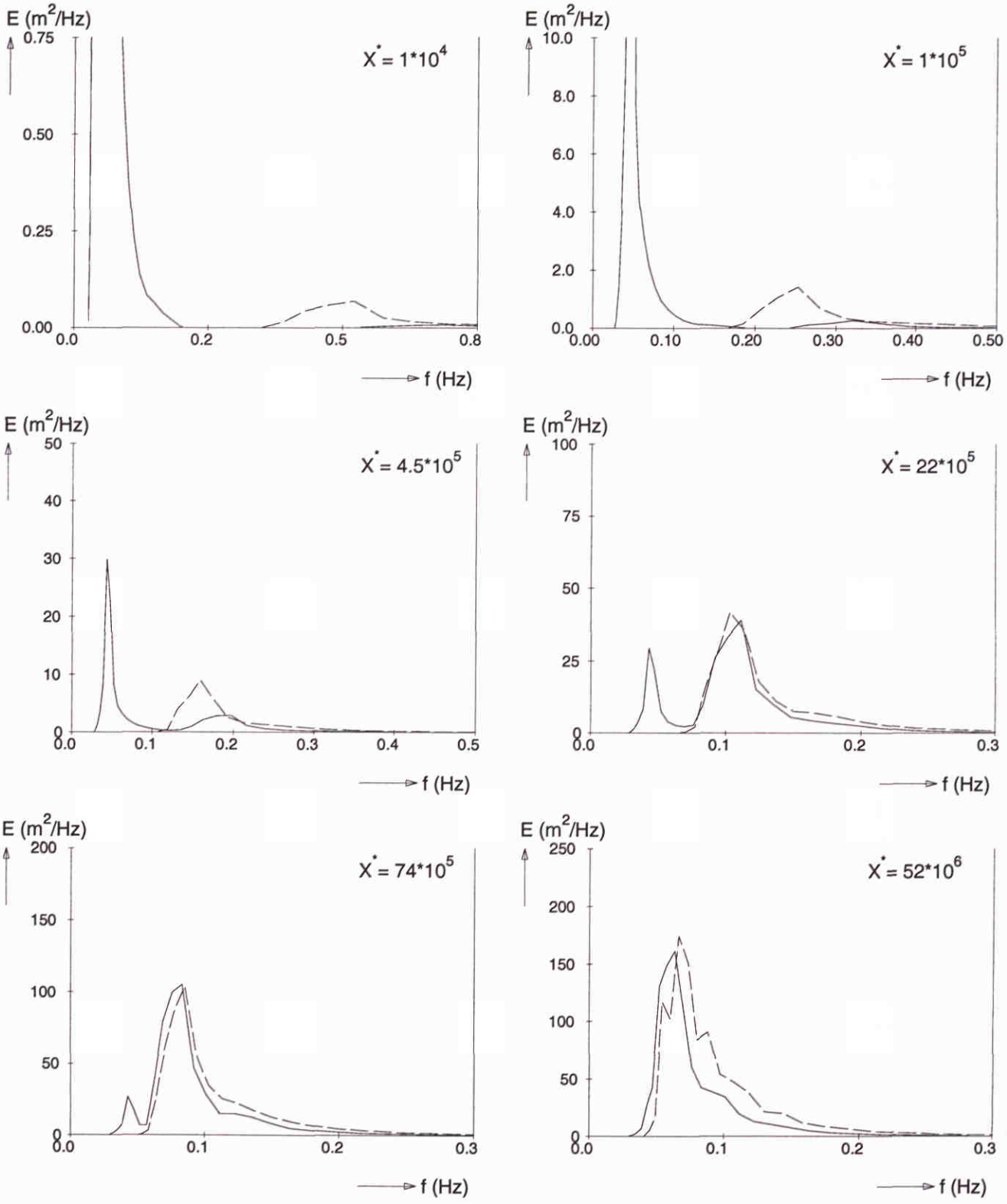


Frequency spectra at different locations ($U_{10}$ = 20 m/s)

With incident low frequency waves

SWAN 40.00

WL | delft hydraulics

H3529

Fig. 5.15.c

Extended Komen et al. (1984) expression with $\beta^0$

Standard option: GEN3, without incident low frequency waves

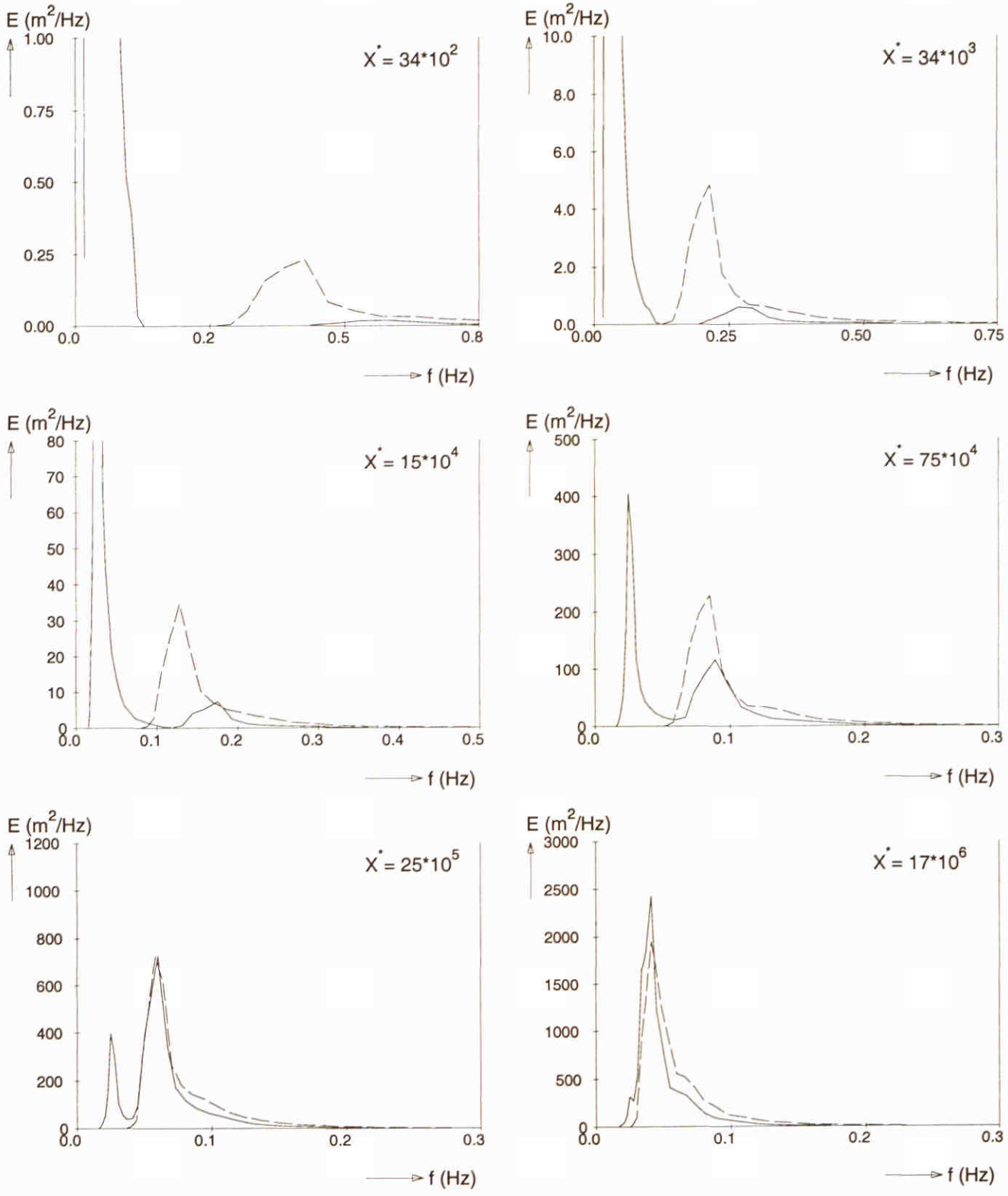


Frequency spectra at different locations ($U_{10}$ = 30 m/s)

With incident low frequency waves

SWAN 40.00

WL | delft hydraulics

H3529

Fig. 5.15.d

October 1999

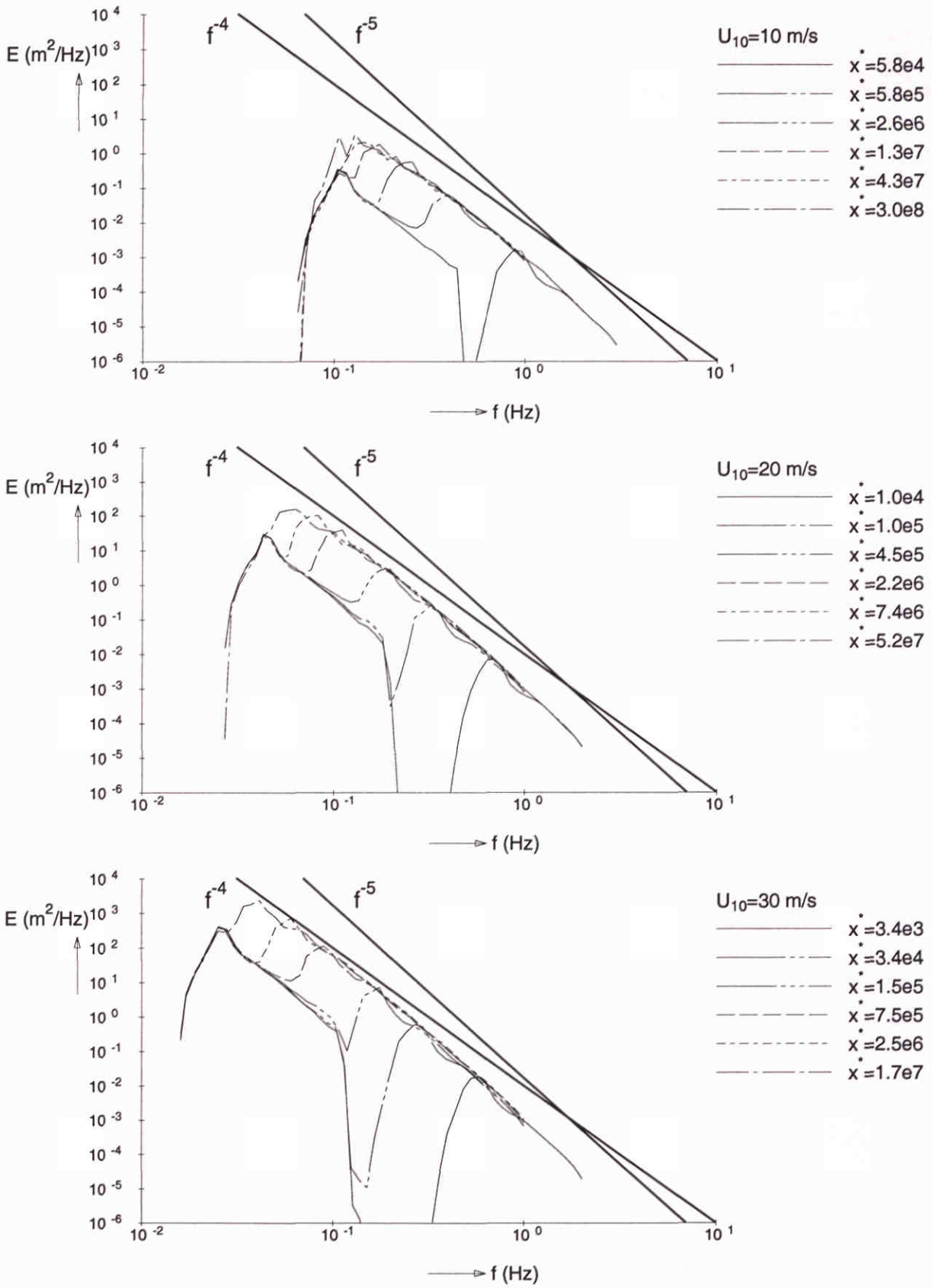


Wave spectra at different fetches
Extended Komen et al. (1984) expression with $\beta^0$
With incident low frequency waves

SWAN 40.00

WL | delft hydraulics

H3529

Fig. 5.15.e

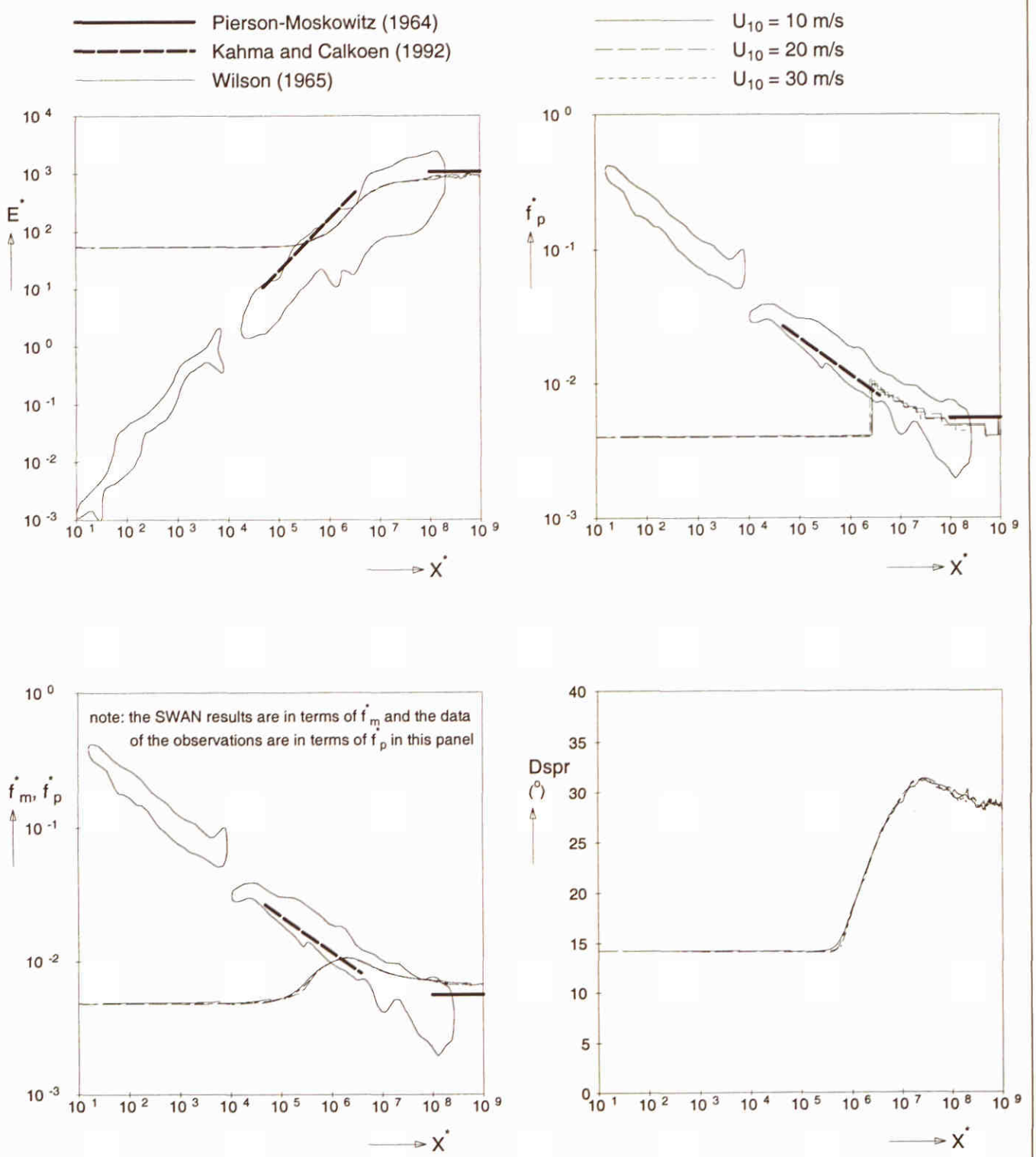


| | | |
|---|---|---|
| Fetch limited wave growth (deep water)<br>Extended Komen et al. (1984) expression with $\beta^{0.5}$<br>With incident low frequency waves | SWAN 40.00 | |
| WL \| delft hydraulics | H3529 | Fig. 5.16.a |

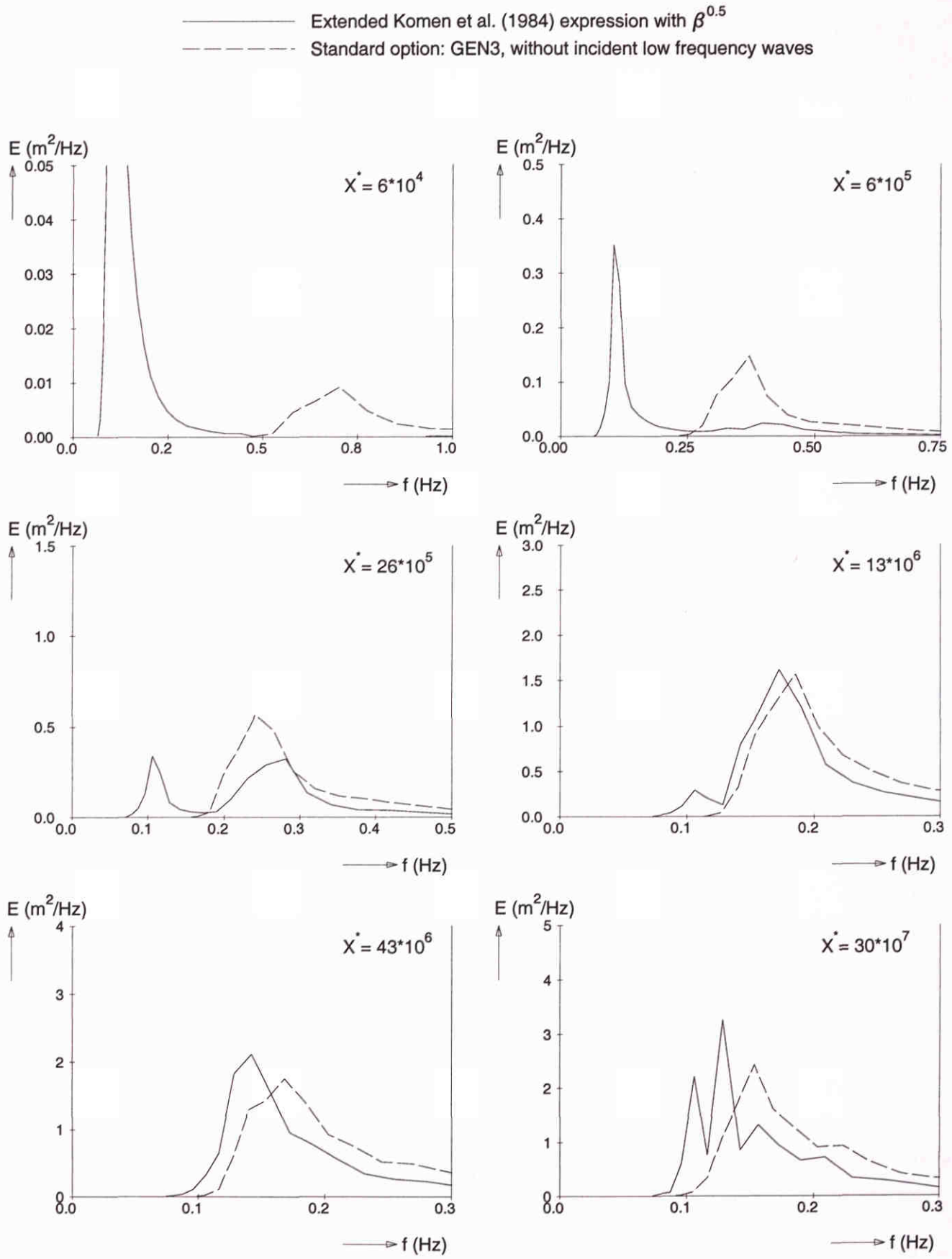


Frequency spectra at different locations ($U_{10}$ = 10 m/s)
With incident low frequency waves

SWAN 40.00

WL | delft hydraulics

H3529

Fig. 5.16.b

Extended Komen et al. (1984) expression with $\beta^{0.5}$

Standard option: GEN3, without incident low frequency waves

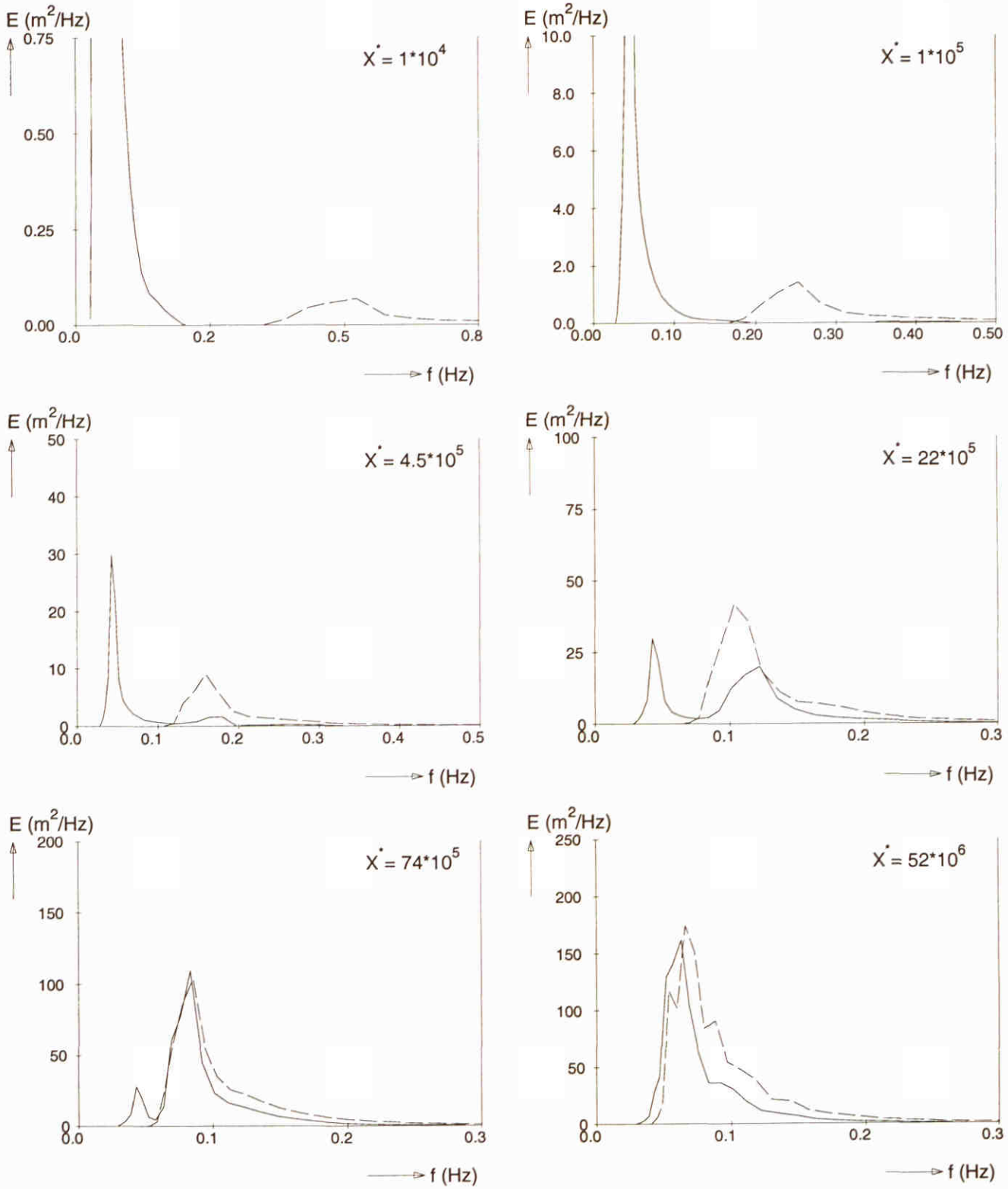


Frequency spectra at different locations ($U_{10}$ = 20 m/s)

With incident low frequency waves

SWAN 40.00

WL | delft hydraulics

H3529

Fig. 5.16.c

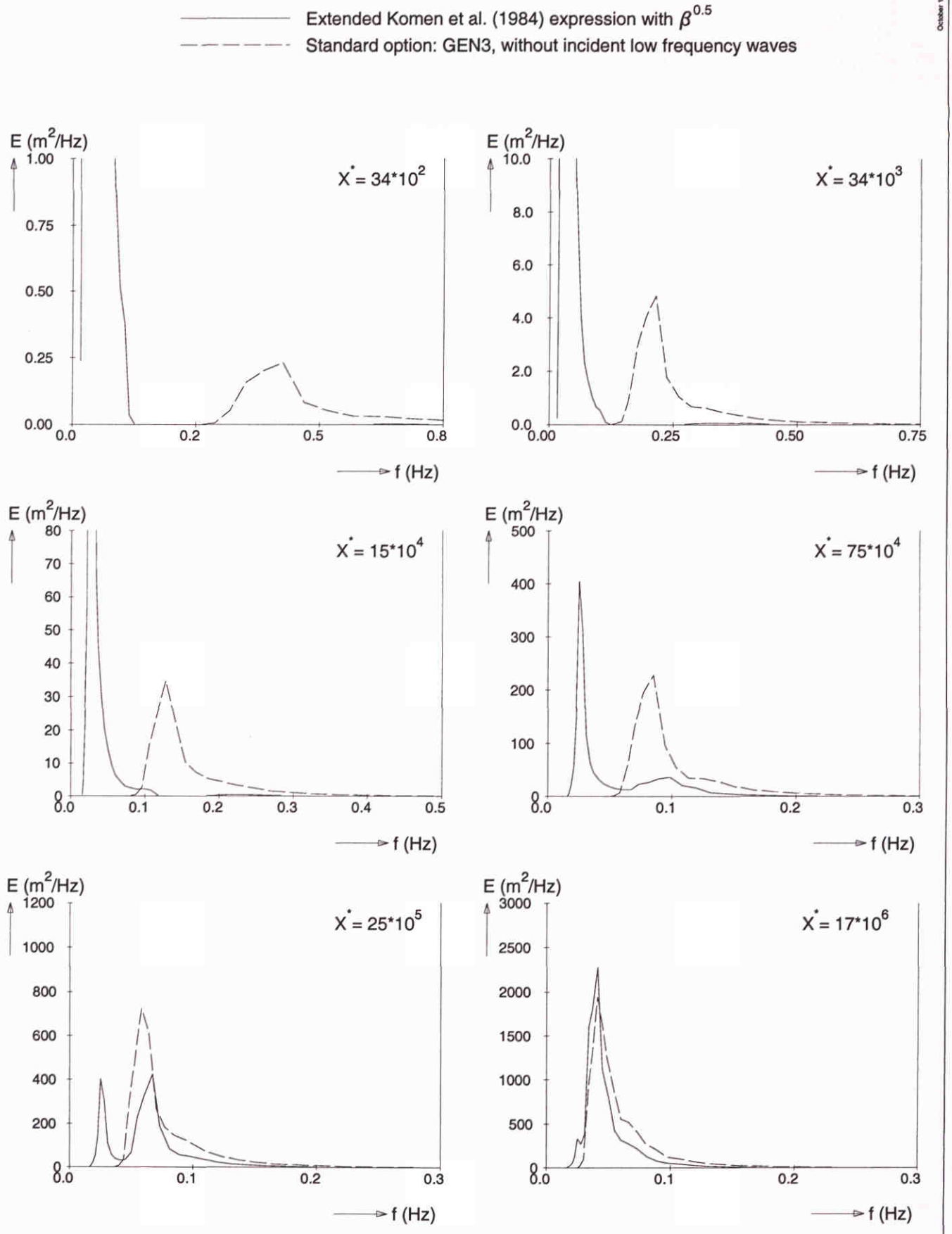


Frequency spectra at different locations ($U_{10}$ = 30 m/s)
With low frequency waves

SWAN 40.00

WL | delft hydraulics

H3529

Fig. 5.16.d

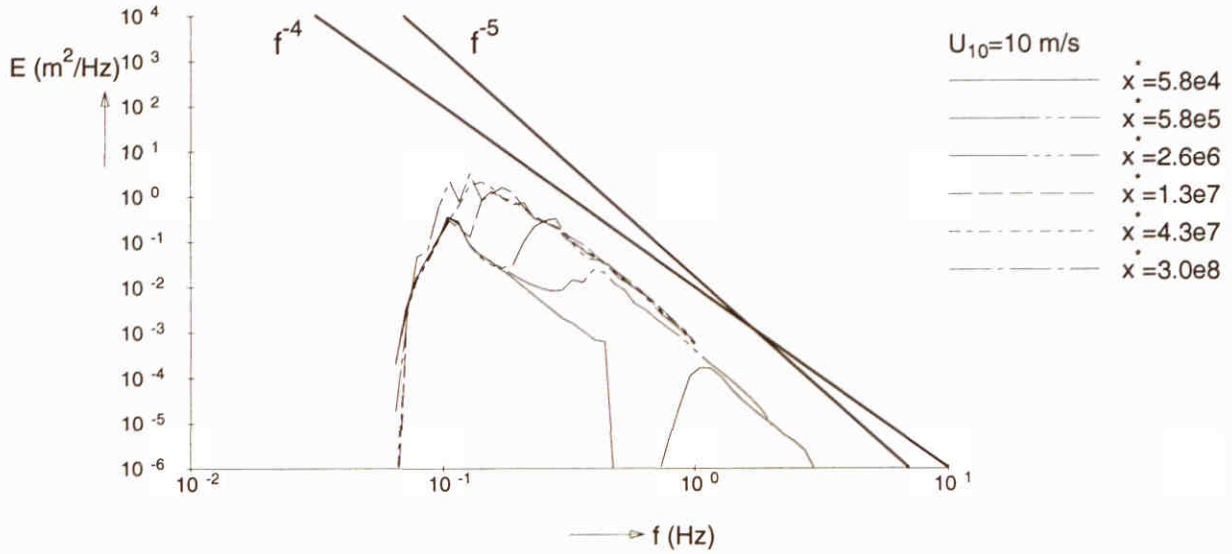


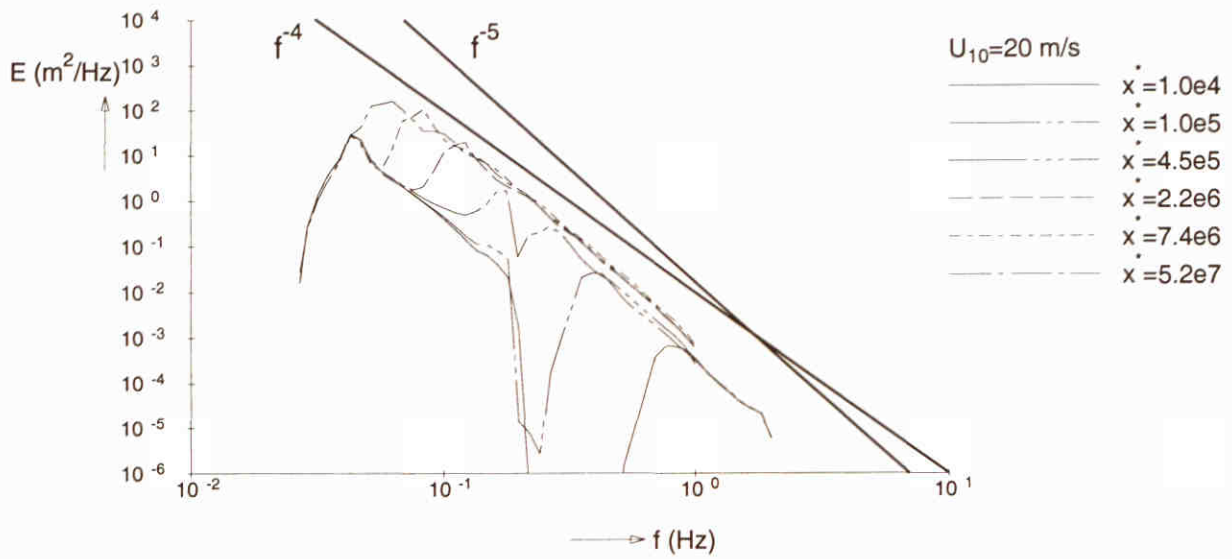


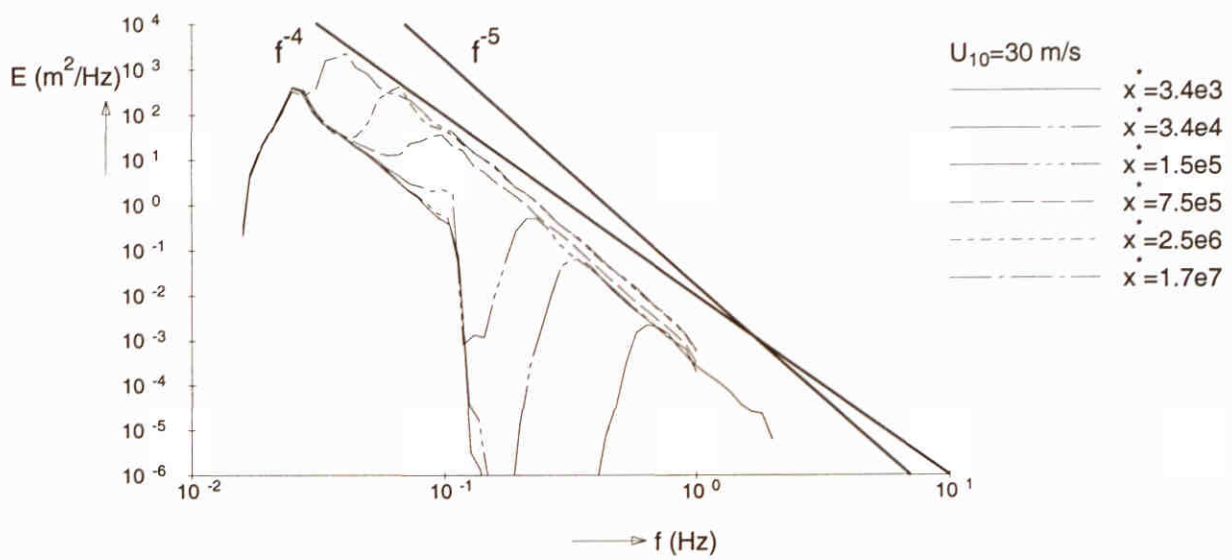


Wave spectra at different fetches
Extended Komen et al. (1984) expression with $\beta^{0.5}$
With incident low frequency waves

SWAN 40.00

WL | delft hydraulics

H3529

Fig. 5.16.e

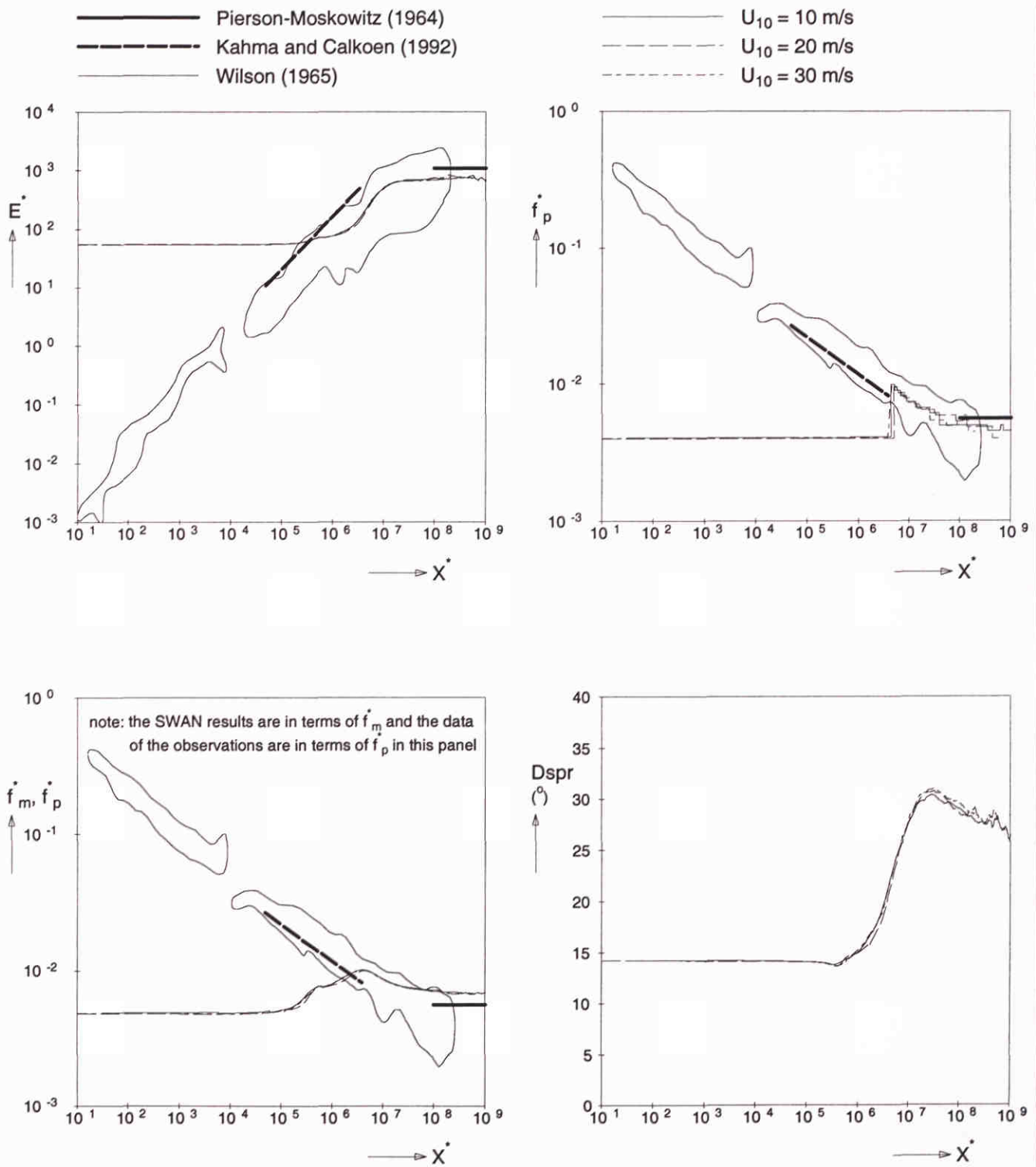


Fetch limited wave growth (deep water)
Extended Komen et al. (1984) expression with $\beta$ [1]
With incident low frequency waves

SWAN 40.00

WL | delft hydraulics

H3529

Fig. 5.17.a

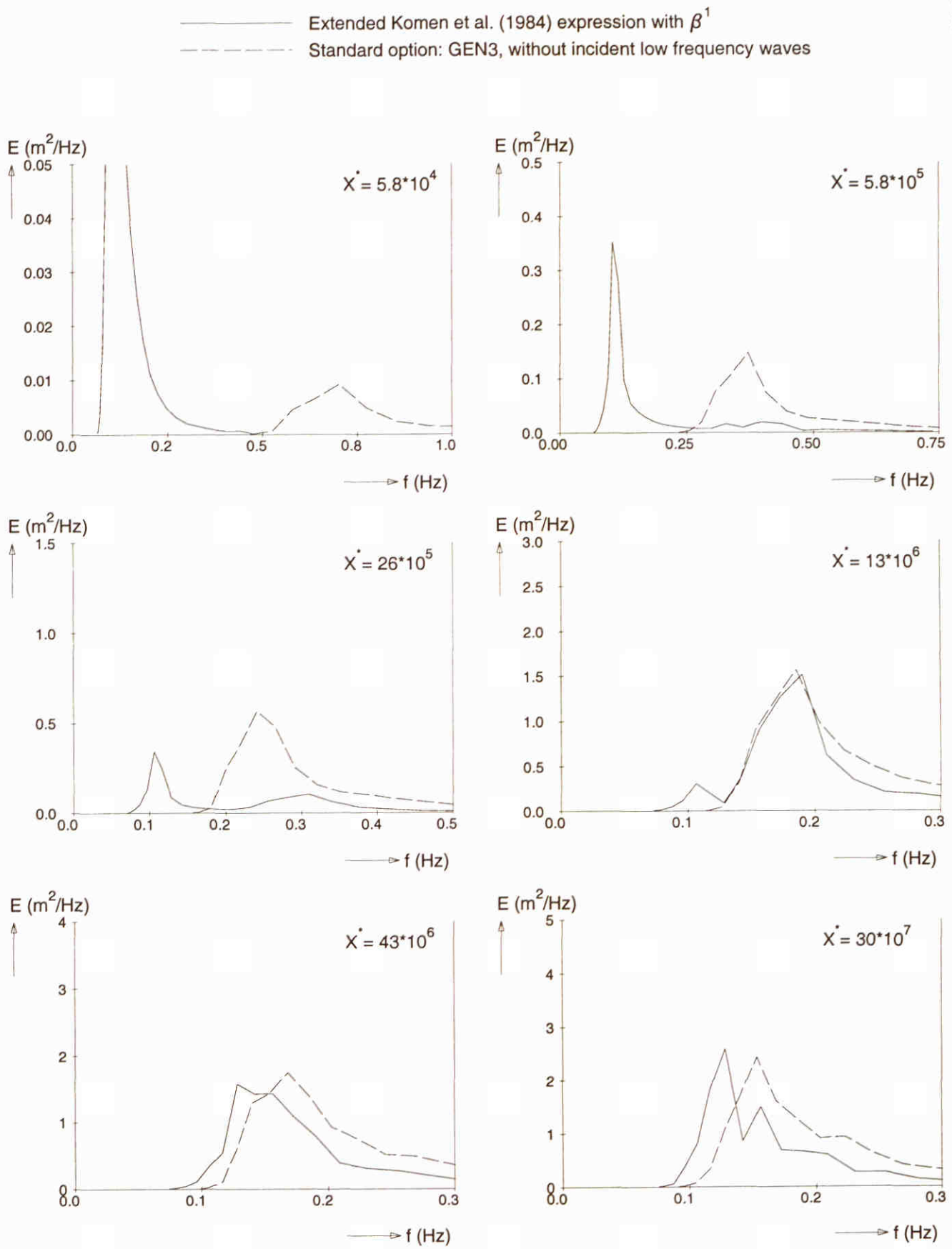


Frequency spectra at different locations ($U_{10}$ = 10 m/s)
With incident low frequency waves

SWAN 40.00

WL | delft hydraulics

H3529

Fig. 5.17.b

October 1998

Extended Komen et al. (1984) expression with $\beta^1$

Standard option: GEN3, without incident low frequency waves

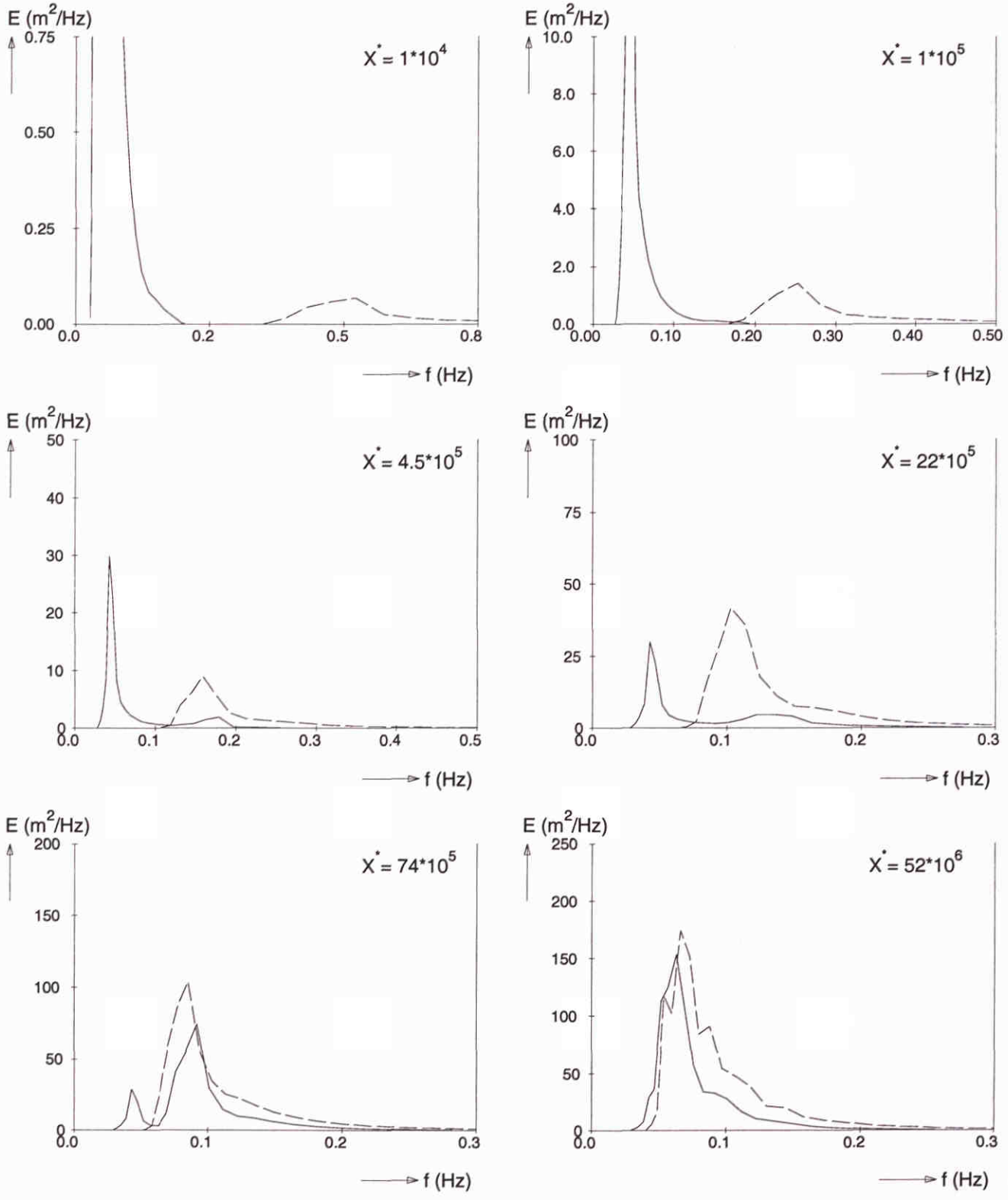


Frequency spectra at different locations ($U_{10}$ = 20 m/s)

With incident low frequency waves

SWAN 40.00

WL | delft hydraulics

H3529

Fig. 5.17.c

Frequency spectra at different locations ($U_{10}$ = 30 m/s)
With incident low frequency waves

SWAN 40.00

WL | delft hydraulics

H3529

Fig. 5.17.d

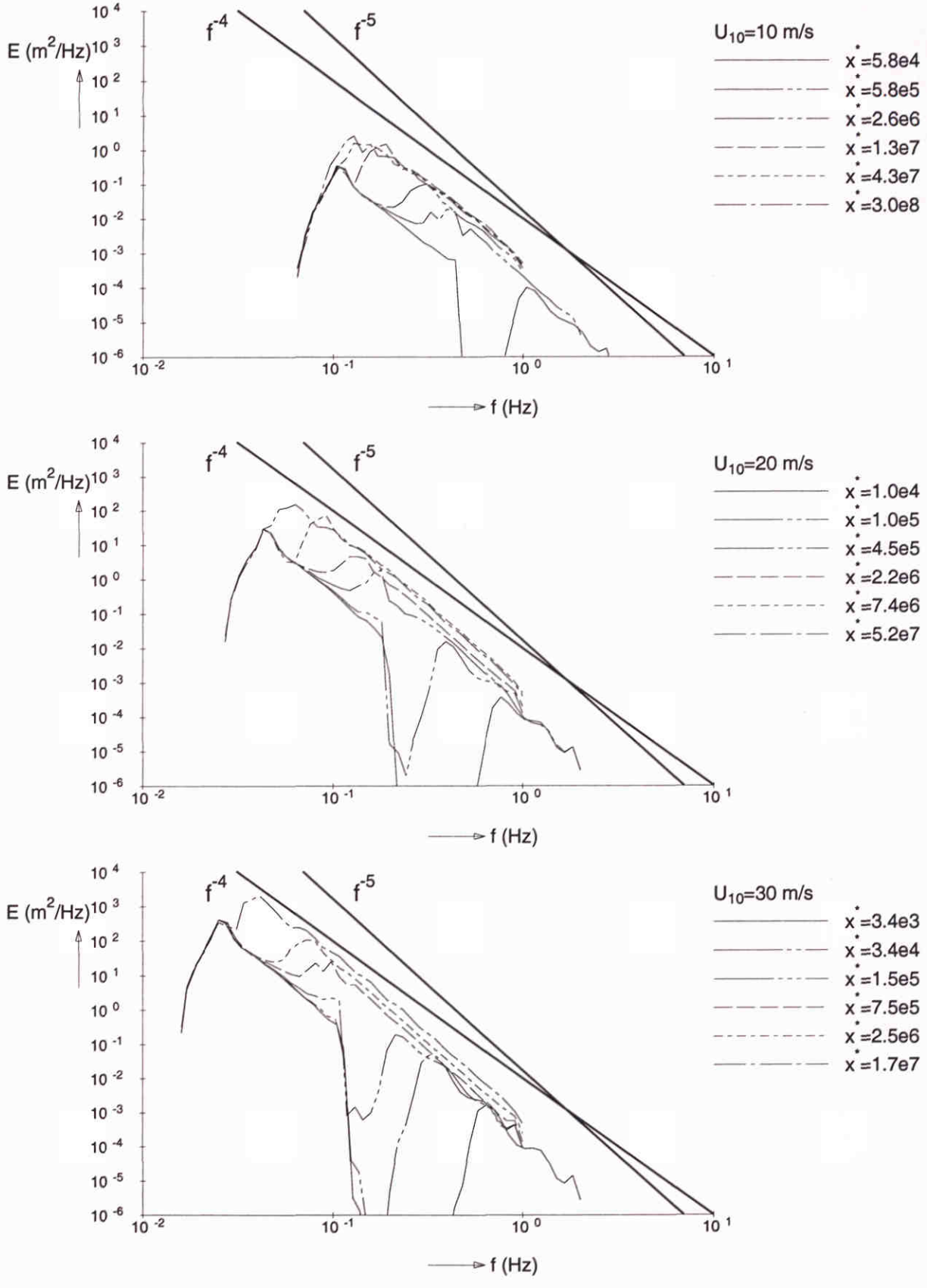


Wave spectra at different fetches

Extended Komen et al. (1984) expression with $\beta^1$

With incident low frequency waves

SWAN 40.00

WL | delft hydraulics

H3529

Fig. 5.17.e

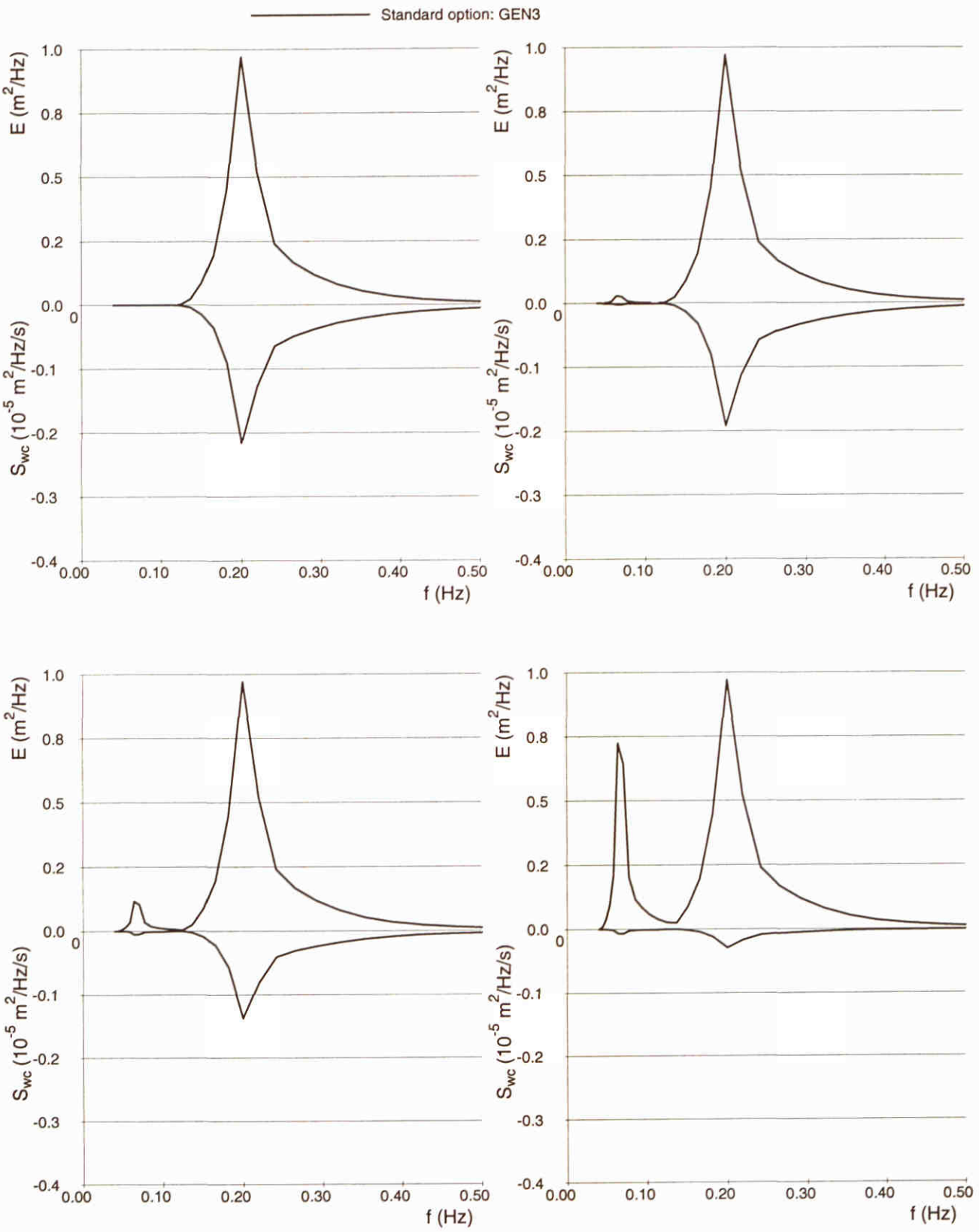


Whitecapping source term $S_{wc}$, for predescibed spectral shapes
Standard option: GEN3

SWAN 40.00

WL | delft hydraulics

H3529

Fig. 5.18

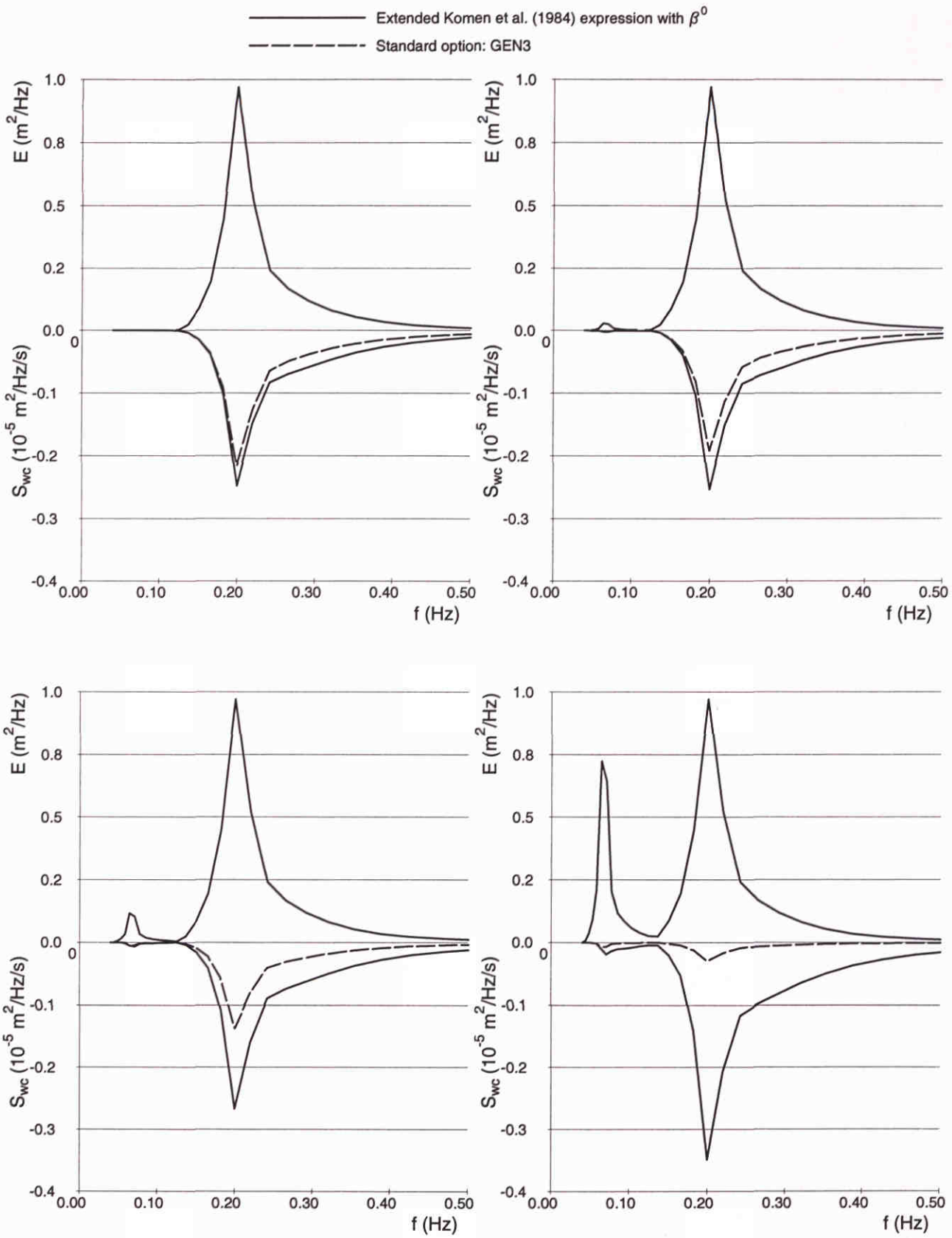


Whitecapping source term $S_{wc}$, for predescibed spectral shapes.
Extended Komen et al. (1984) expression with $\beta^0$

SWAN 40.00

WL | delft hydraulics

H3529

Fig. 5.19

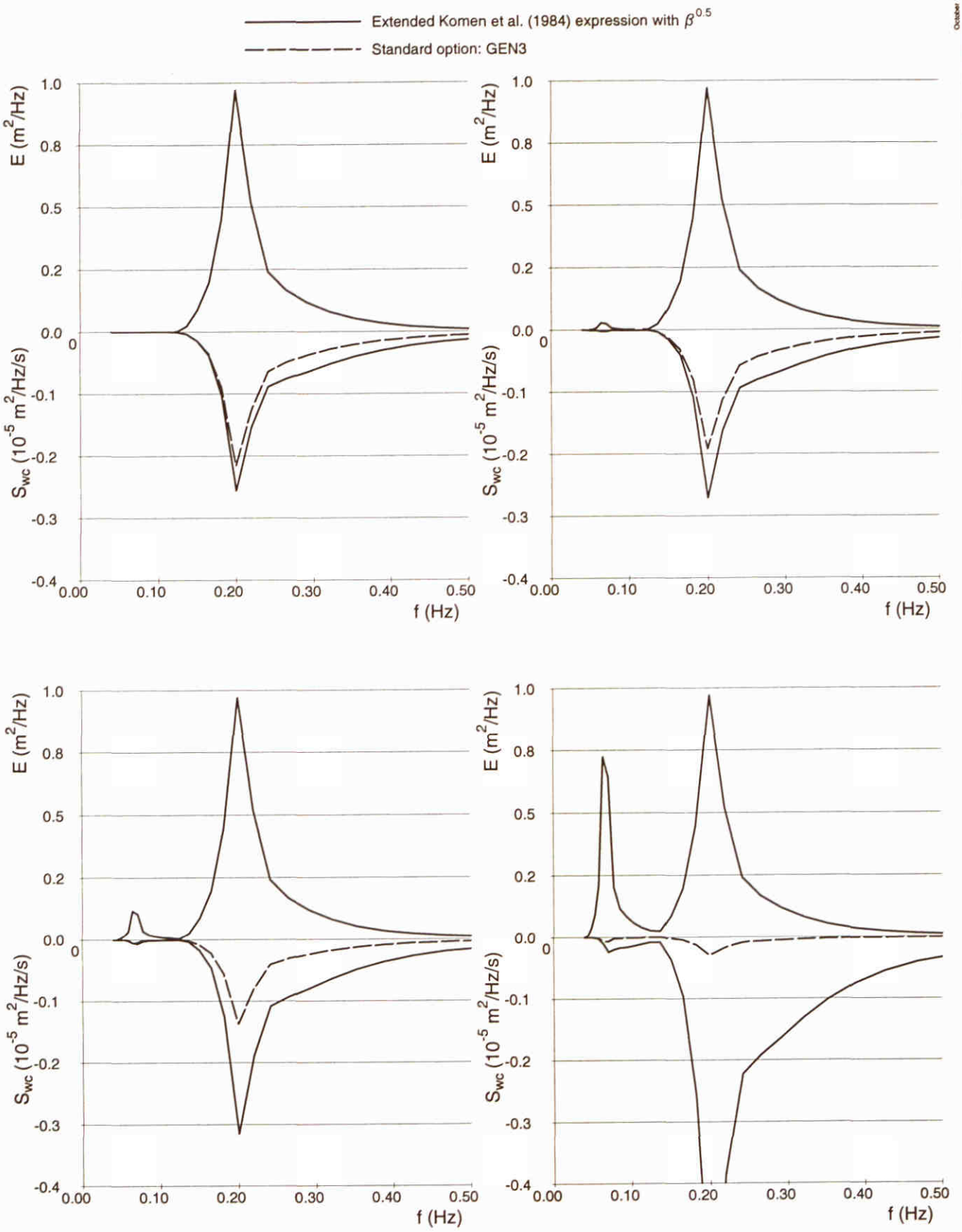


Whitecapping source term $S_{wc}$, for predescibed spectral shapes.
Extended Komen et al. (1984) expression with $\beta^{0.5}$

SWAN 40.00

WL | delft hydraulics

H3529

Fig. 5.20

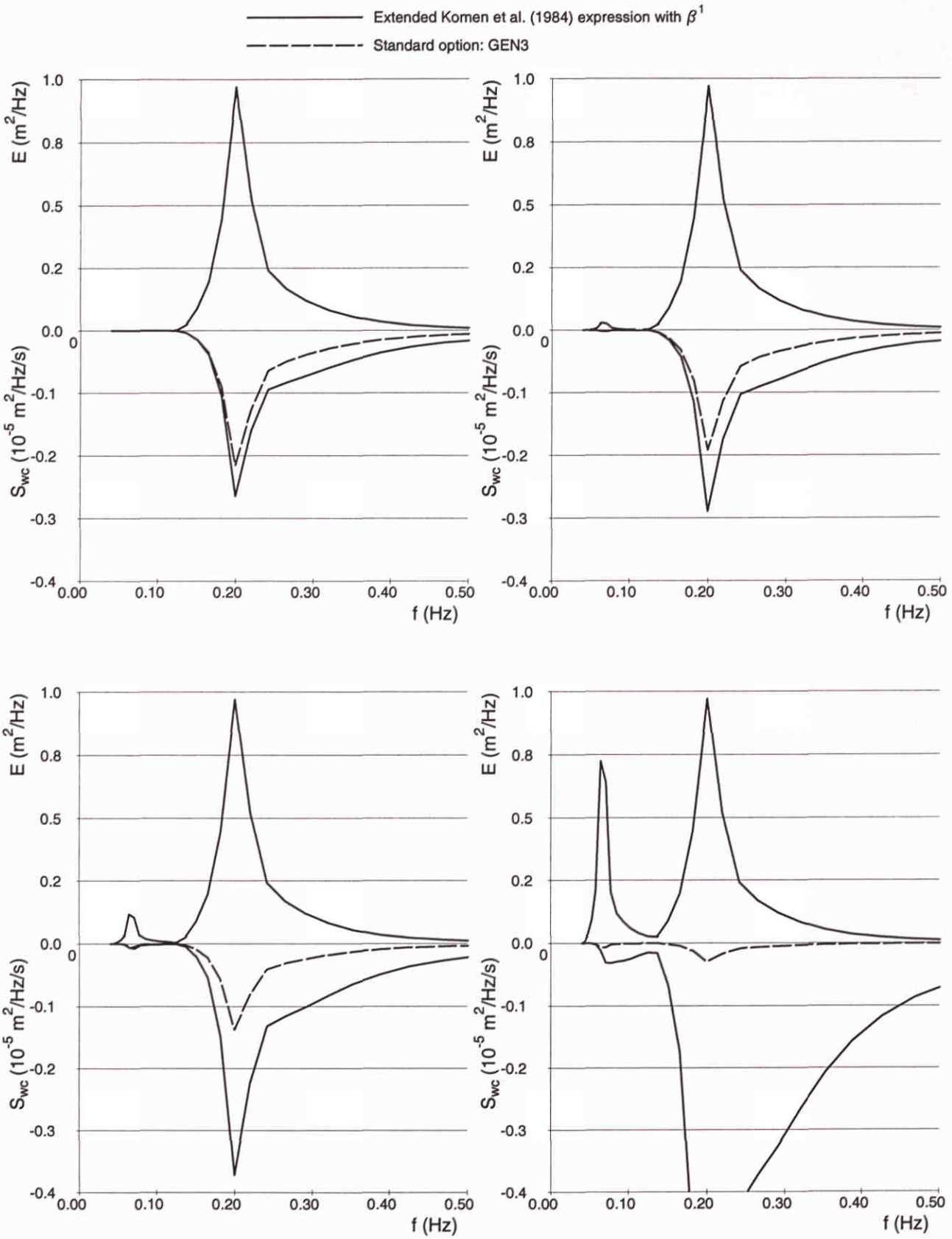


Whitecapping source term $S_{wc}$, for predescibed spectral shapes.
Extended Komen et al. (1984) expression with $\beta^1$

SWAN 40.00

WL | delft hydraulics

H3529

Fig. 5.21

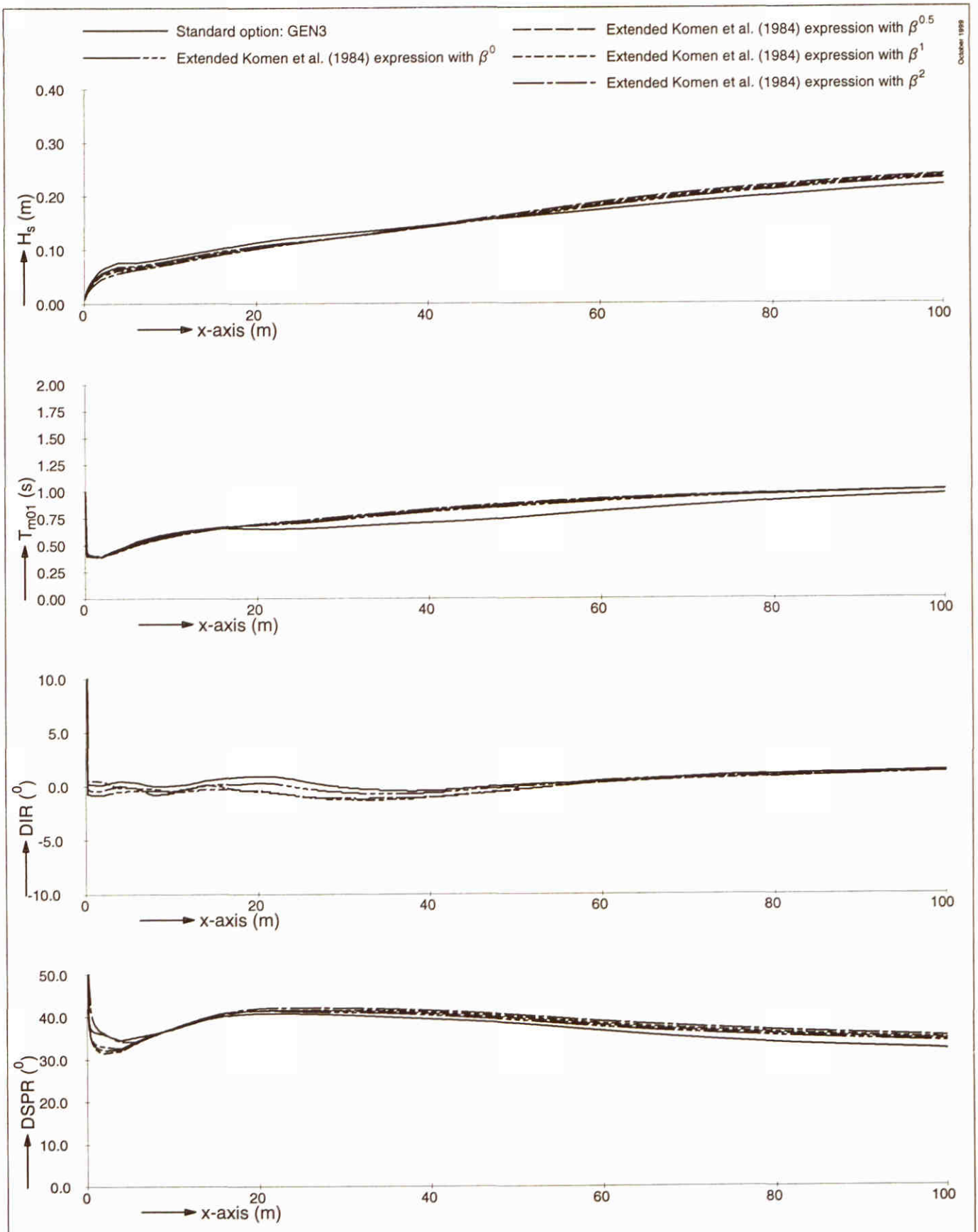


SWAN model results for Donelan (1987) experiment
Wind sea conditions without low frequency waves

SWAN 40.00

WL | delft hydraulics

H3529

Fig. 6.1.a

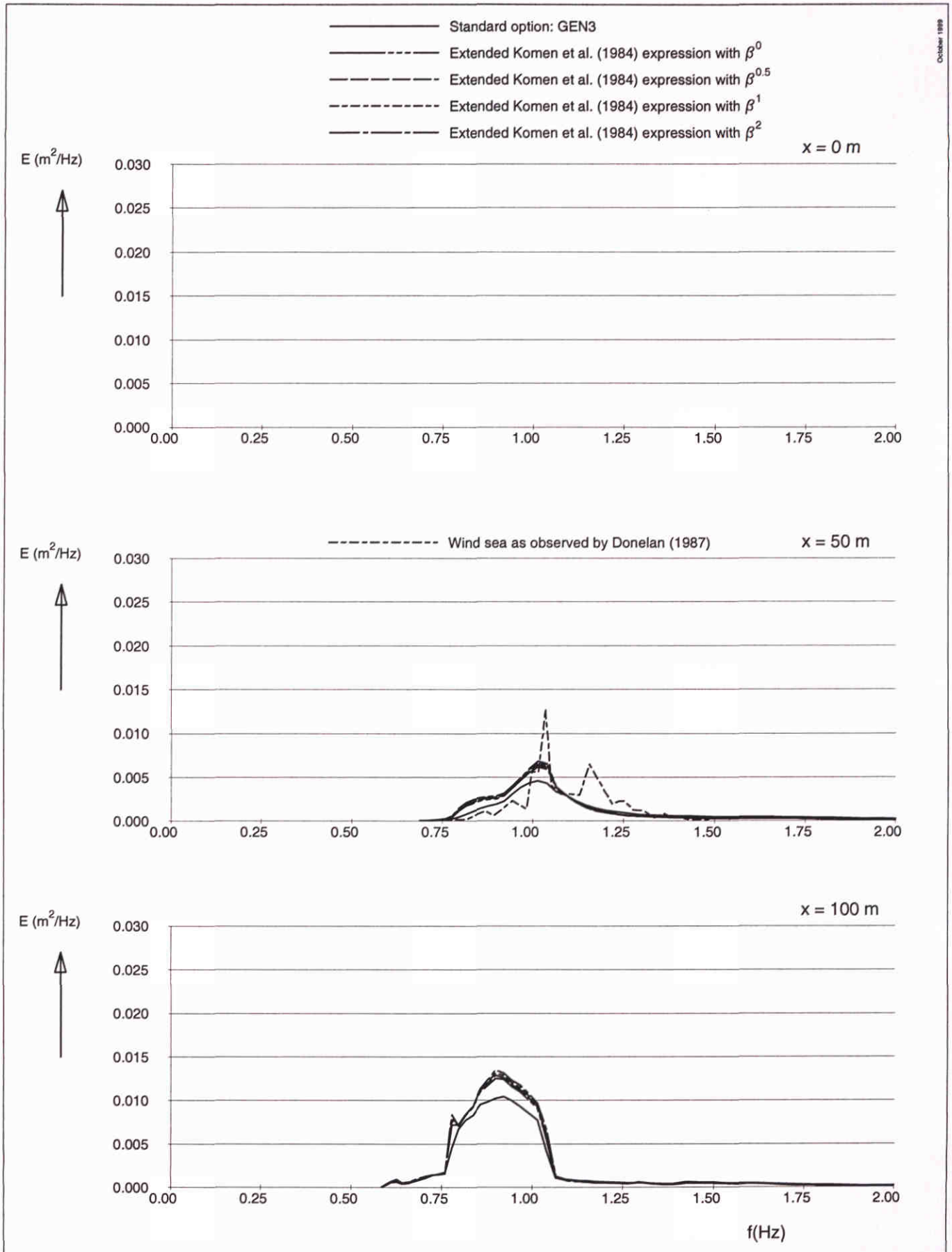


| | | |
|---|---|---|
| SWAN model results for Donelan (1987) experiment<br>Wind sea conditions without low frequency waves | SWAN 40.00 | |
| WL \| delft hydraulics | H3529 | Fig. 6.1.b |

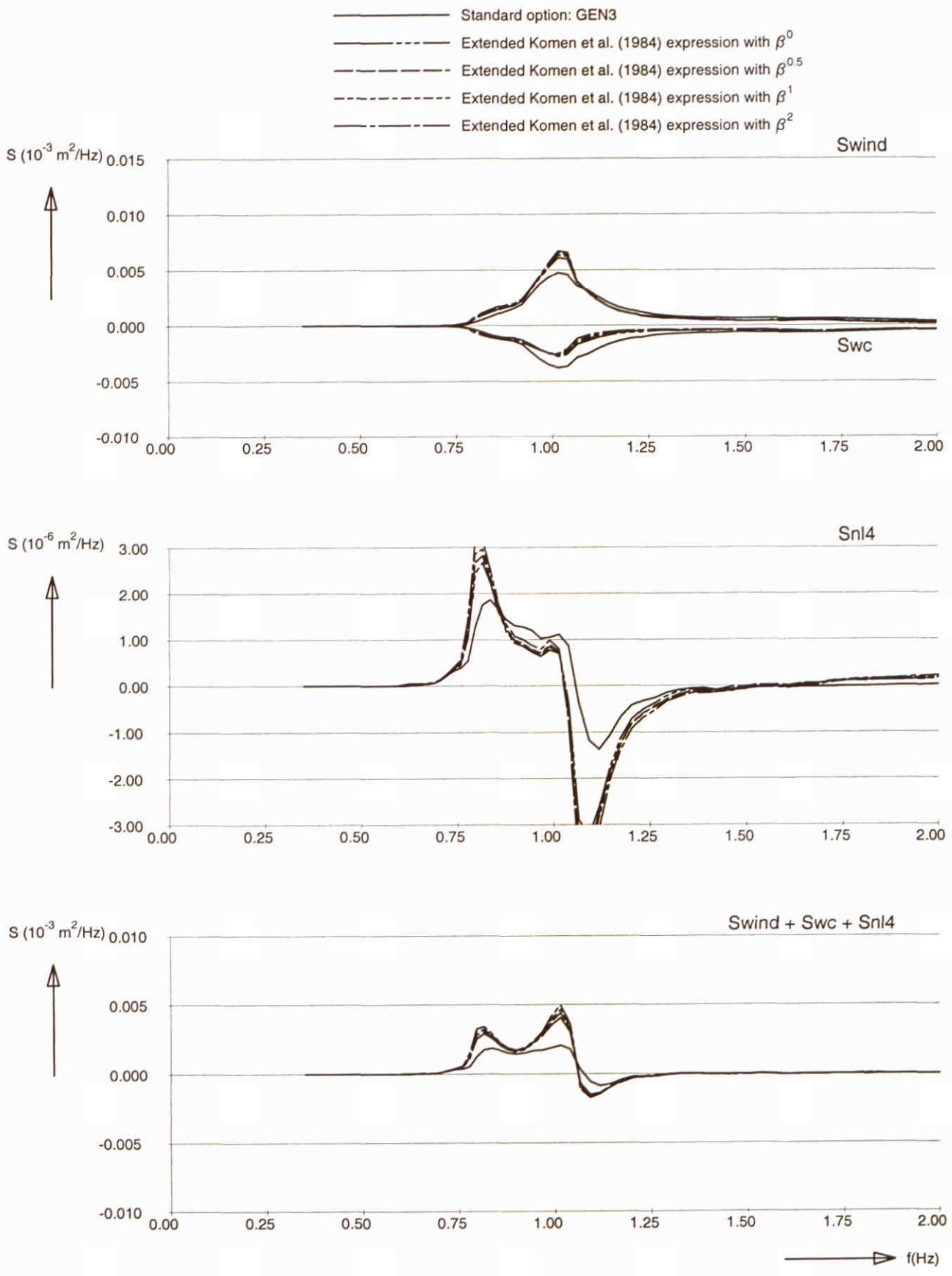


SWAN model results for Donelan (1987) experiment
Source terms at x = 50 m
Wind sea conditions without low frequency waves

SWAN 40.00

WL | delft hydraulics

H3529

Fig. 6.1.c

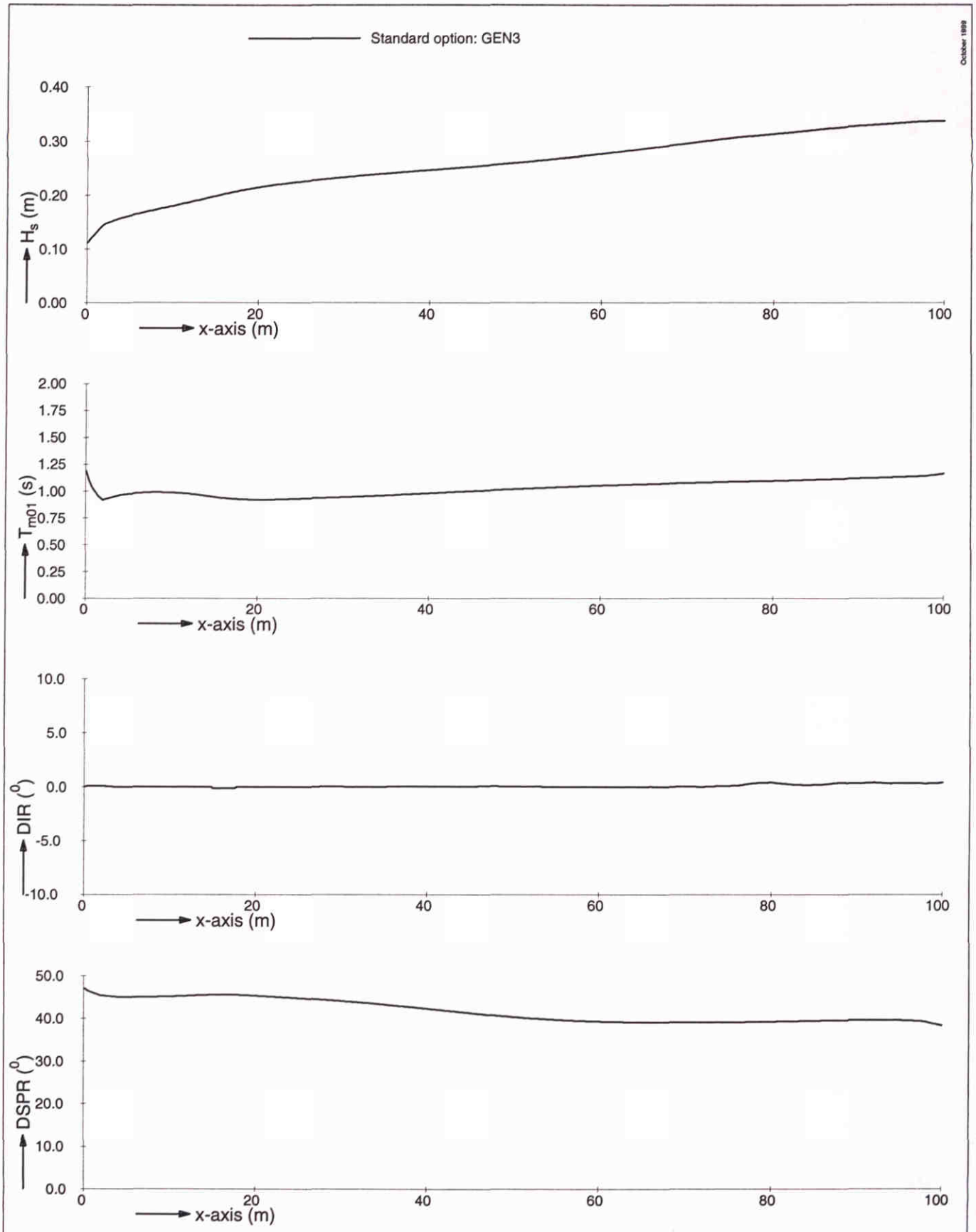


SWAN model results for Donelan (1987) experiment
Standard option: GEN3

SWAN 40.00

WL | delft hydraulics

H3529

Fig. 6.2.a

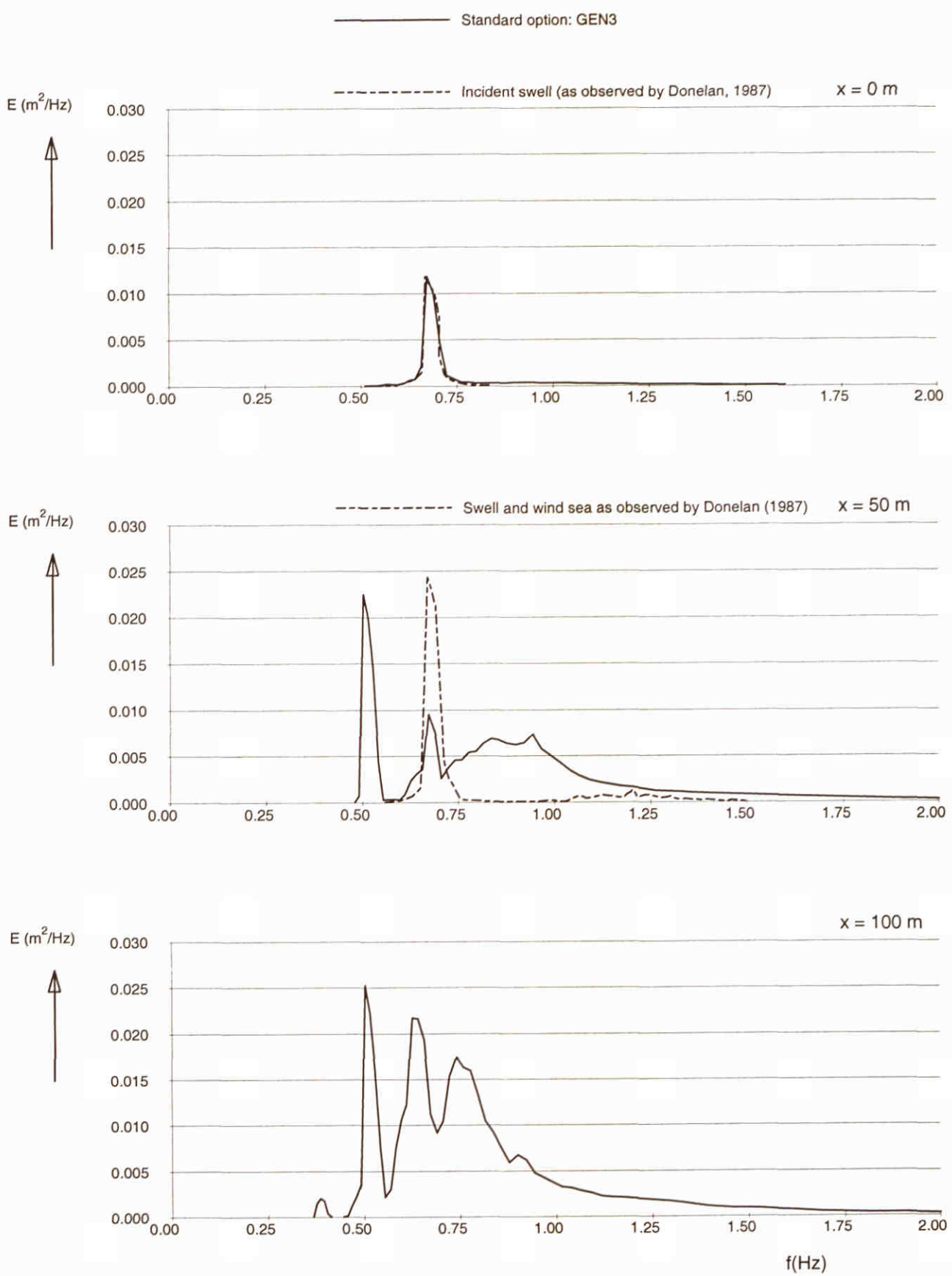


SWAN model results for Donelan (1987) experiment
Computed wave spectra with standard option: GEN3

SWAN 40.00

WL | delft hydraulics

H3529

Fig. 6.2.b

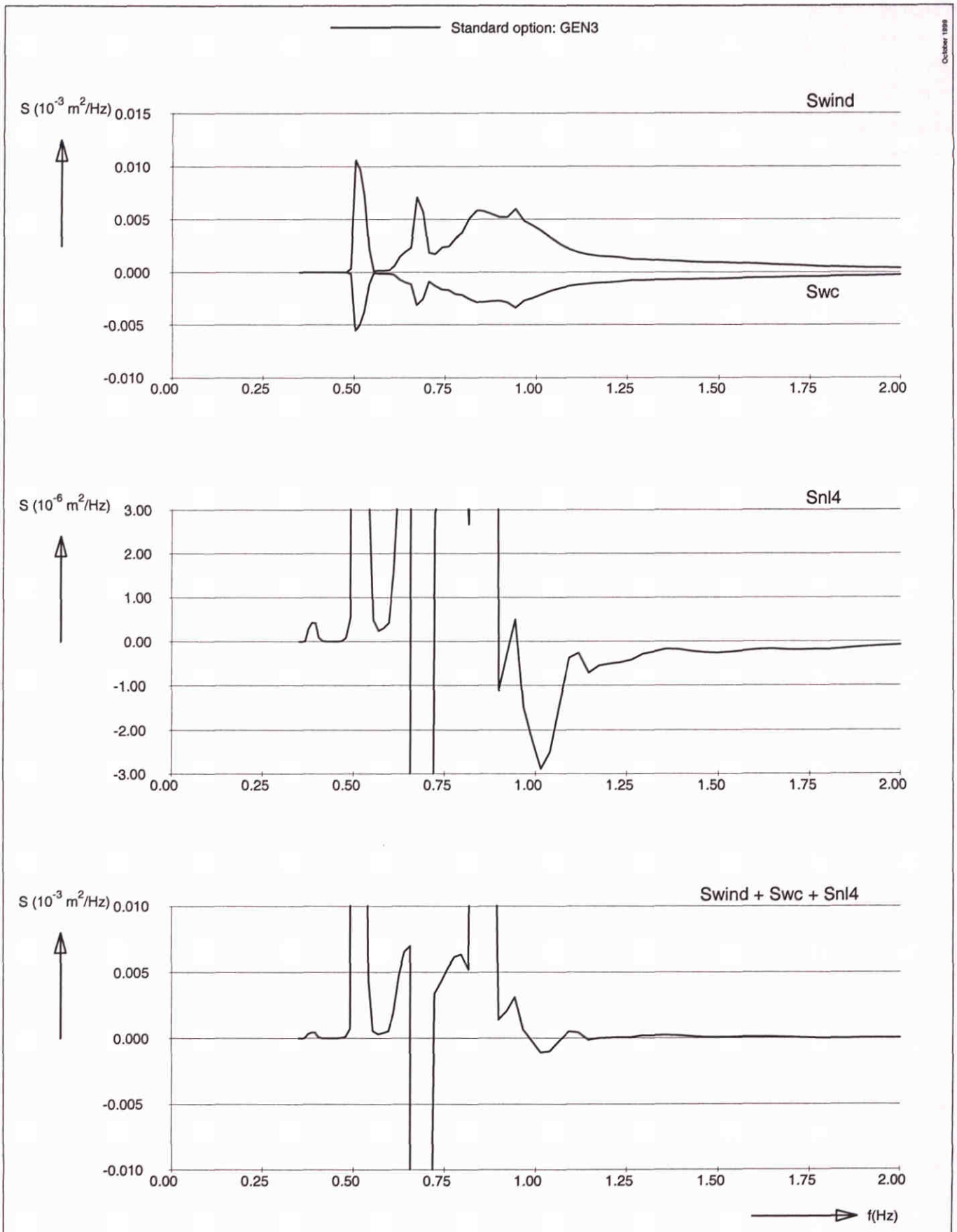


SWAN model results for Donelan (1987) experiment
Source terms at x = 50 m

SWAN 40.00

WL | delft hydraulics

H3529

Fig. 6.2.c

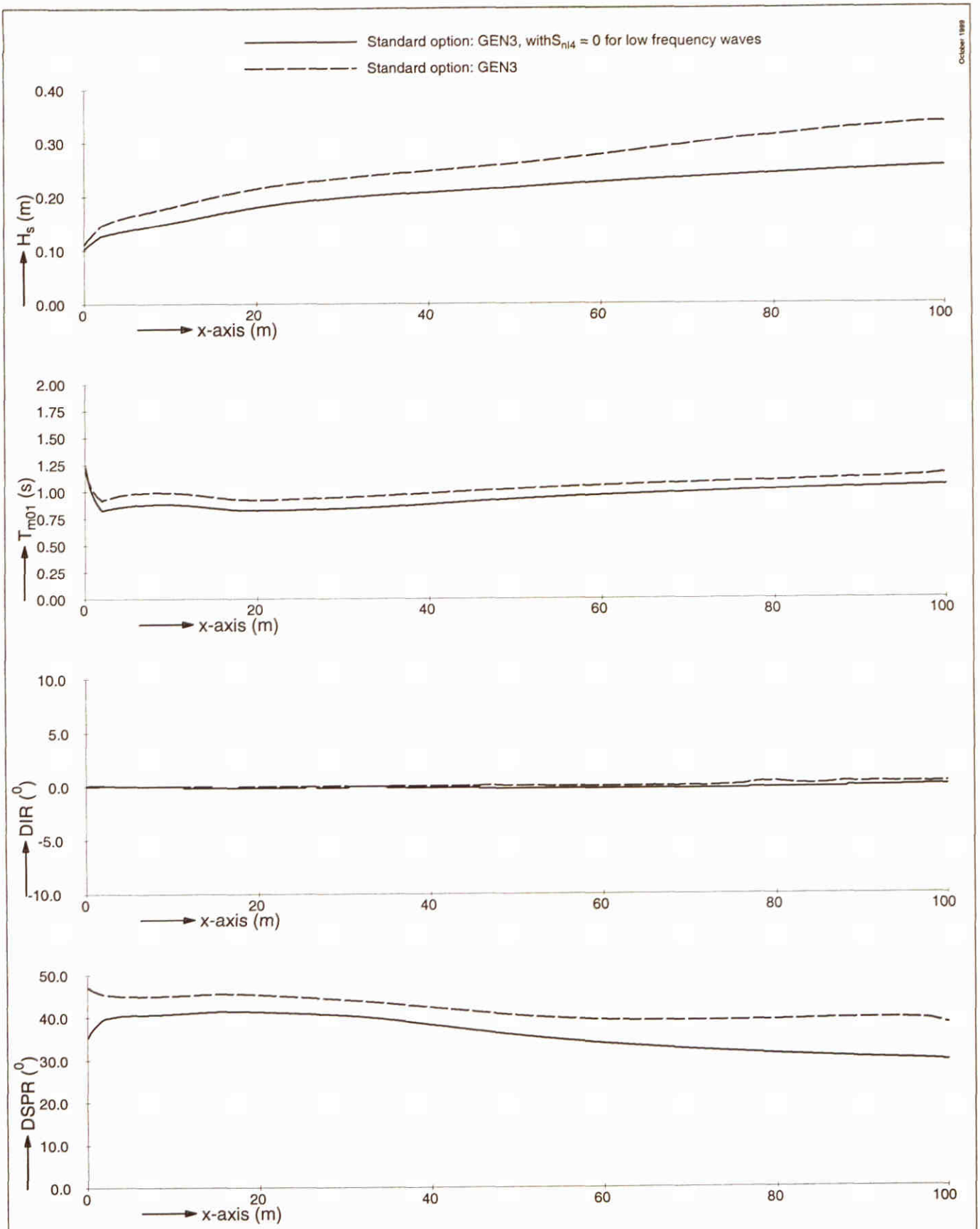


SWAN model results for Donelan (1987) experiment
Standard option: GEN3

SWAN 40.00

WL | delft hydraulics

H3529

Fig. 6.3.a

October 1998

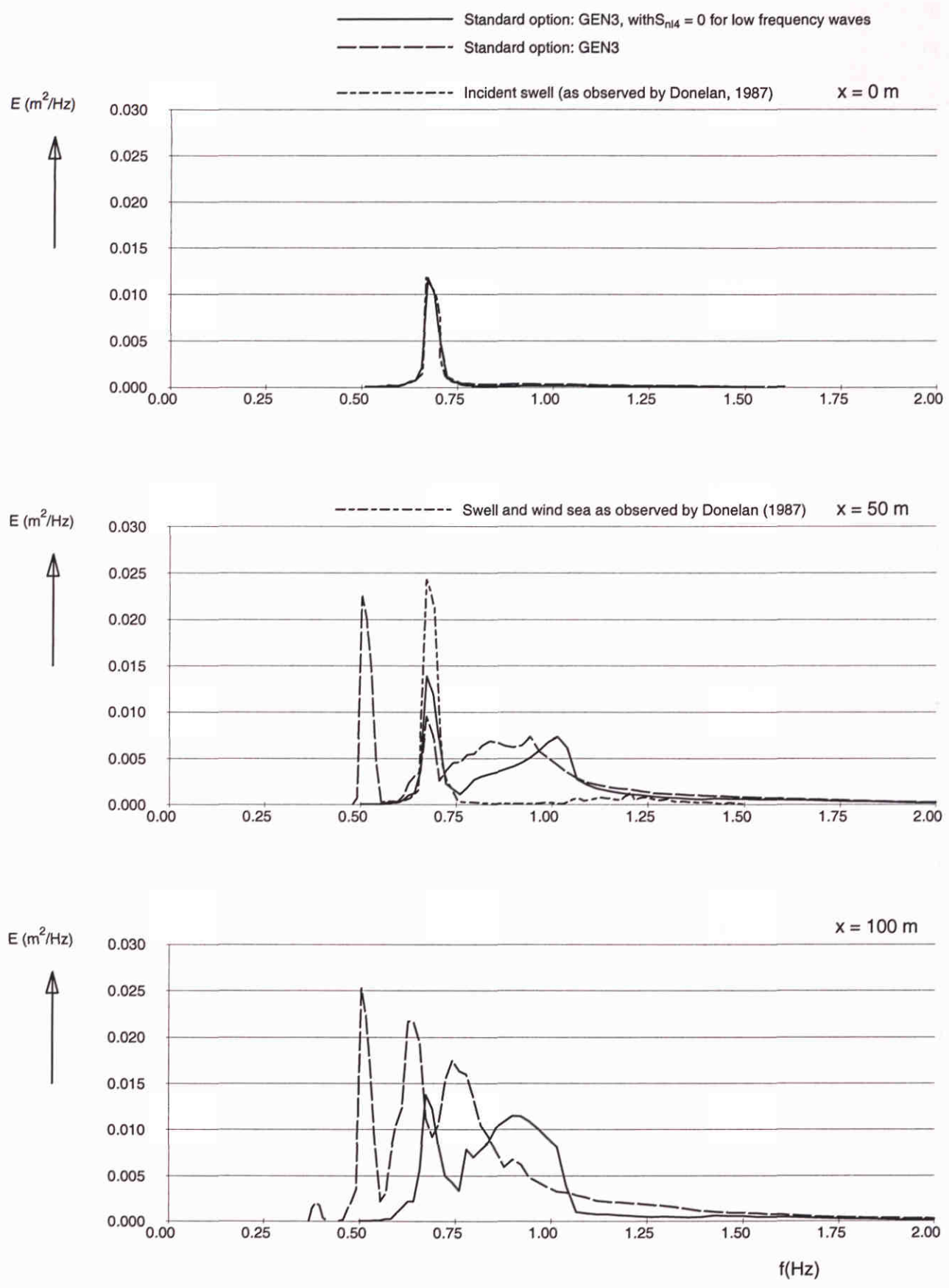


| | | |
|---|---|---|
| SWAN model results for Donelan (1987) experiment<br>Computed waves spectra with standard option: GEN3 | SWAN 40.00 | |
| WL \| delft hydraulics | H3529 | Fig. 6.3.b |

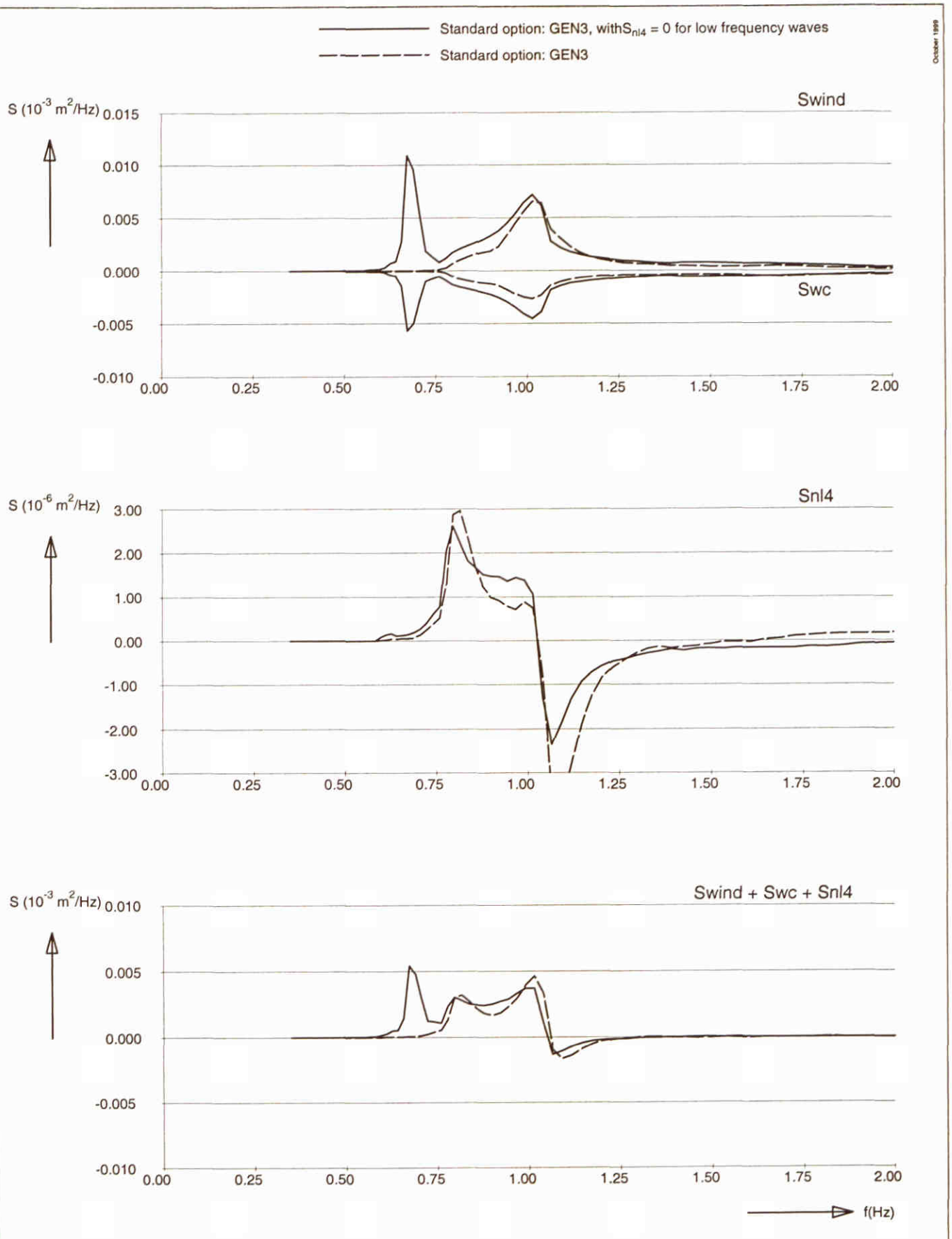


| | | |
|---|---|---|
| SWAN model results for Donelan (1987) experiment<br>Source terms at x = 50 m | SWAN 40.00 | |
| WL \| delft hydraulics | H3529 | Fig. 6.3.c |

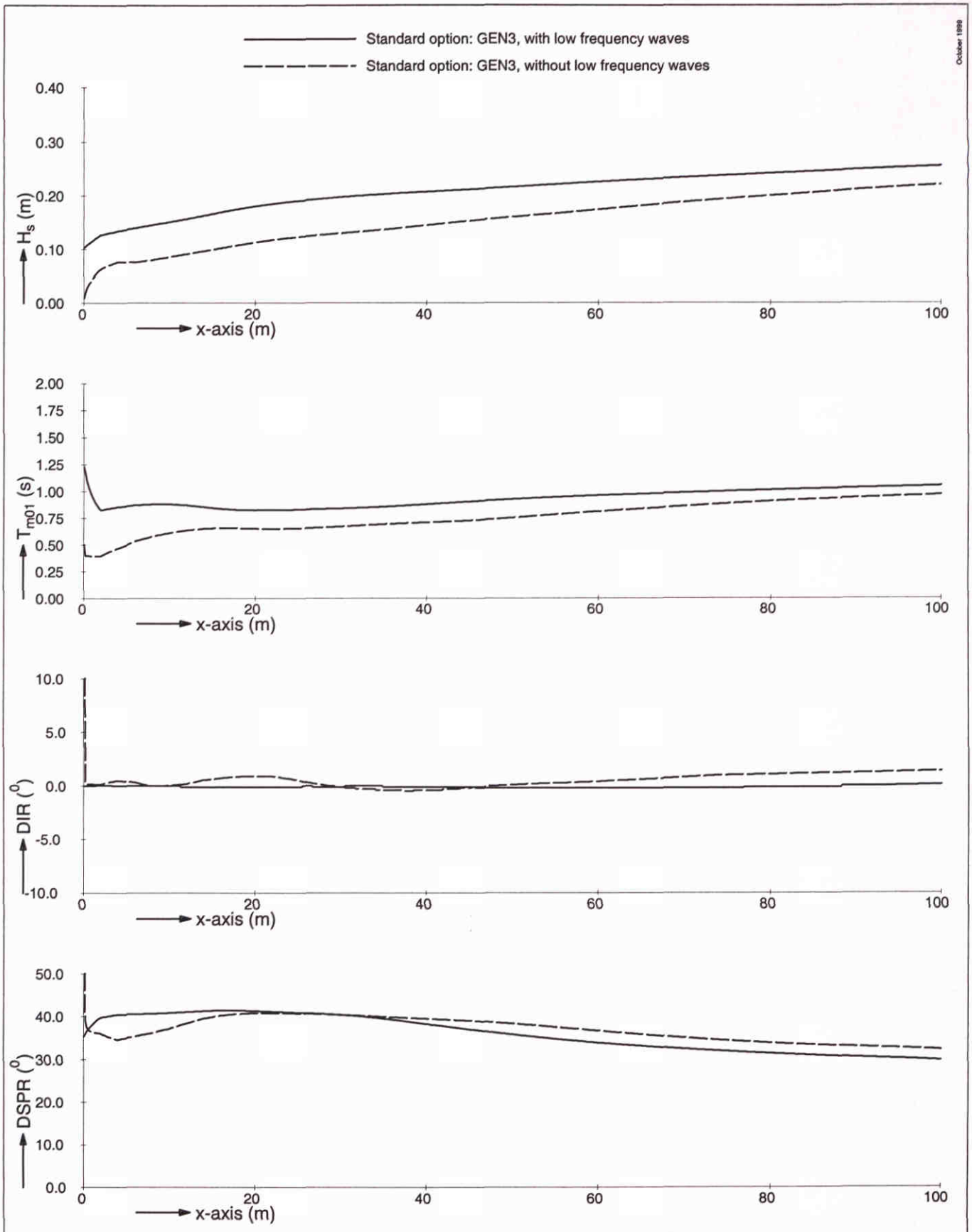


SWAN model results for Donelan (1987) experiment
Standard option: GEN3

SWAN 40.00

WL | delft hydraulics

H3529

Fig. 6.4.a

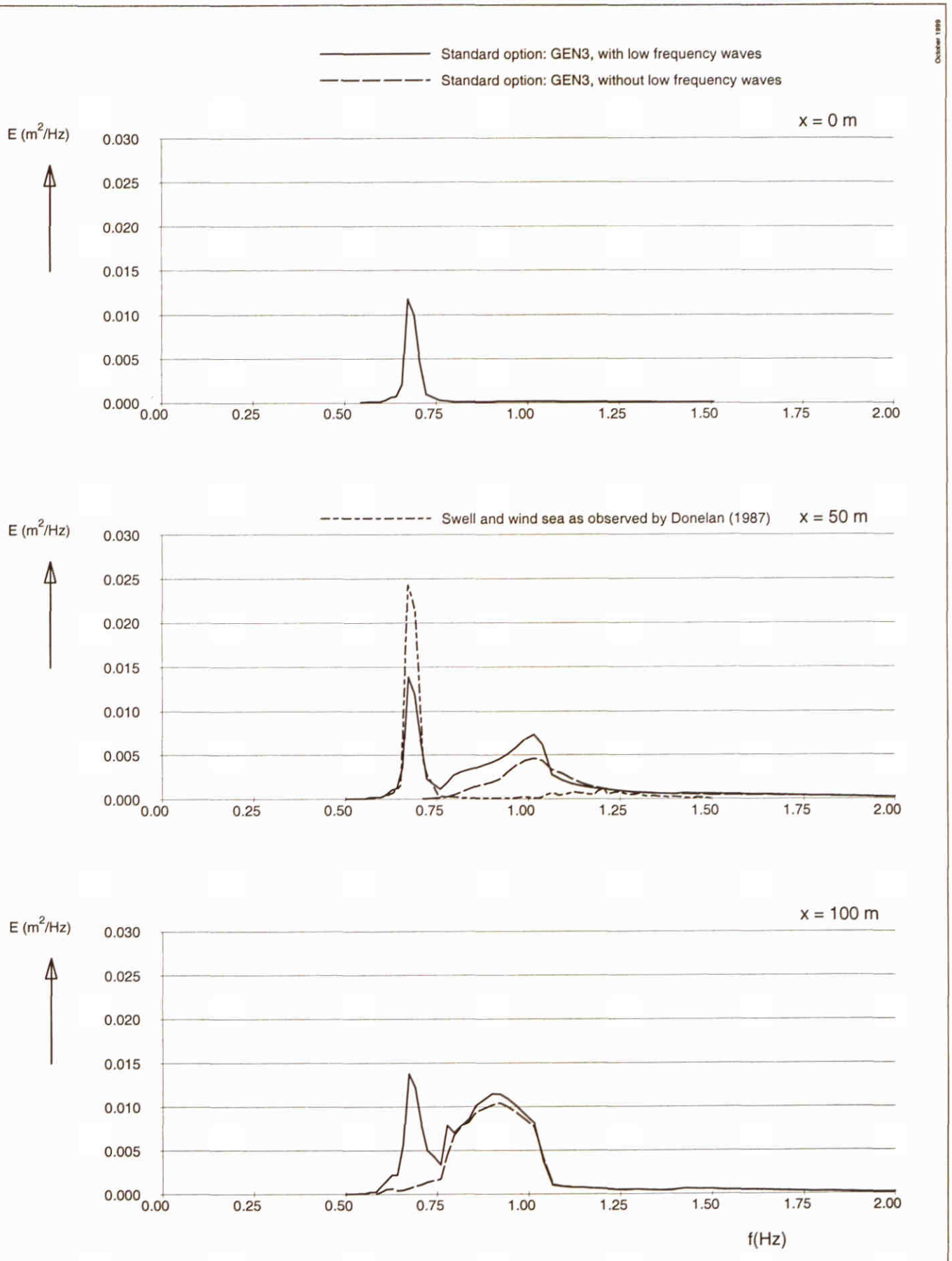


SWAN model results for Donelan (1987) experiment
Computed wave spectra with standard option: GEN3

SWAN 40.00

WL | delft hydraulics

H3529

Fig. 6.4.b

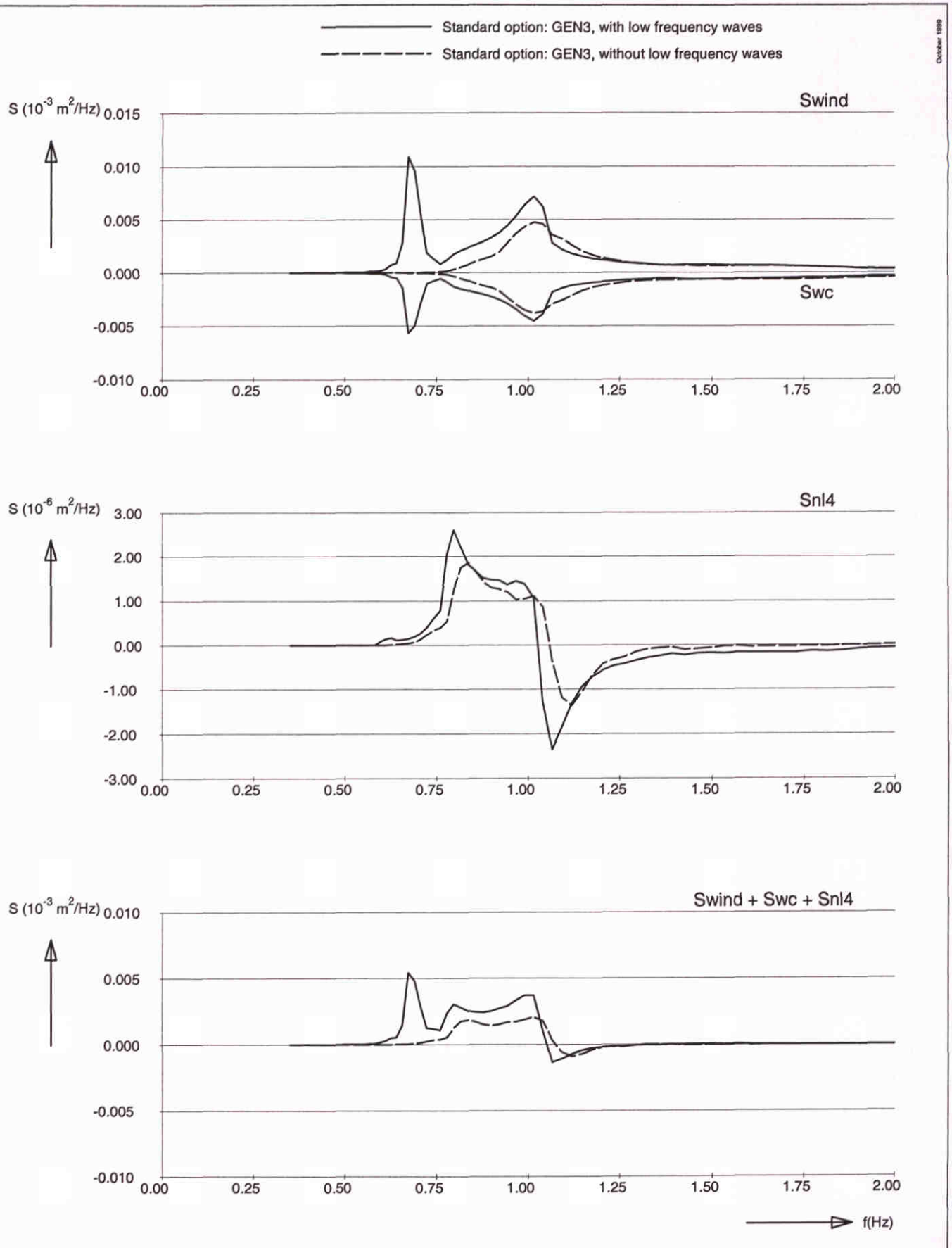


| | | |
|---|---|---|
| SWAN model results for Donelan (1987) experiment<br>Source terms at x = 50 m | SWAN 40.00 | |
| WL \| delft hydraulics | H3529 | Fig. 6.4.c |

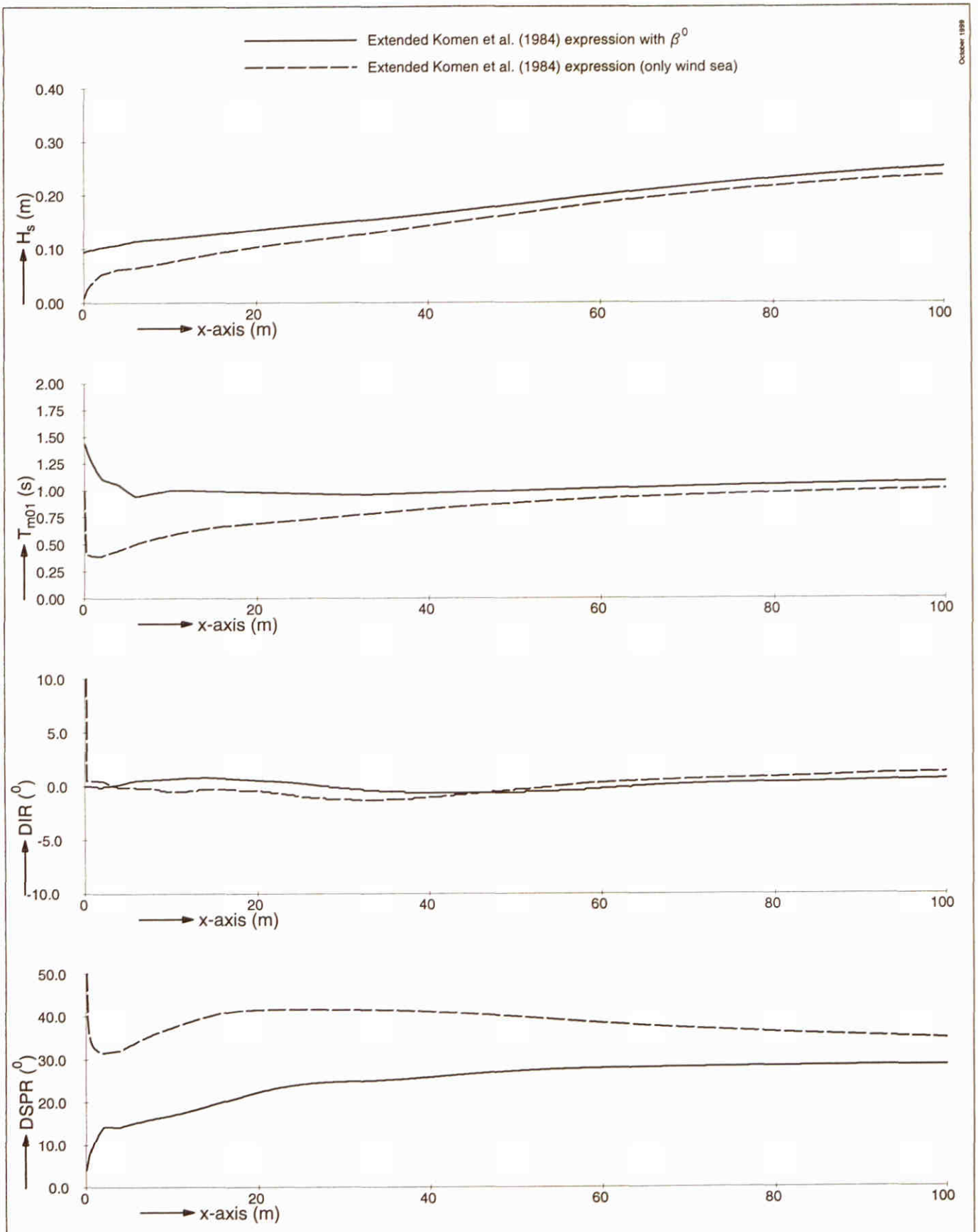


SWAN model results for Donelan (1987) experiment
Extended Komen et al. (1984) expression with $\beta^0$

SWAN 40.00

WL | delft hydraulics

H3529

Fig. 6.5.a

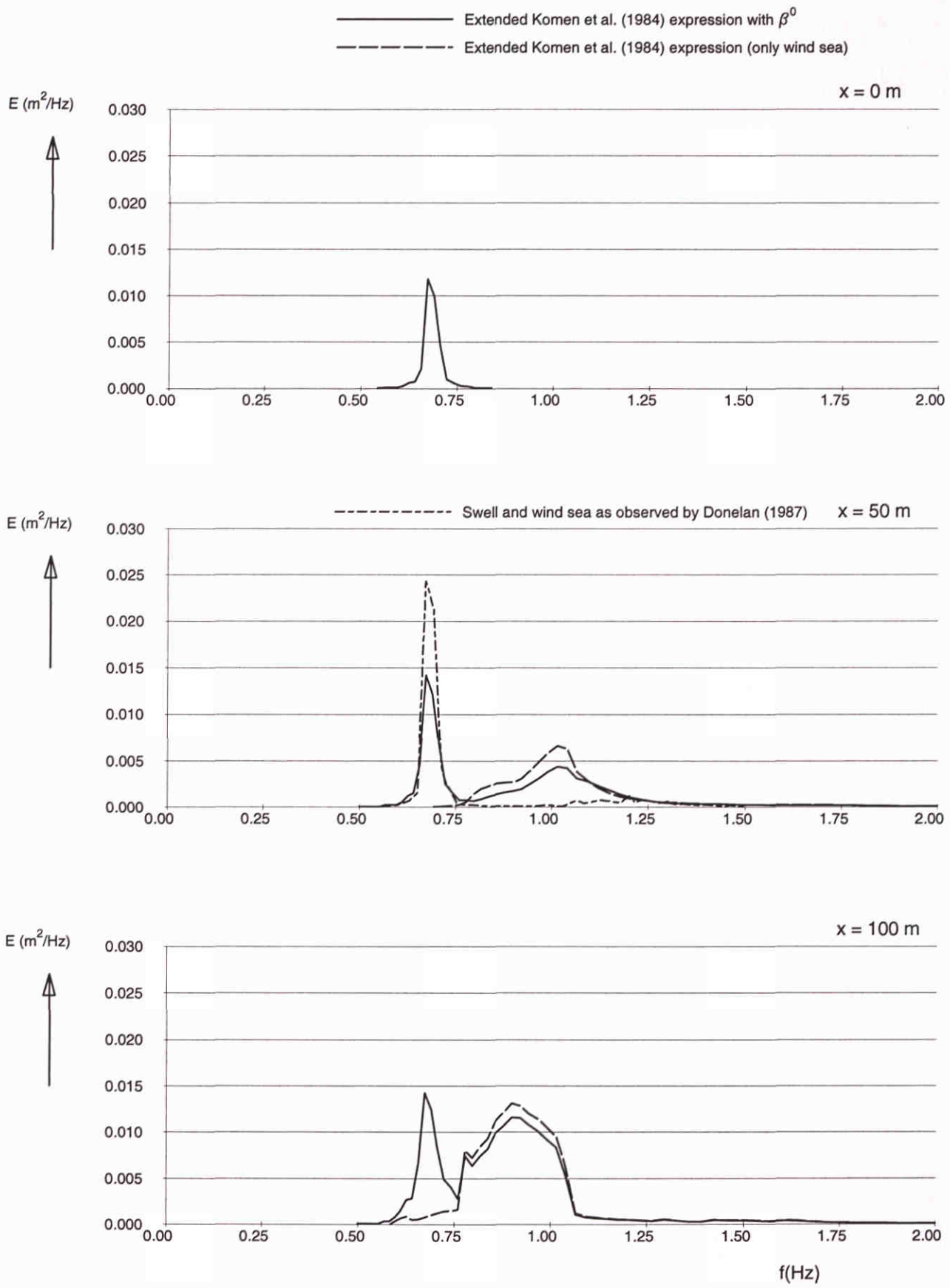


| | | |
|---|---|---|
| SWAN model results for Donelan (1987) experiment<br>Computed wave spectra with<br>extended Komen et al. (1984) expression with $\beta^0$ | SWAN 40.00 | |
| WL \| delft hydraulics | H3529 | Fig. 6.5.b |

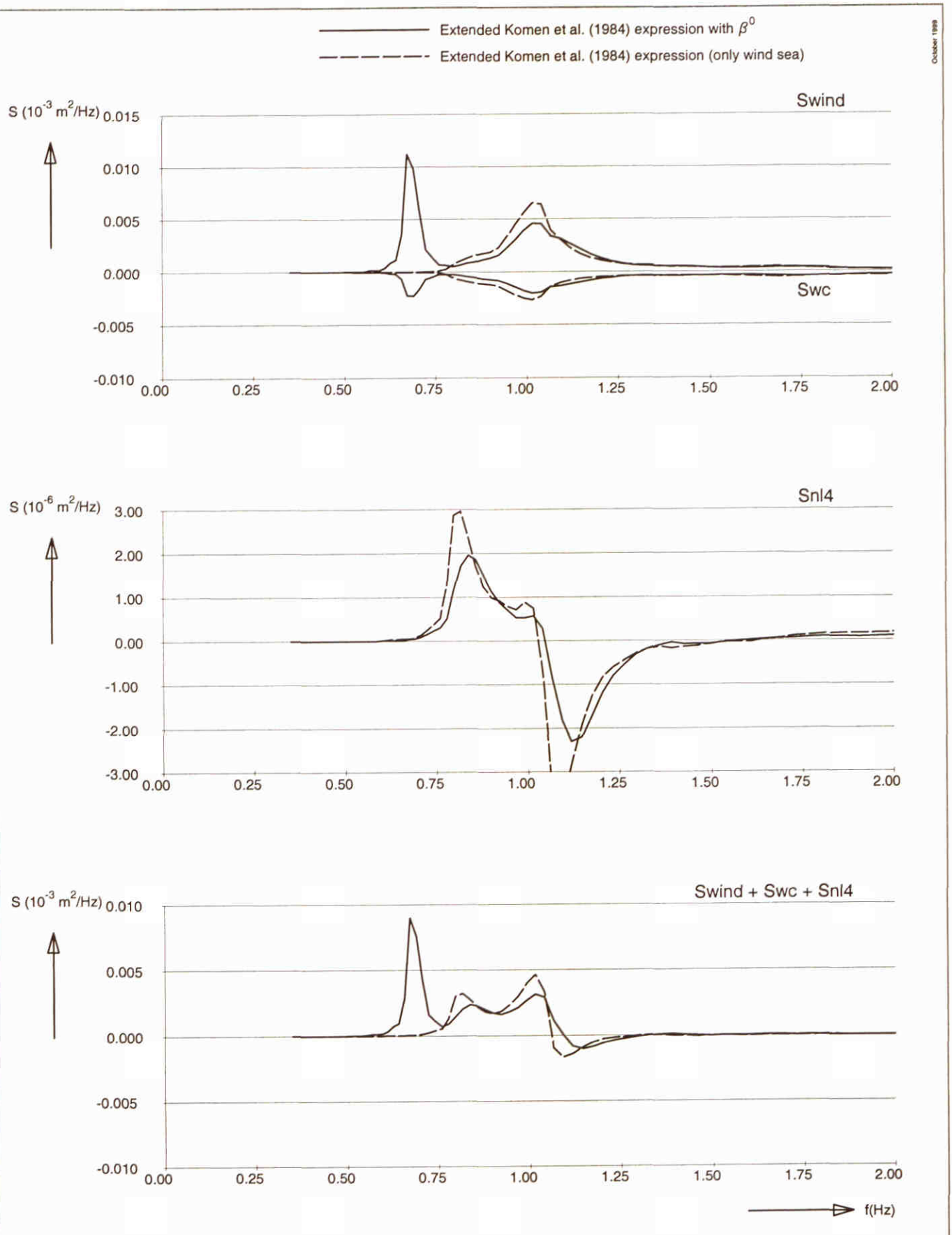


SWAN model results for Donelan (1987) experiment
Source terms at x = 50 m

SWAN 40.00

WL | delft hydraulics

H3529

Fig. 6.5.c

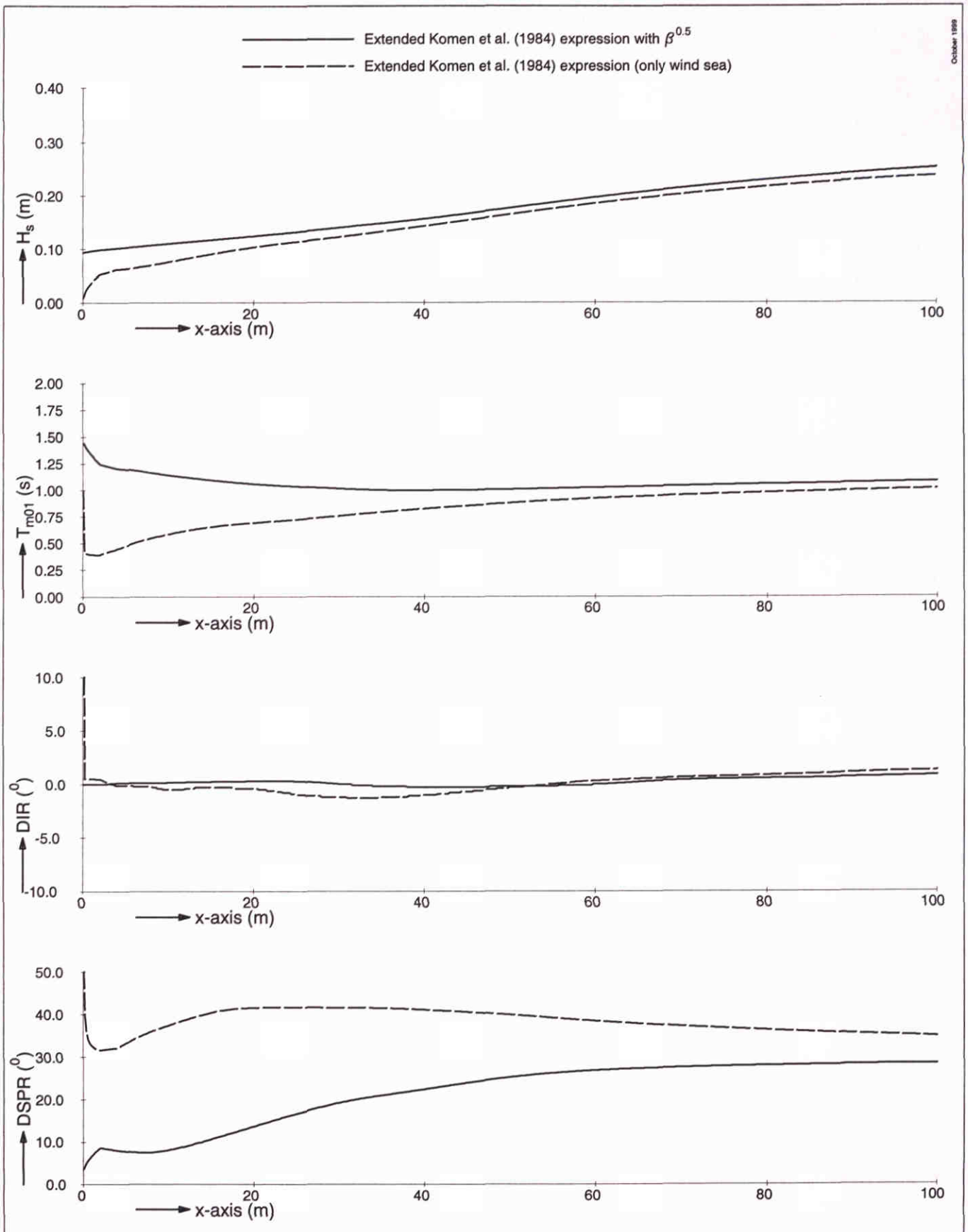


SWAN model results for Donelan (1987) experiment
Extended Komen et al. (1984) expression with $\beta^{0.5}$

SWAN 40.00

WL | delft hydraulics

H3529

Fig. 6.6.a

October 1999

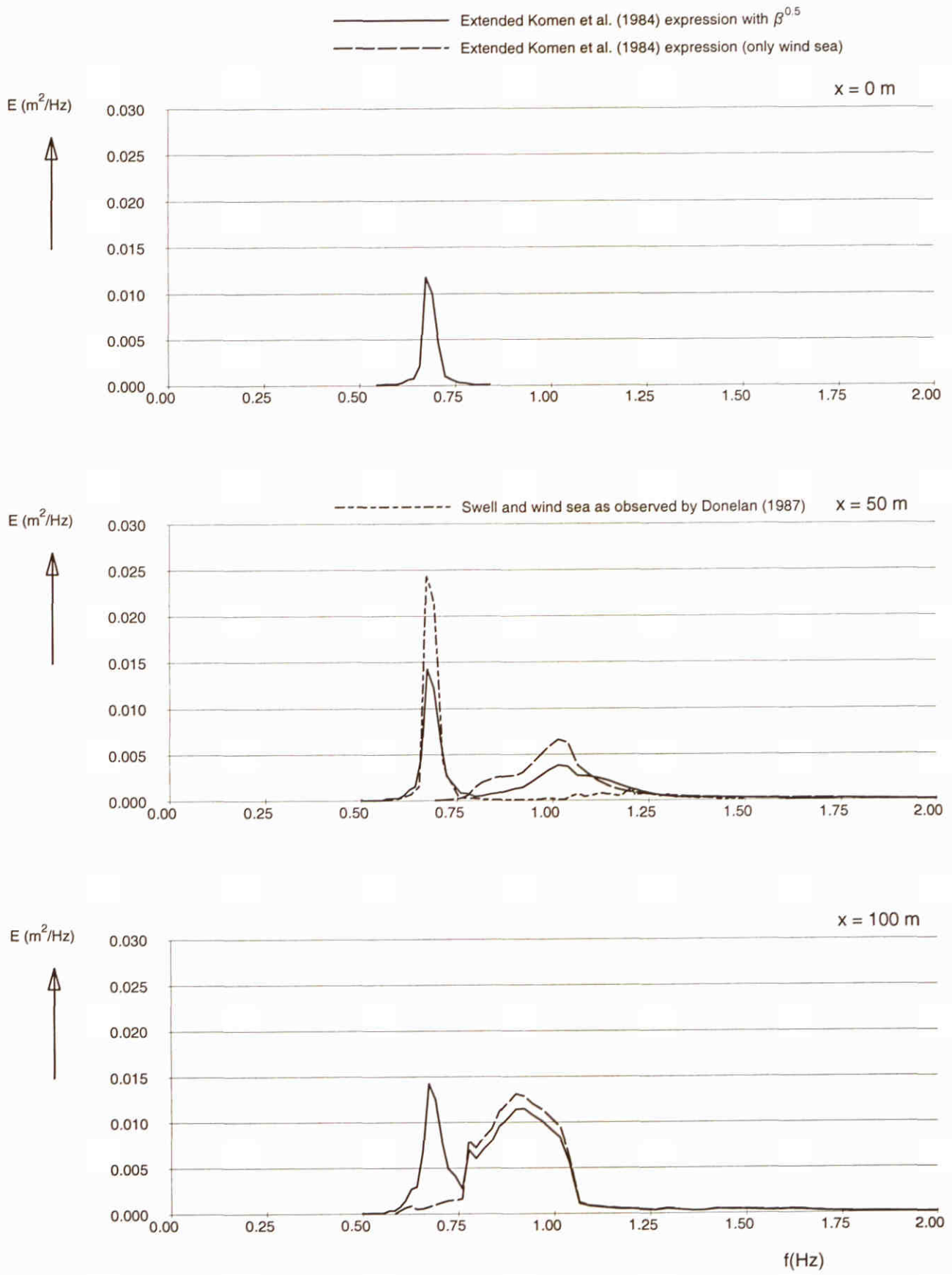


SWAN model results for Donelan (1987) experiment
Computed wave spectra with
extended Komen et al. (1984) expression with $\beta^{0.5}$

SWAN 40.00

WL | delft hydraulics

H3529

Fig. 6.6.b

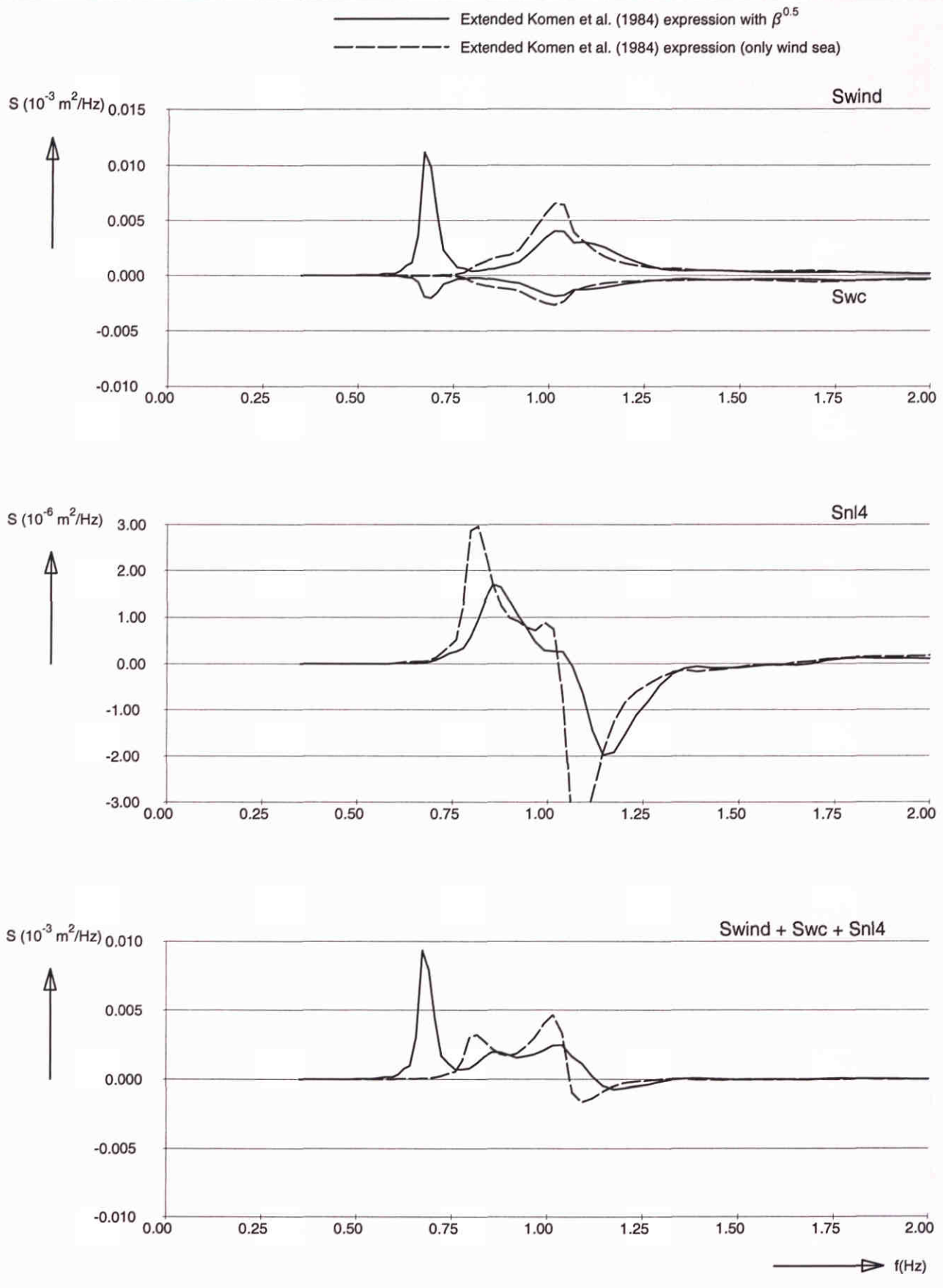


| | | |
|---|---|---|
| SWAN model results for Donelan (1987) experiment<br>Source terms at x = 50 m | SWAN 40.00 | |
| WL \| delft hydraulics | H3529 | Fig. 6.6.c |

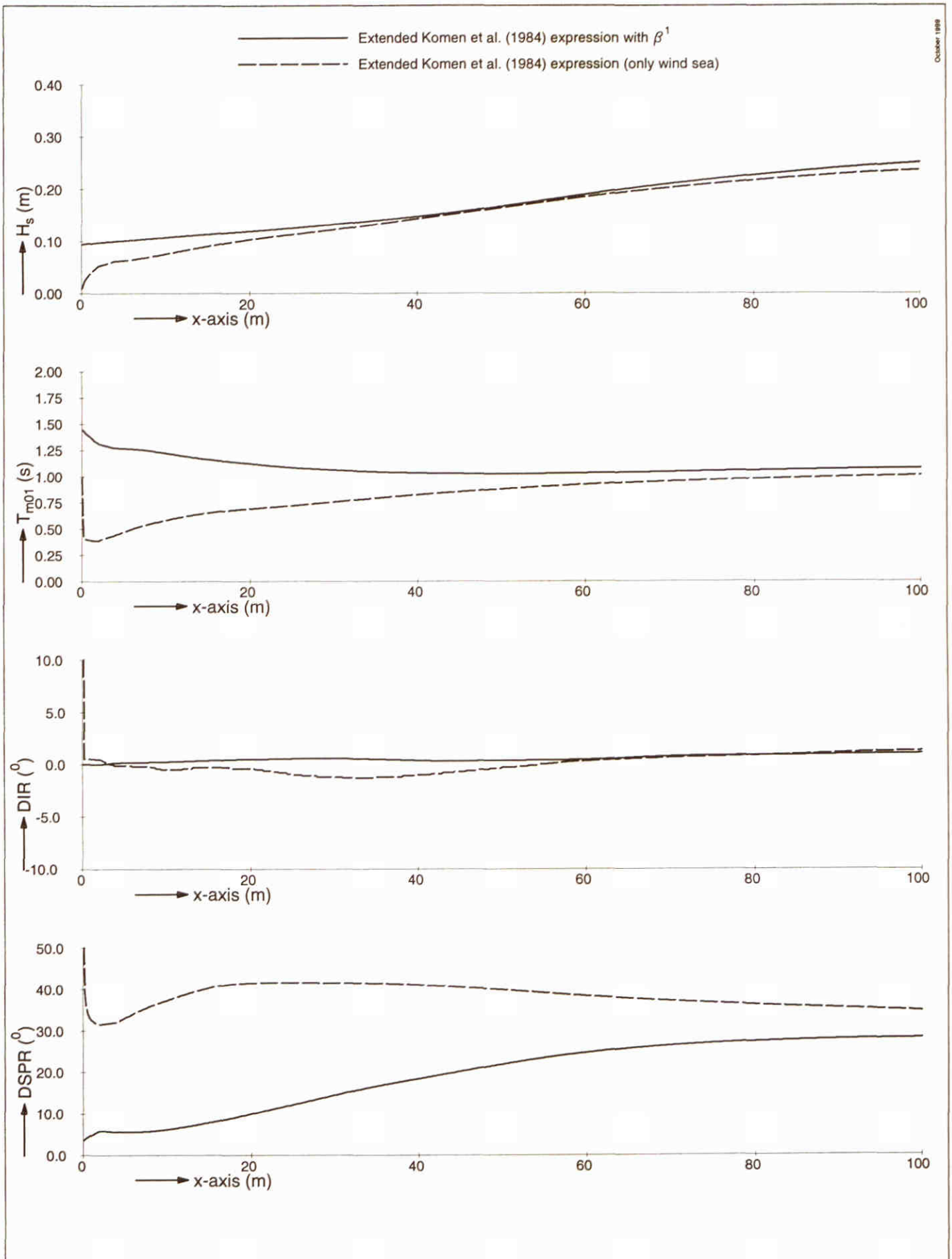


SWAN model results for Donelan (1987) experiment
Extended Komen et al. (1984) expression with $\beta^1$

SWAN 40.00

WL | delft hydraulics

H3529

Fig. 6.7.a

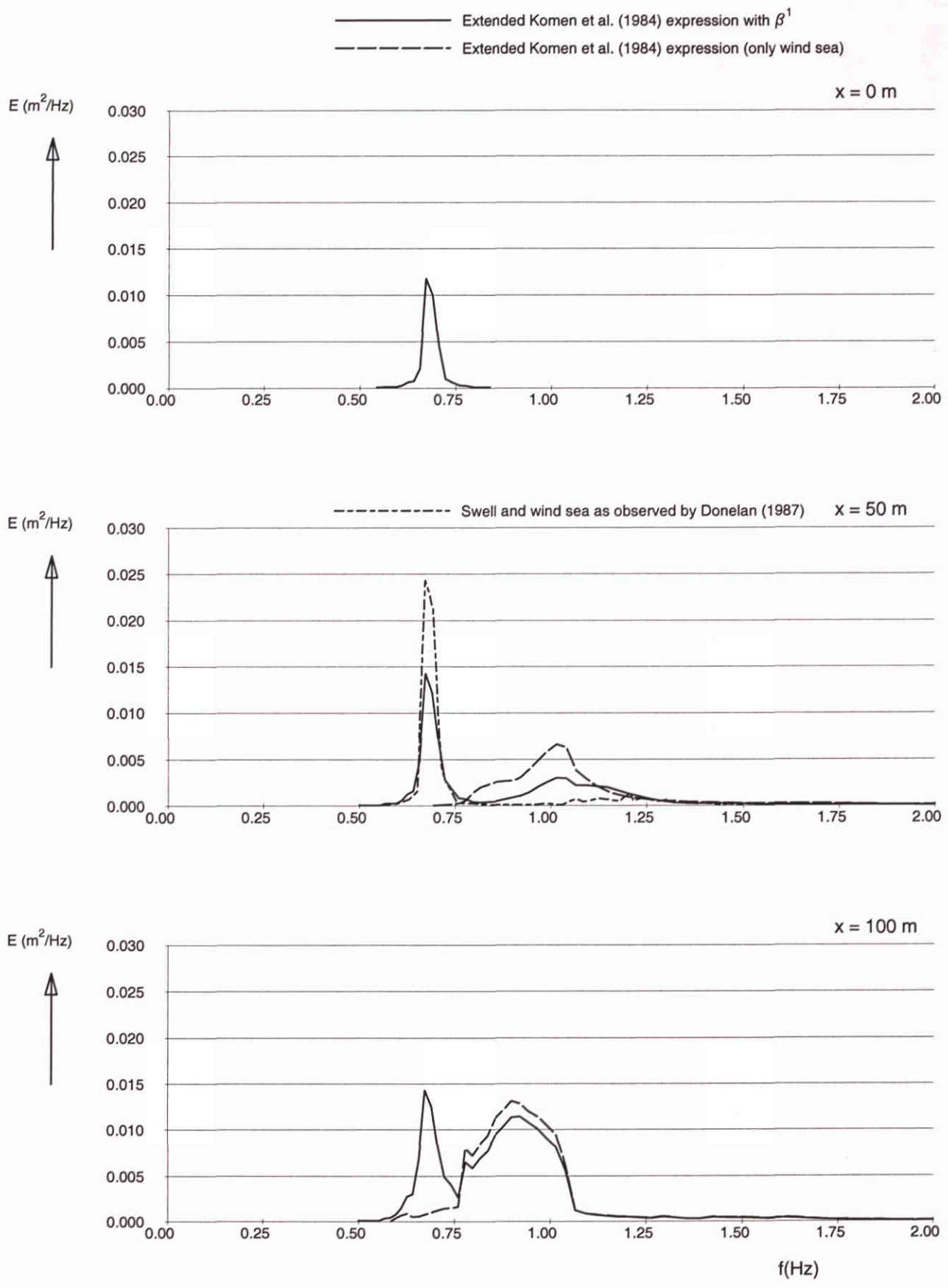


| | | |
|---|---|---|
| SWAN model results for Donelan (1987) experiment<br>Computed wave spectra with<br>extended Komen et al. (1984) expression with $\beta^1$ | SWAN 40.00 | |
| WL \| delft hydraulics | H3529 | Fig. 6.7.b |

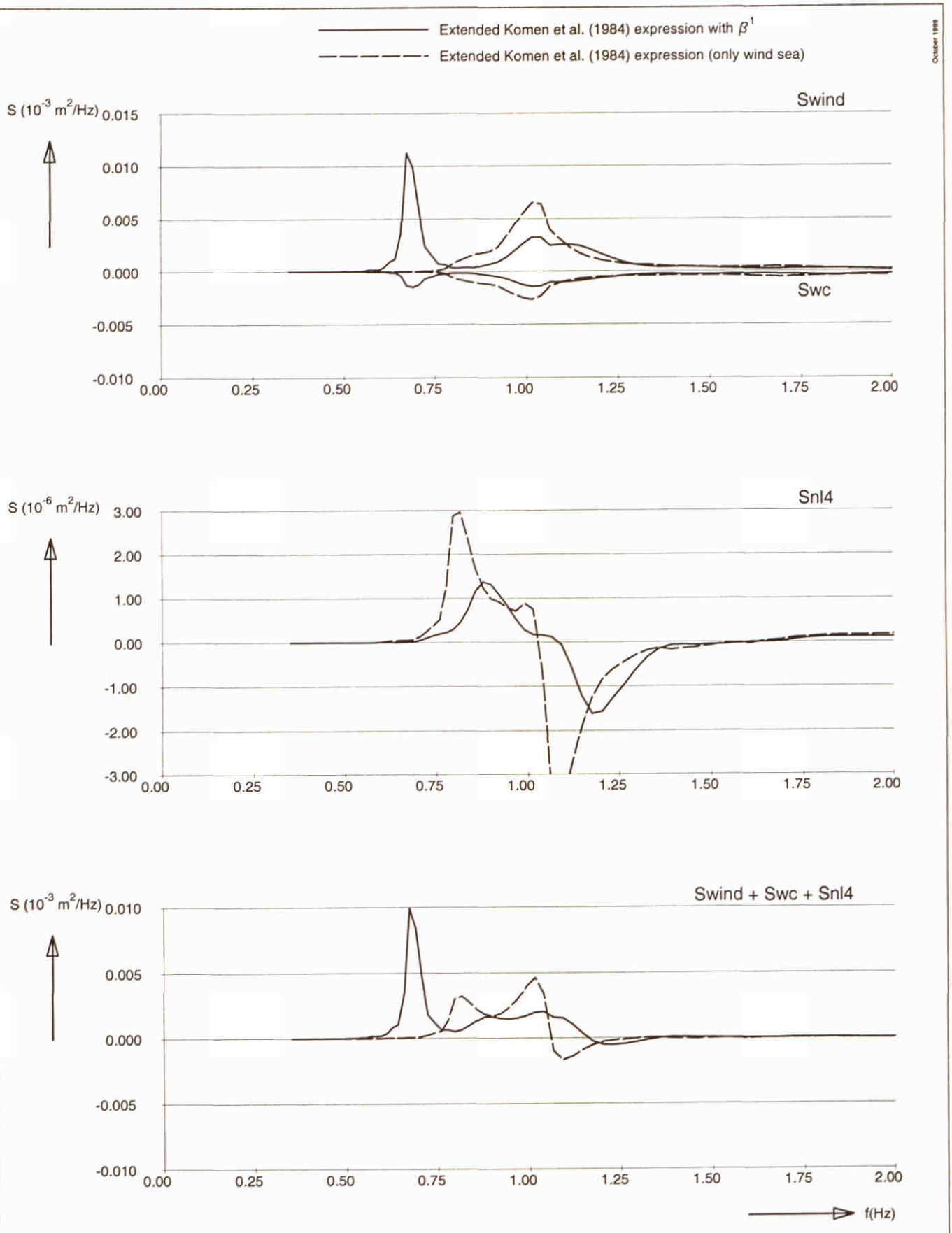


SWAN model results for Donelan (1987) experiment
Source terms at x = 50 m

SWAN 40.00

WL | delft hydraulics

H3529

Fig. 6.7.c

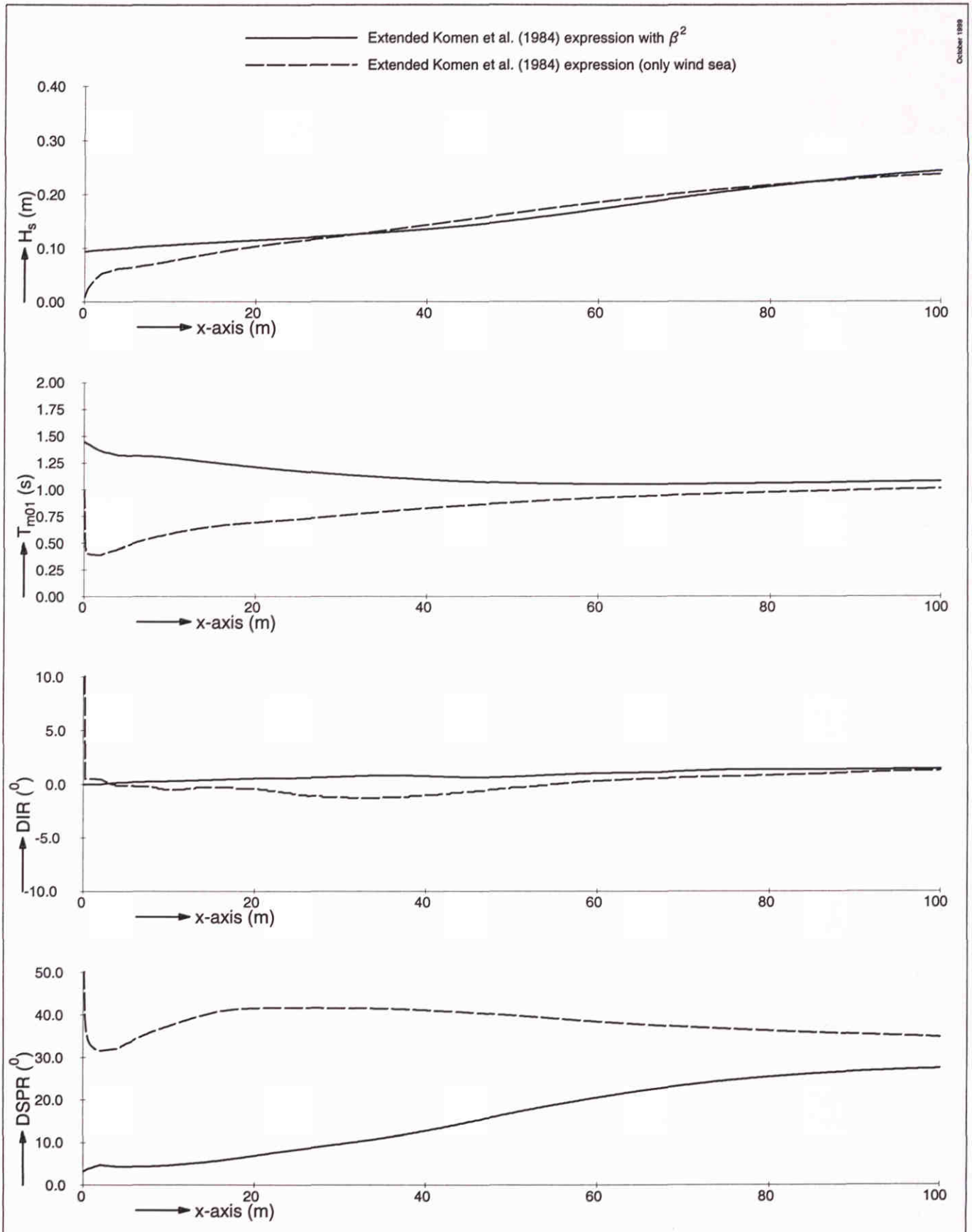


SWAN model results for Donelan (1987) experiment
Extended Komen et al. (1984) expression with $\beta^2$

SWAN 40.00

WL | delft hydraulics

H3529

Fig. 6.8.a

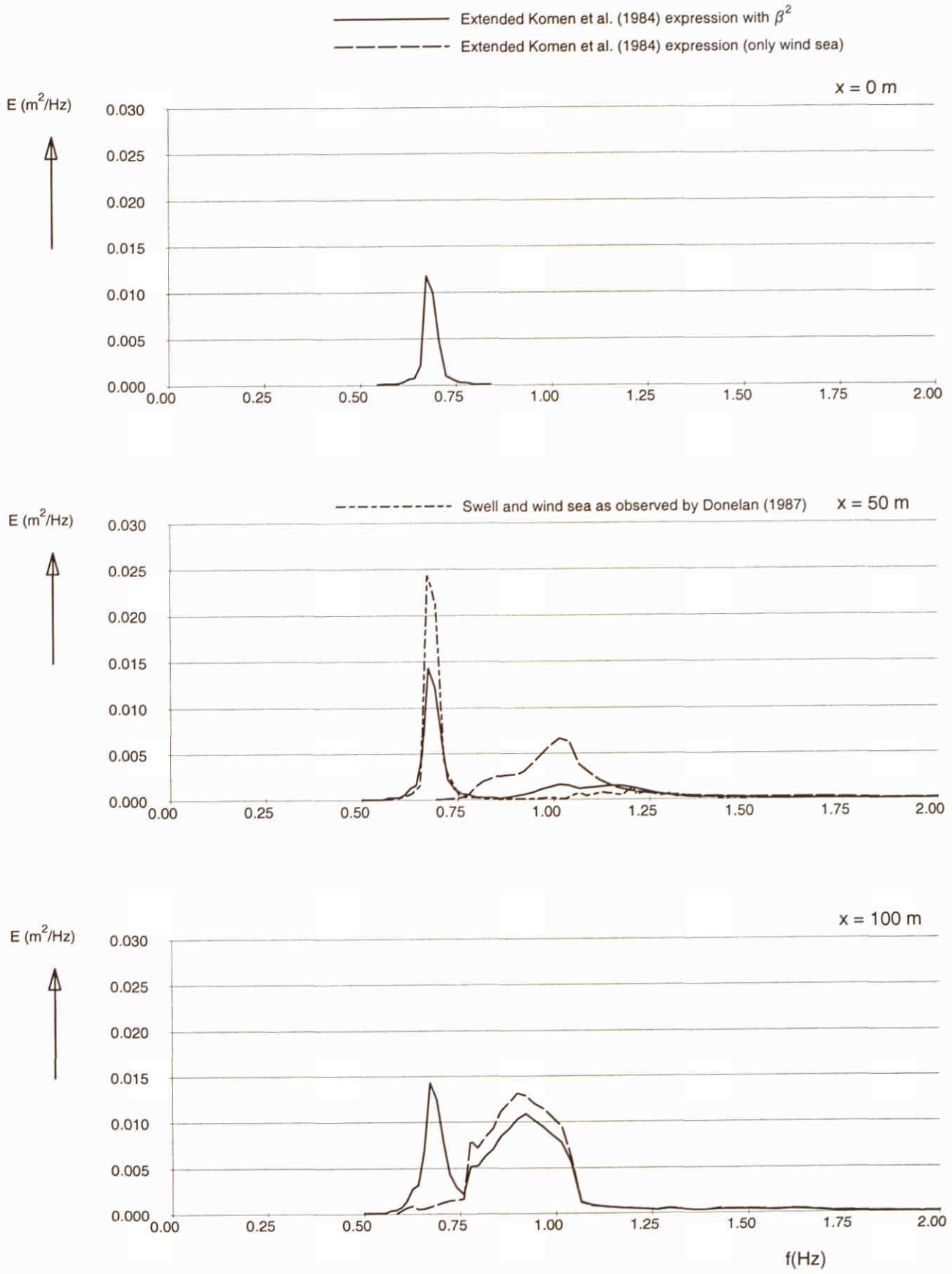


SWAN model results for Donelan (1987) experiment
Computed wave spectra with
extended Komen et al. (1984) expression with $\beta^2$

SWAN 40.00

WL | delft hydraulics

H3529

Fig. 6.8.b

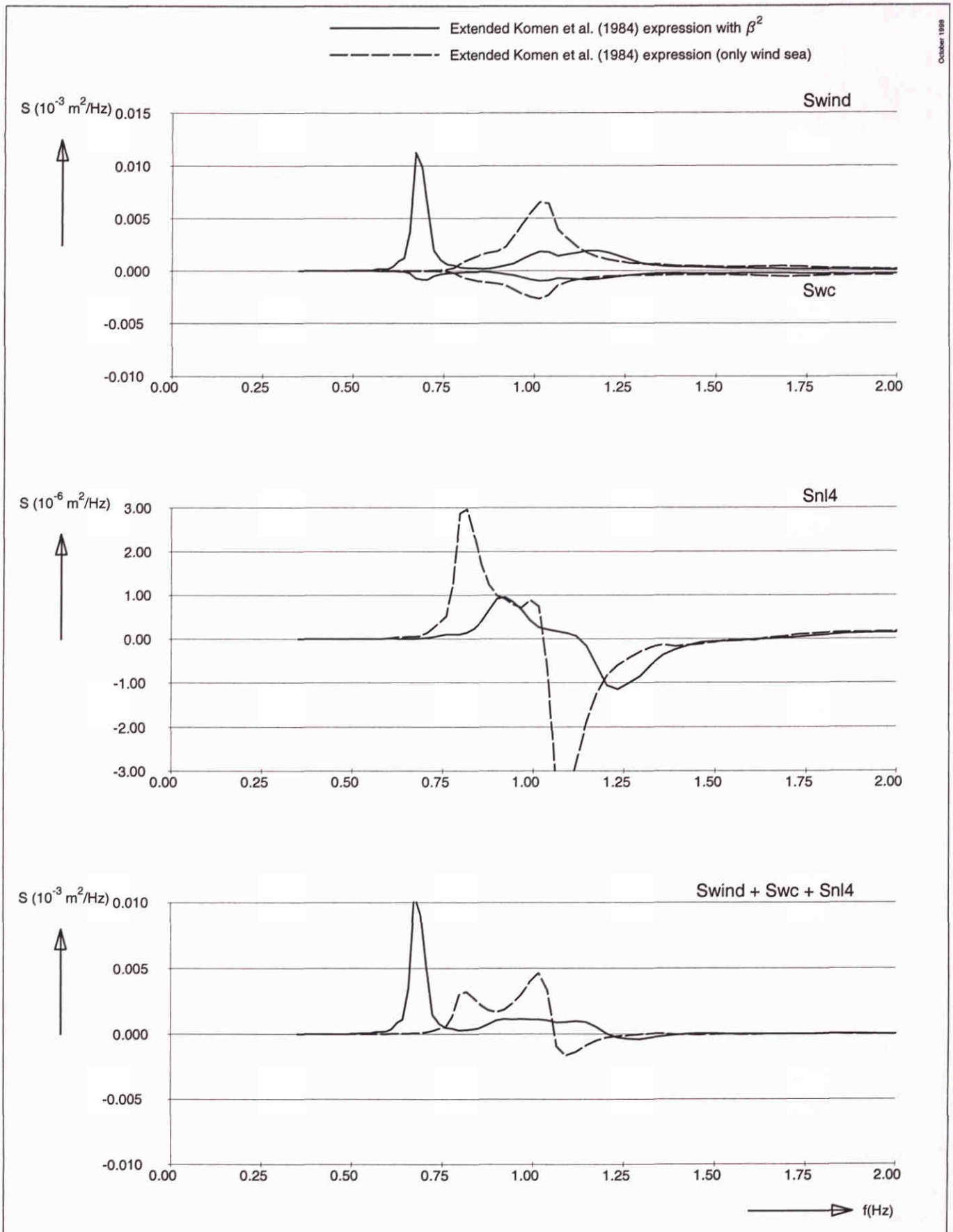


| | | |
|---|---|---|
| SWAN model results for Donelan (1987) experiment<br>Source terms at x = 50 m | SWAN 40.00 | |
| | | |
| WL \| delft hydraulics | H3529 | Fig. 6.8.c |

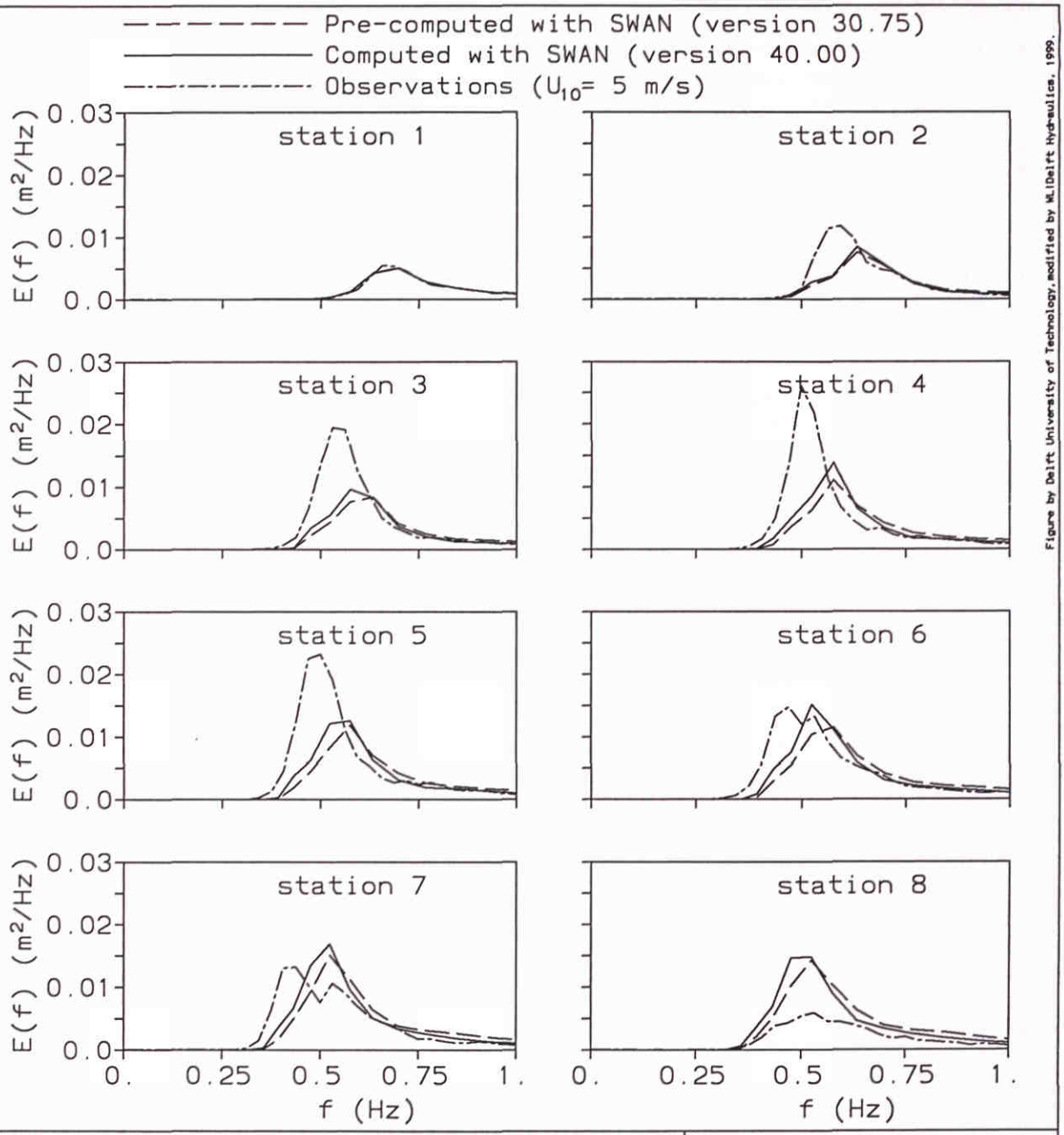


Figure by Delft University of Technology, modified by WL|Delft Hydraulics, 1999.

October 1999

F41lakegR1 F41a

Lake George: low wind speed

| | | |
|---|---|---|
| Lake George field experiment<br>Extended Komen et al. (1984) expression with $\beta^0$ | SWAN 40.00 | |
| WL \| delft hydraulics | H3529 | Fig. 7.1.a |

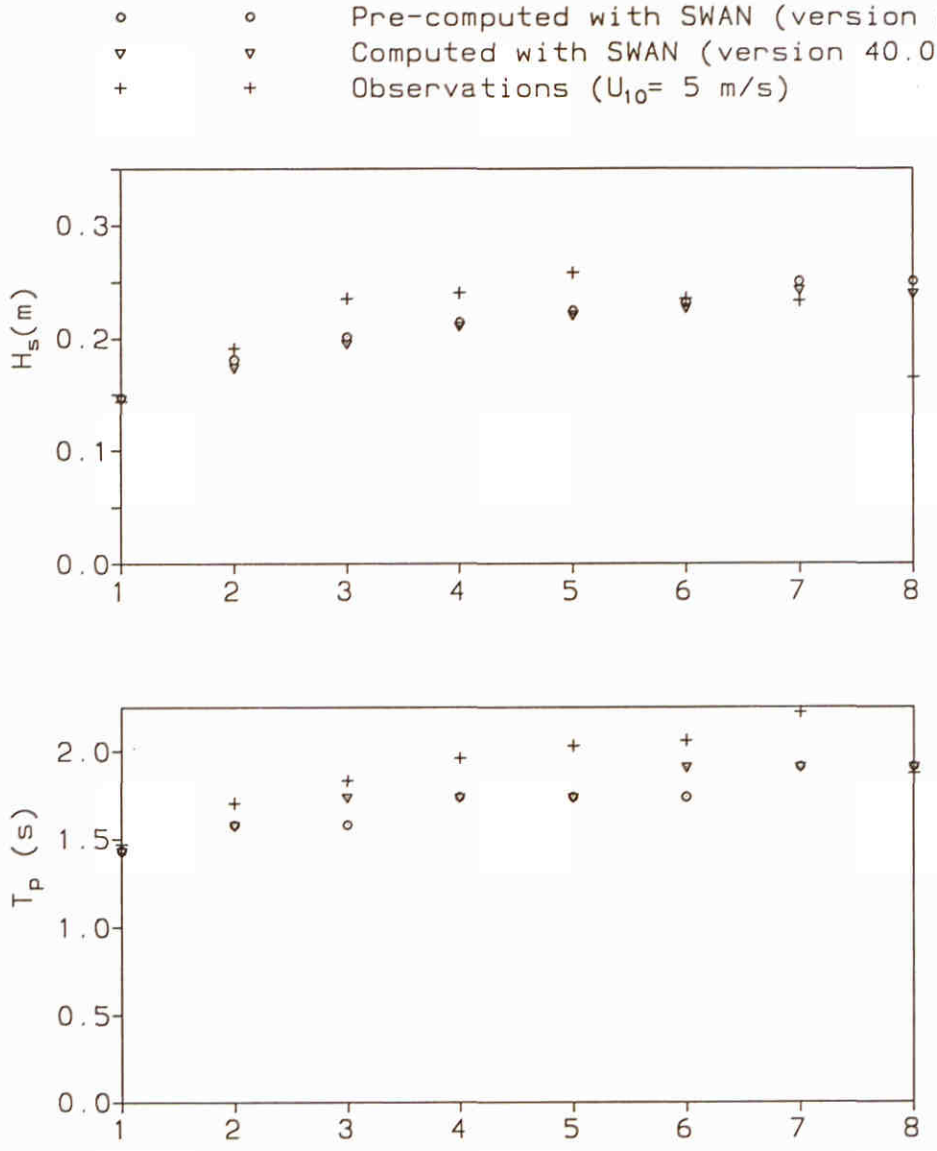




F41LakgR1 F41b

Lage George: low wind speed

Lake George field experiment

Extended Komen et al. (1984) expression with $\beta^0$

SWAN 40.00

WL | delft hydraulics

H3529

Fig. 7.1.b

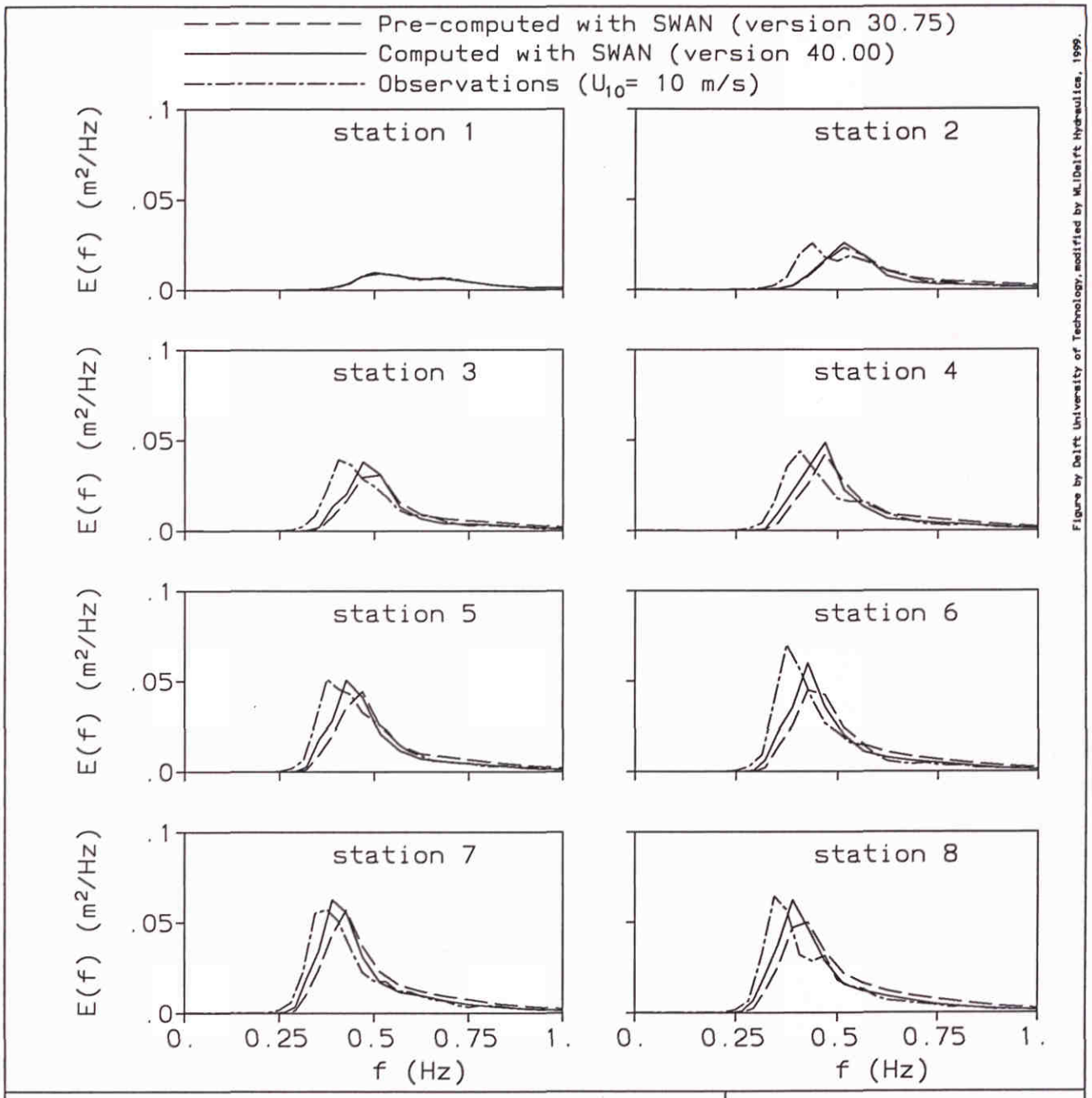


F41lakegR2 F41c

Lake George: moderate wind speed

| | | |
|---|---|---|
| Lake George field experiment<br>Extended Komen et al. (1984) expression with $\beta^0$ | SWAN 40.00 | |
| WL \| delft hydraulics | H3529 | Fig. 7.1.c |

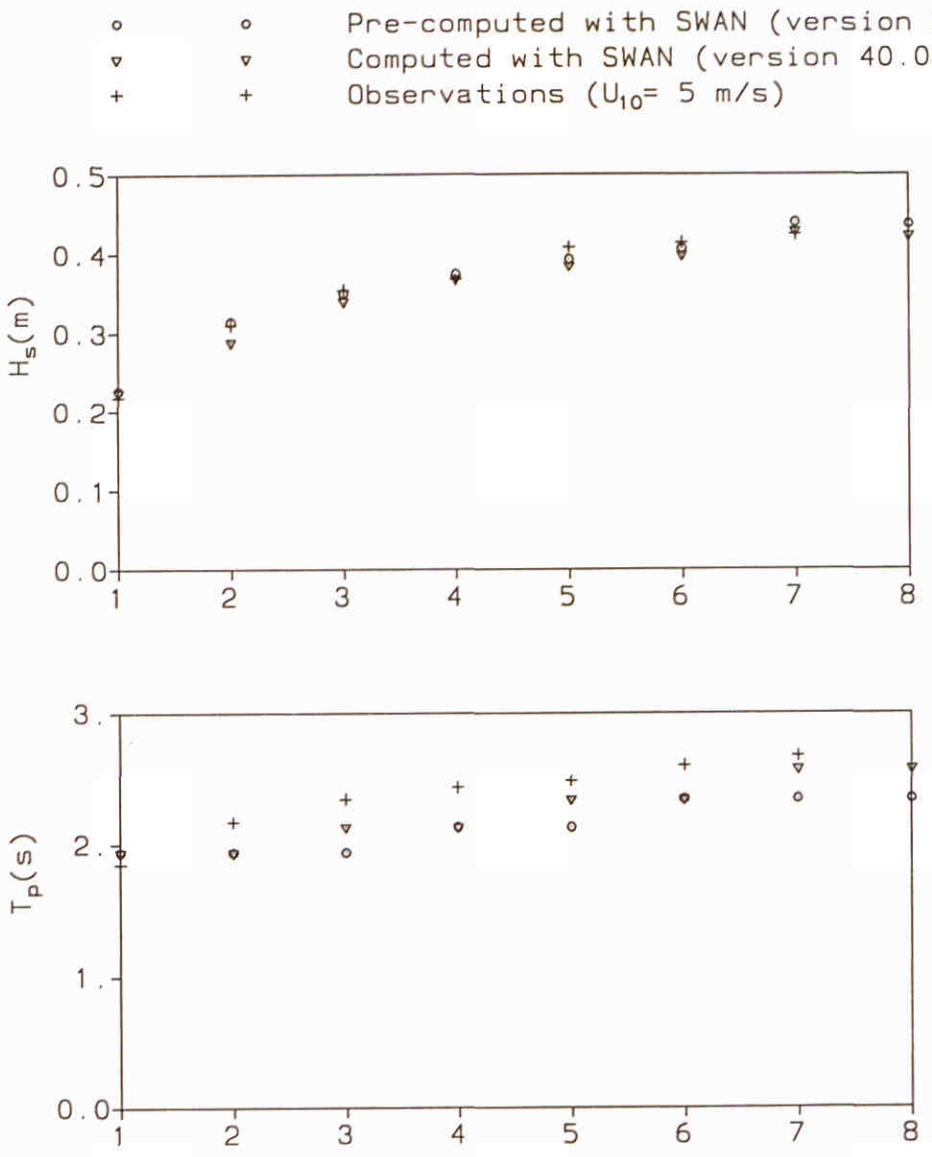


F41LakgR2 F41d

Lage George: moderate wind speed

Lake George field experiment

Extended Komen et al. (1984) expression with $\beta^0$

SWAN 40.00

WL | delft hydraulics

H3529

Fig. 7.1.d

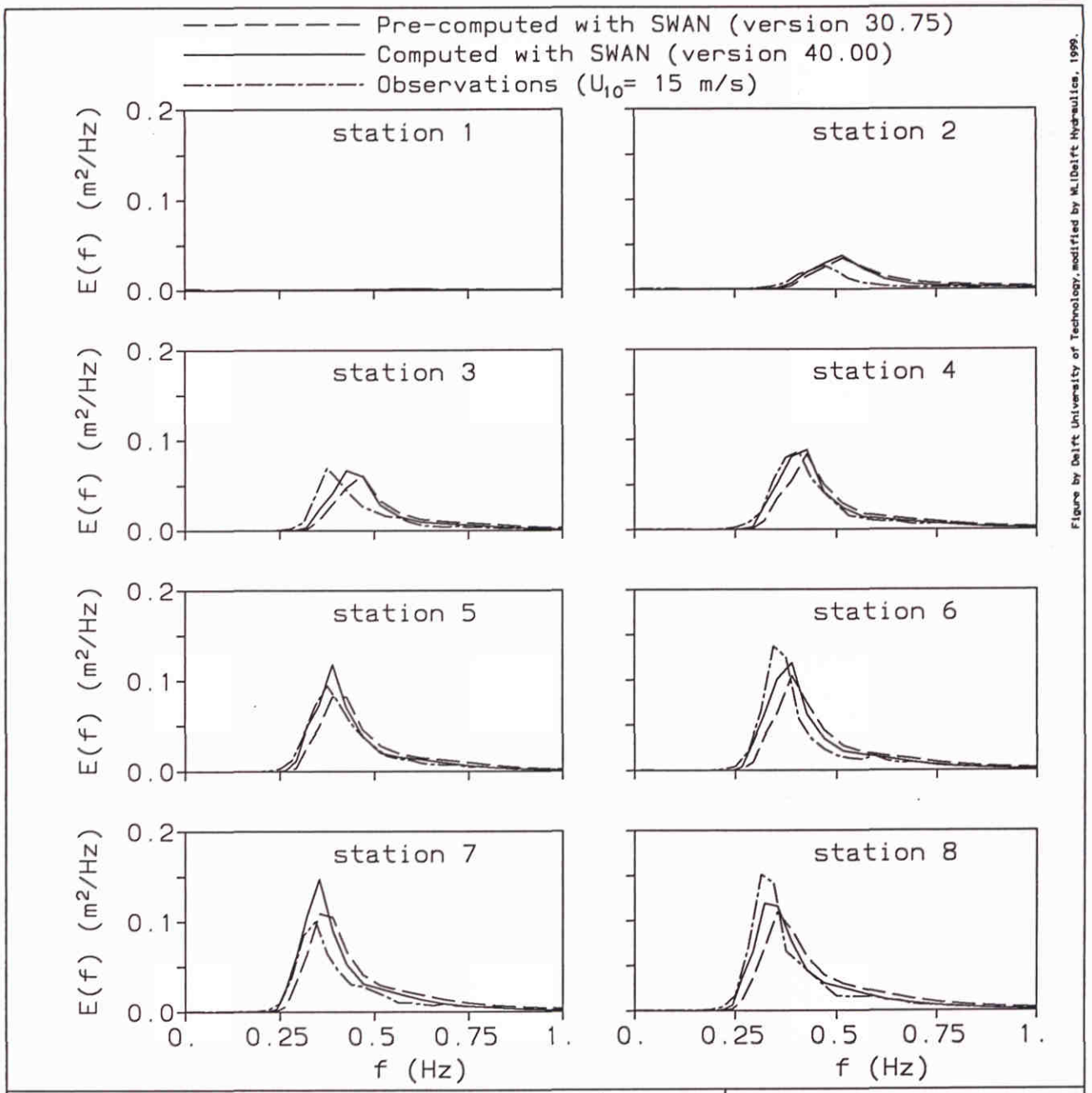


Figure by Delft University of Technology, modified by WL|Delft Hydraulics, 1999.

October 1999

F41lakegR3 F41e

Lake George: high wind speed

| | | |
|---|---|---|
| Lake George field experiment<br>Extended Komen et al. (1984) expression with $\beta^0$ | SWAN 40.00 | |
| WL \| delft hydraulics | H3529 | Fig. 7.1.e |

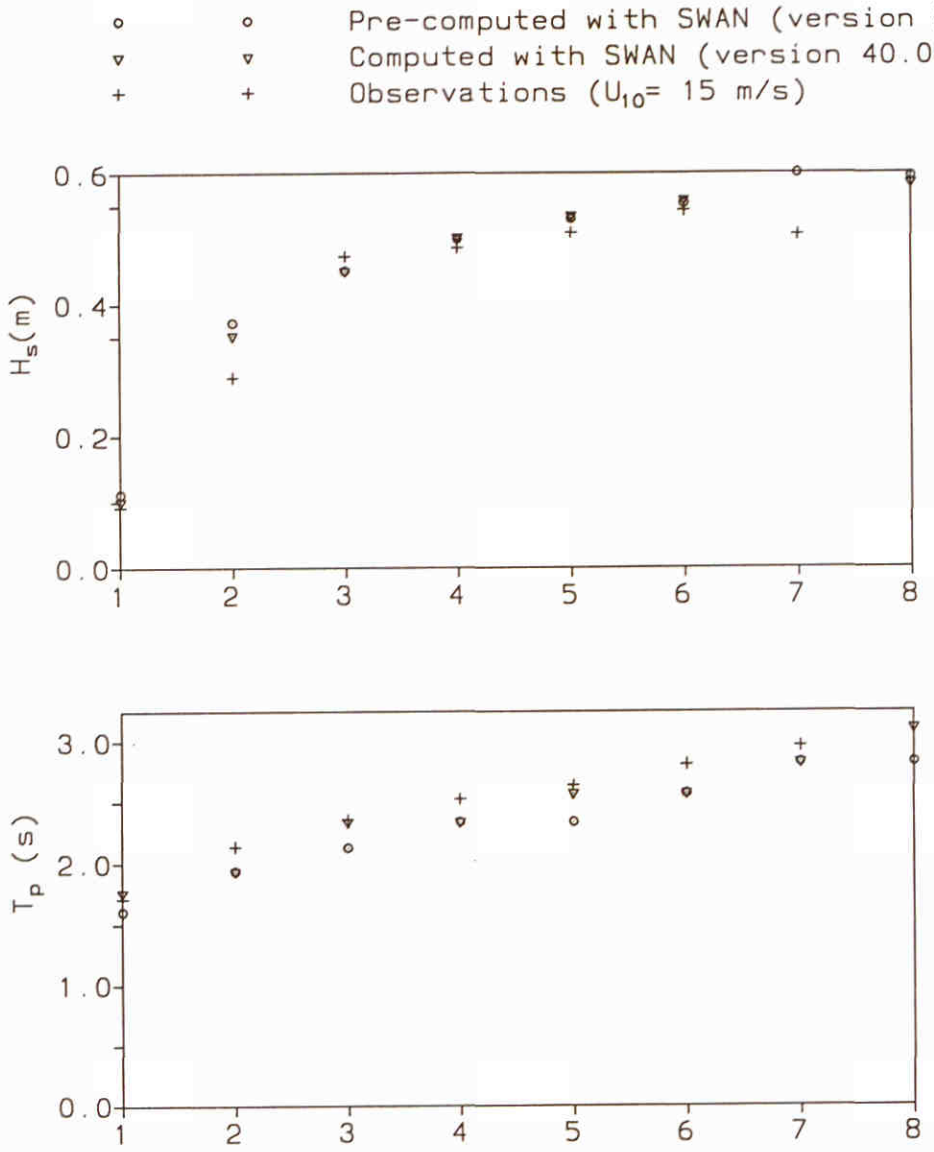


F41LakgR3 F41f

Lage George: high wind speed

Lake George field experiment

Extended Komen et al. (1984) expression with $\beta^0$

SWAN 40.00

WL | delft hydraulics

H3529

Fig. 7.1.f

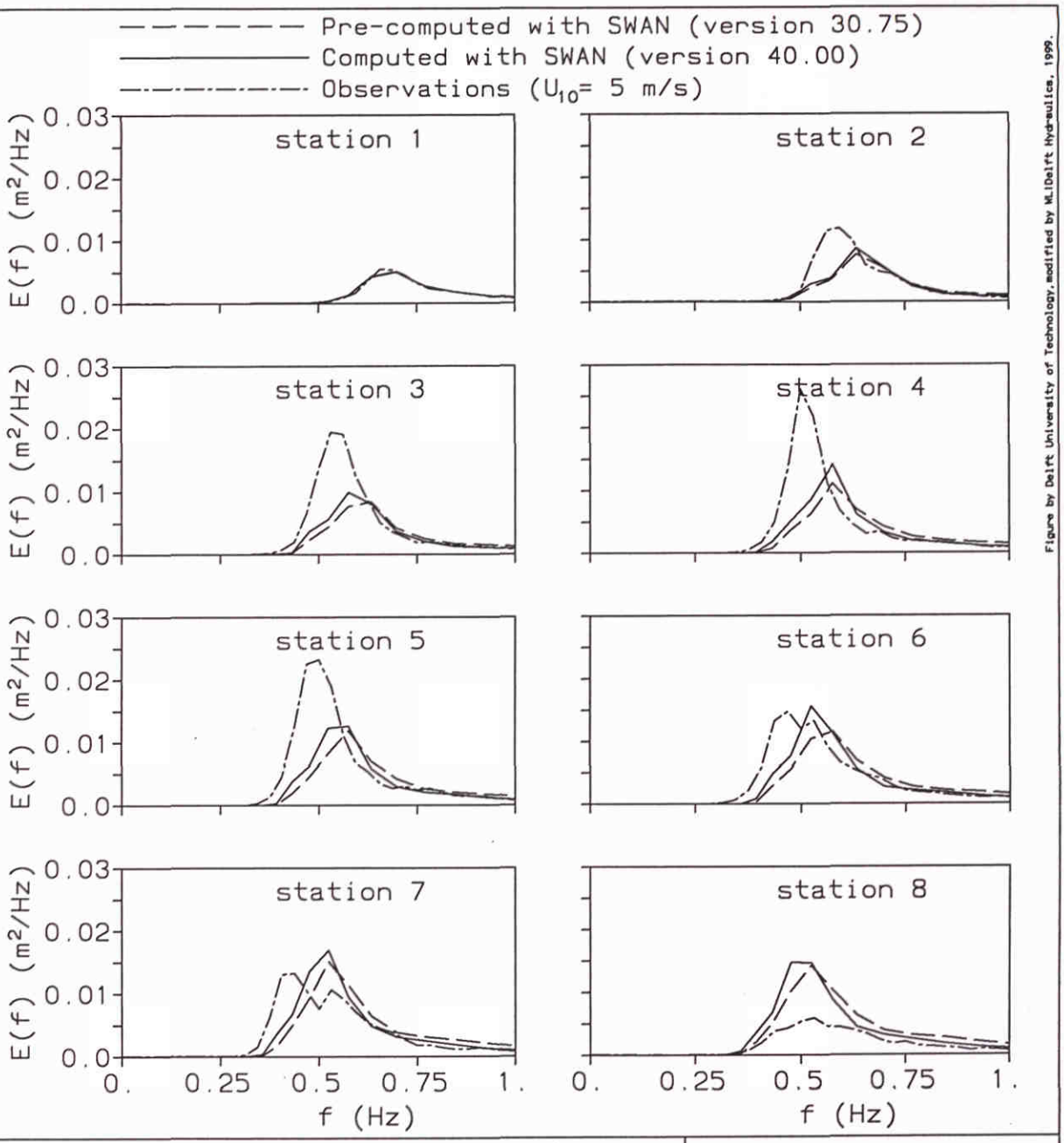


F41lakegR1 F41a

Lake George: low wind speed

| | | |
|---|---|---|
| Lake George field experiment<br>Extended Komen et al. (1984) expression with $\beta^{0.5}$ | SWAN 40.00 | |
| WL \| delft hydraulics | H3529 | Fig. 7.2.a |

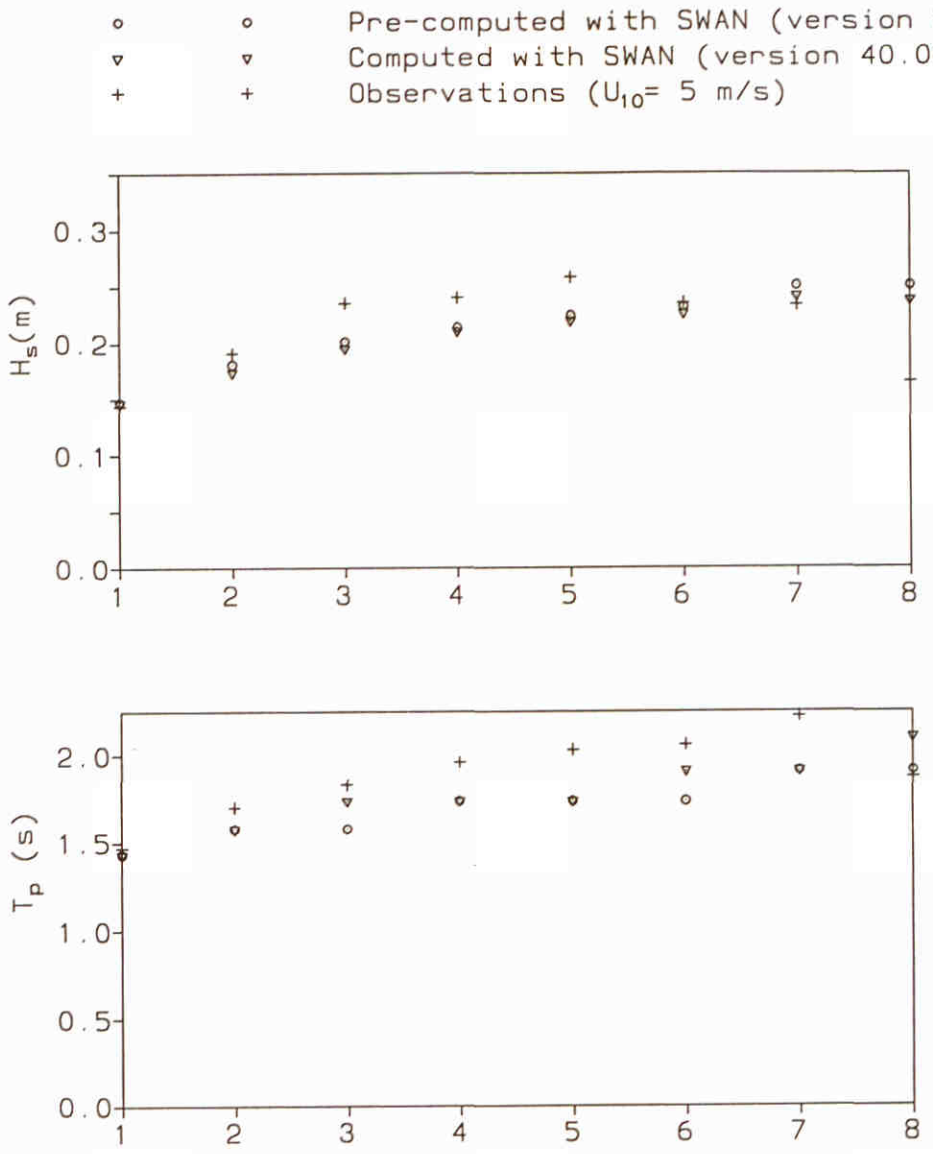


F41LakgR1 F41b

Lage George: low wind speed

Lake George field experiment

Extended Komen et al. (1984) expression with $\beta^{0.5}$

SWAN 40.00

WL | delft hydraulics

H3529

Fig. 7.2.b

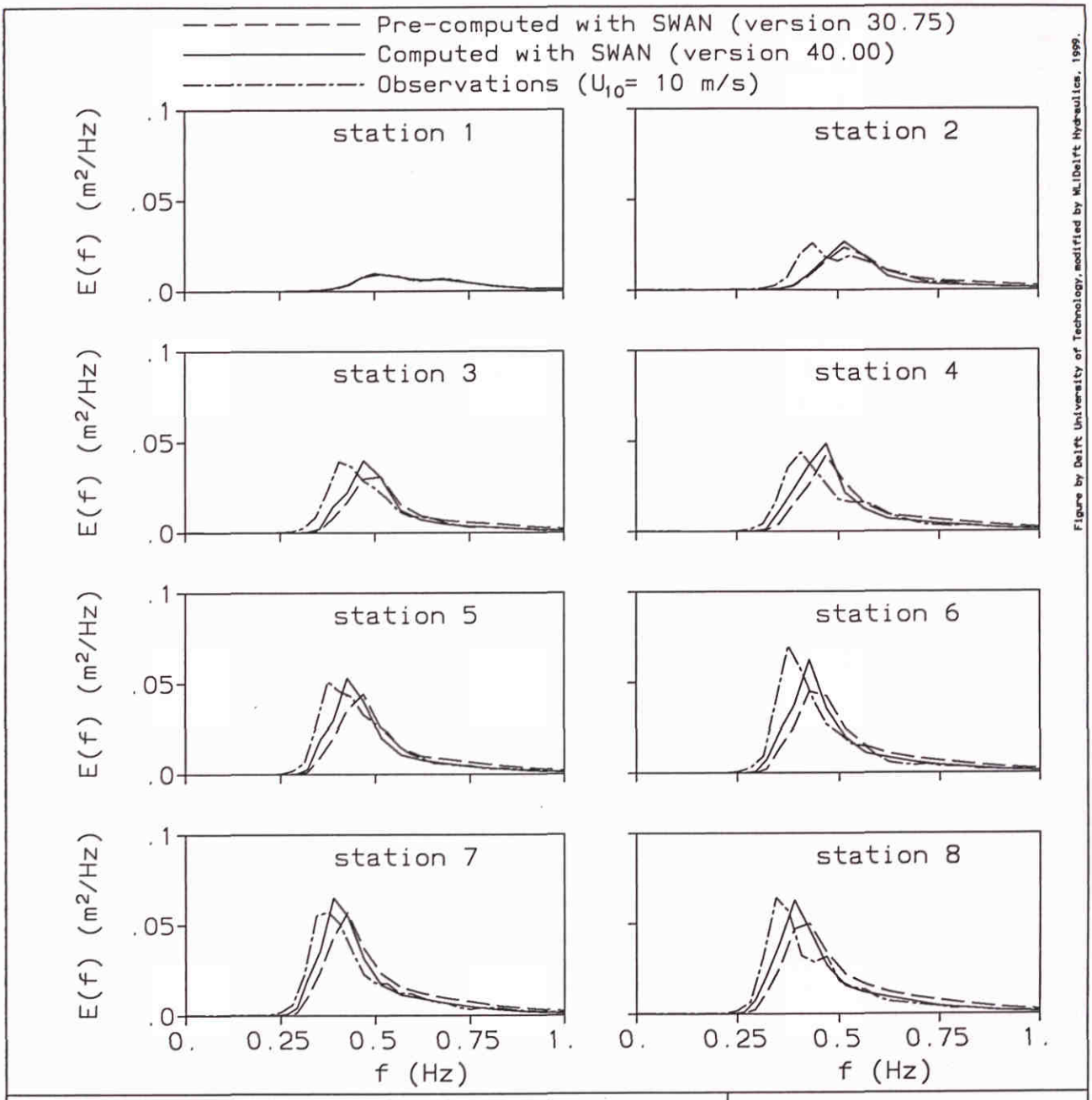


Figure by Delft University of Technology, modified by WL|Delft Hydraulics, 1999.

October 1999

F41lakegR2 F41c

Lake George: moderate wind speed

Lake George field experiment

Extended Komen et al. (1984) expression with $\beta^{0.5}$

SWAN 40.00

WL | delft hydraulics

H3529

Fig. 7.2.c

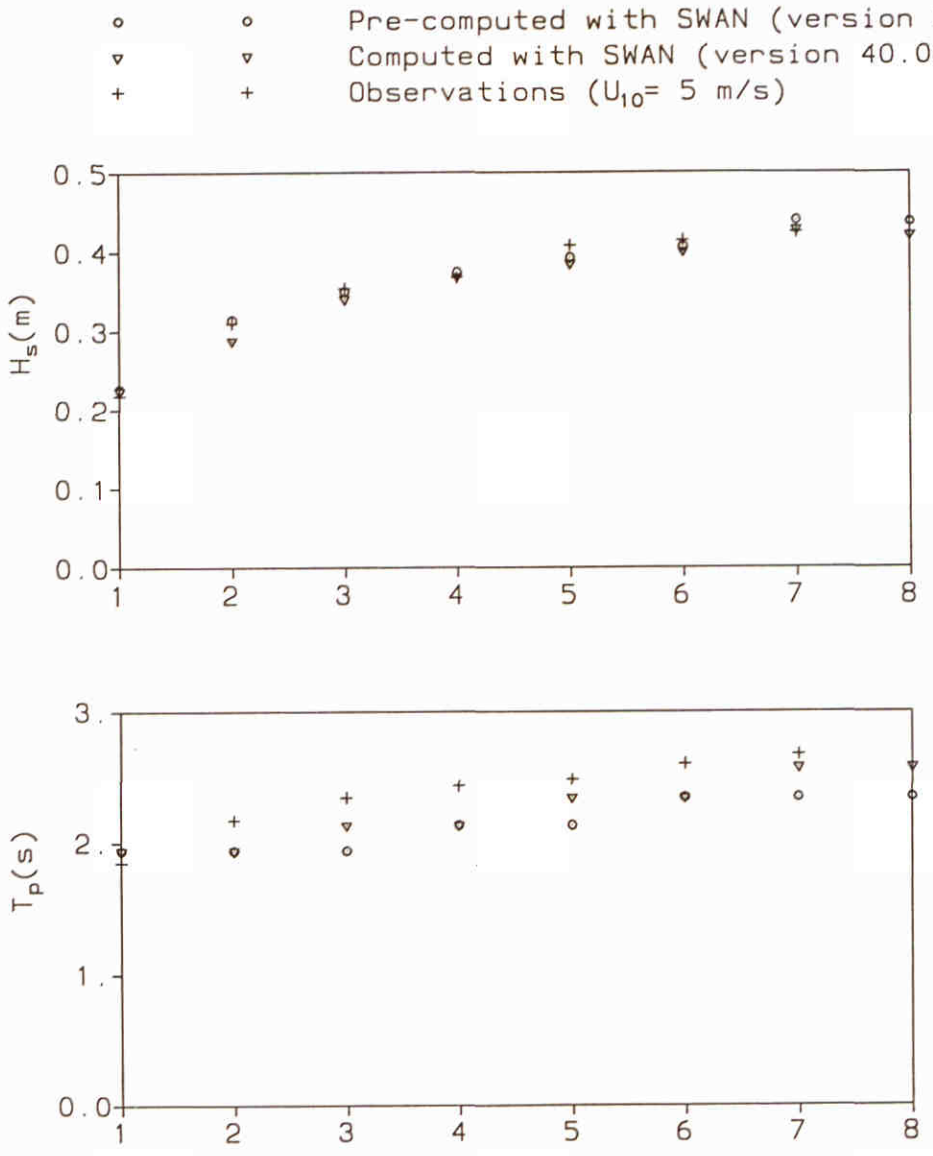




F41LakgR2 F41d

Lage George: moderate wind speed

Lake George field experiment

Extended Komen et al. (1984) expression with $\beta^{0.5}$

SWAN 40.00

WL | delft hydraulics

H3529

Fig. 7.2.d

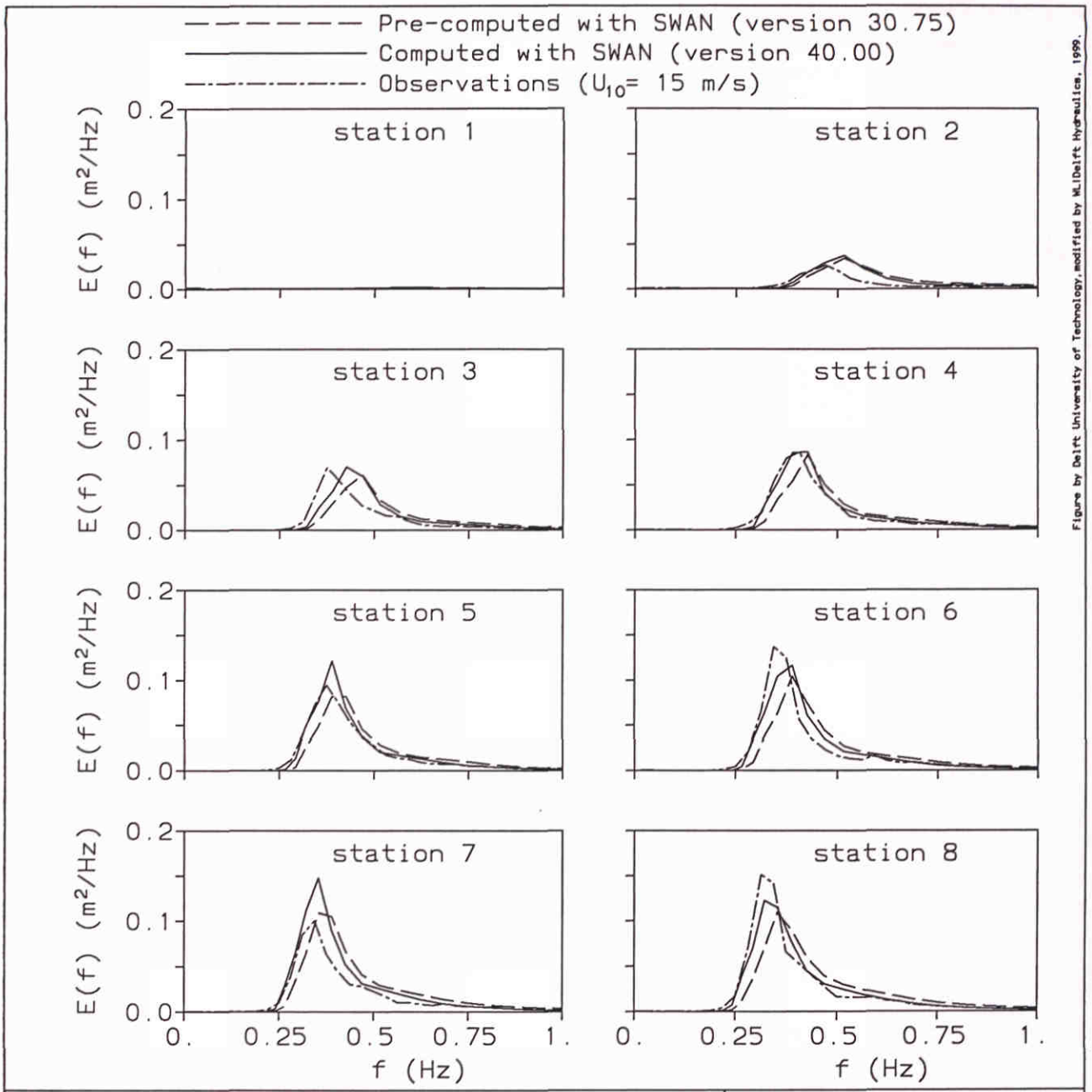


F41lakegR3 F41e

Lake George: high wind speed

| | | |
|---|---|---|
| Lake George field experiment<br>Extended Komen et al. (1984) expression with $\beta^{0.5}$ | SWAN 40.00 | |
| WL \| delft hydraulics | H3529 | Fig. 7.2.e |

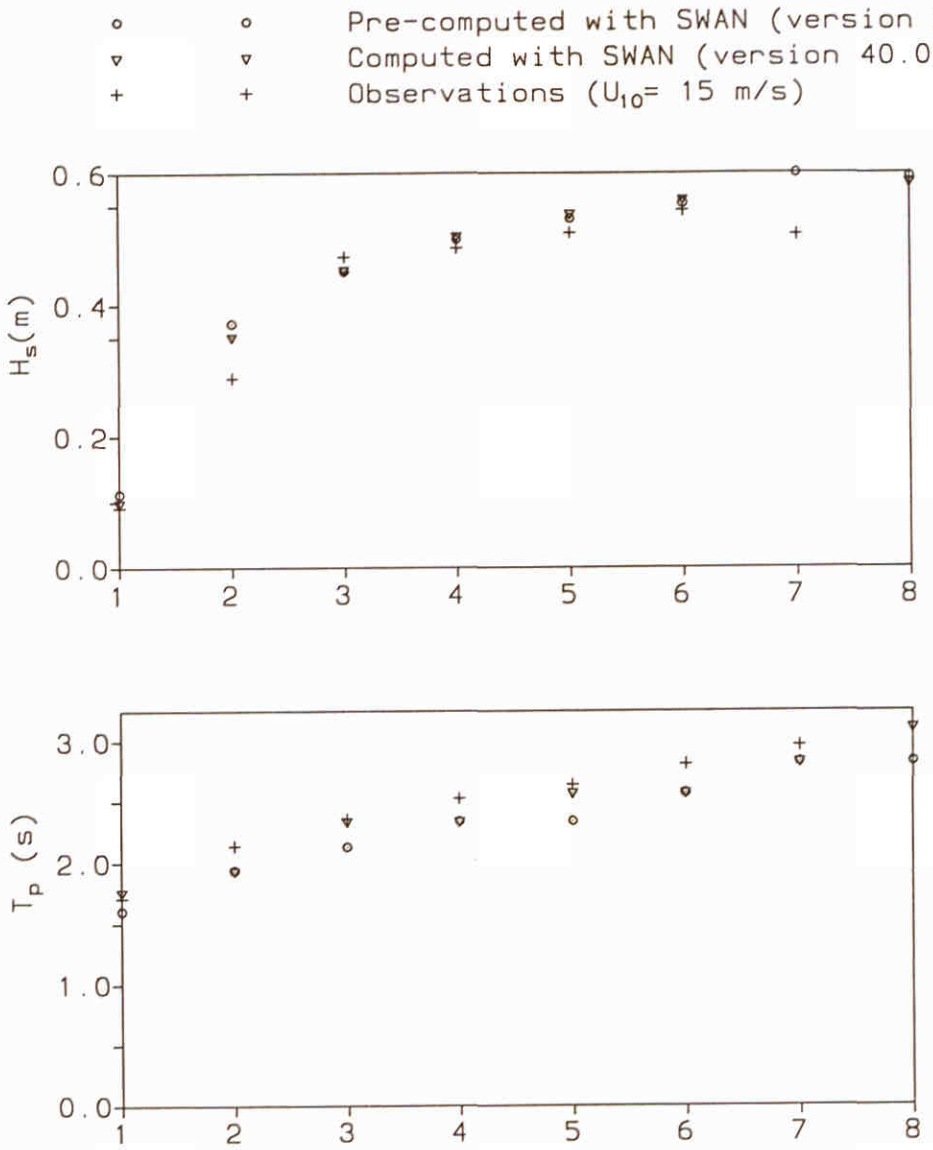


F41LakgR3 F41f

Lage George: high wind speed

Lake George field experiment

Extended Komen et al. (1984) expression with $\beta^{0.5}$

SWAN 40.00

WL | delft hydraulics

H3529

Fig. 7.2.f

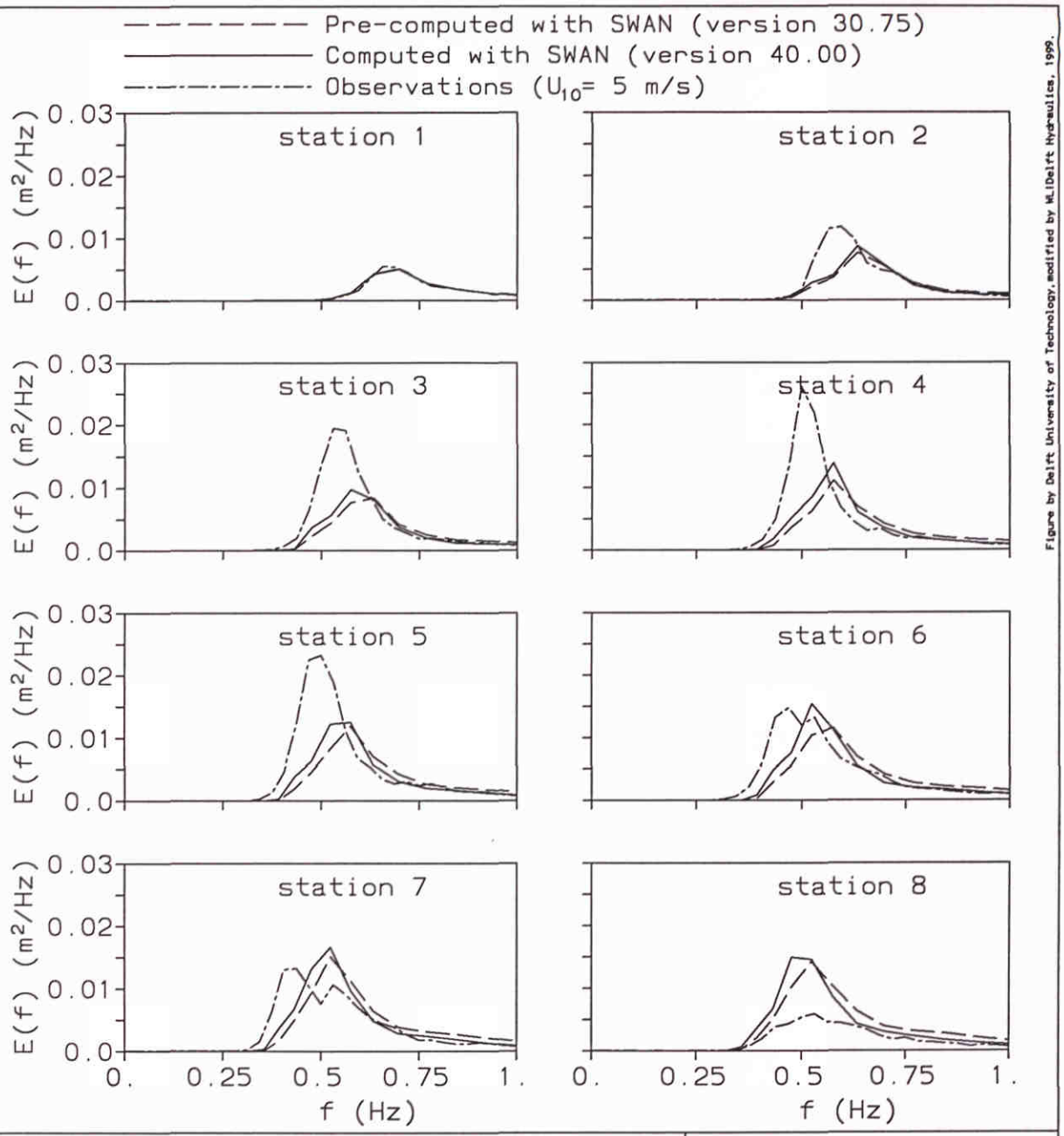


Figure by Delft University of Technology, modified by WL|Delft Hydraulics, 1999.

October 1999

F41lakegR1 F41a

Lake George: low wind speed

Lake George field experiment

Extended Komen et al. (1984) expression with $\beta^1$

SWAN 40.00

WL | delft hydraulics

H3529

Fig. 7.3.a

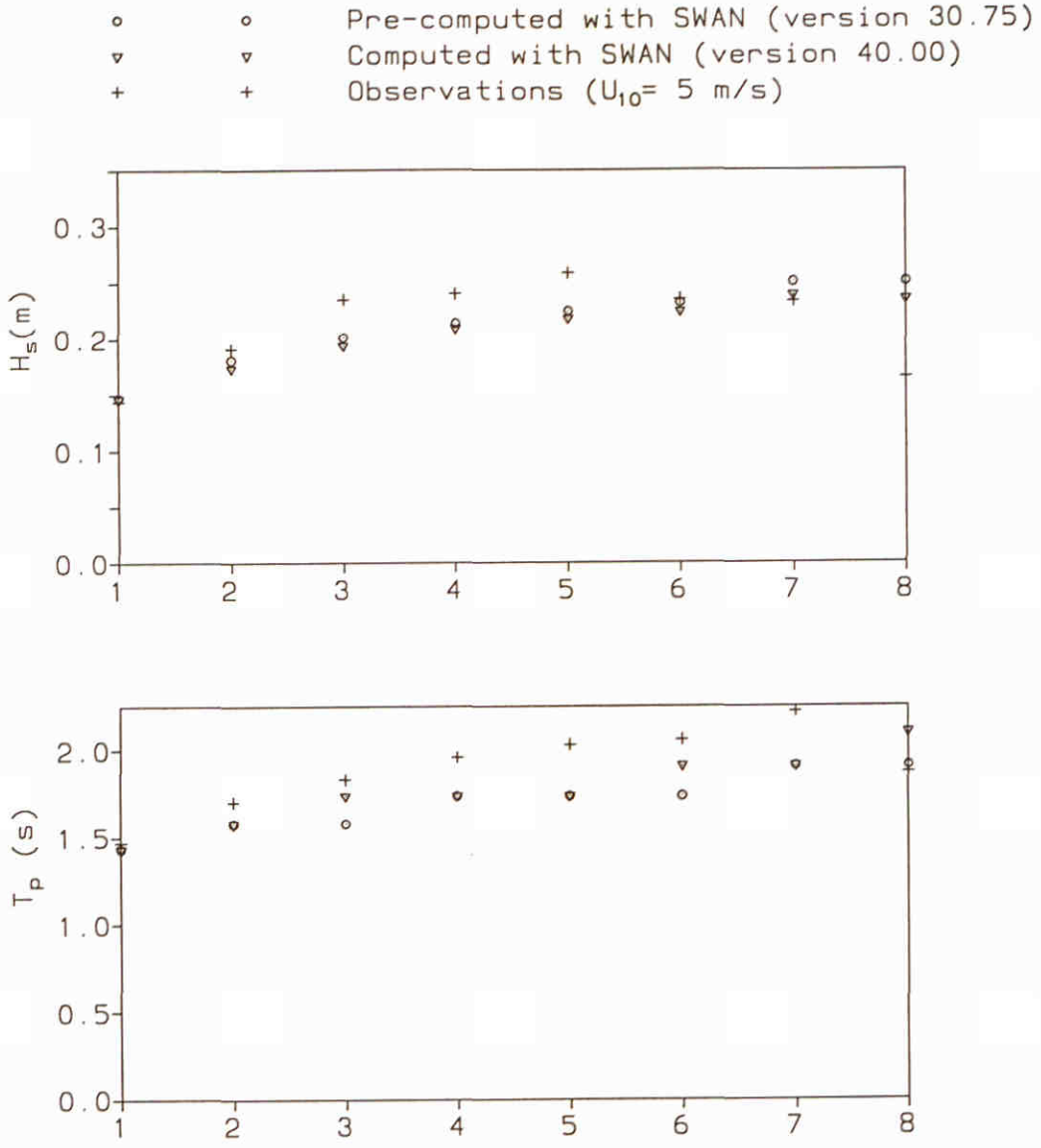


F41LakgR1 F41b

Lage George: low wind speed

| | | |
|---|---|---|
| Lake George field experiment<br>Extended Komen et al. (1984) expression with $\beta^1$ | SWAN 40.00 | |
| WL \| delft hydraulics | H3529 | Fig. 7.3.b |

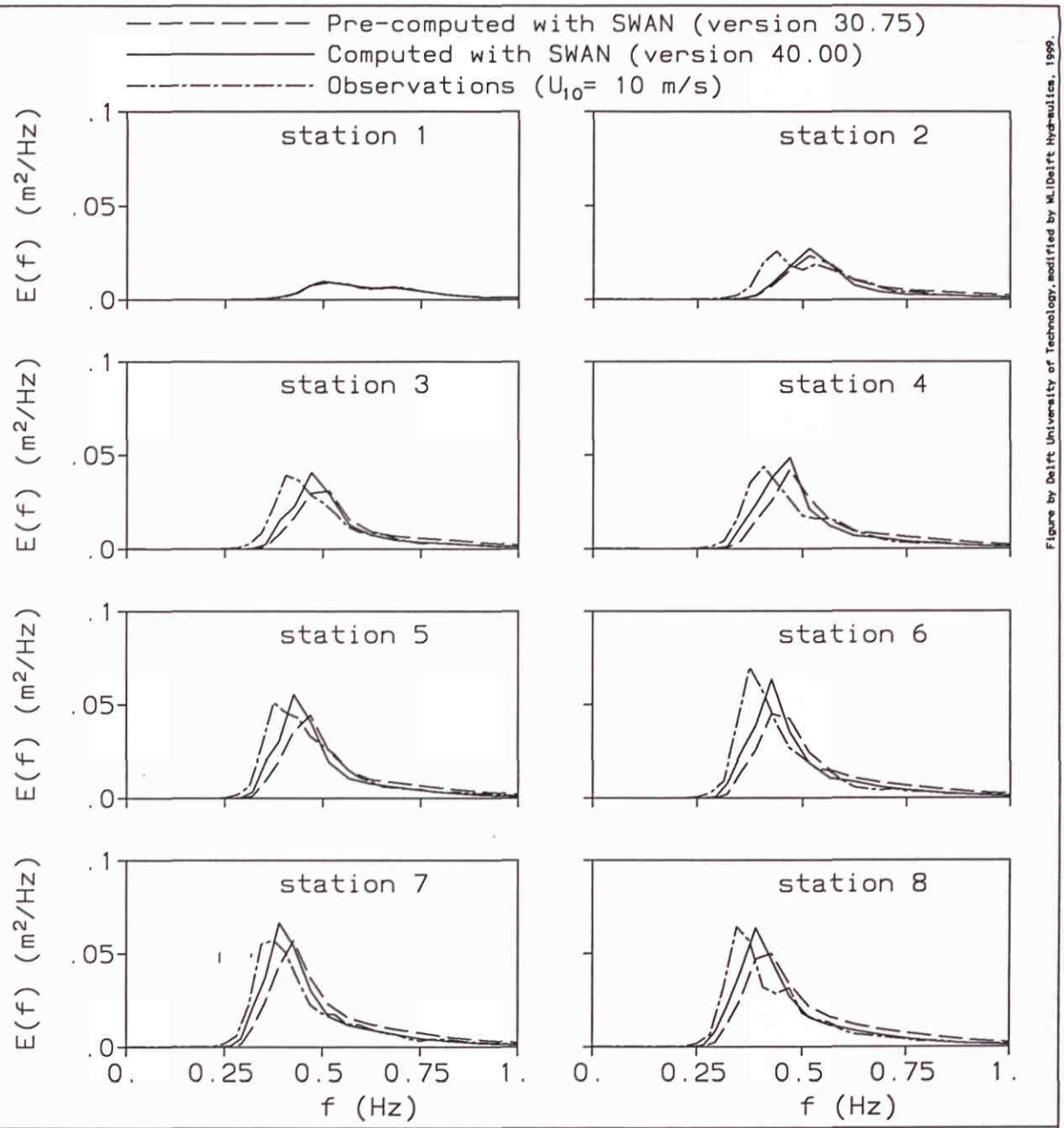




F41lakegR2 F41c

Lake George: moderate wind speed

Lake George field experiment

Extended Komen et al. (1984) expression with $\beta$[1]

SWAN 40.00

WL | delft hydraulics

H3529

Fig. 7.3.c

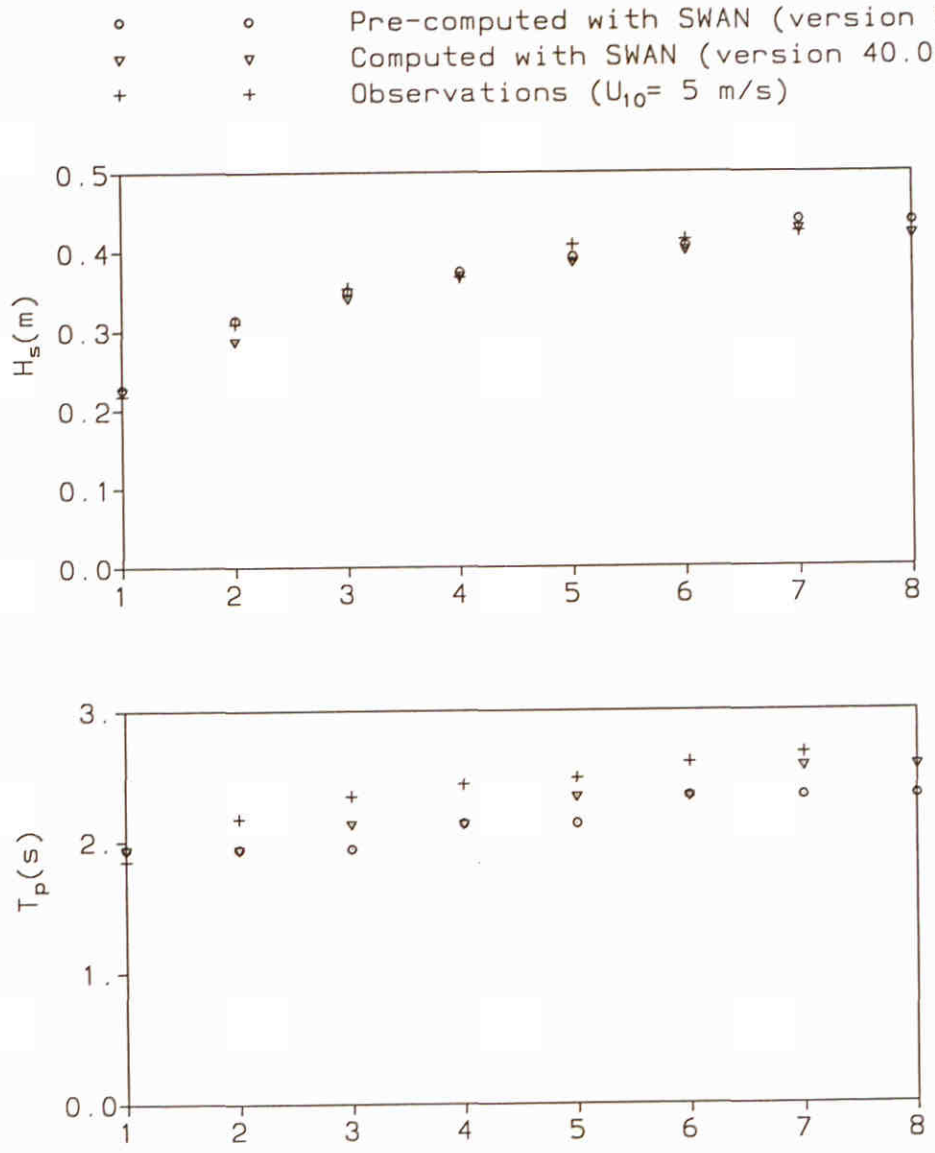


F41LakgR2 F41d

Lage George: moderate wind speed

Lake George field experiment

Extended Komen et al. (1984) expression with $\beta^1$

SWAN 40.00

WL | delft hydraulics

H3529

Fig. 7.3.d

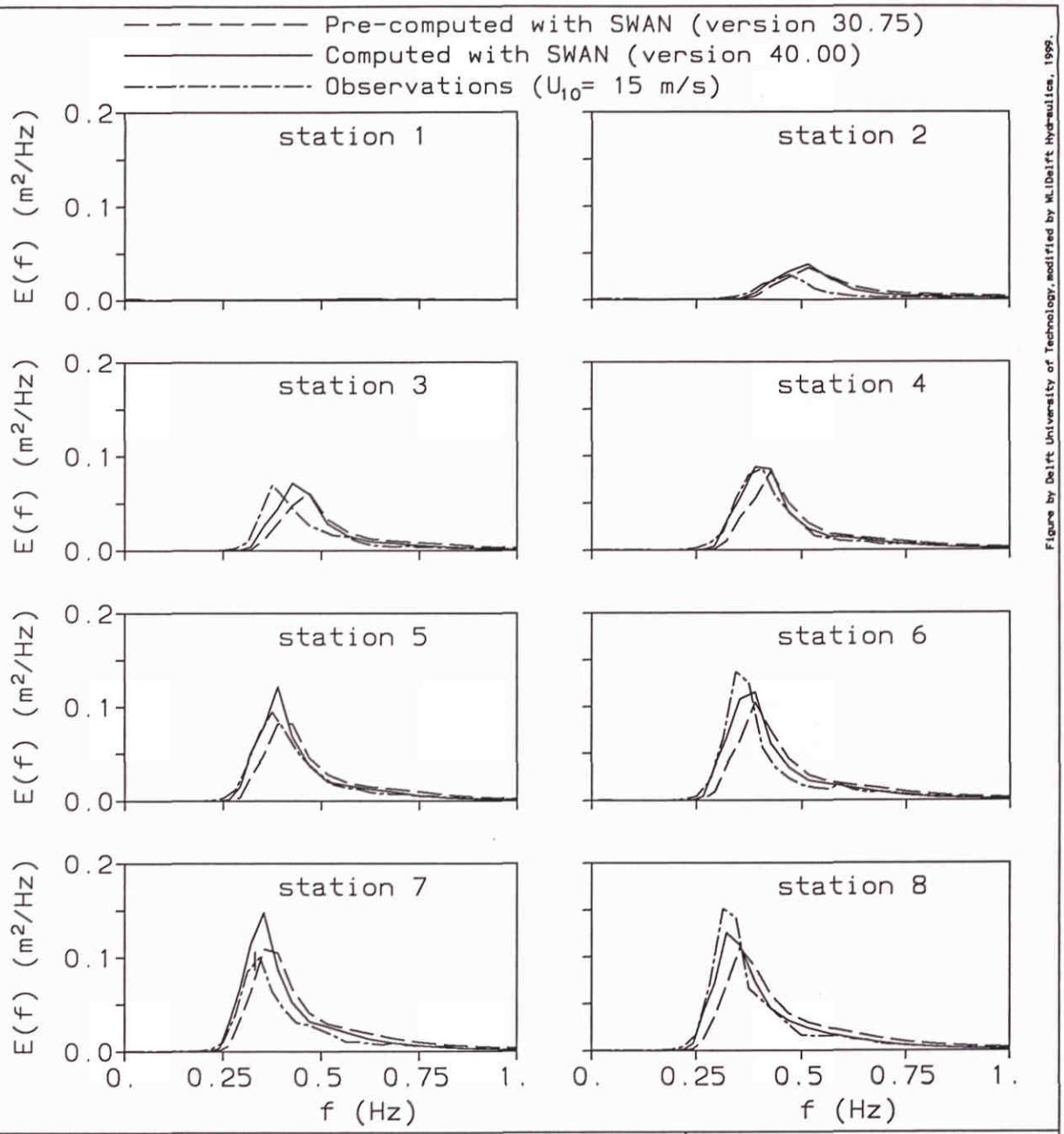


Figure by Delft University of Technology, modified by WL|Delft Hydraulics, 1999.

October 1999

F41lakegR3 F41e

Lake George: high wind speed

Lake George field experiment

Extended Komen et al. (1984) expression with $\beta^1$

SWAN 40.00

WL | delft hydraulics

H3529

Fig. 7.3.e

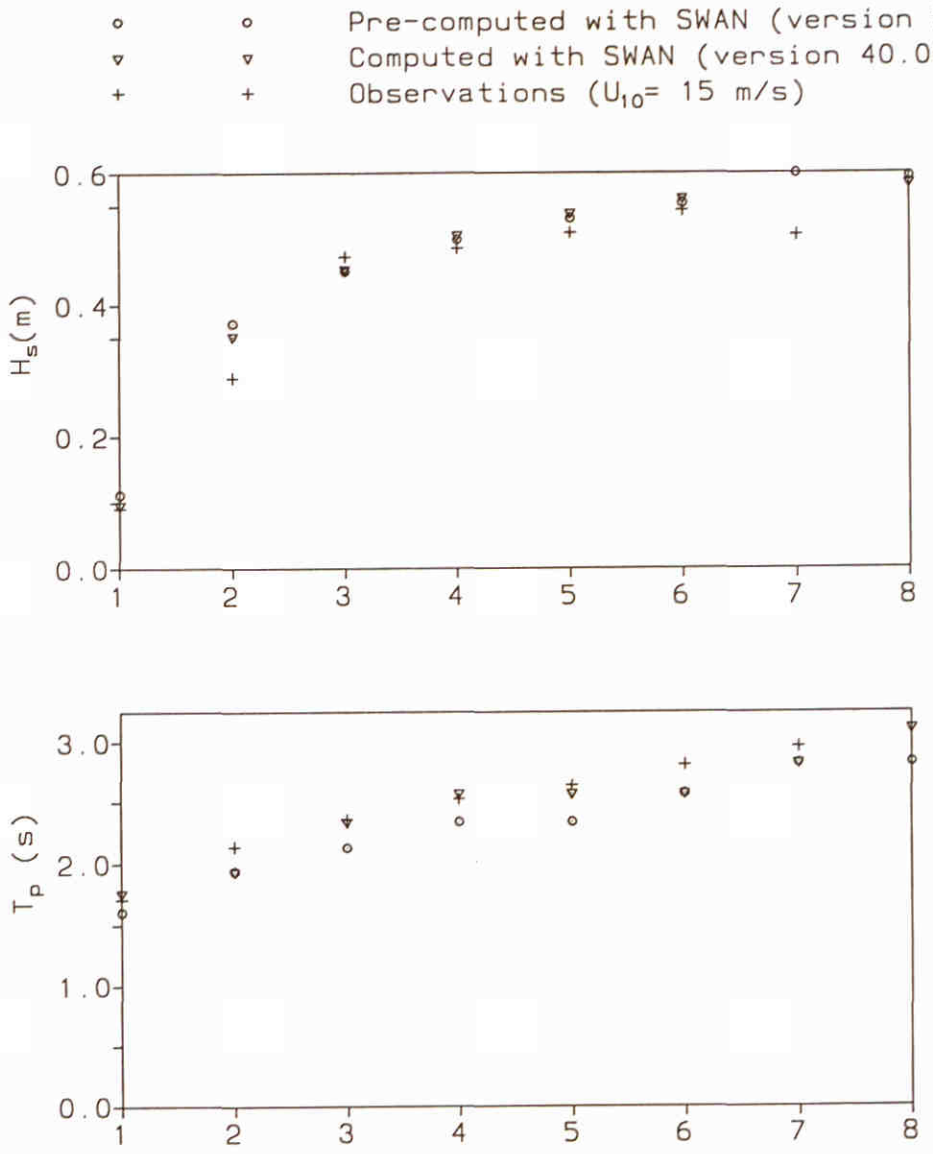


F41LakgR3 F41f

Lage George: high wind speed

| | | |
|---|---|---|
| Lake George field experiment<br>Extended Komen et al. (1984) expression with $\beta^1$ | SWAN 40.00 | |
| WL \| delft hydraulics | H3529 | Fig. 7.3.f |

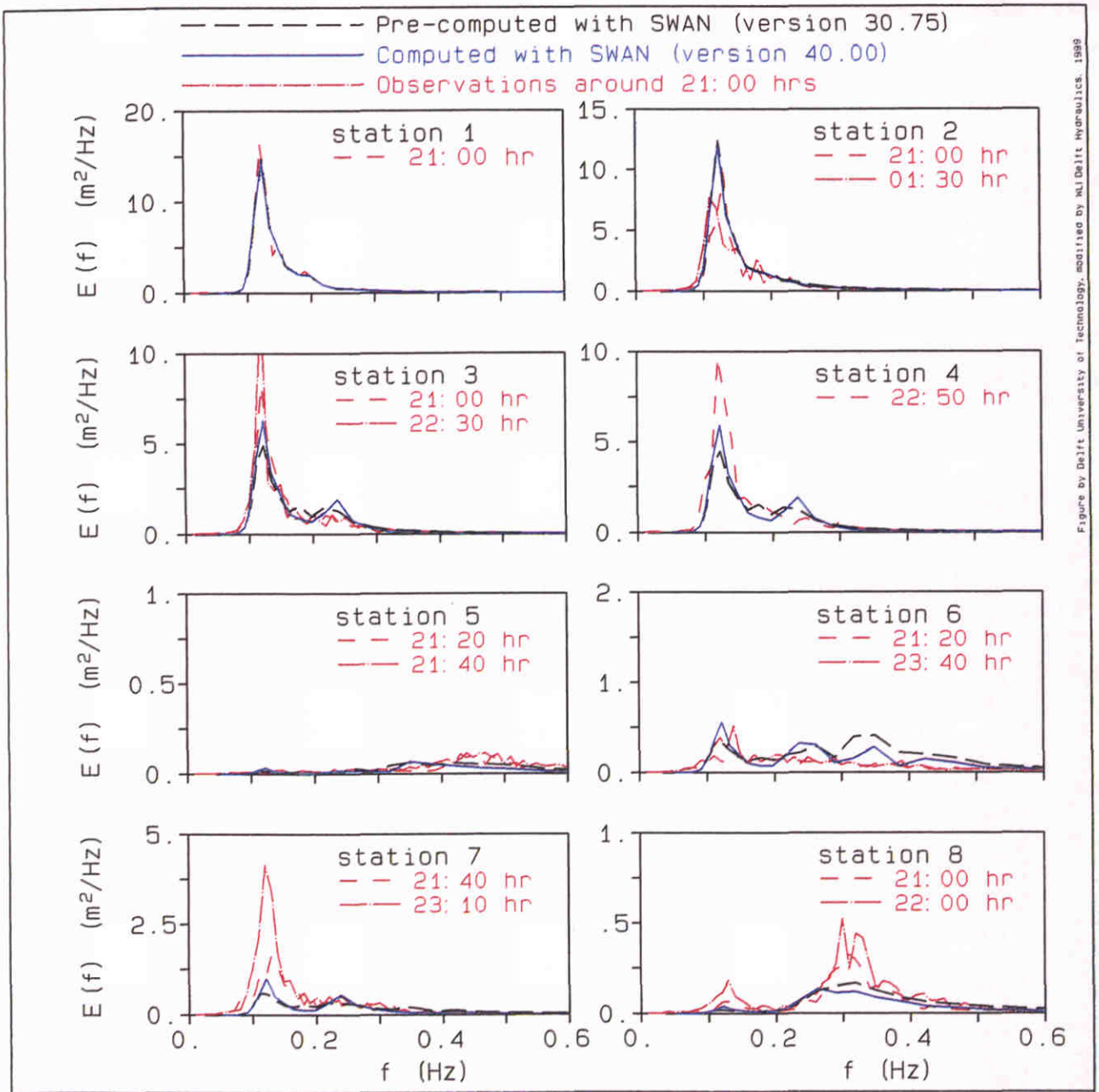


F31harinR1 F31a

Haringvliet: 21:00 UTC (run 1)

Haringvliet estuary field experiment

Extended Komen et al. (1984) expression with $\beta^0$

SWAN 40.00

WL | delft hydraulics

H3529

Fig. 7.4.a

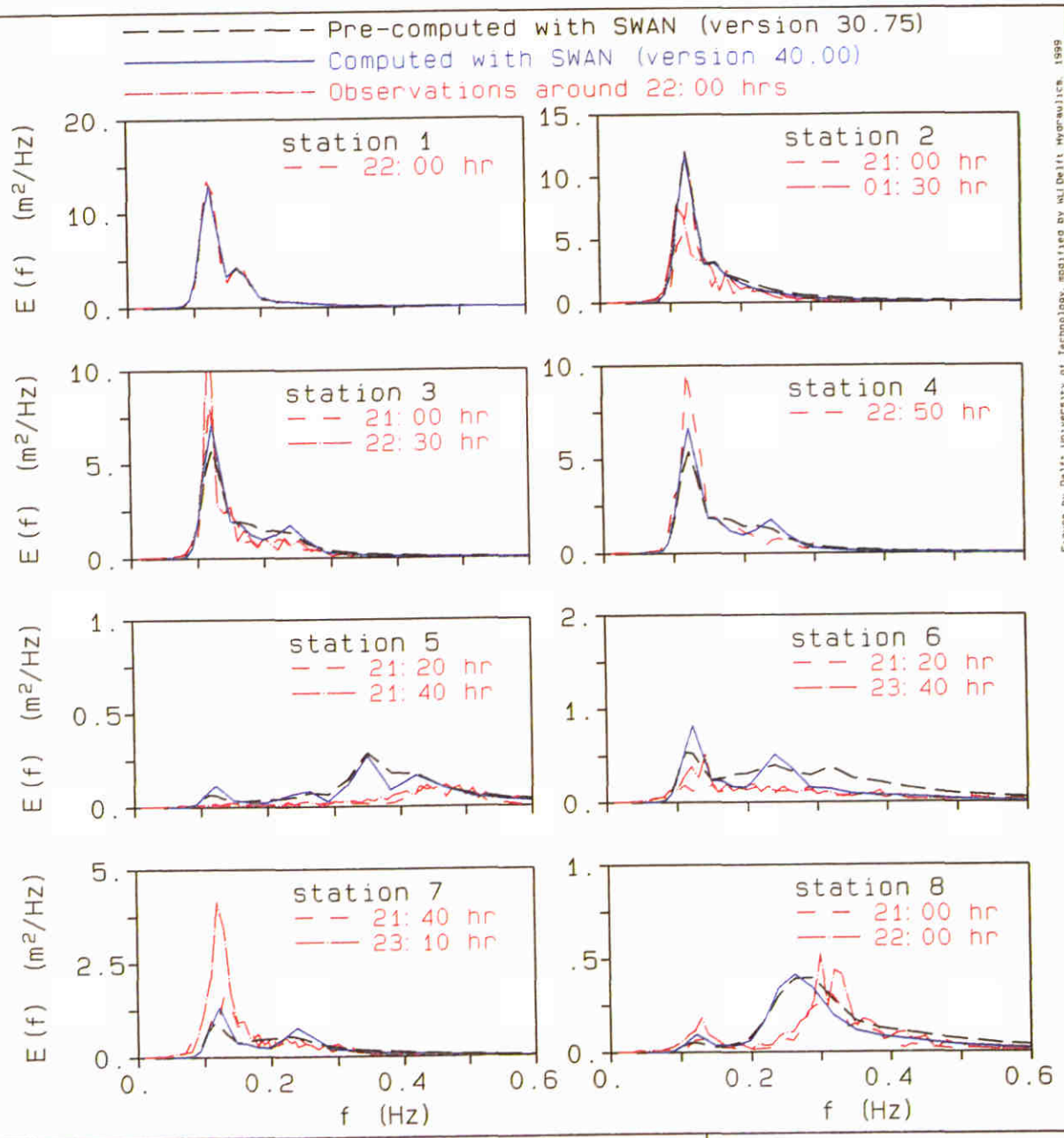


F32harinR2 F32a

Haringvliet: 22:00 UTC (run 2)

Haringvliet estuary field experiment

Extended Komen et al. (1984) expression with $\beta^0$

SWAN 40.00

WL | delft hydraulics

H3529

Fig. 7.4.b

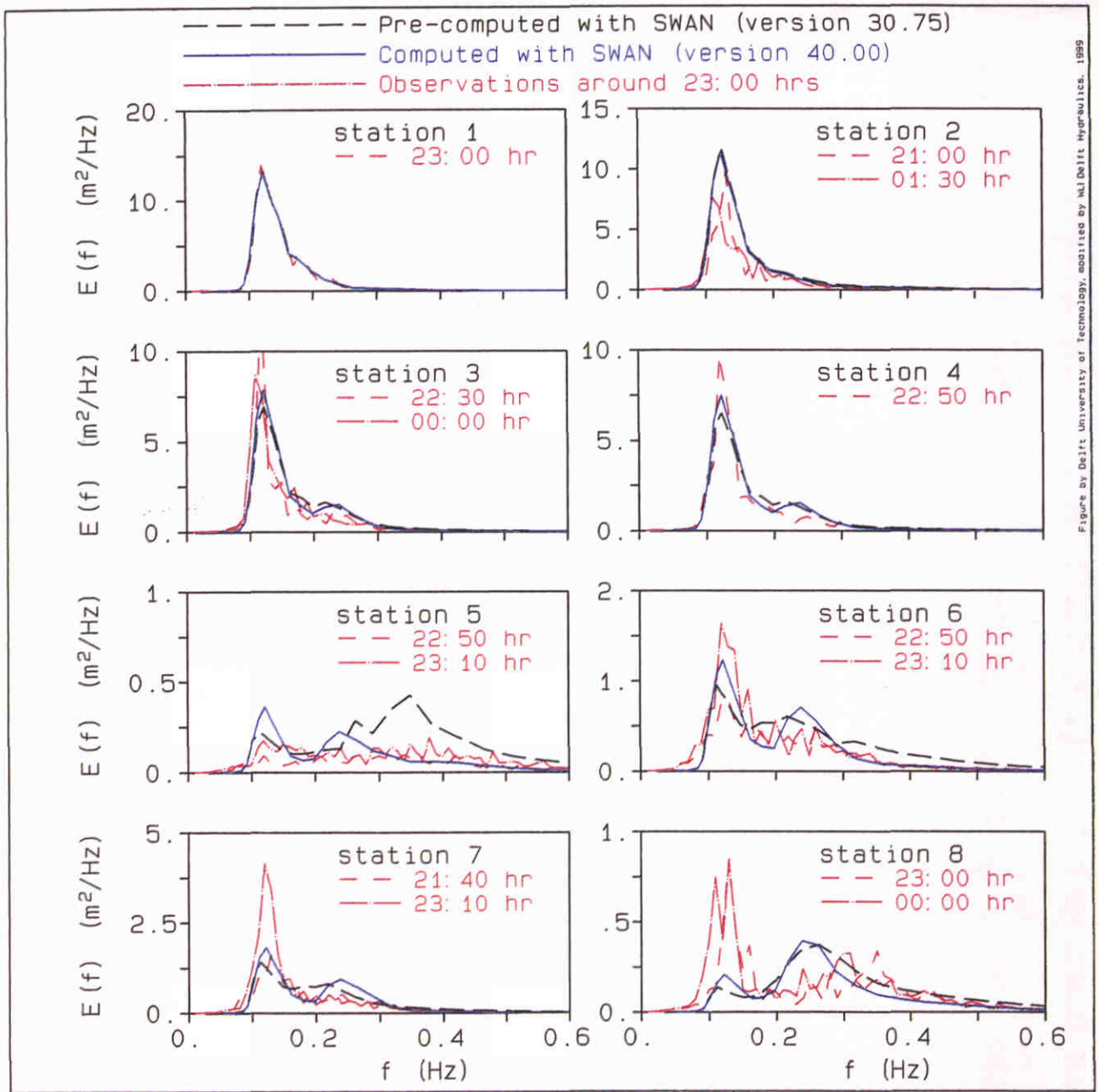


F33harinR3 F33a

Haringvliet: 23:00 UTC (run 3)

Haringvliet estuary field experiment

Extended Komen et al. (1984) expression with $\beta^0$

SWAN 40.00

WL | delft hydraulics

H3529

Fig. 7.4.c

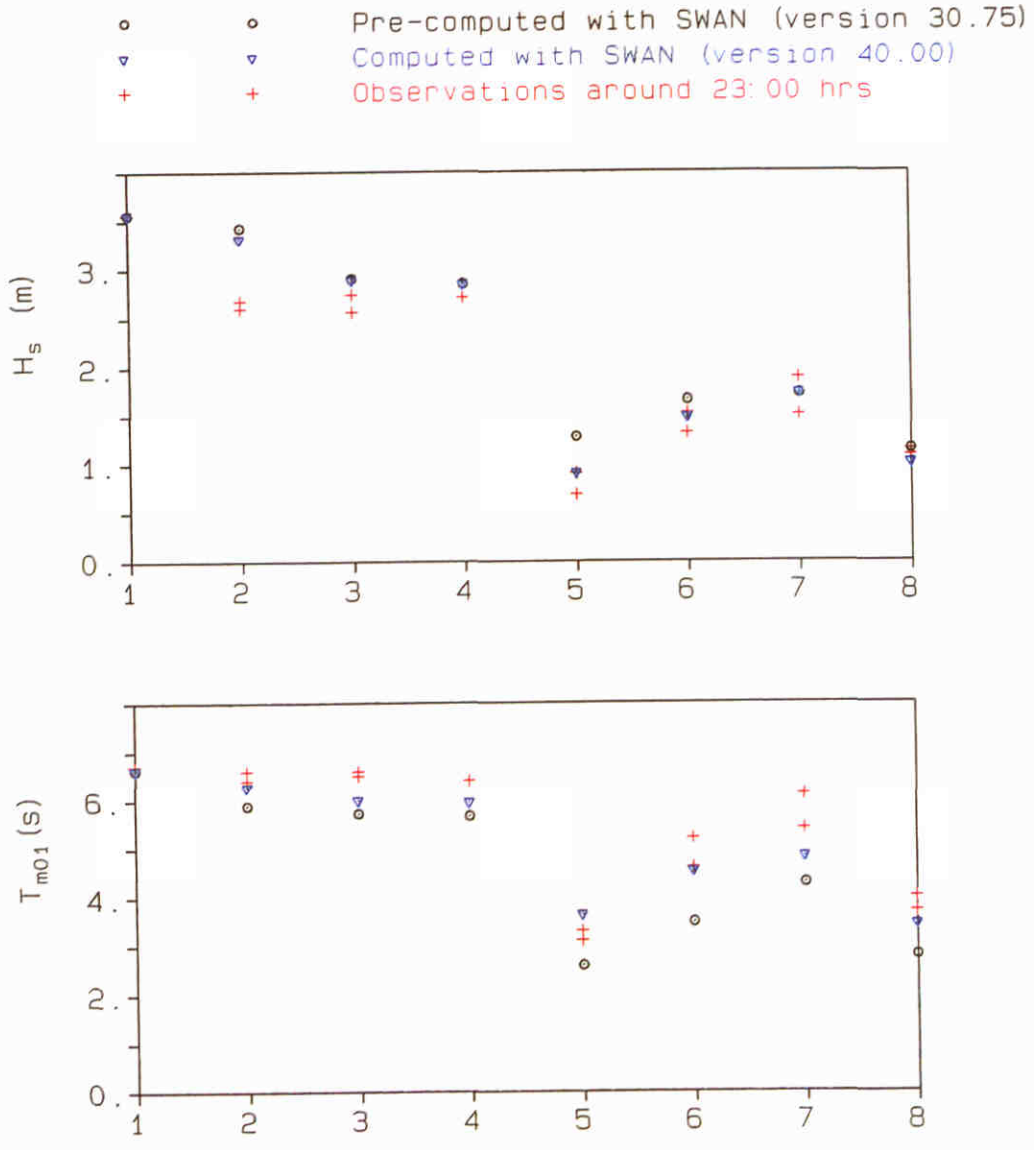


Figure by Delft University of Technology, modified by WL|Delft Hydraulics 1998

October 1999

F33harinR3 F33b

Haringvliet: 23:00 UTC (run 3)

Haringvliet estuary field experiment

Extended Komen et al. (1984) expression with $\beta^0$

SWAN 40.00

WL | delft hydraulics

H3529

Fig. 7.4.d

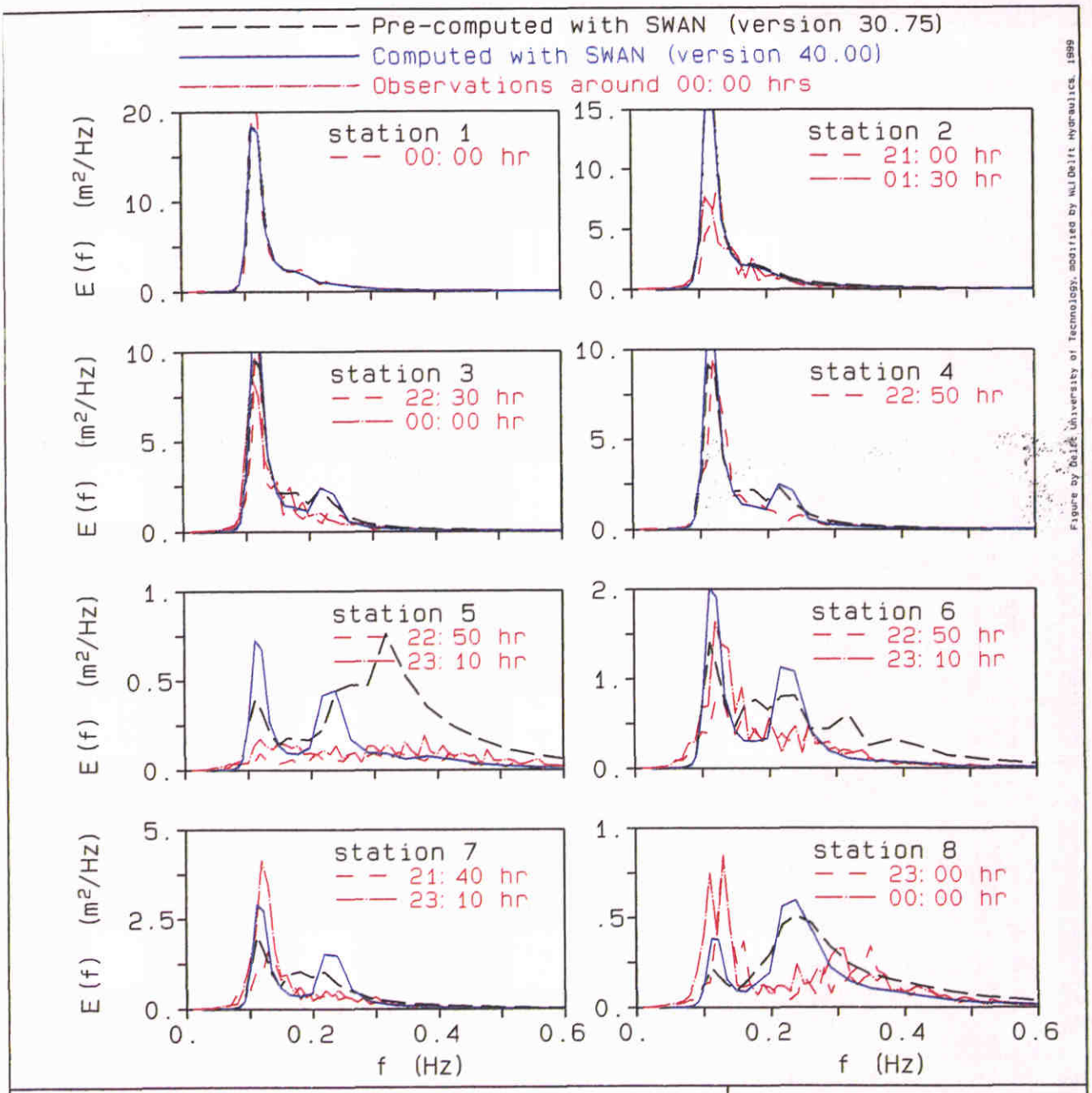


F34harinR4 F34a

Haringvliet: 00:00 UTC (run 4)

Haringvliet estuary field experiment

Extended Komen et al. (1984) expression with $\beta^0$

SWAN 40.00

WL | delft hydraulics

H3529

Fig. 7.4.e

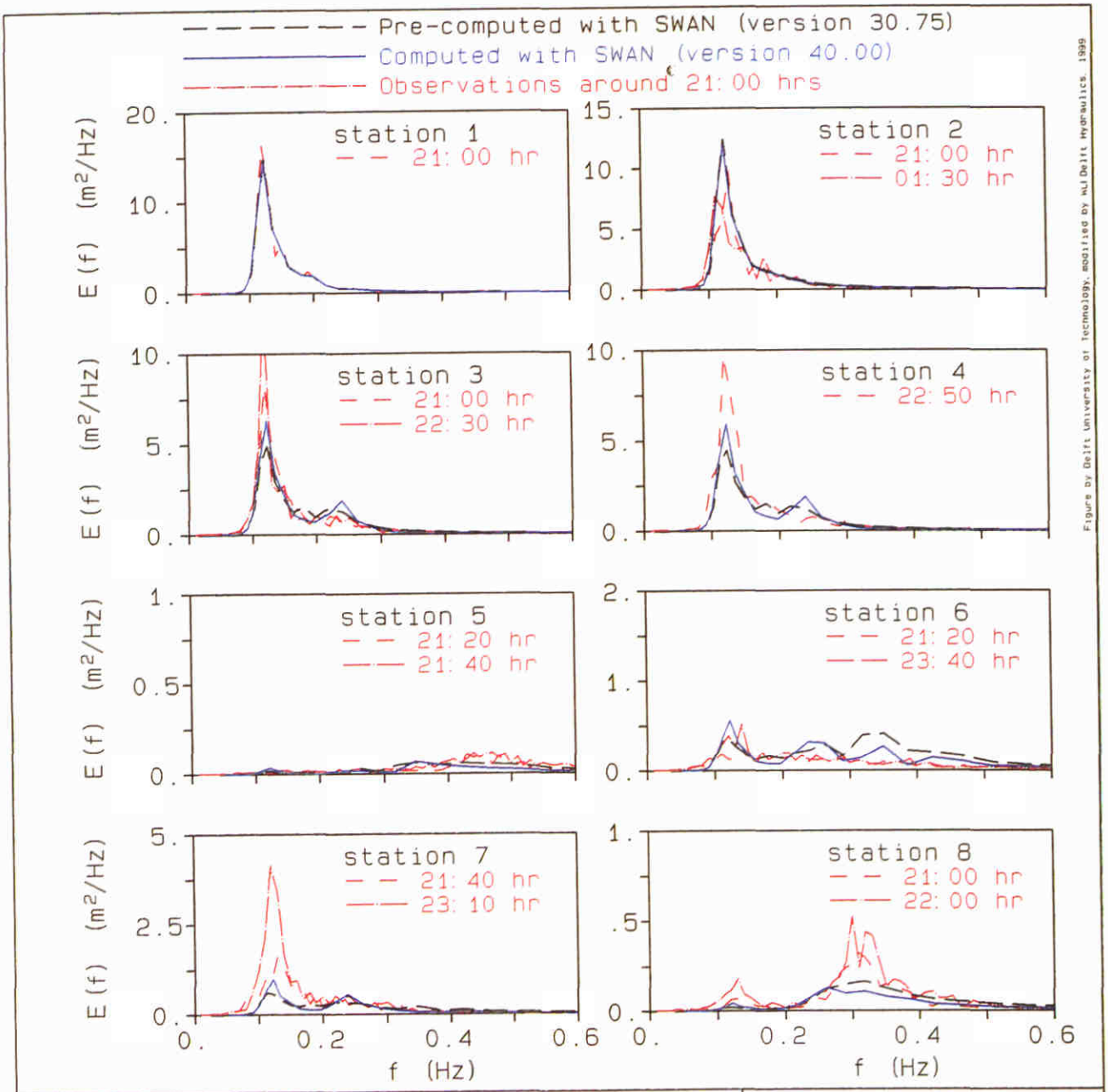


F31harinR1 F31a

Haringvliet: 21:00 UTC (run 1)

Haringvliet estuary field experiment

Extended Komen et al. (1984) expression with $\beta^{0.5}$

SWAN 40.00

WL | delft hydraulics

H3529

Fig. 7.5.a

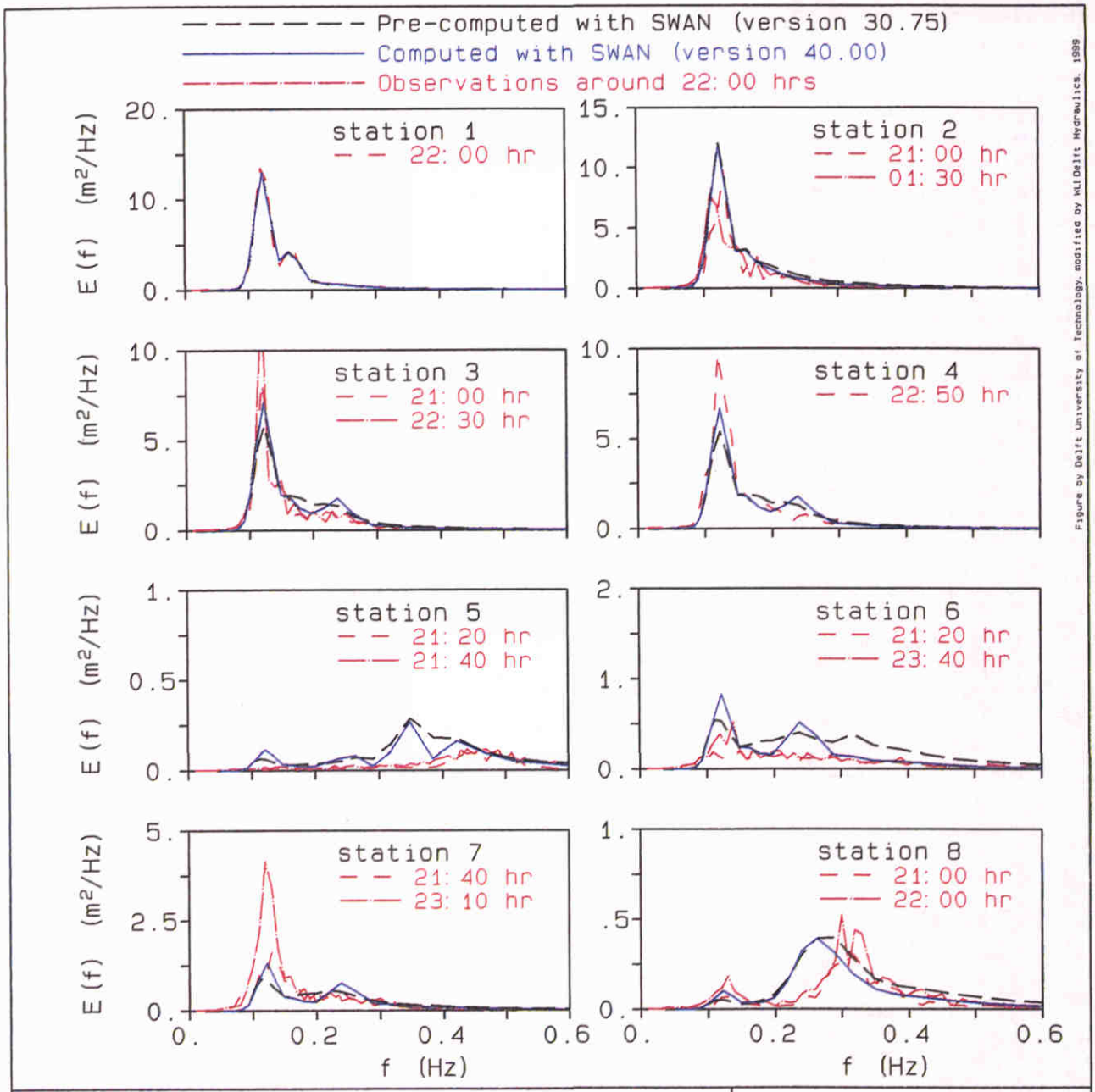


F32harinR2 F32a

Haringvliet: 22:00 UTC (run 2)

| | | |
|---|---|---|
| Haringvliet estuary field experiment<br>Extended Komen et al. (1984) expression with $\beta^{0.5}$ | SWAN 40.00 | |
| WL \| delft hydraulics | H3529 | Fig. 7.5.b |

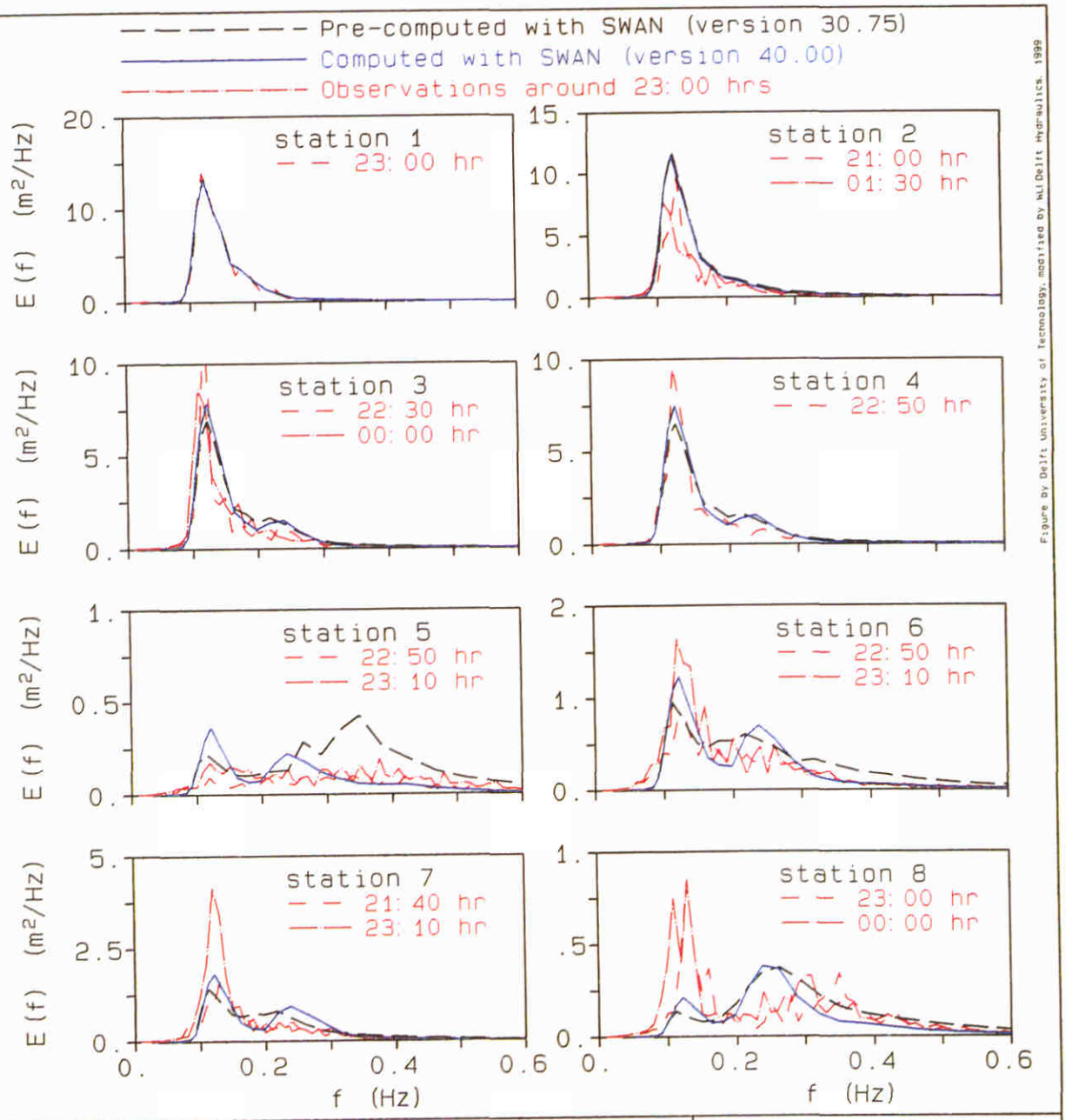


F33harinR3 F33a

Haringvliet: 23:00 UTC (run 3)

Haringvliet estuary field experiment

Extended Komen et al. (1984) expression with $\beta^{0.5}$

SWAN 40.00

WL | delft hydraulics

H3529

Fig. 7.5.c

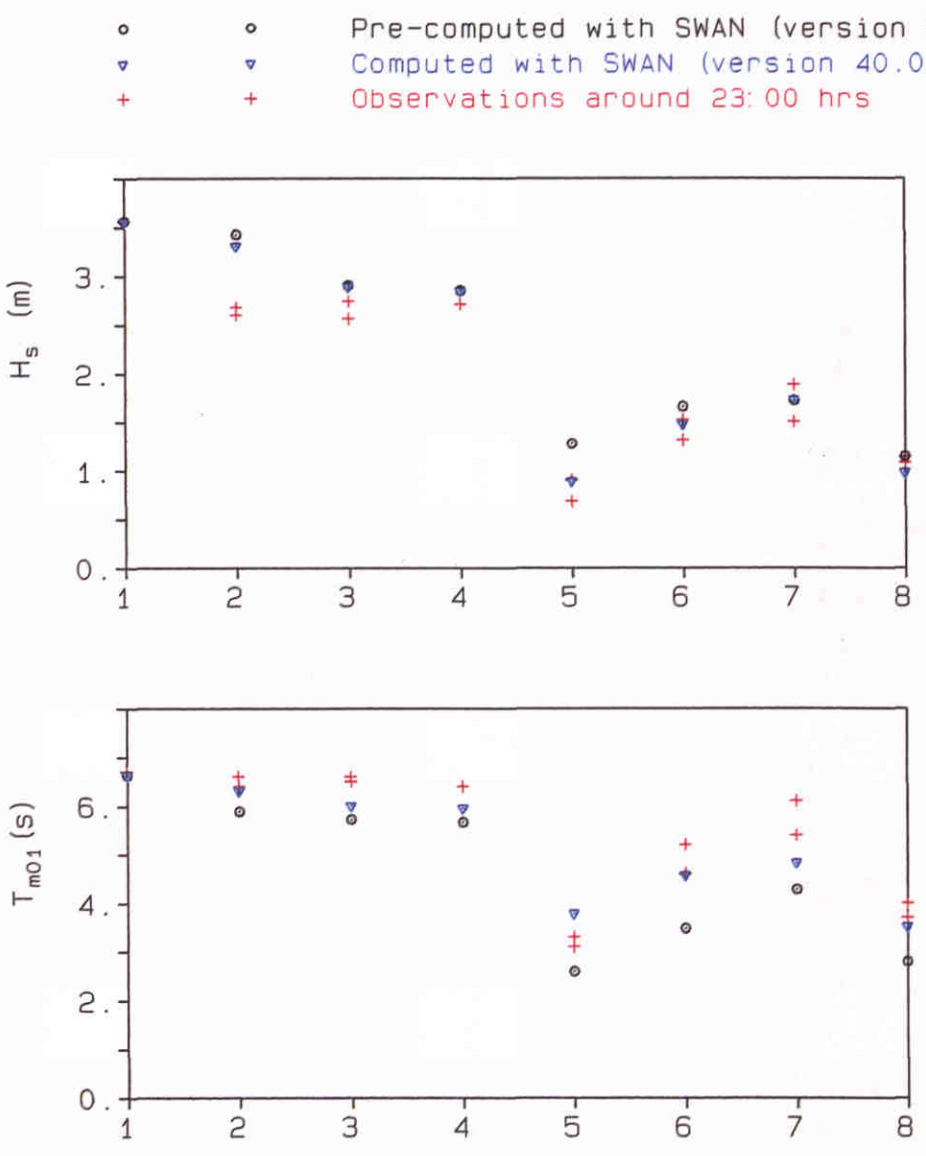




F33harinR3 F33b

Haringvliet: 23:00 UTC (run 3)

Haringvliet estuary field experiment

Extended Komen et al. (1984) expression with $\beta^{0.5}$

SWAN 40.00

WL | delft hydraulics

H3529

Fig. 7.5.d

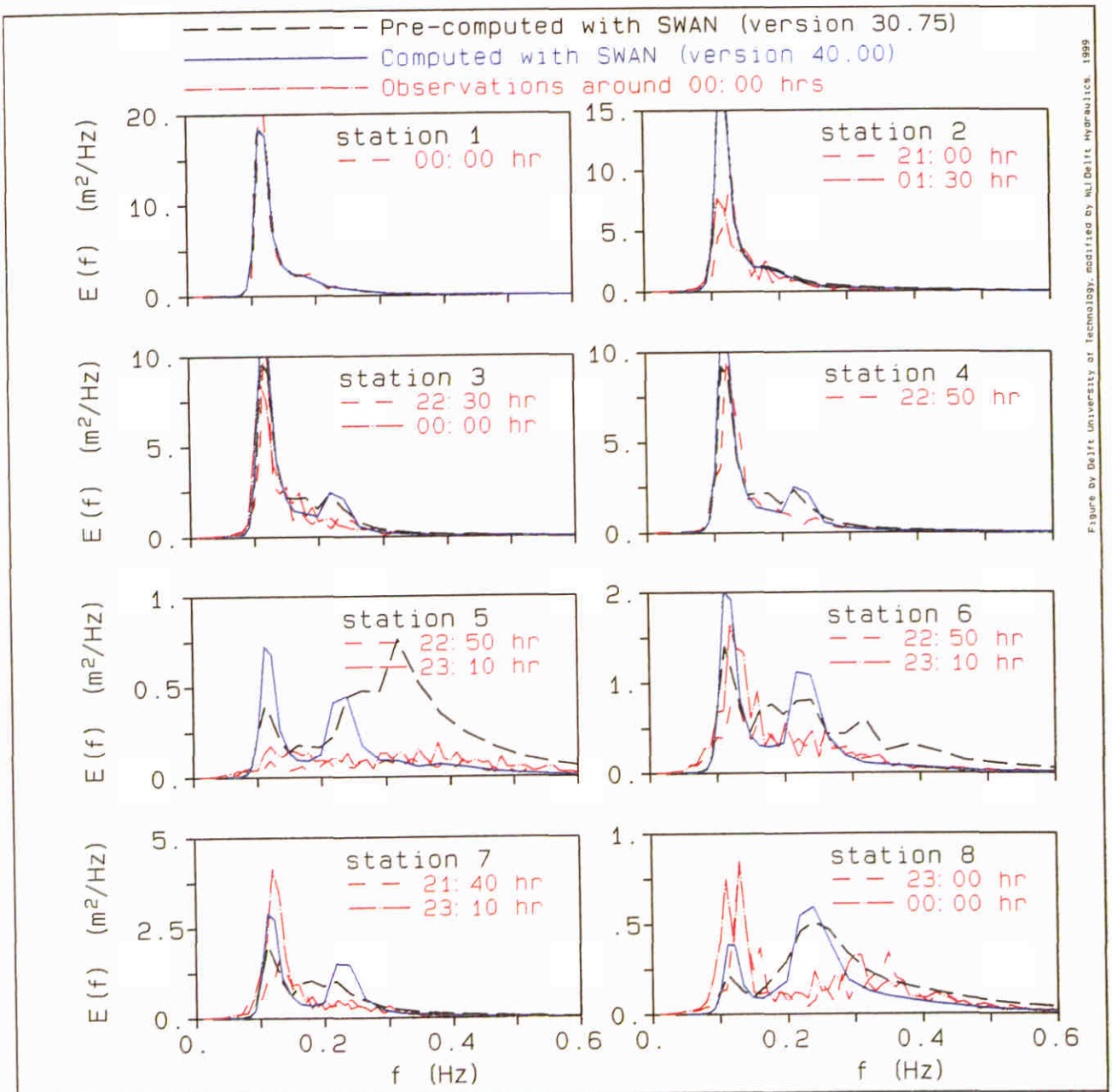


F34harinR4 F34a

Haringvliet: 00:00 UTC (run 4)

Haringvliet estuary field experiment

Extended Komen et al. (1984) expression with $\beta^{0.5}$

SWAN 40.00

WL | delft hydraulics

H3529

Fig. 7.5.e

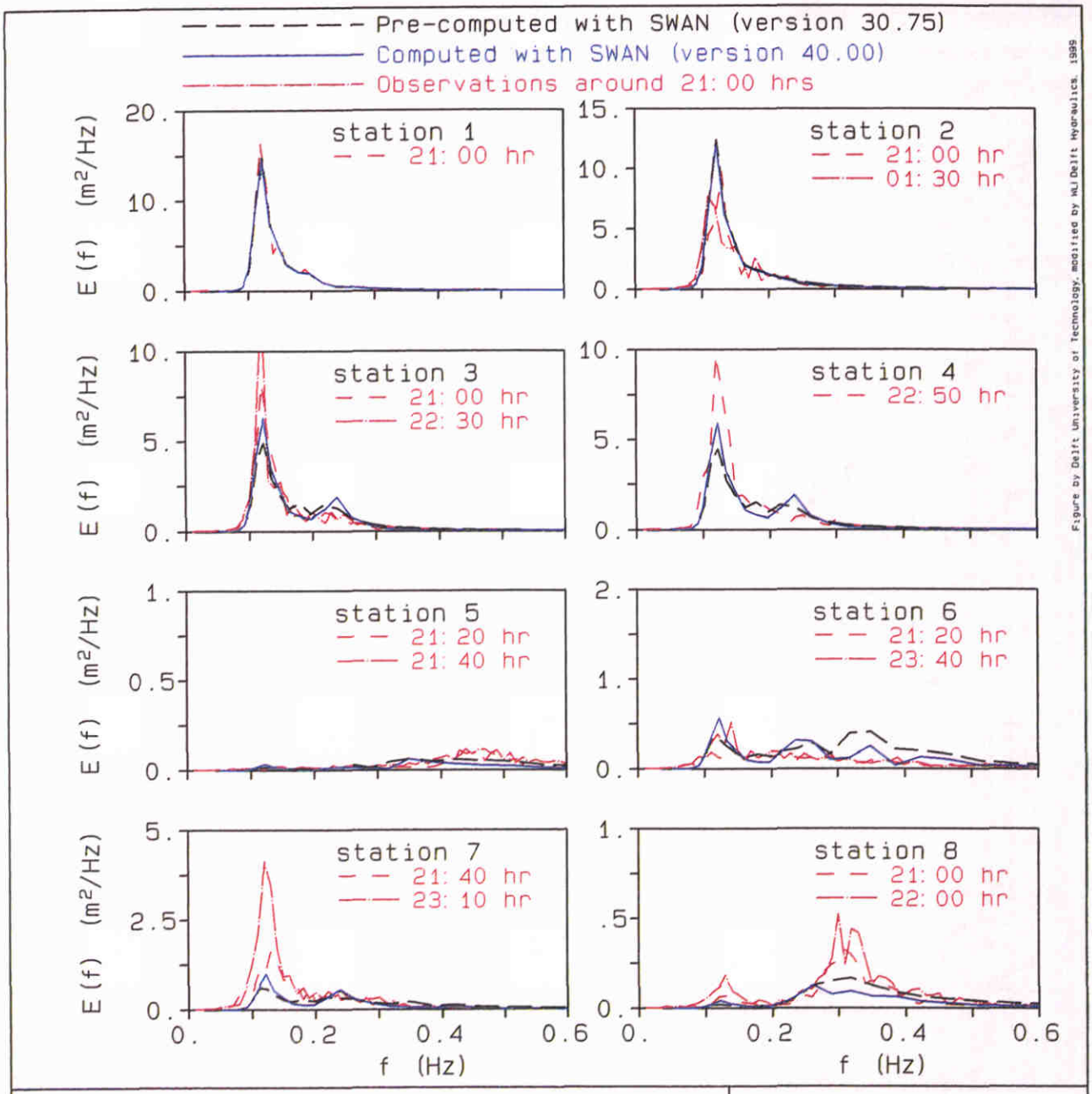


F31harinR1 F31a

Haringvliet: 21:00 UTC (run 1)

Haringvliet estuary field experiment

Extended Komen et al. (1984) expression with $\beta^1$

SWAN 40.00

WL | delft hydraulics

H3529

Fig. 7.6.a

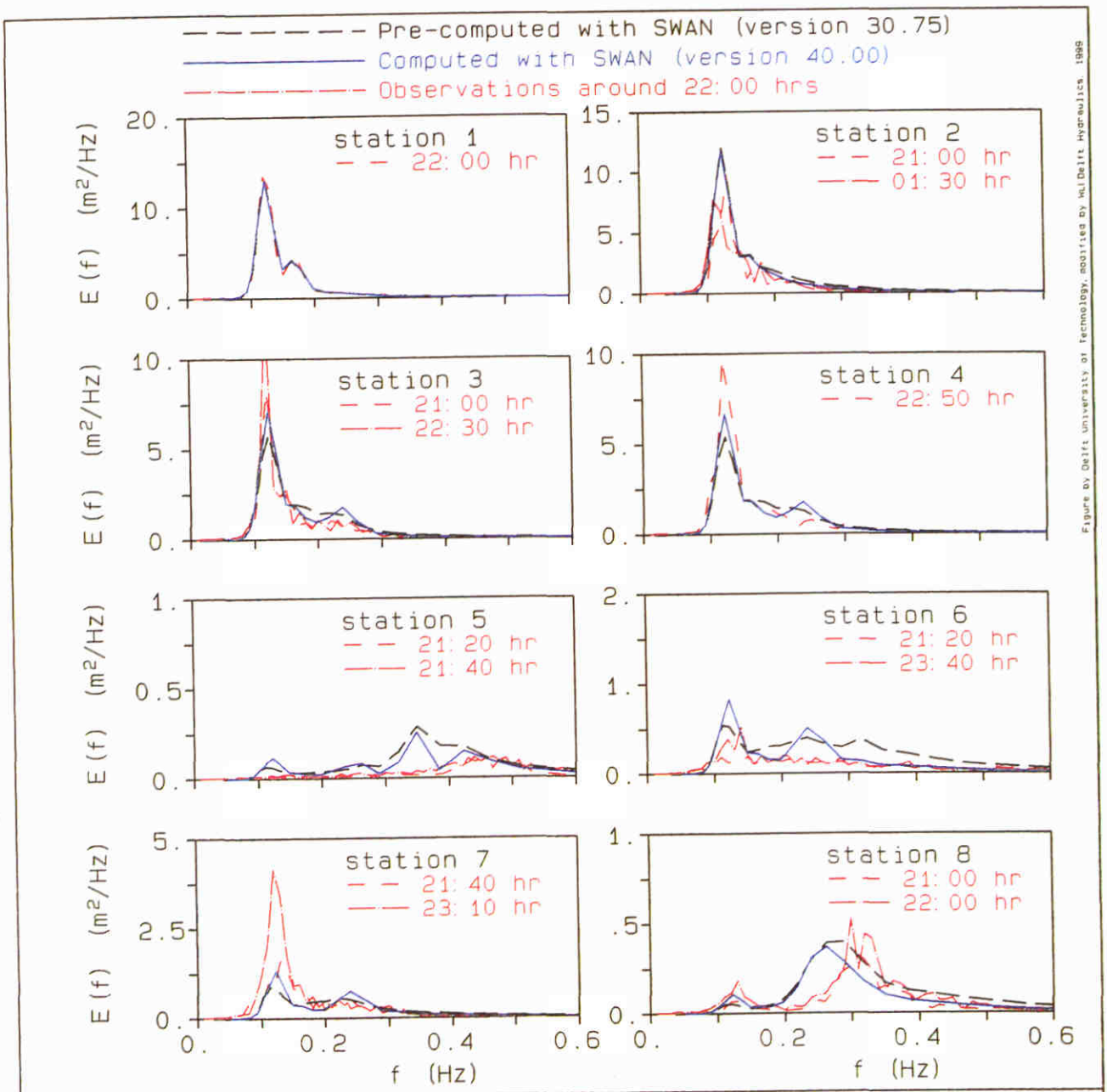


F32harinR2 F32a

Haringvliet: 22:00 UTC (run 2)

Haringvliet estuary field experiment

Extended Komen et al. (1984) expression with $\beta^1$

SWAN 40.00

WL | delft hydraulics

H3529

Fig. 7.6.b

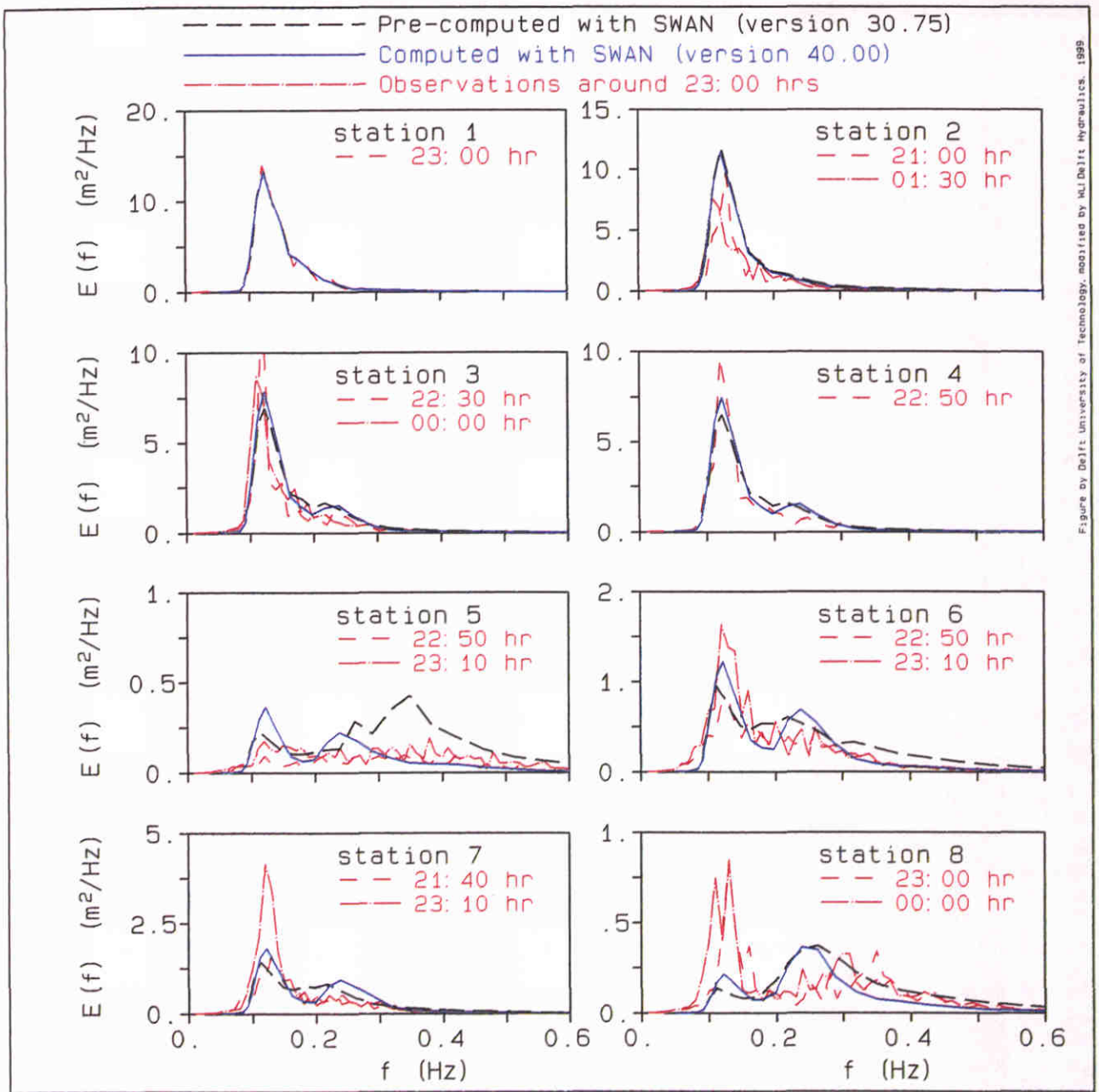


F33harinR3 F33a

Haringvliet: 23:00 UTC (run 3)

Haringvliet estuary field experiment

Extended Komen et al. (1984) expression with $\beta^1$

SWAN 40.00

WL | delft hydraulics

H3529

Fig. 7.6.c

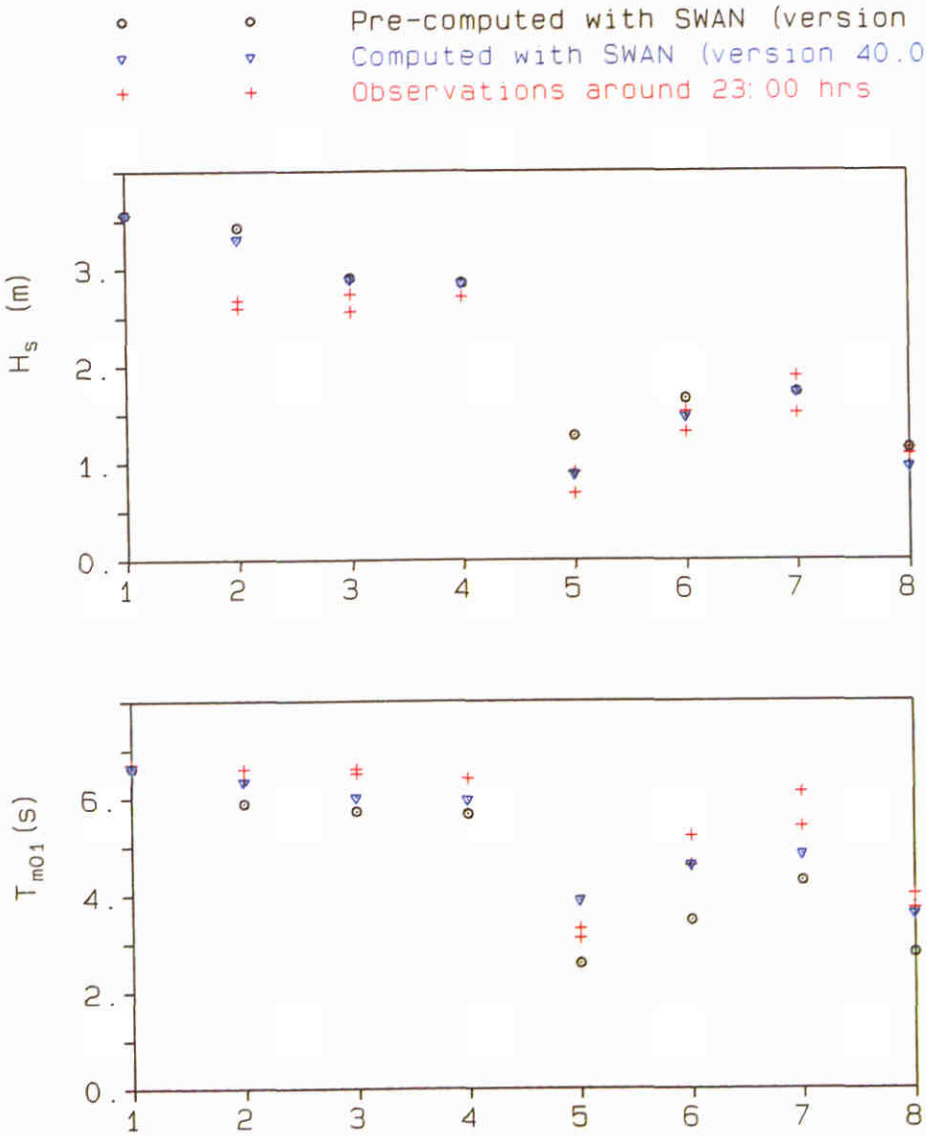




F33harinR3 F33b

Haringvliet: 23:00 UTC (run 3)

Haringvliet estuary field experiment

Extended Komen et al. (1984) expression with $\beta$[1]

SWAN 40.00

WL | delft hydraulics

H3529

Fig. 7.6.d

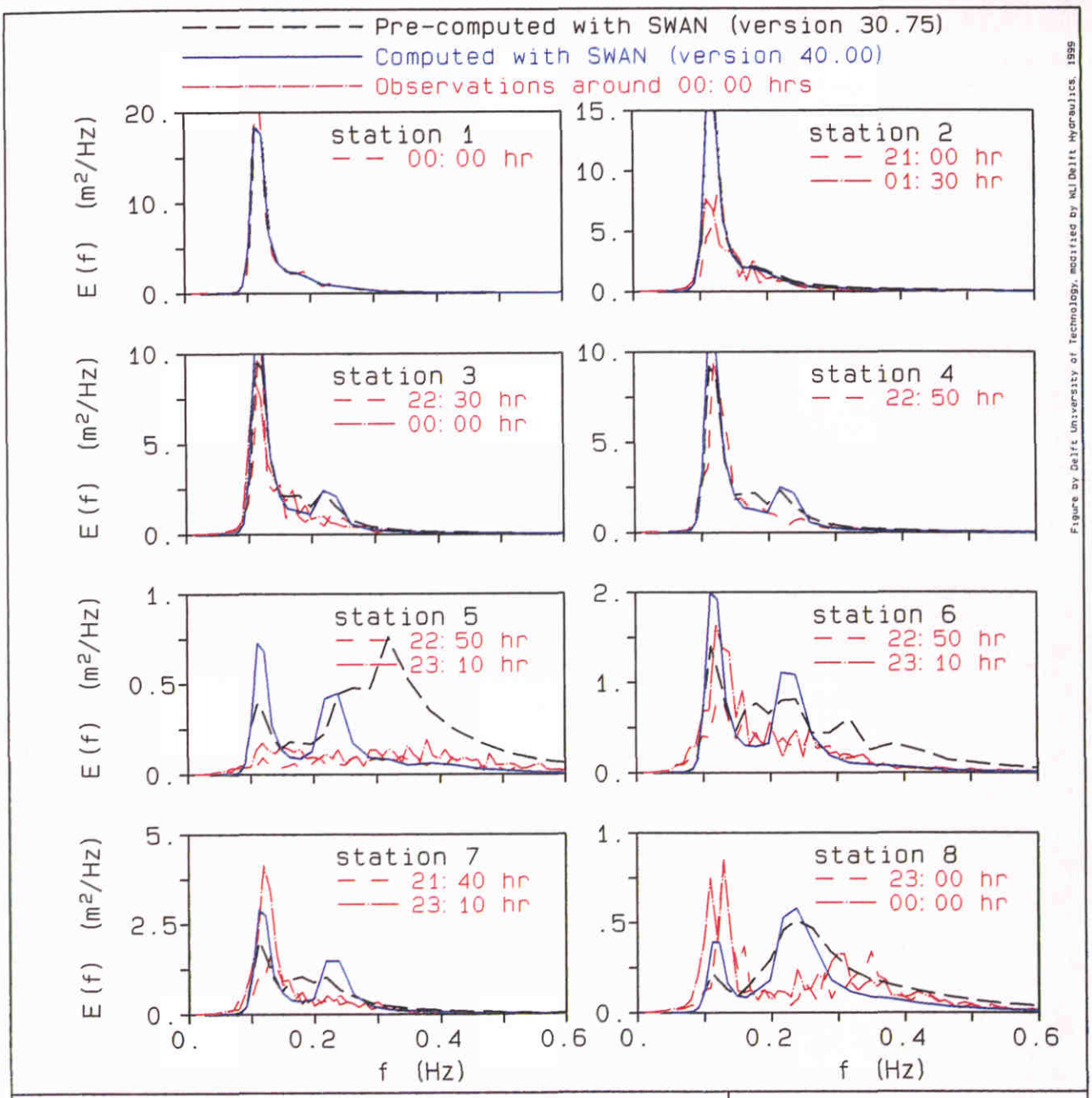


F34harinR4 F34a

Haringvliet: 00:00 UTC (run 4)

Haringvliet estuary field experiment

Extended Komen et al. (1984) expression with $\beta^1$

SWAN 40.00

WL | delft hydraulics

H3529

Fig. 7.6.e

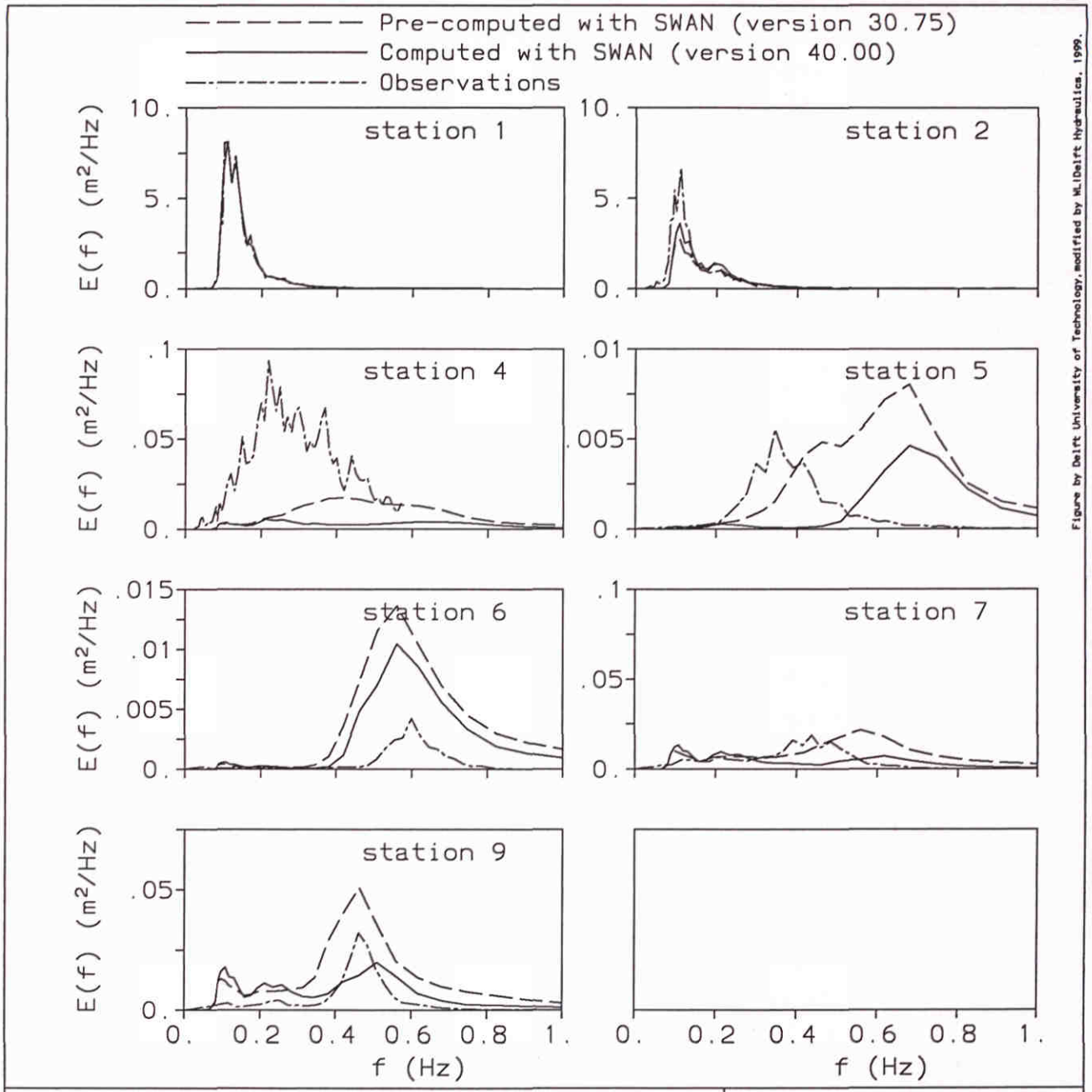


F81Nord1 F81a

Norderney :

| | | |
|---|---|---|
| Norderneyer Seegat field experiment<br>Extended Komen et al. (1984) expression with $\beta^0$ | SWAN 40.00 | |
| WL \| delft hydraulics | H3529 | Fig. 7.7.a |

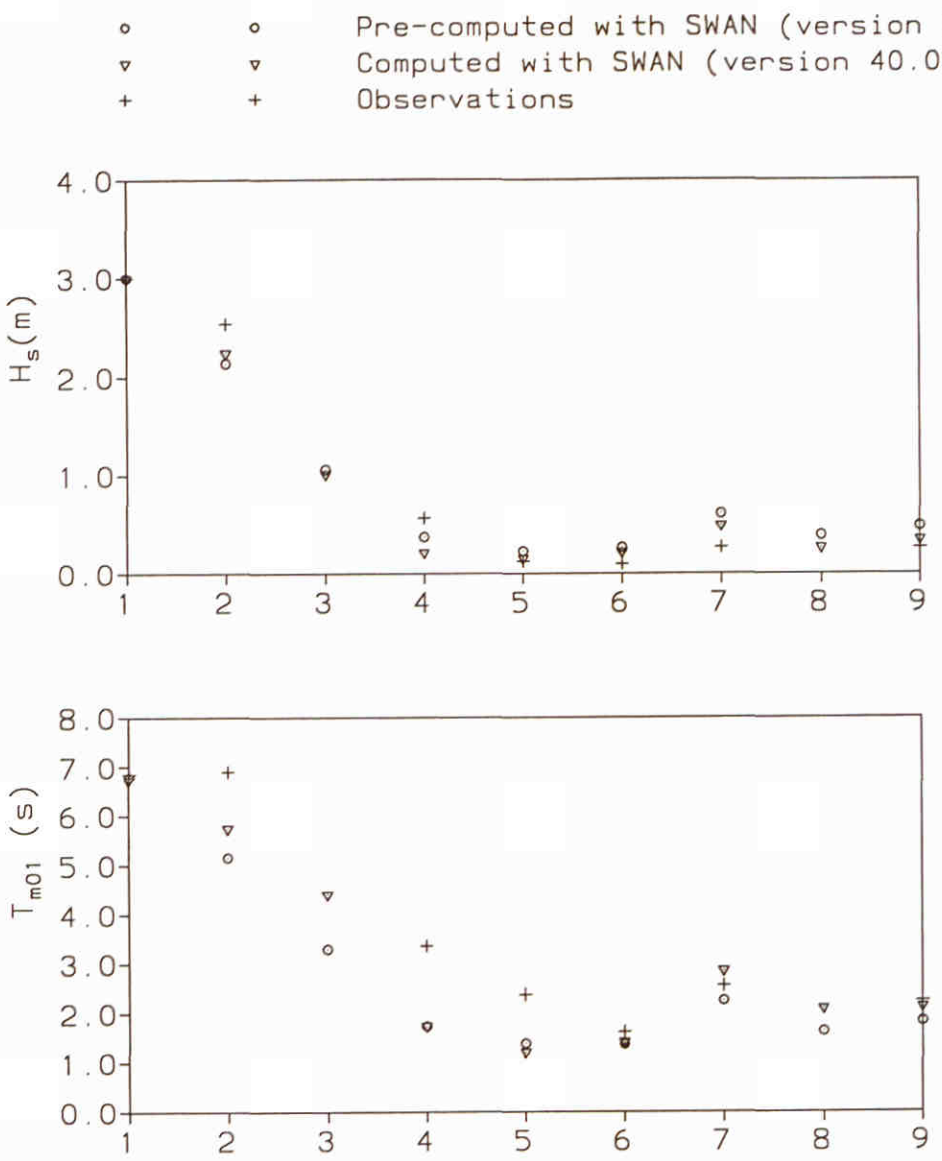


F81Nord1 F81b

Norderney :

Norderneyer Seegat field experiment

Extended Komen et al. (1984) expression with $\beta^0$

SWAN 40.00

WL | delft hydraulics

H3529

Fig. 7.7.b

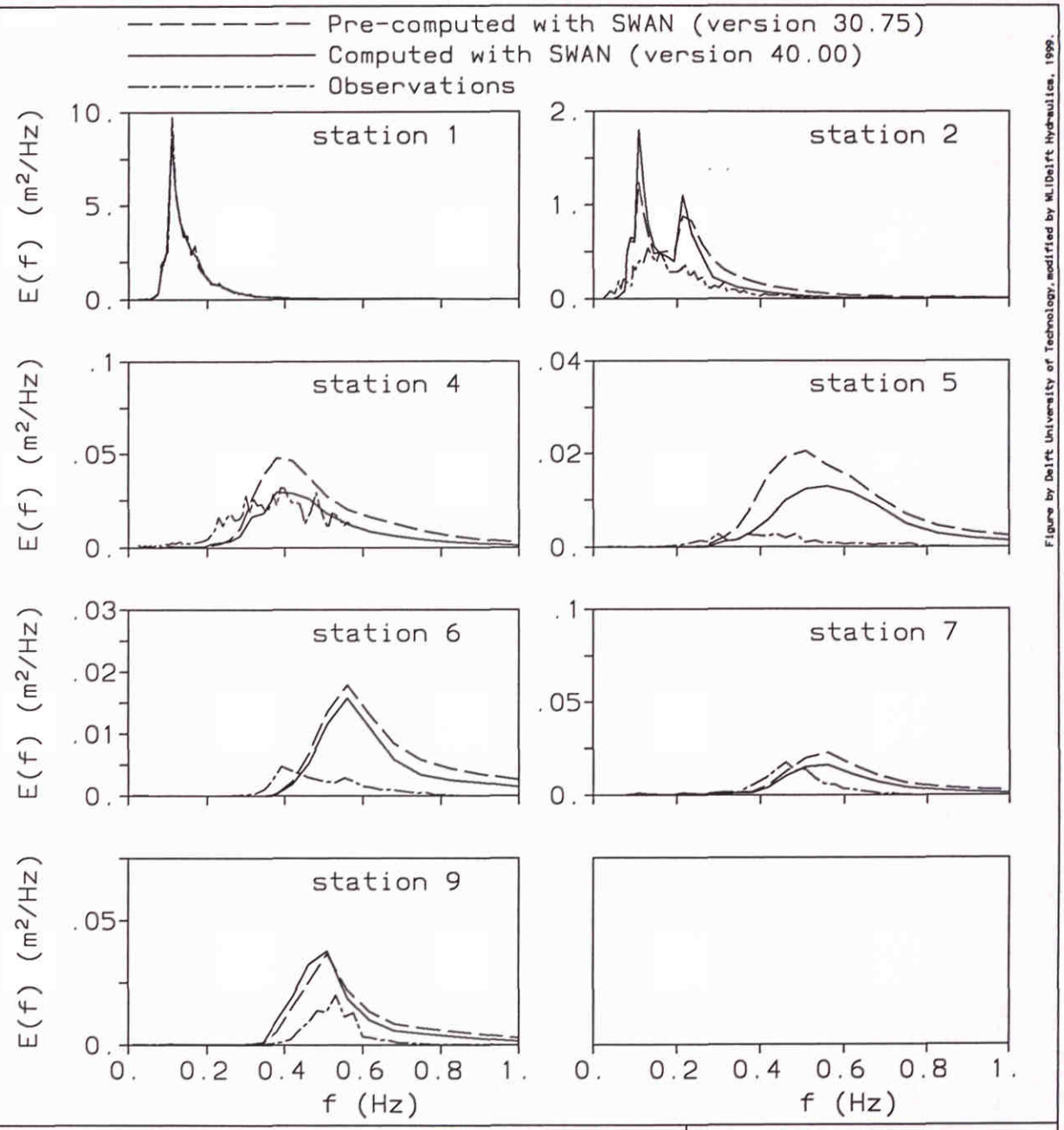


F81Nord2 F81c

Norderney :

Norderneyer Seegat field experiment

Extended Komen et al. (1984) expression with $\beta^0$

SWAN 40.00

WL | delft hydraulics

H3529

Fig. 7.7.c

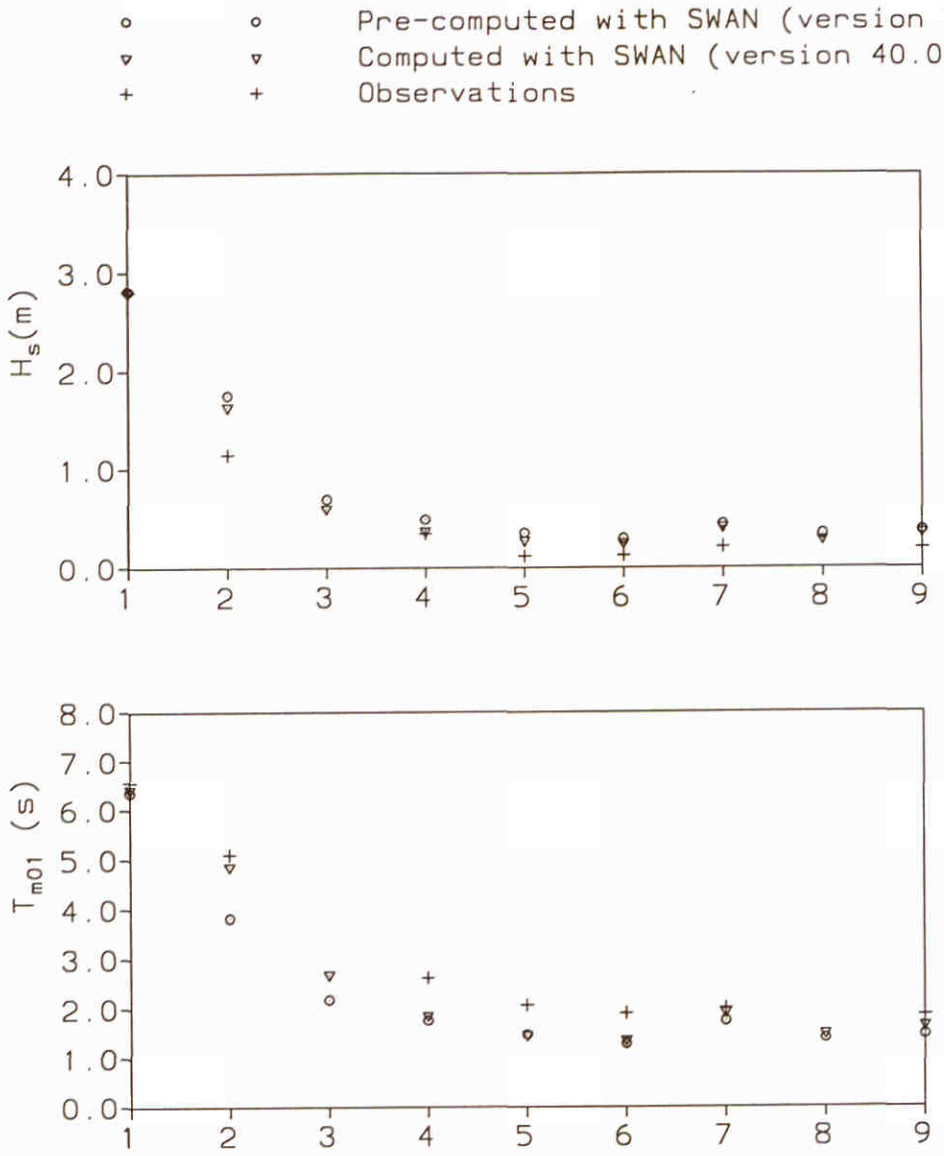


F81Nord2 F81d

Norderney :

Norderneyer Seegat field experiment

Extended Komen et al. (1984) expression with $\beta^0$

SWAN 40.00

WL | delft hydraulics

H3529

Fig. 7.7.d

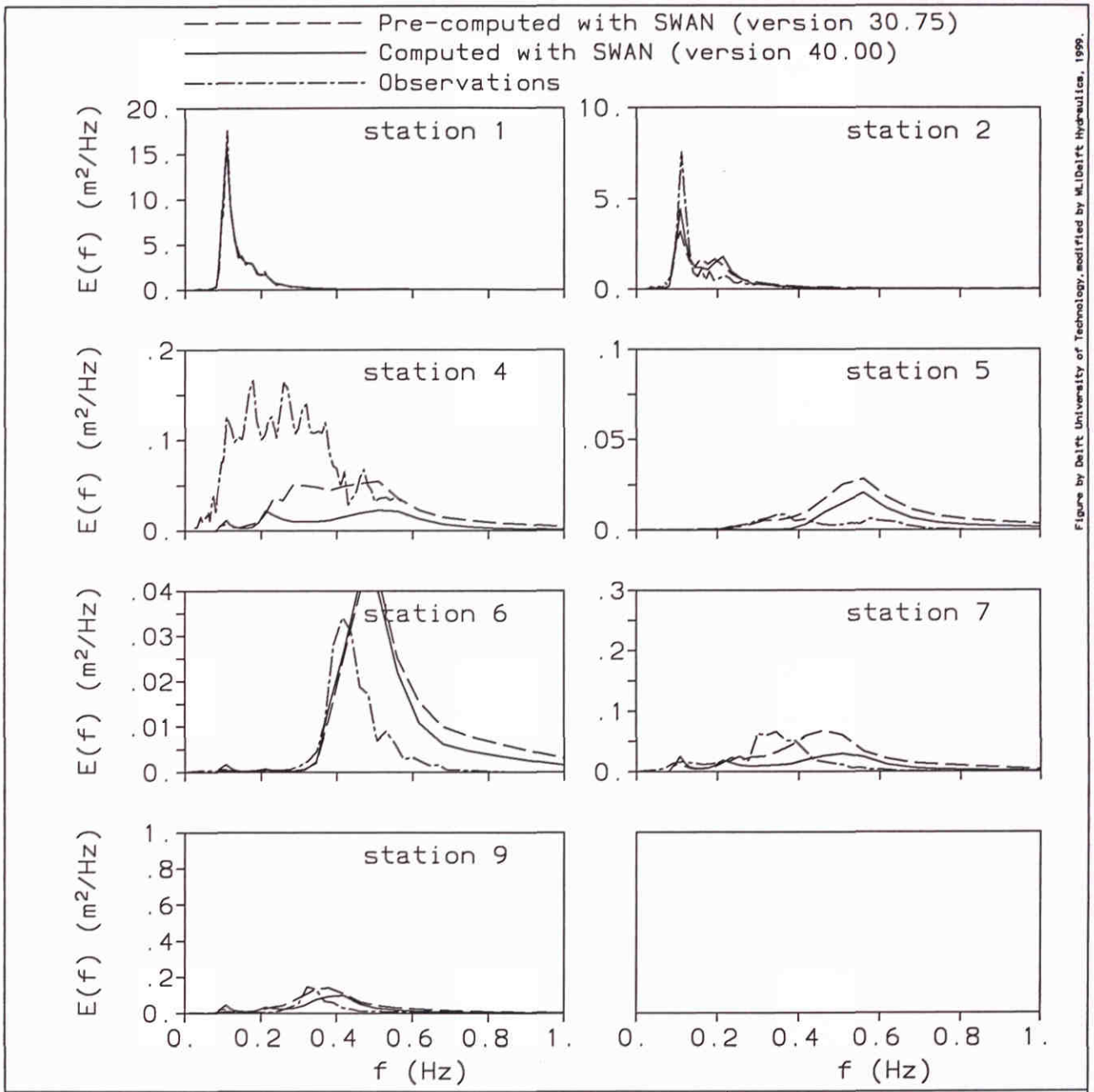


F81Nord3 F81e

Norderney :

Norderneyer Seegat field experiment

Extended Komen et al. (1984) expression with $\beta^0$

SWAN 40.00

WL | delft hydraulics

H3529

Fig. 7.7.e

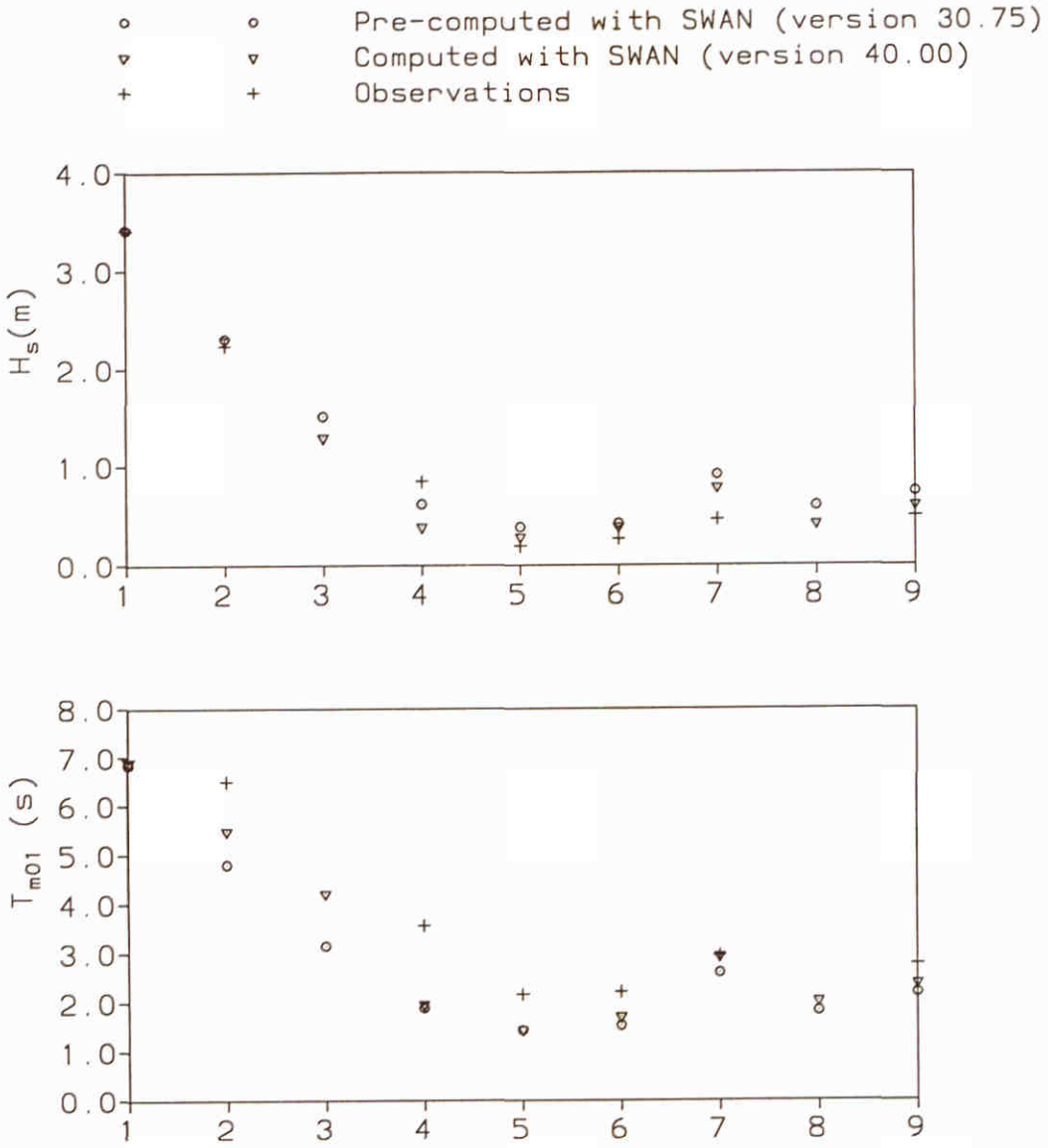


F81Nord1 F81f

Norderney:

Norderneyer Seegat field experiment

Extended Komen et al. (1984) expression with $\beta^0$

SWAN 40.00

WL | delft hydraulics

H3529

Fig. 7.7.f

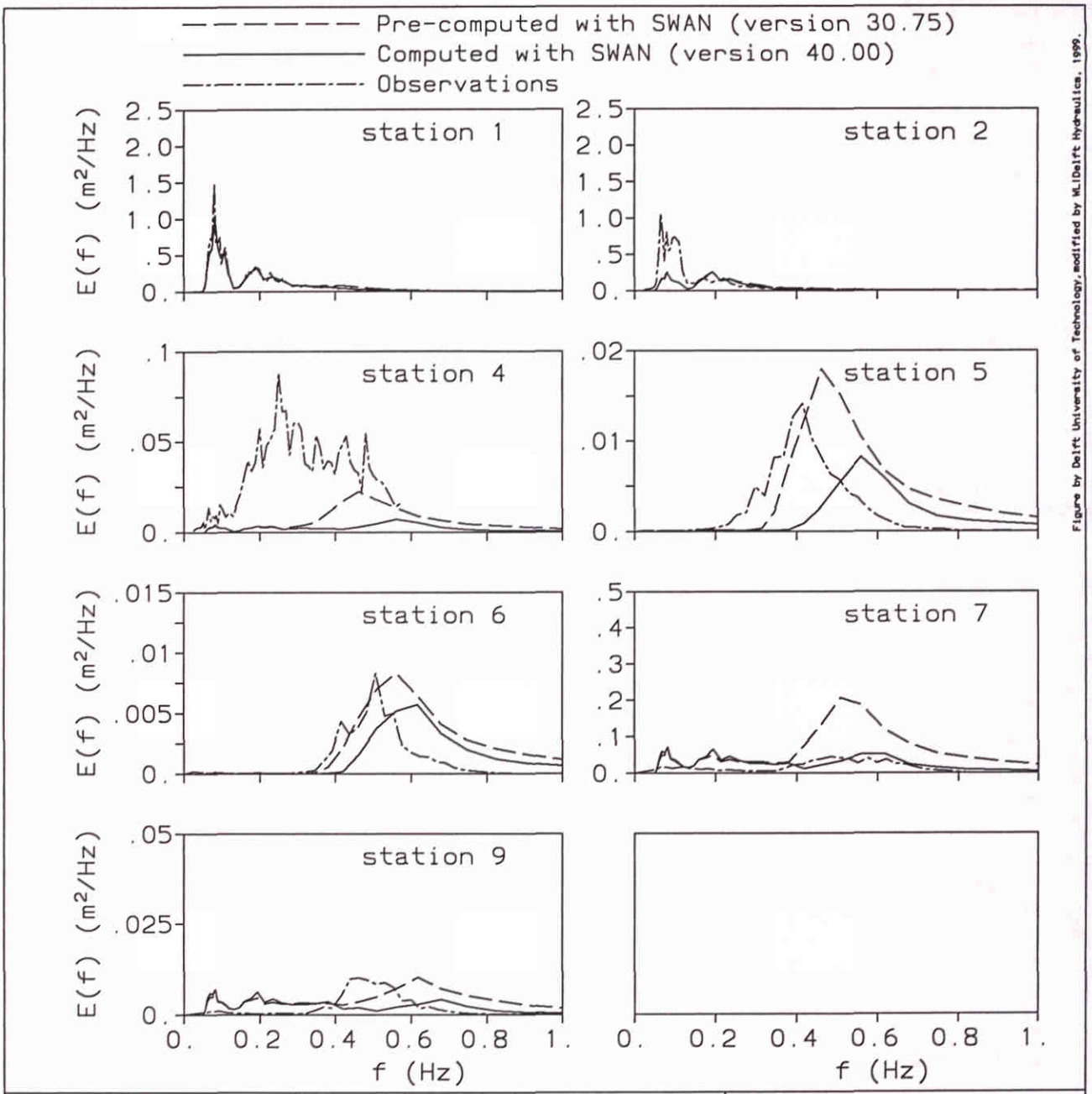


F81nord4 F81g

Norderney:

Norderneyer Seegat field experiment

Extended Komen et al. (1984) expression with $\beta^0$

SWAN 40.00

WL | delft hydraulics

H3529

Fig. 7.7.g

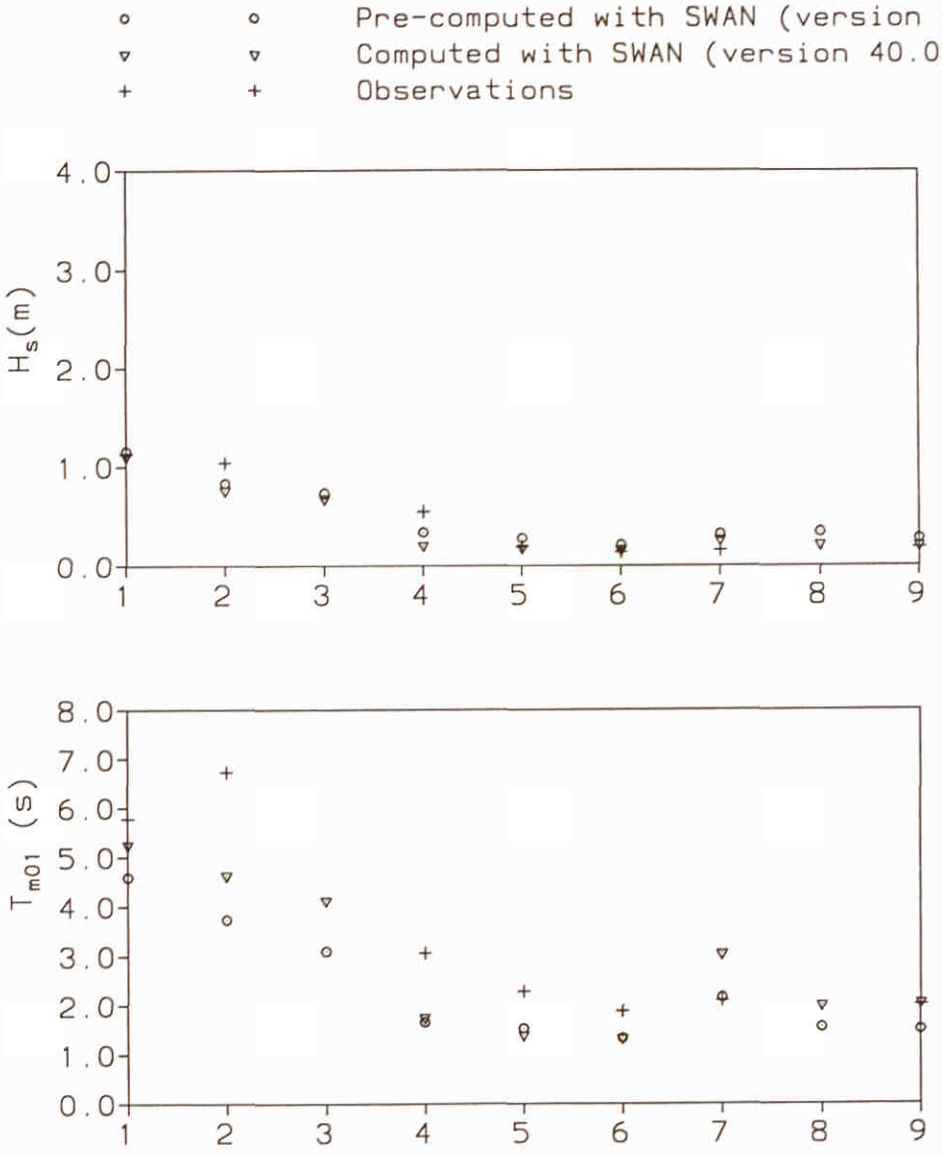


F81Nord1 F81h

Norderney :

Norderneyer Seegat field experiment

Extended Komen et al. (1984) expression with $\beta^0$

SWAN 40.00

WL | delft hydraulics

H3529

Fig. 7.7.h

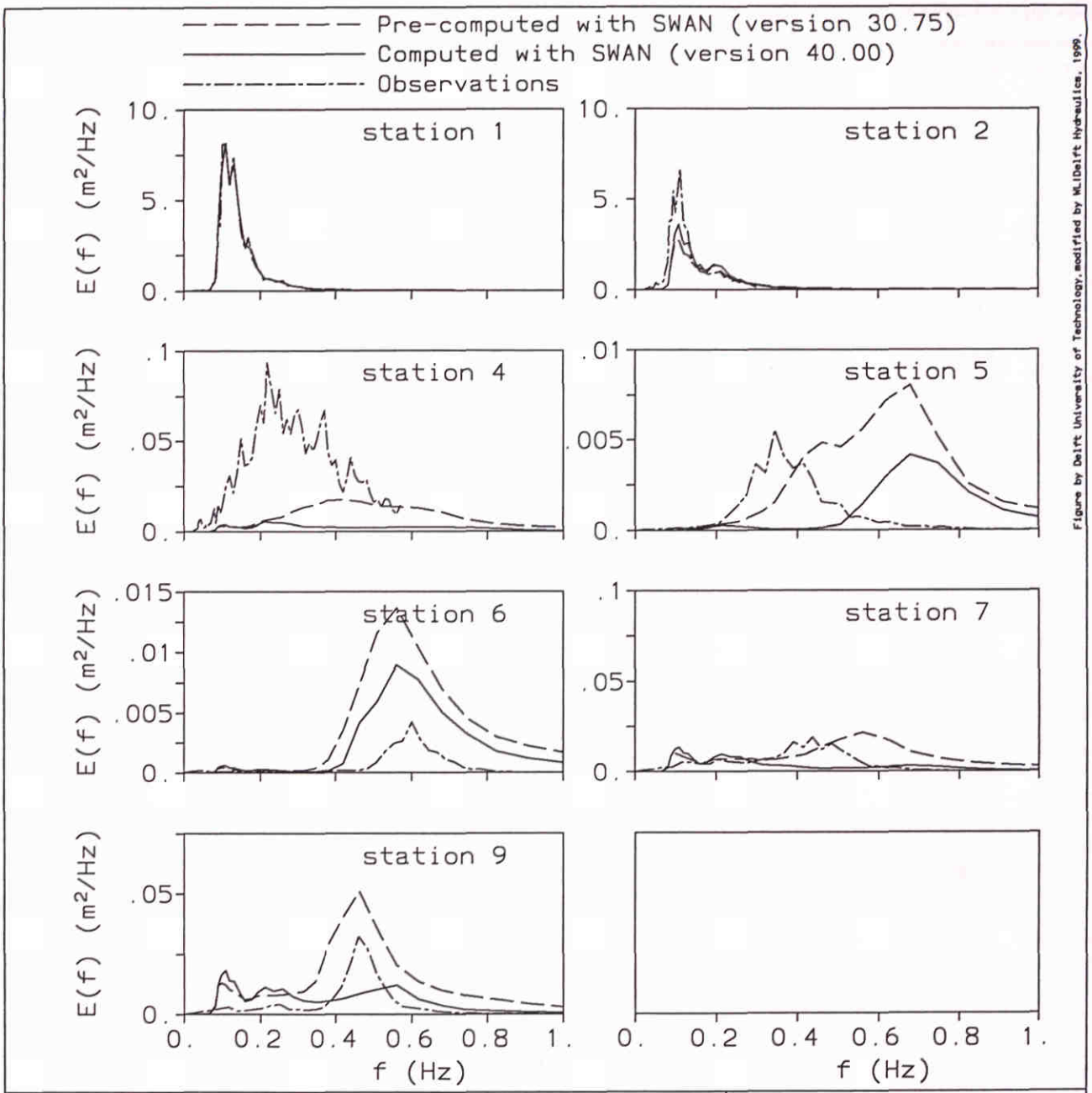


F81Nord1 F81a

Norderney :

Norderneyer Seegat field experiment

Extended Komen et al. (1984) expression with $\beta^{0.5}$

SWAN 40.00

WL | delft hydraulics

H3529

Fig. 7.8.a

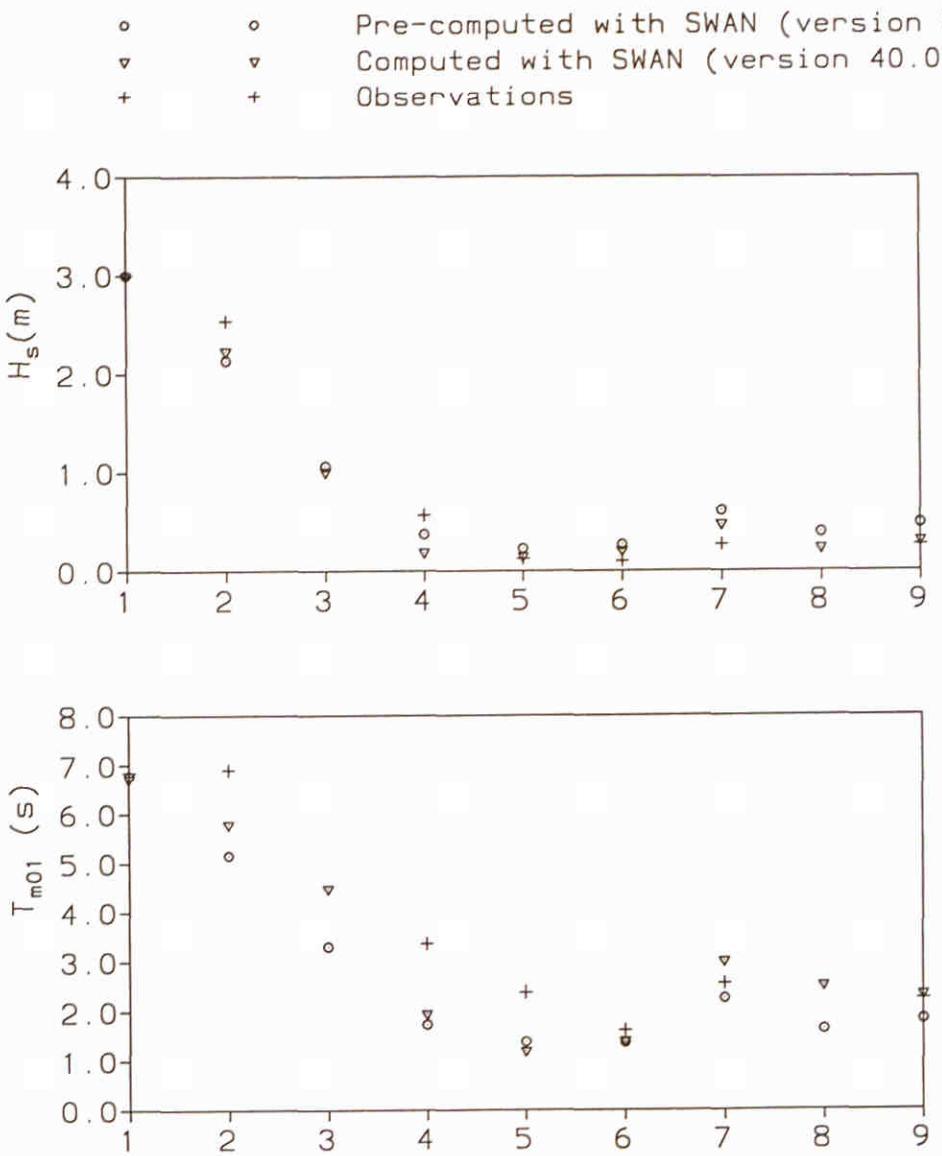


F81Nord1 F81b

Norderney:

Norderneyer Seegat field experiment

Extended Komen et al. (1984) expression with $\beta^{0.5}$

SWAN 40.00

WL | delft hydraulics

H3529

Fig. 7.8.b

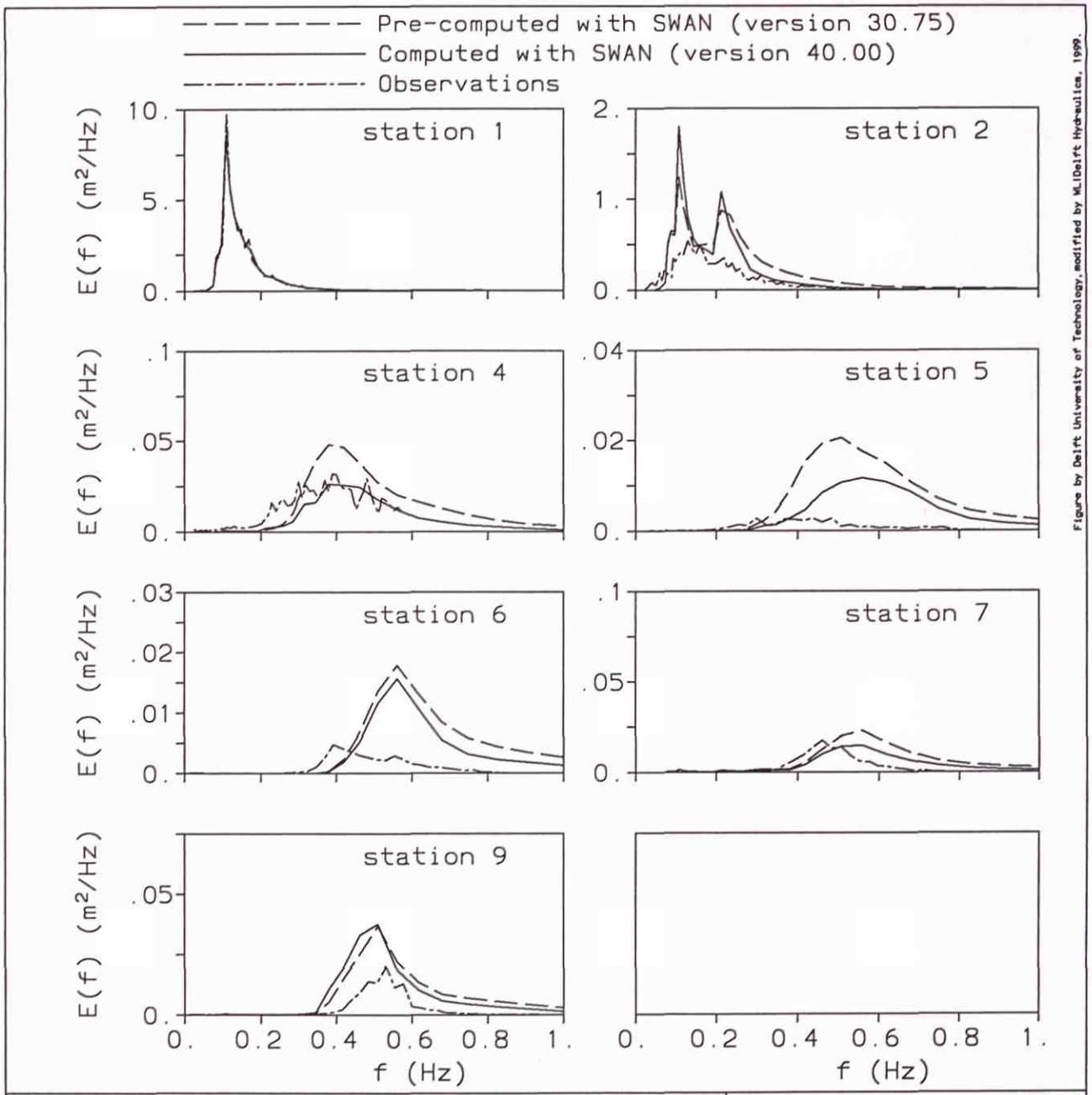


F81Nord2 F81c

Norderney :

Norderneyer Seegat field experiment

Extended Komen et al. (1984) expression with $\beta^{0.5}$

SWAN 40.00

WL | delft hydraulics

H3529

Fig. 7.8.c

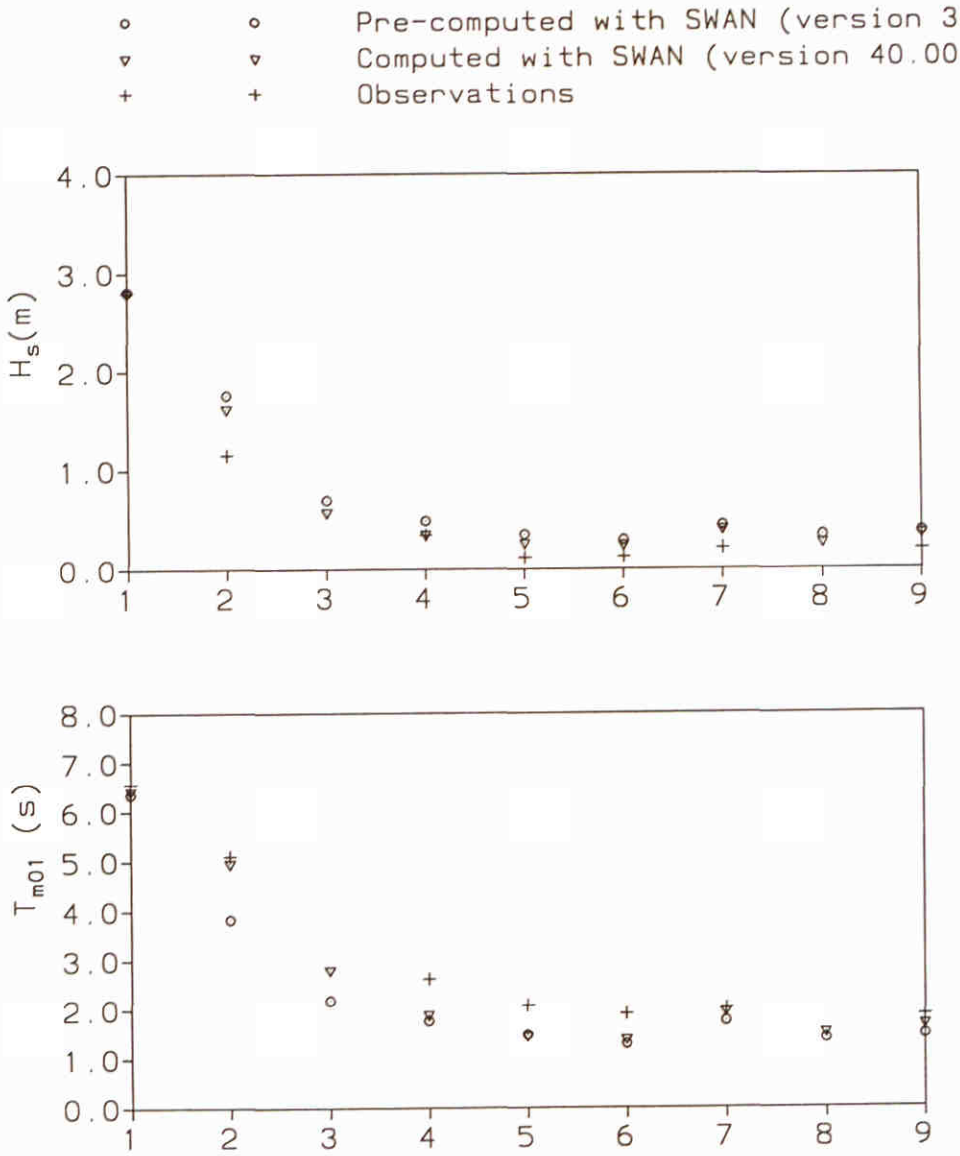


F81Nord2 F81d

Norderney:

Norderneyer Seegat field experiment

Extended Komen et al. (1984) expression with $\beta^{0.5}$

SWAN 40.00

WL | delft hydraulics

H3529

Fig. 7.8.d

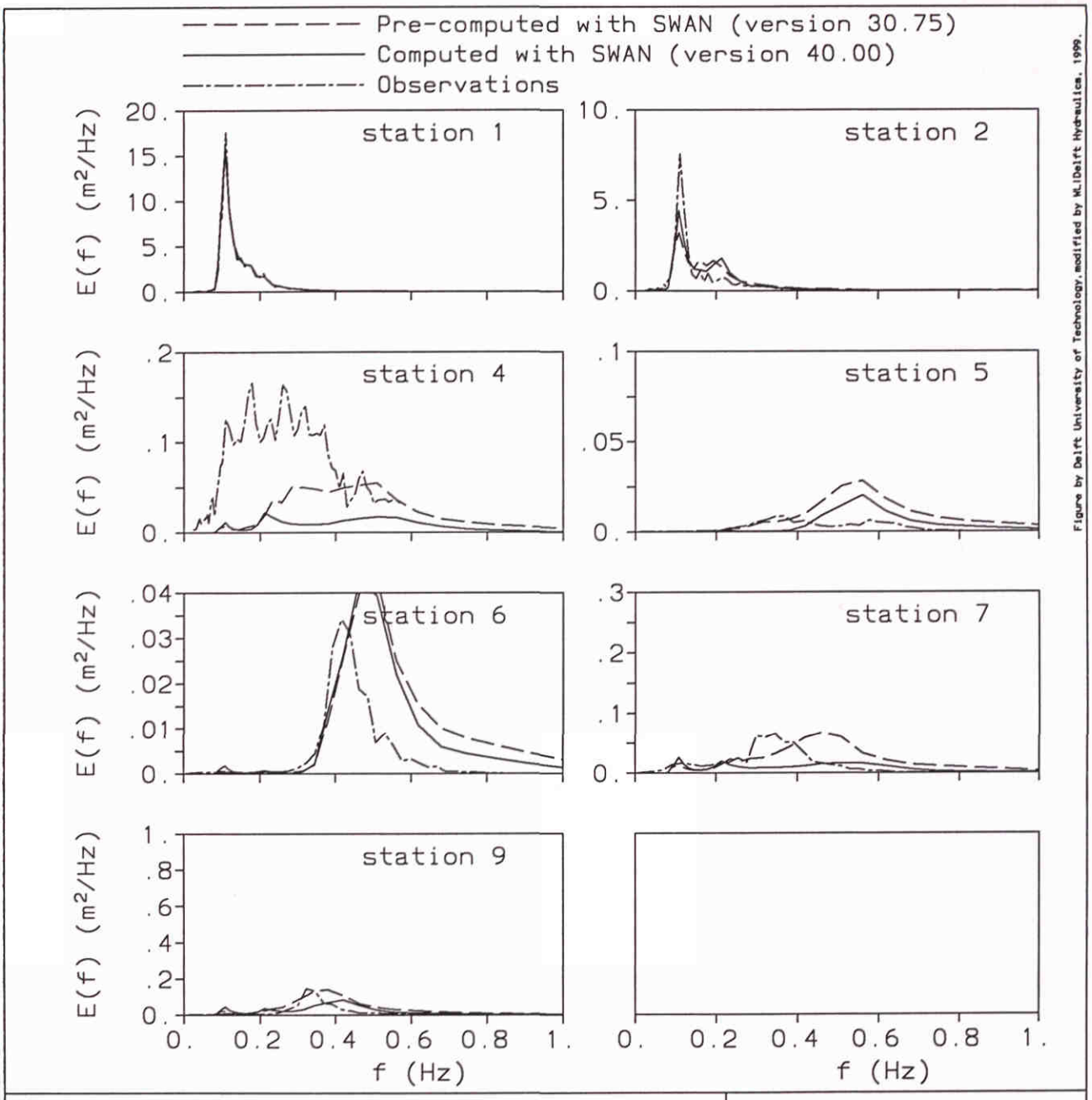


F81Nord3 F81e

Norderney :

Norderneyer Seegat field experiment

Extended Komen et al. (1984) expression with $\beta^{0.5}$

SWAN 40.00

WL | delft hydraulics

H3529

Fig. 7.8.e

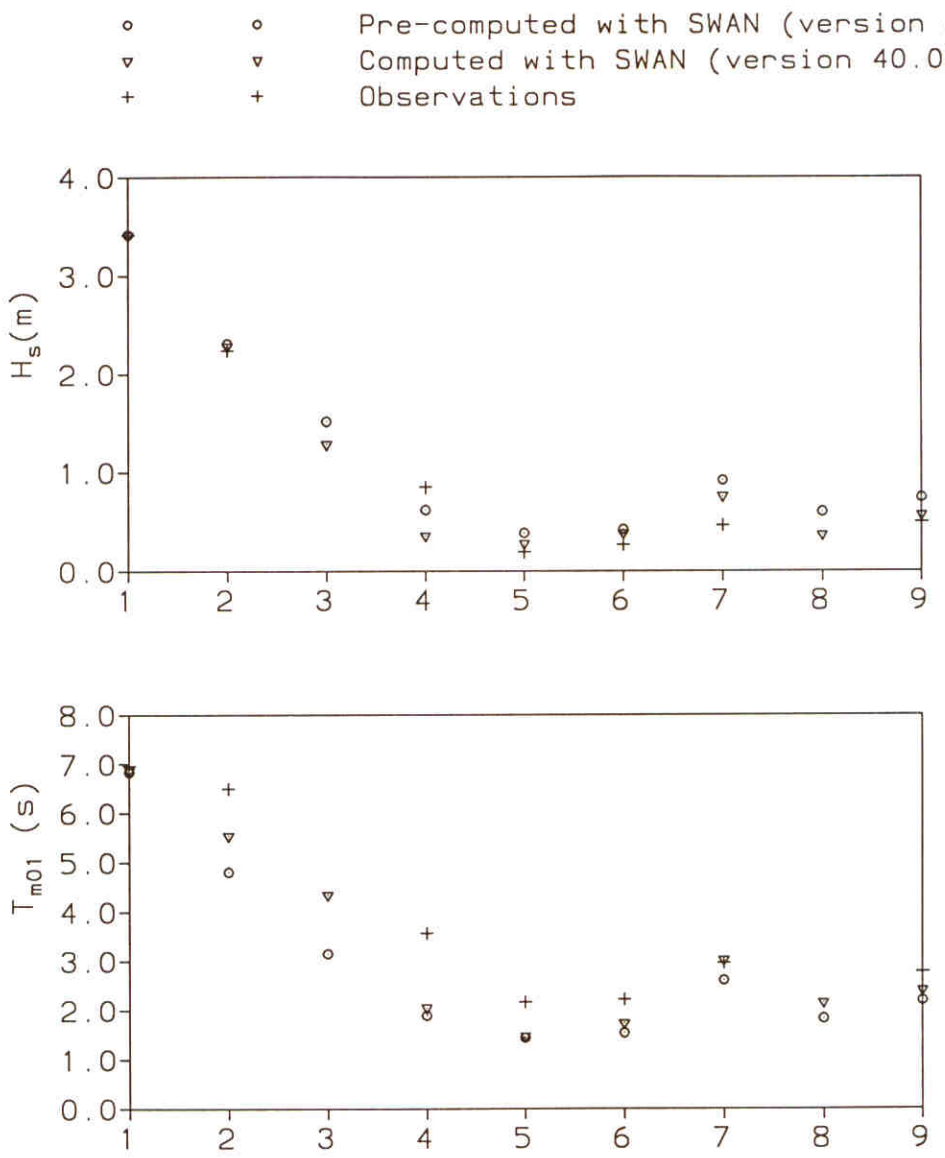


F81Nord1 F81f

Norderney :

Norderneyer Seegat field experiment

Extended Komen et al. (1984) expression with $\beta^{0.5}$

SWAN 40.00

WL | delft hydraulics

H3529

Fig. 7.8.f

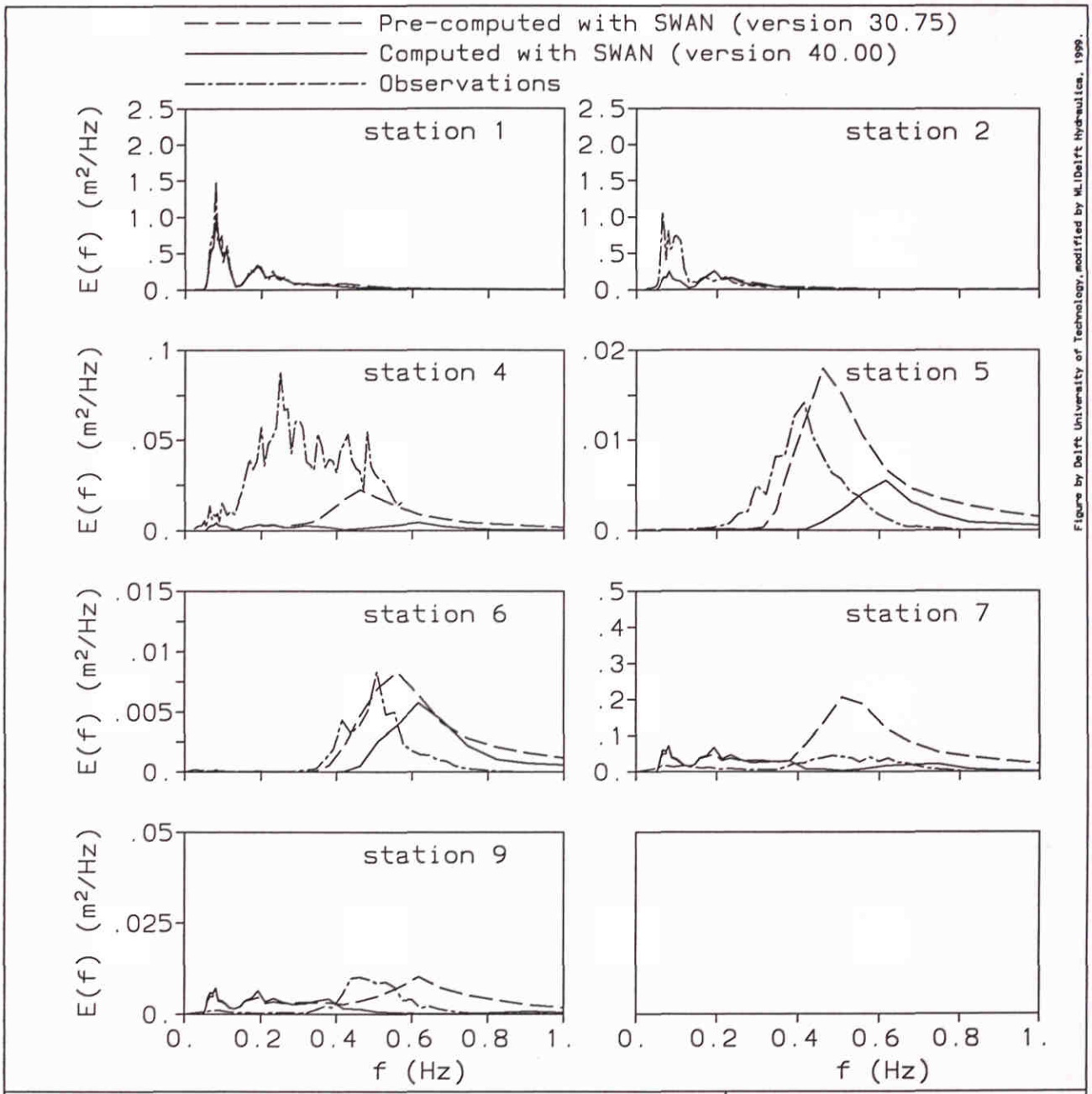


F81nord4 F81g

Norderney:

Norderneyer Seegat field experiment

Extended Komen et al. (1984) expression with $\beta^{0.5}$

SWAN 40.00

WL | delft hydraulics

H3529

Fig. 7.8.g

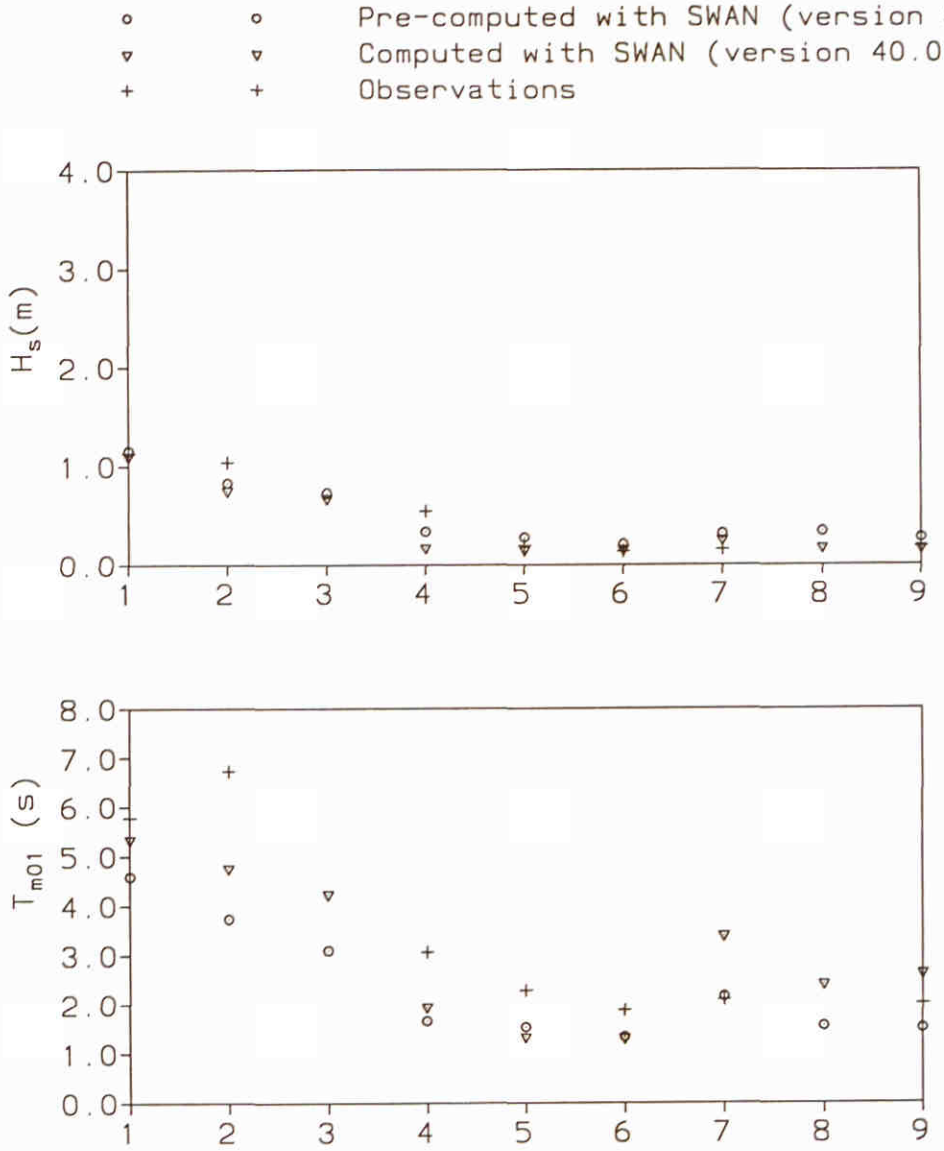


F81Nord1 F81h

Norderney:

Norderneyer Seegat field experiment

Extended Komen et al. (1984) expression with $\beta^{0.5}$

SWAN 40.00

WL | delft hydraulics

H3529

Fig. 7.8.h

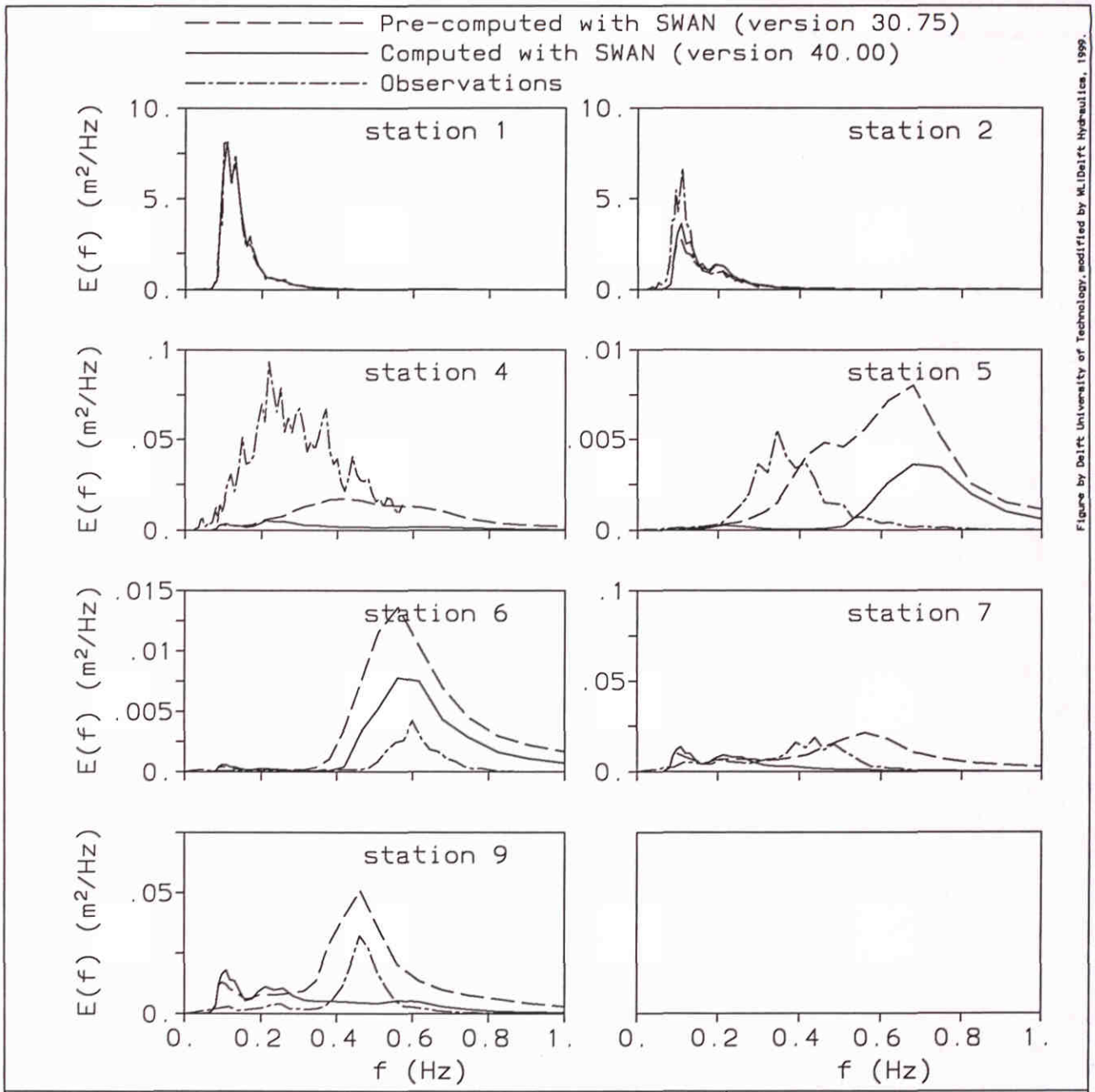


F81Nord1 F81a

Norderney:

Norderneyer Seegat field experiment

Extended Komen et al. (1984) expression with $\beta^1$

SWAN 40.00

WL | delft hydraulics

H3529

Fig. 7.9.a

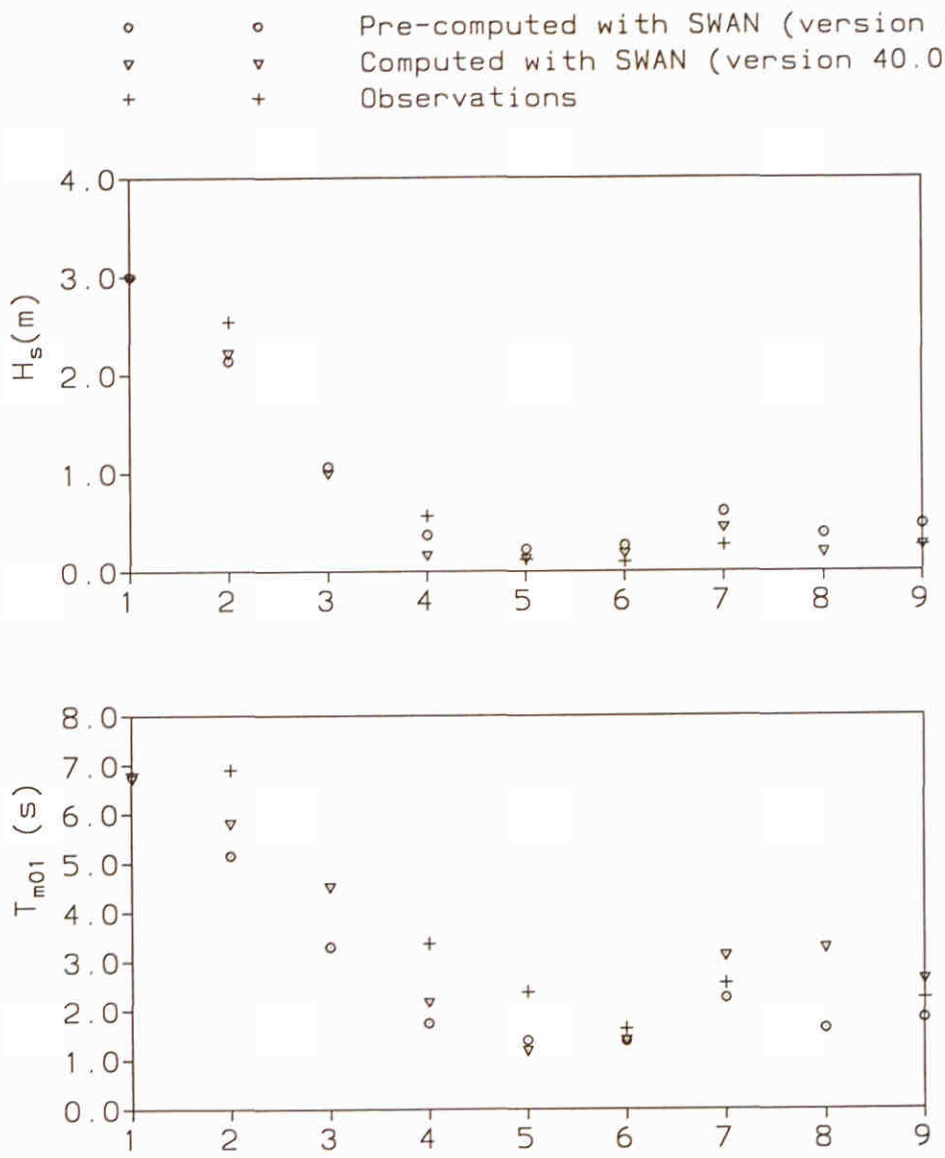


F81Nord1 F81b

Norderney:

Norderneyer Seegat field experiment

Extended Komen et al. (1984) expression with $\beta$[1]

SWAN 40.00

WL | delft hydraulics

H3529

Fig. 7.9.b

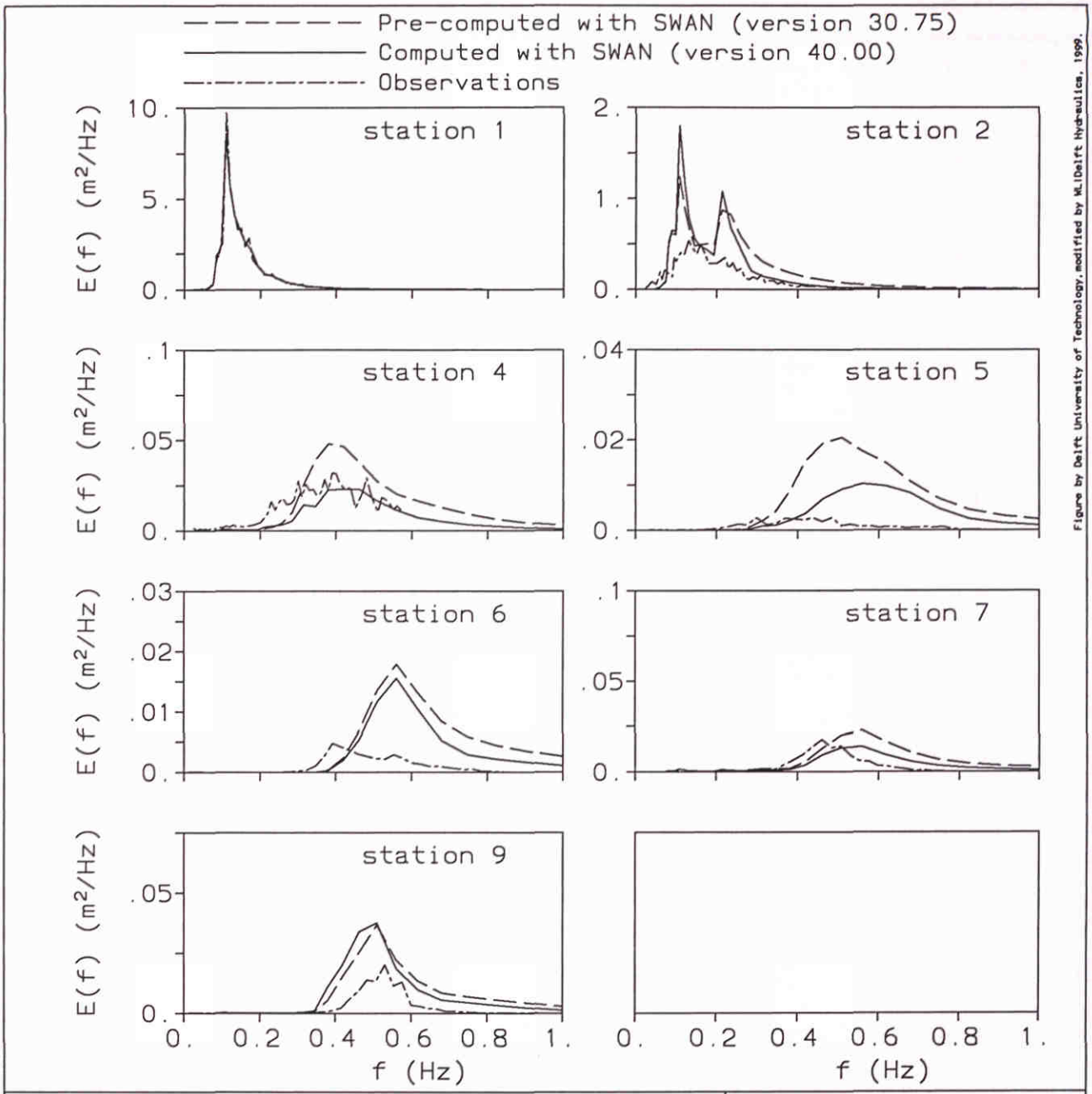


F81Nord2 F81c

Norderney:

Norderneyer Seegat field experiment

Extended Komen et al. (1984) expression with $\beta^1$

SWAN 40.00

WL | delft hydraulics

H3529

Fig. 7.9.c

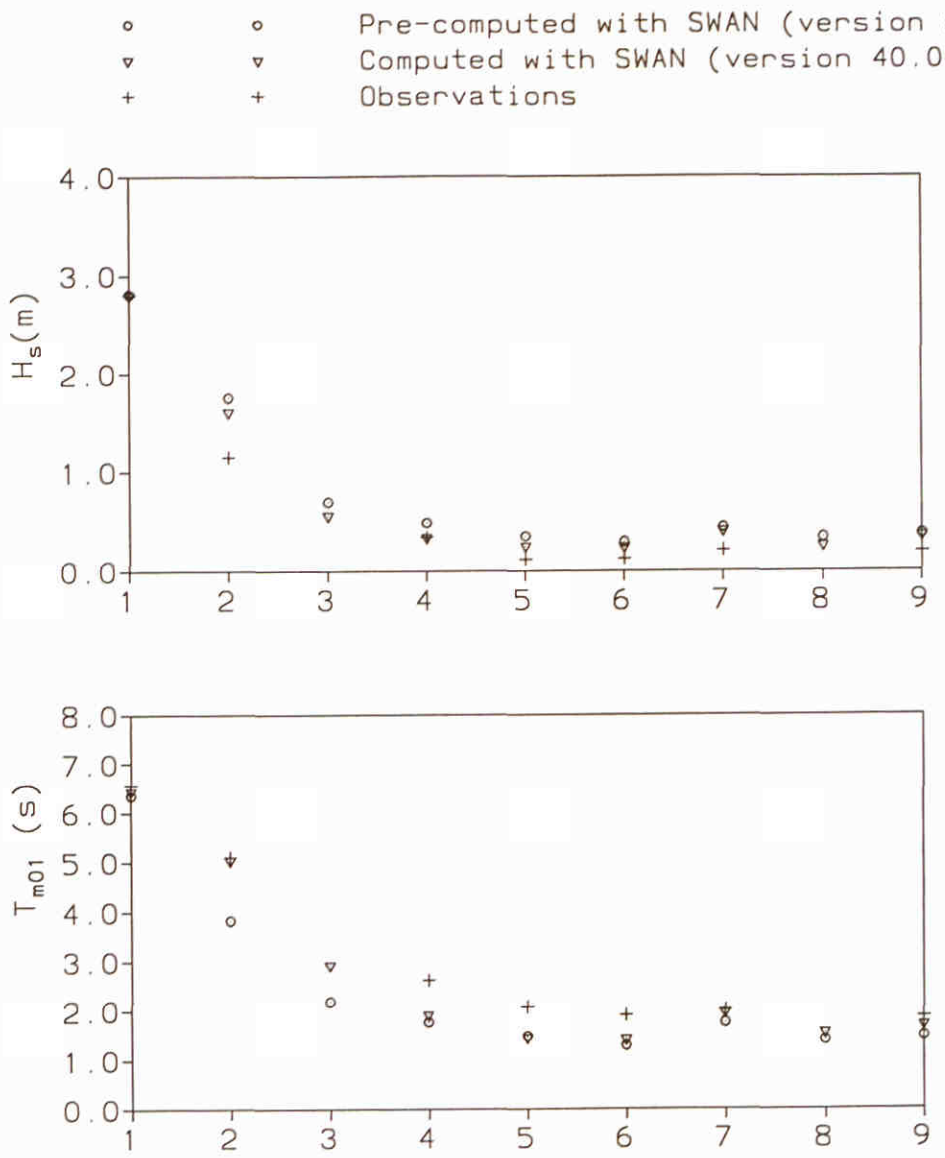


F81Nord2 F81d

Norderney:

Norderneyer Seegat field experiment

Extended Komen et al. (1984) expression with $\beta$[1]

SWAN 40.00

WL | delft hydraulics

H3529

Fig. 7.9.d

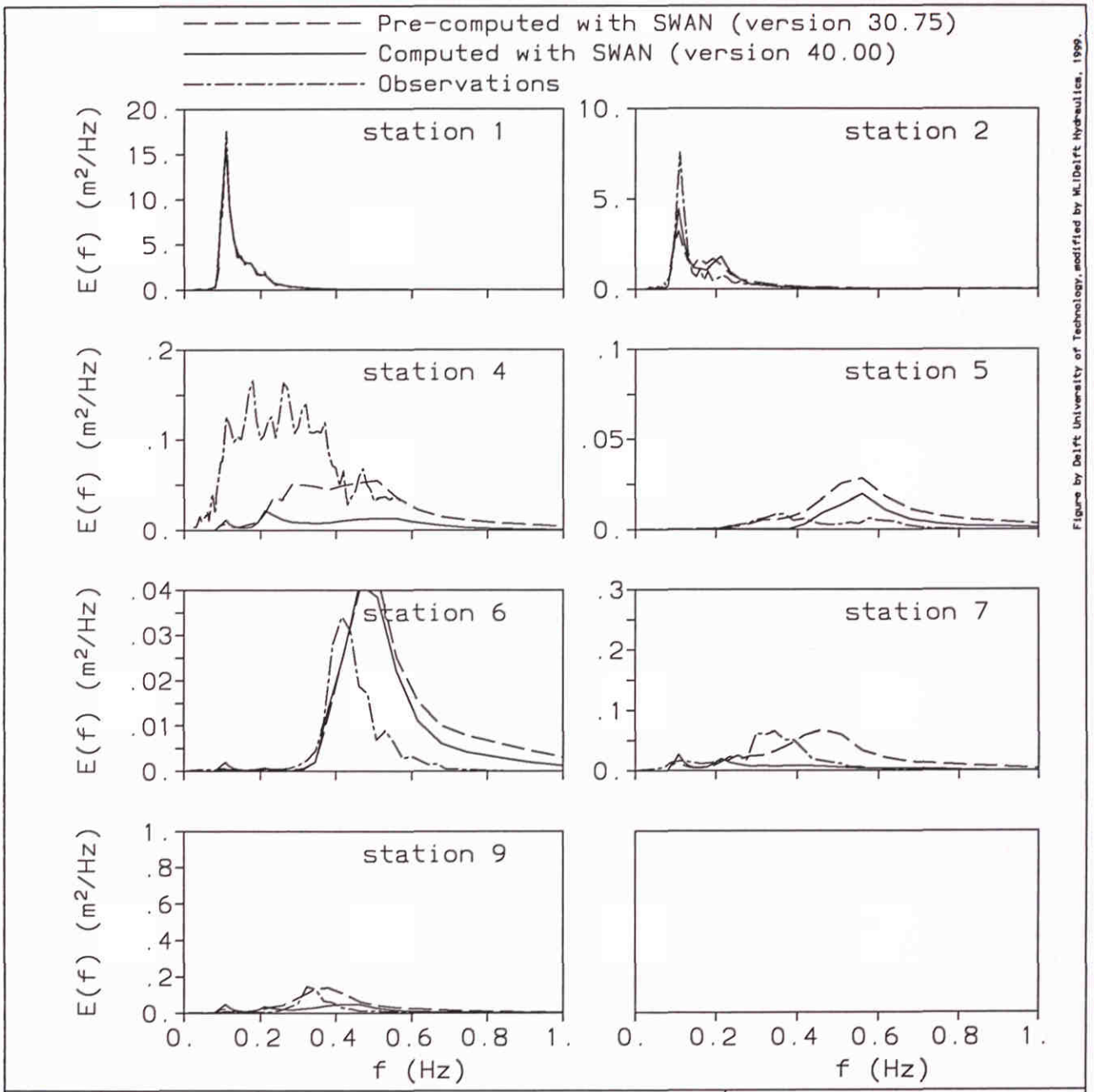


F81Nord3 F81e

Norderney:

Norderneyer Seegat field experiment

Extended Komen et al. (1984) expression with $\beta^1$

SWAN 40.00

WL | delft hydraulics

H3529

Fig. 7.9.e

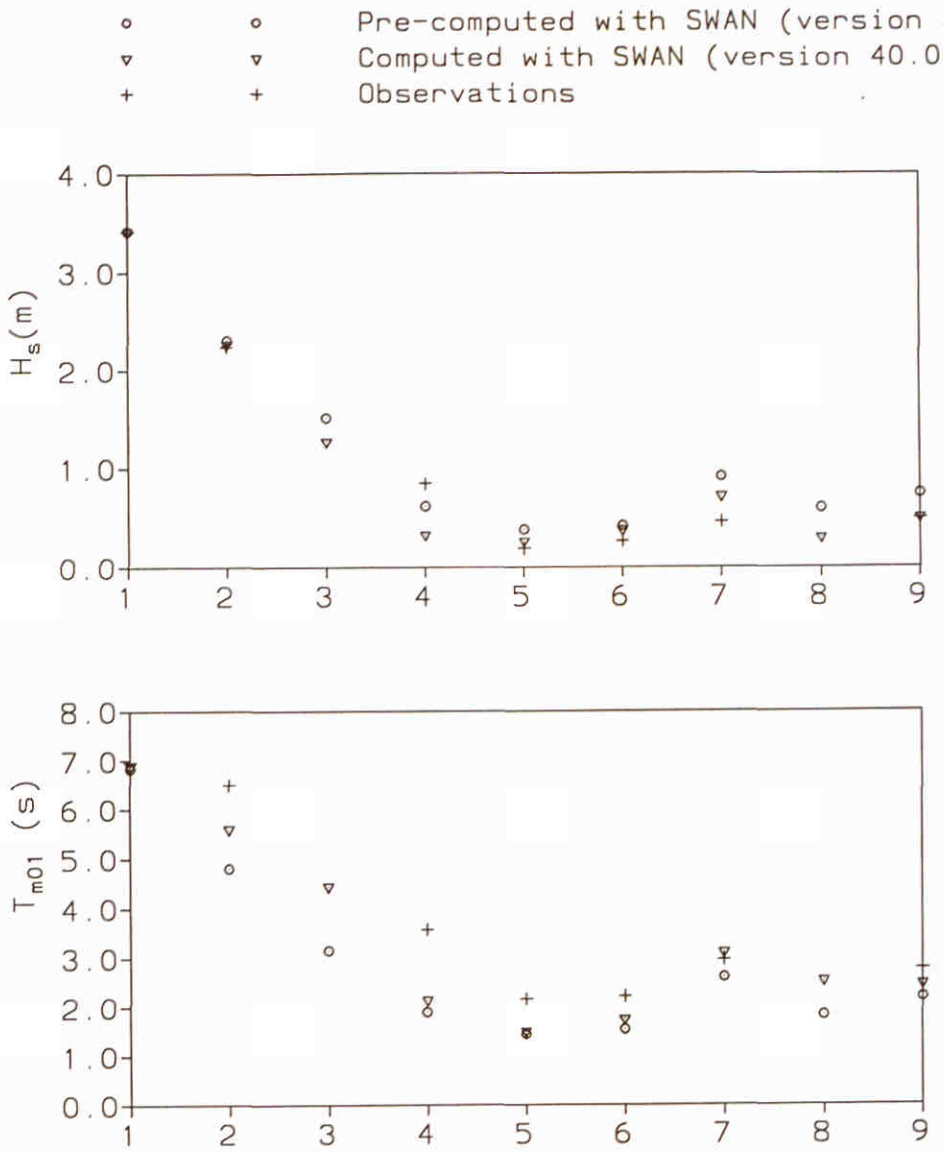


F81Nord1 F81f

Norderney :

Norderneyer Seegat field experiment

Extended Komen et al. (1984) expression with $\beta^1$

SWAN 40.00

WL | delft hydraulics

H3529

Fig. 7.9.f

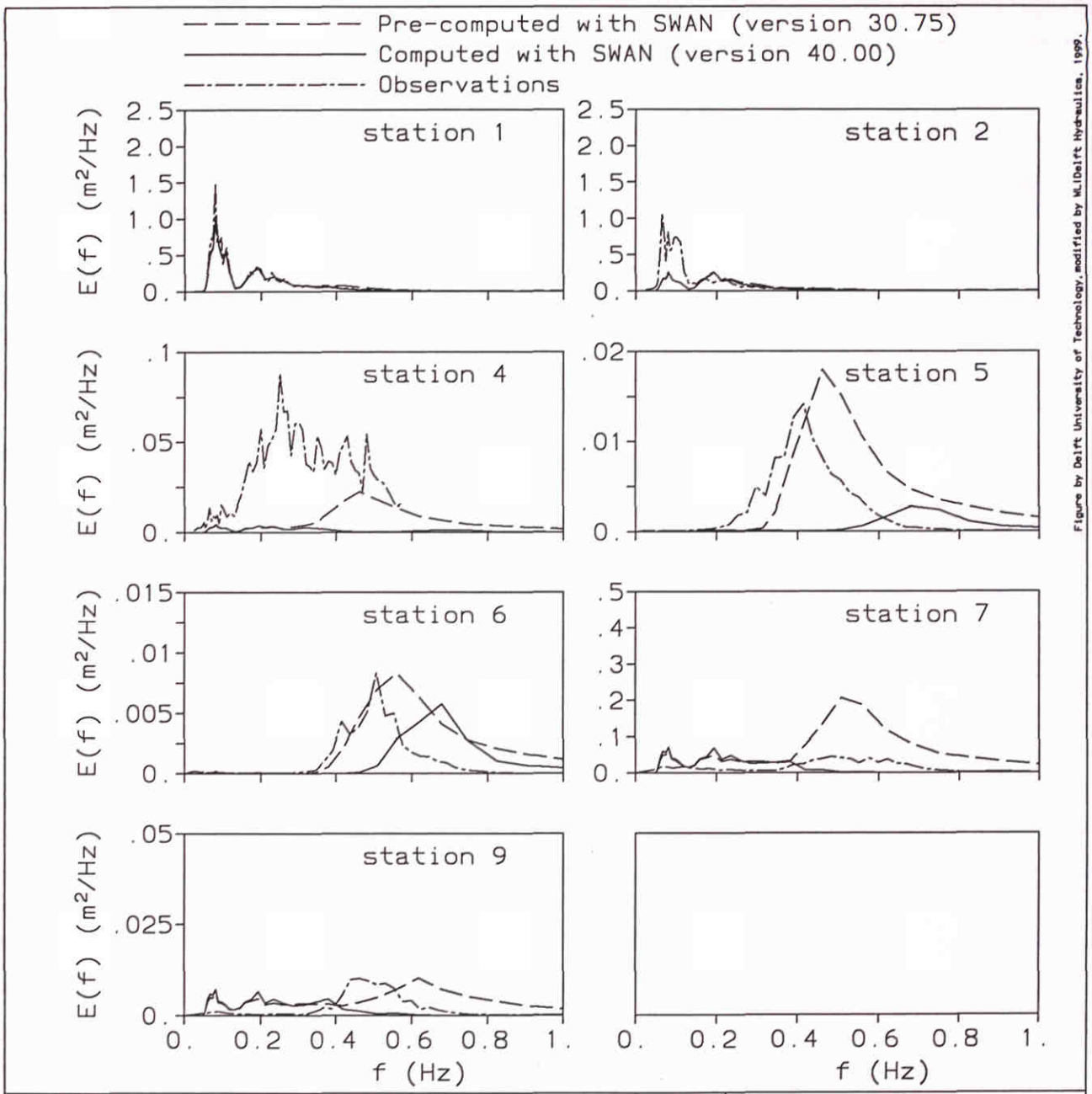


F81nord4 F81g

Norderney:

Norderneyer Seegat field experiment

Extended Komen et al. (1984) expression with $\beta^1$

SWAN 40.00

WL | delft hydraulics

H3529

Fig. 7.9.g

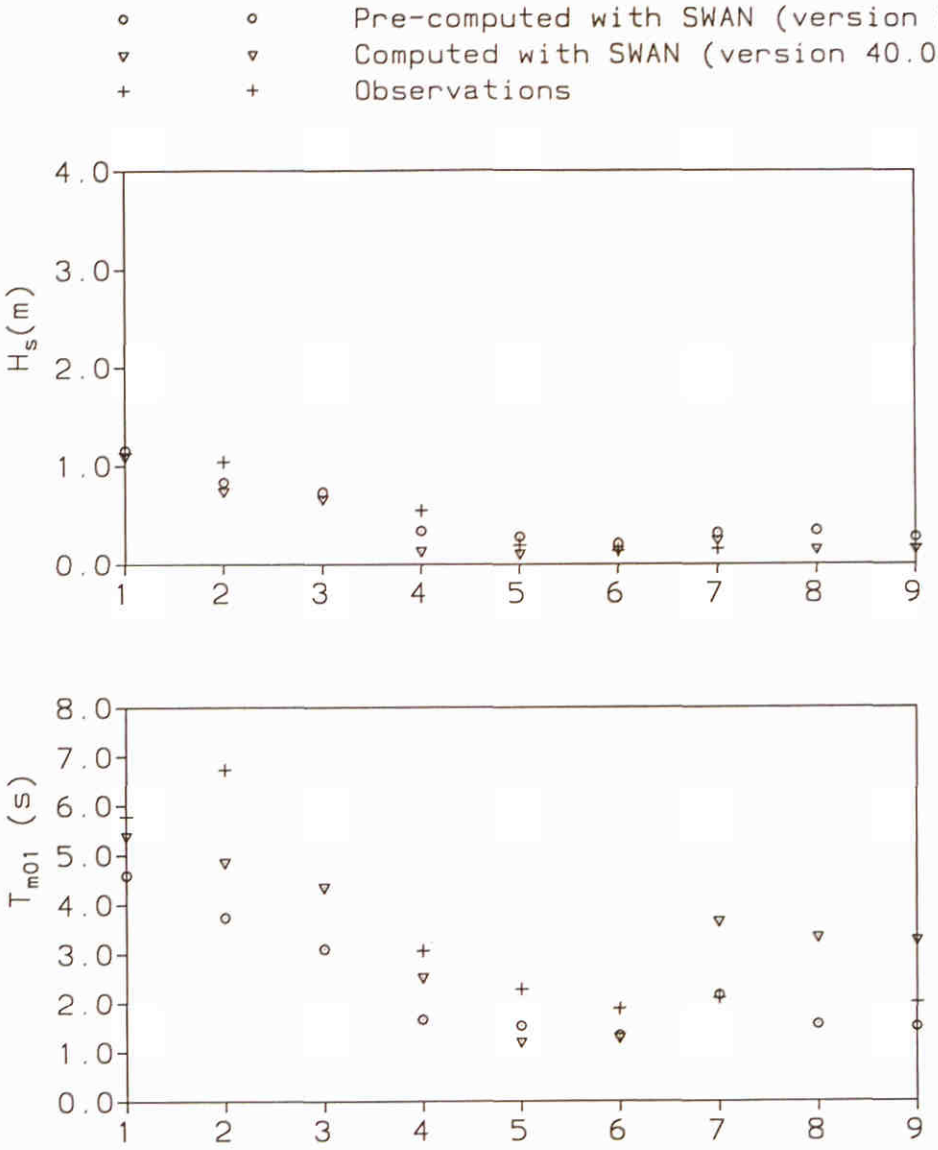


F81Nord1 F81h

Norderney:

Norderneyer Seegat field experiment

Extended Komen et al. (1984) expression with $\beta$[1]

SWAN 40.00

WL | delft hydraulics

H3529

Fig. 7.9.h

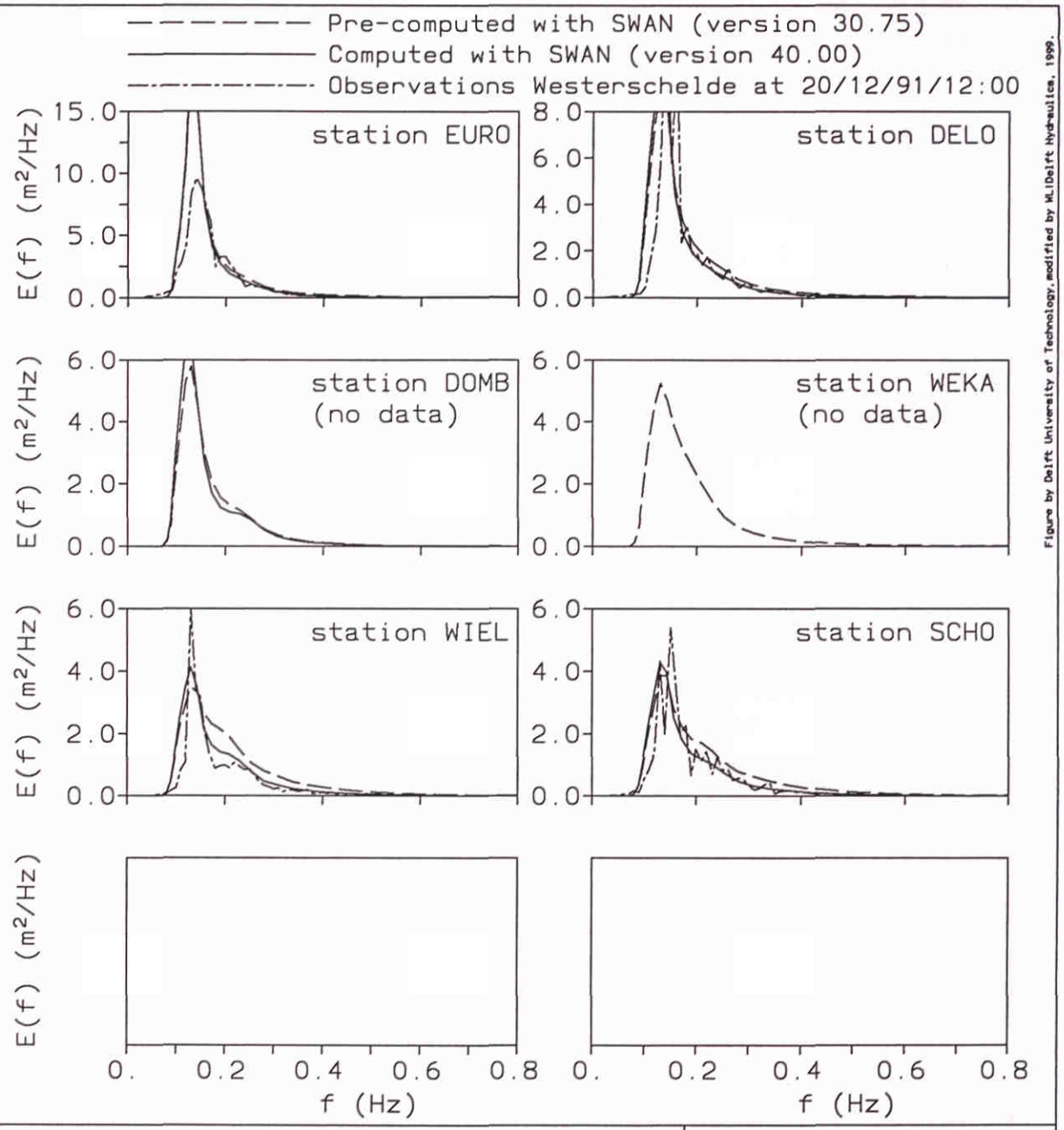


F61WesC1 F61a

Westerschelde Estuary

Westerschelde estuary

Extended Komen et al. (1984) expression with $\beta^0$

SWAN 40.00

WL | delft hydraulics

H3529

Fig. 7.10.a

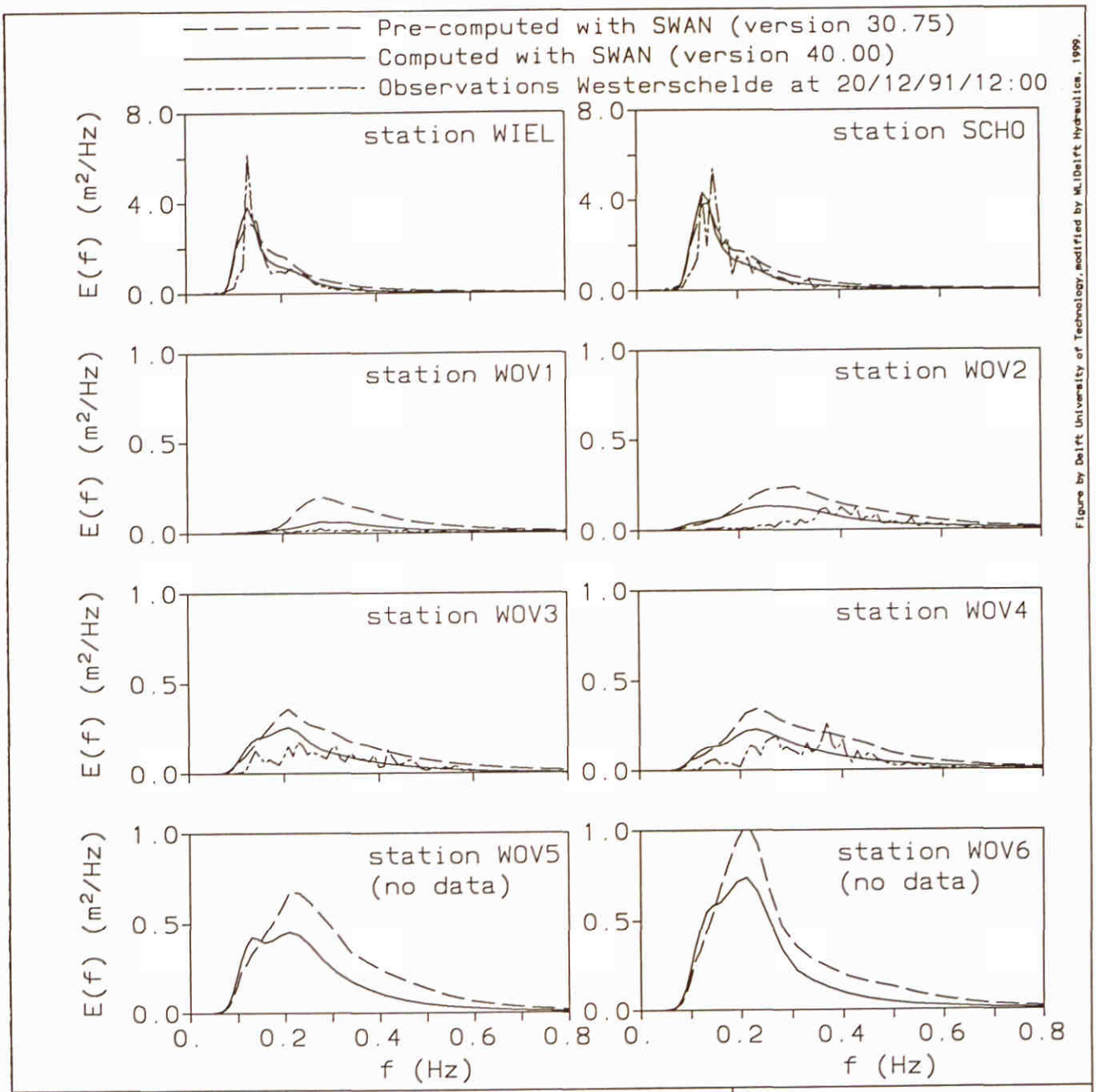


F61WesC1 F61b

Westerschelde Estuary

Westerschelde estuary

Extended Komen et al. (1984) expression with $\beta^0$

SWAN 40.00

WL | delft hydraulics

H3529

Fig. 7.10.b

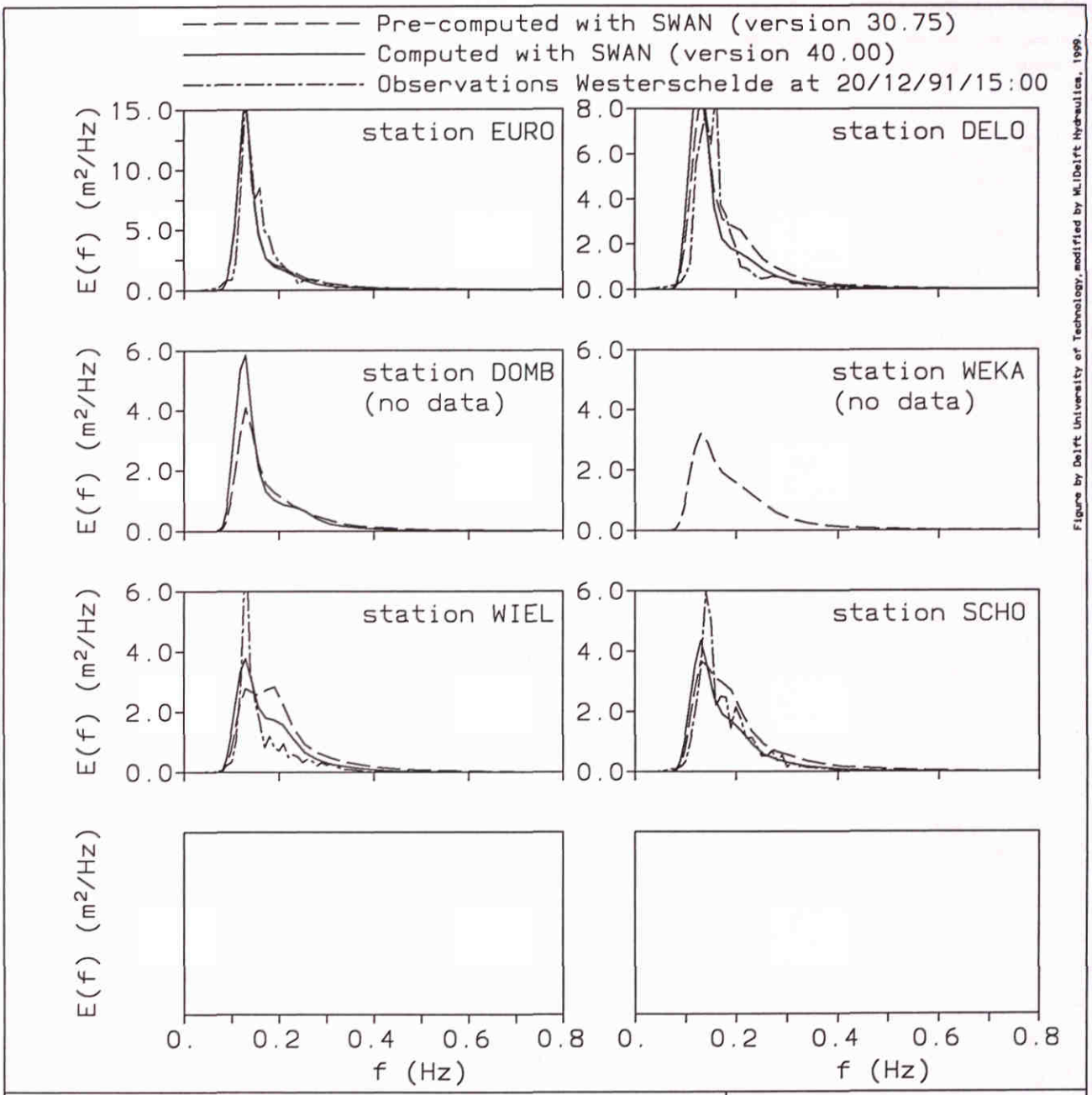


F61WesC2 F61c

Westerschelde Estuary

Westerschelde estuary

Extended Komen et al. (1984) expression with $\beta^0$

SWAN 40.00

WL | delft hydraulics

H3529

Fig. 7.10.c

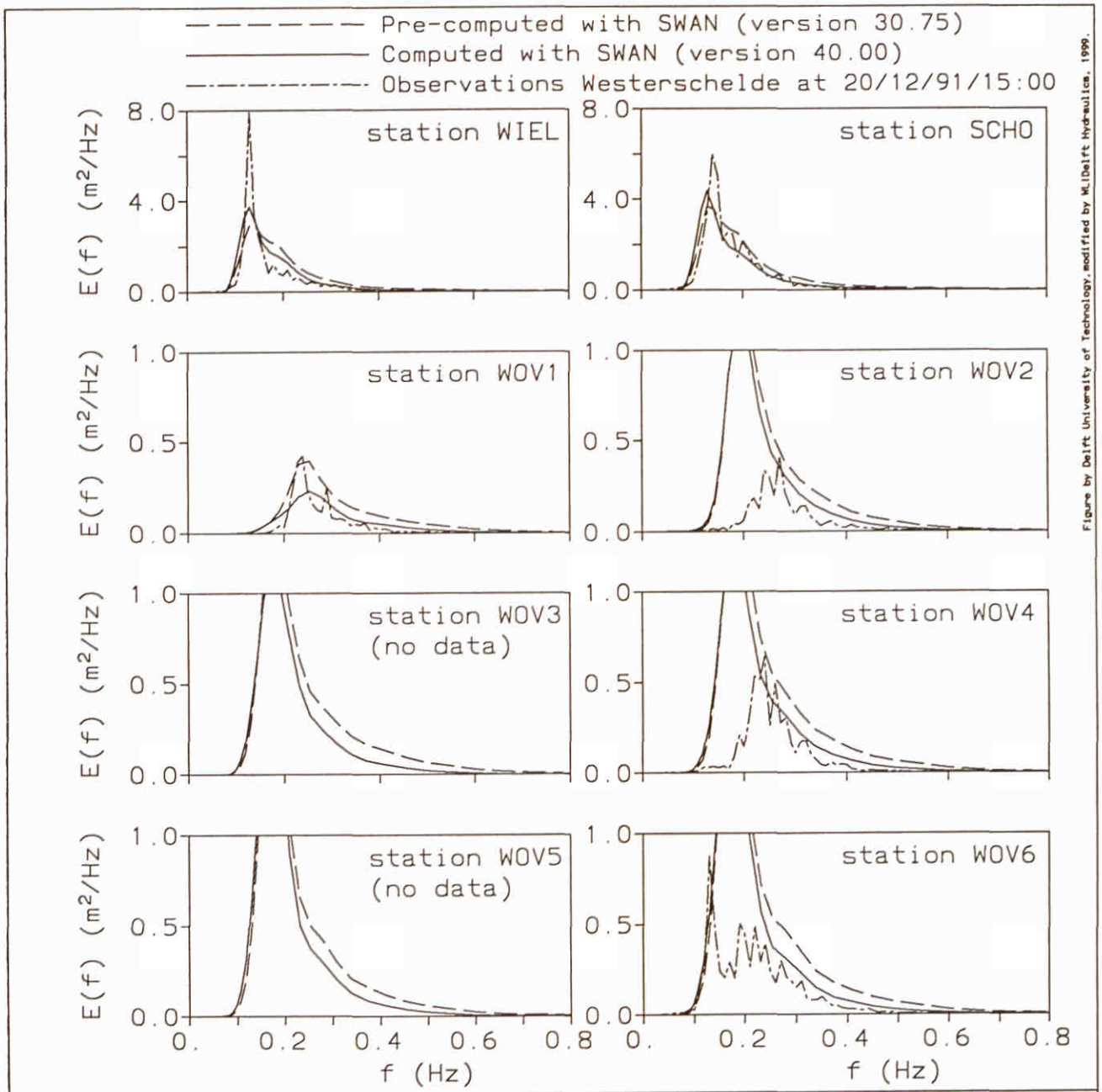


F61WesC2 F61d

Westerschelde Estuary

| | | |
|---|---|---|
| Westerschelde estuary<br>Extended Komen et al. (1984) expression with $\beta^0$ | SWAN 40.00 | |
| WL \| delft hydraulics | H3529 | Fig. 7.10.d |

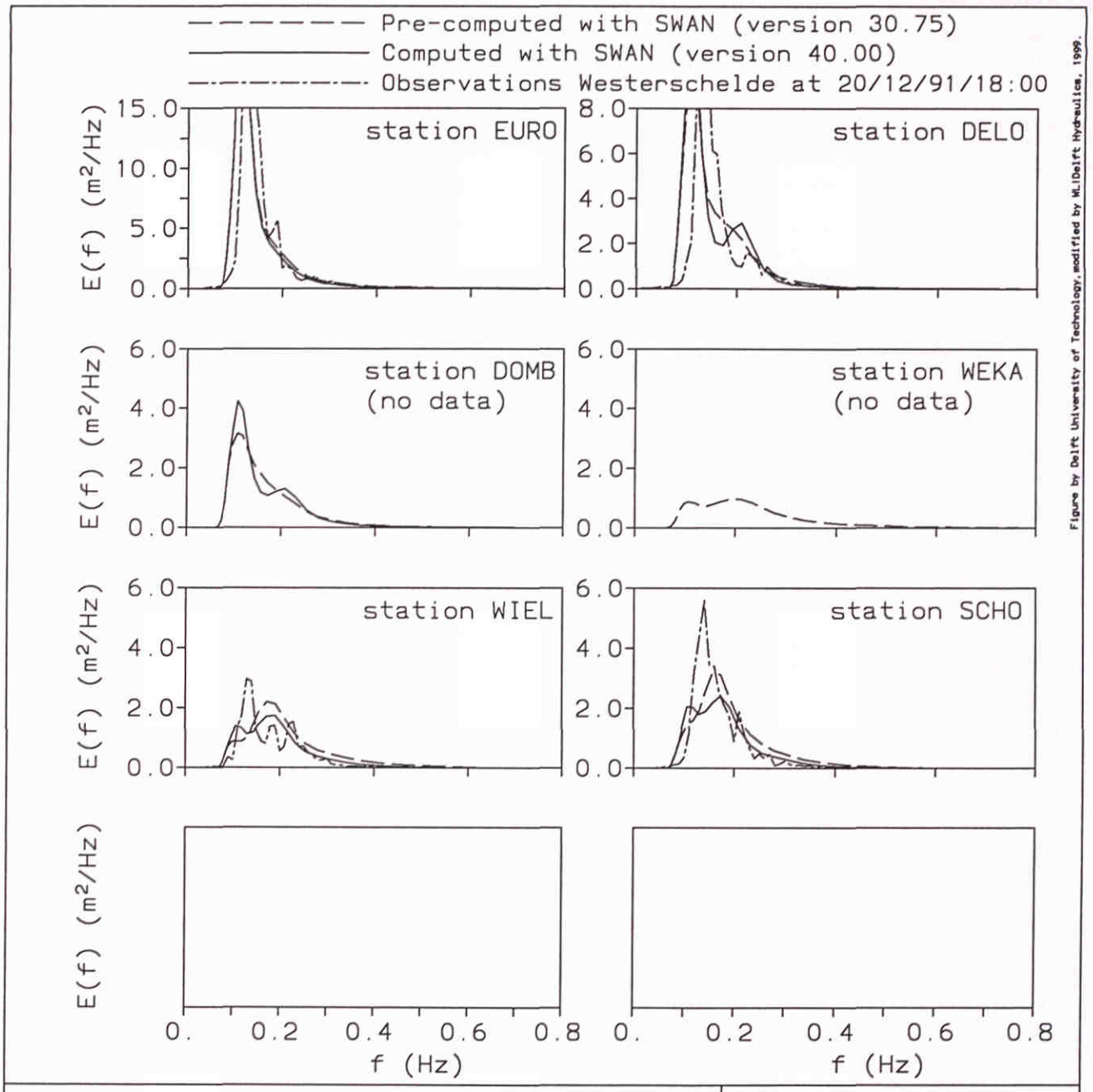


F61WesC3 F61e

Westerschelde Estuary

| | | |
|---|---|---|
| Westerschelde estuary<br>Extended Komen et al. (1984) expression with $\beta^0$ | SWAN 40.00 | |
| WL \| delft hydraulics | H3529 | Fig. 7.10.e |

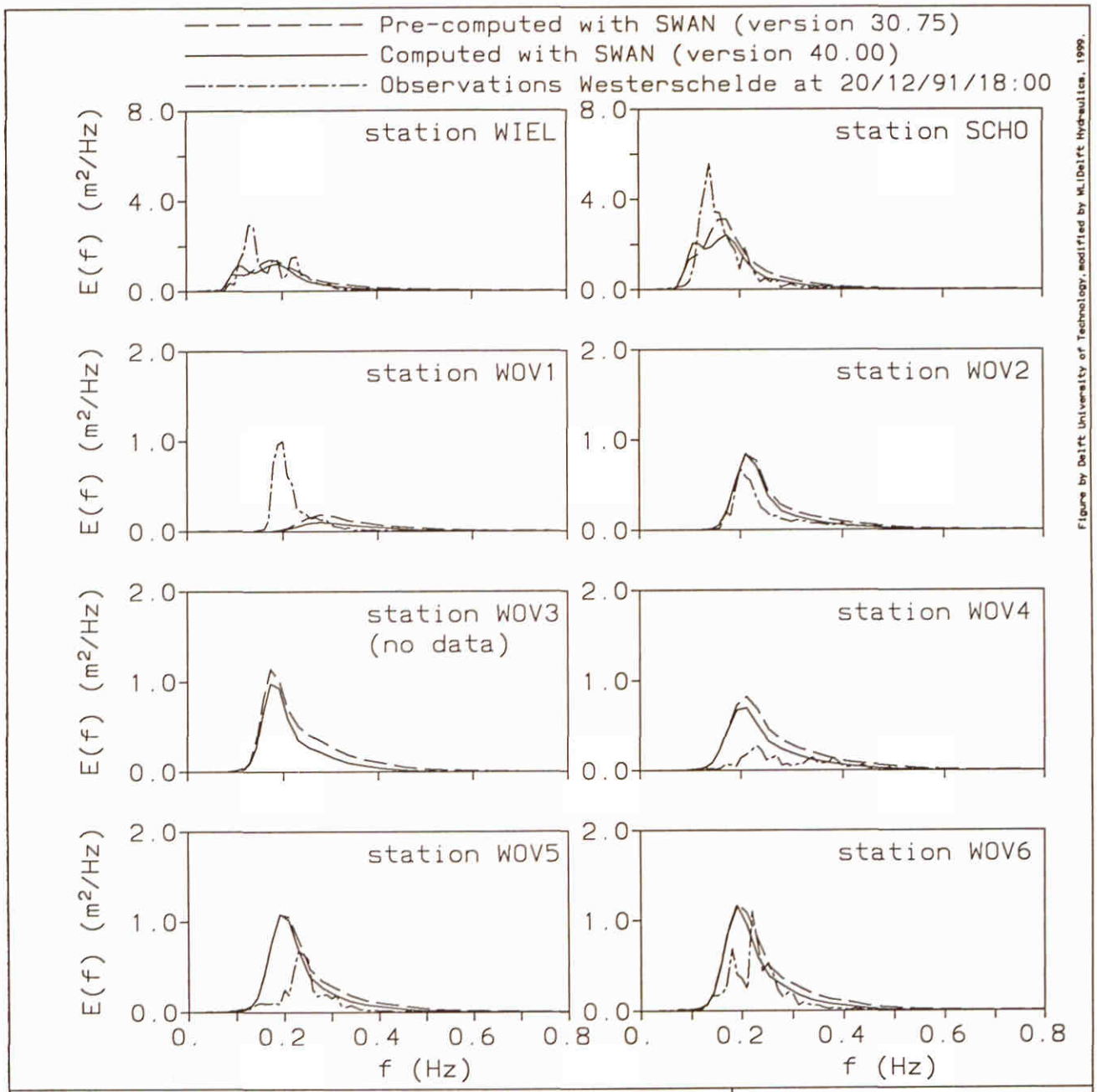


F61WesC2 F61f

Westerschelde Estuary

Westerschelde estuary

Extended Komen et al. (1984) expression with $\beta^0$

SWAN 40.00

WL | delft hydraulics

H3529

Fig. 7.10.f

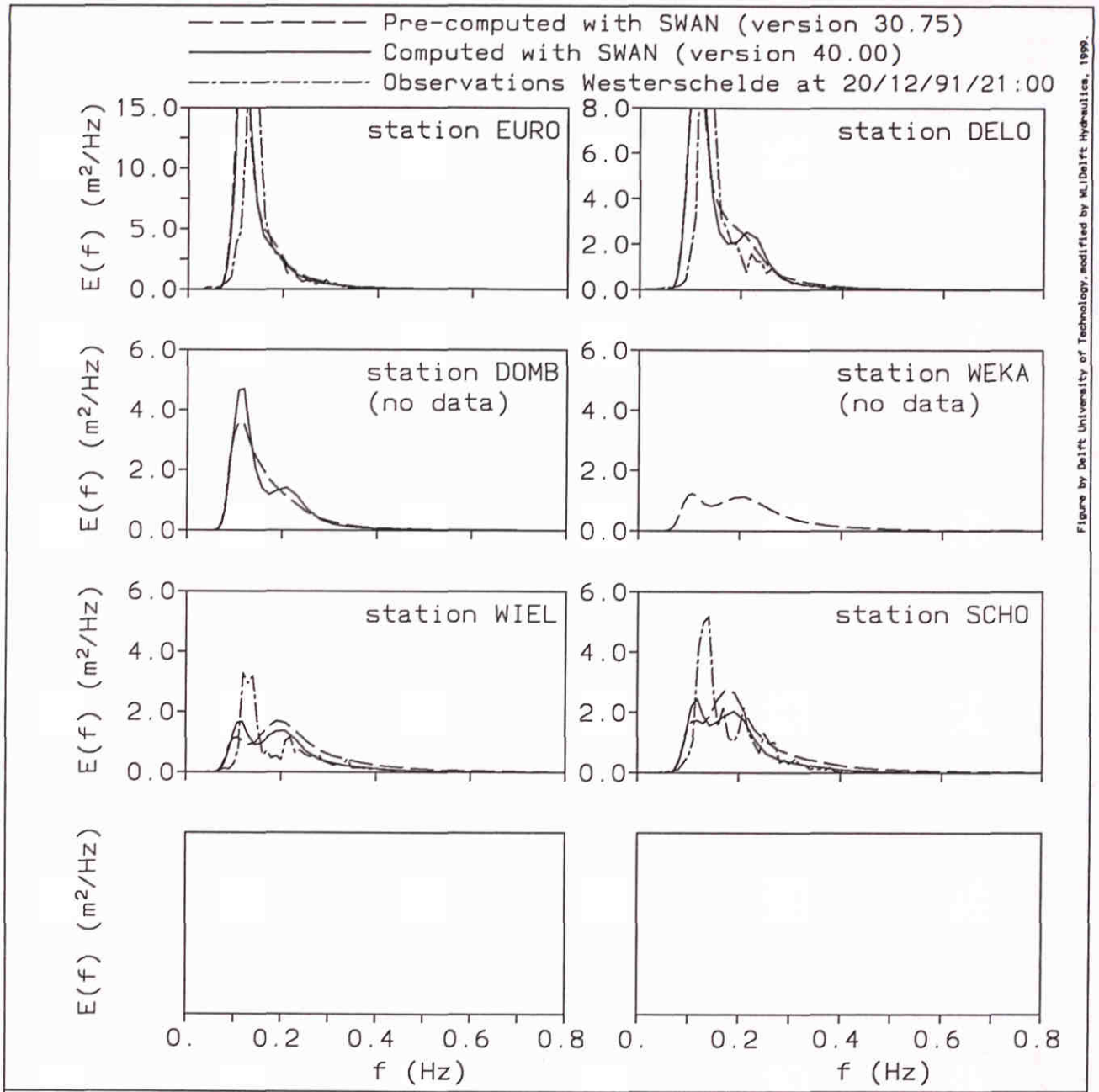


F61WesC4 F61g

Westerschelde Estuary

| | | |
|---|---|---|
| Westerschelde estuary<br>Extended Komen et al. (1984) expression with $\beta^0$ | SWAN 40.00 | |
| WL \| delft hydraulics | H3529 | Fig. 7.10.g |

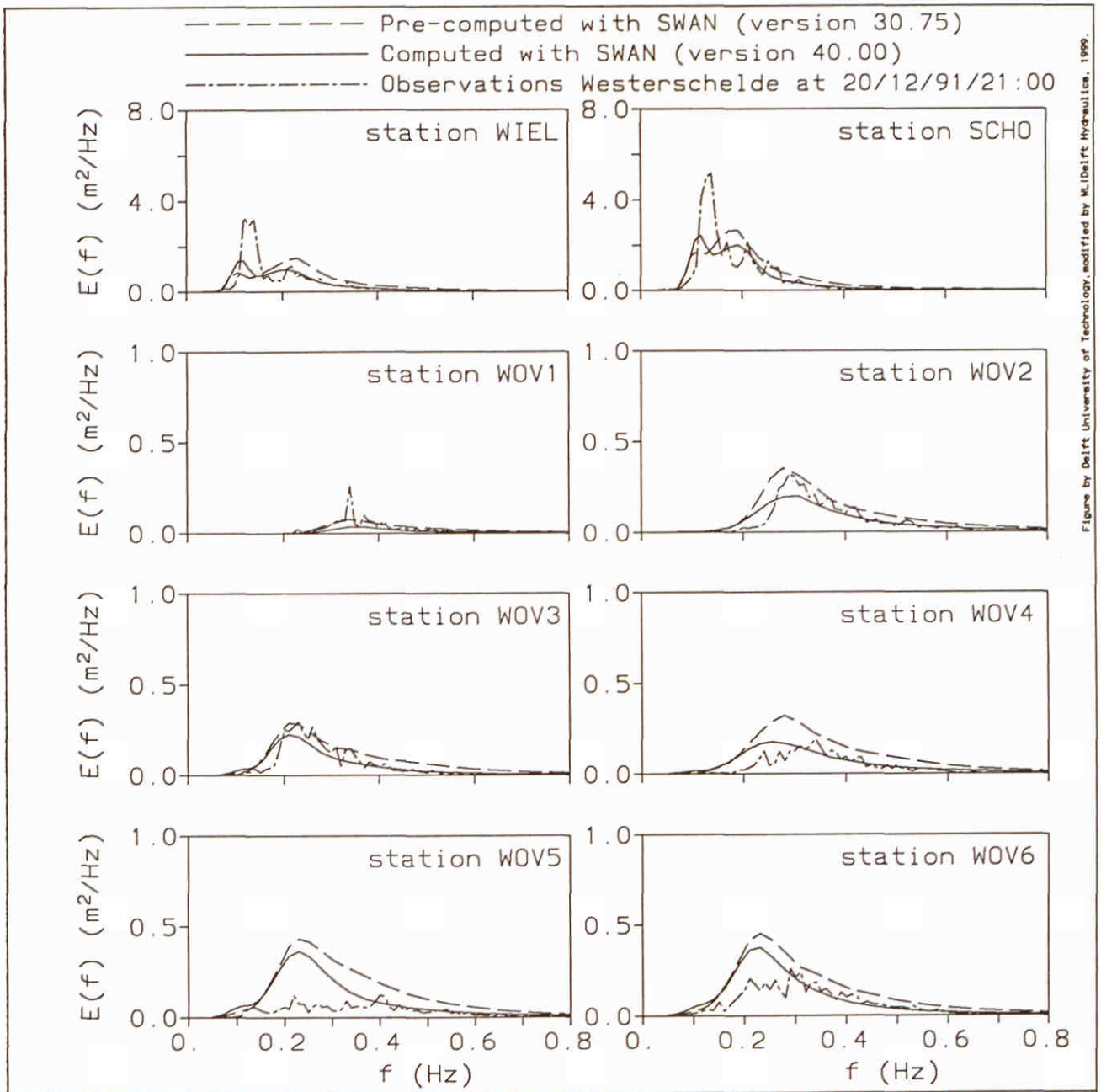


F61WesC4 F61h

Westerschelde Estuary

| | | |
|---|---|---|
| Westerschelde estuary<br>Extended Komen et al. (1984) expression with $\beta^0$ | SWAN 40.00 | |
| WL \| delft hydraulics | H3529 | Fig. 7.10.h |

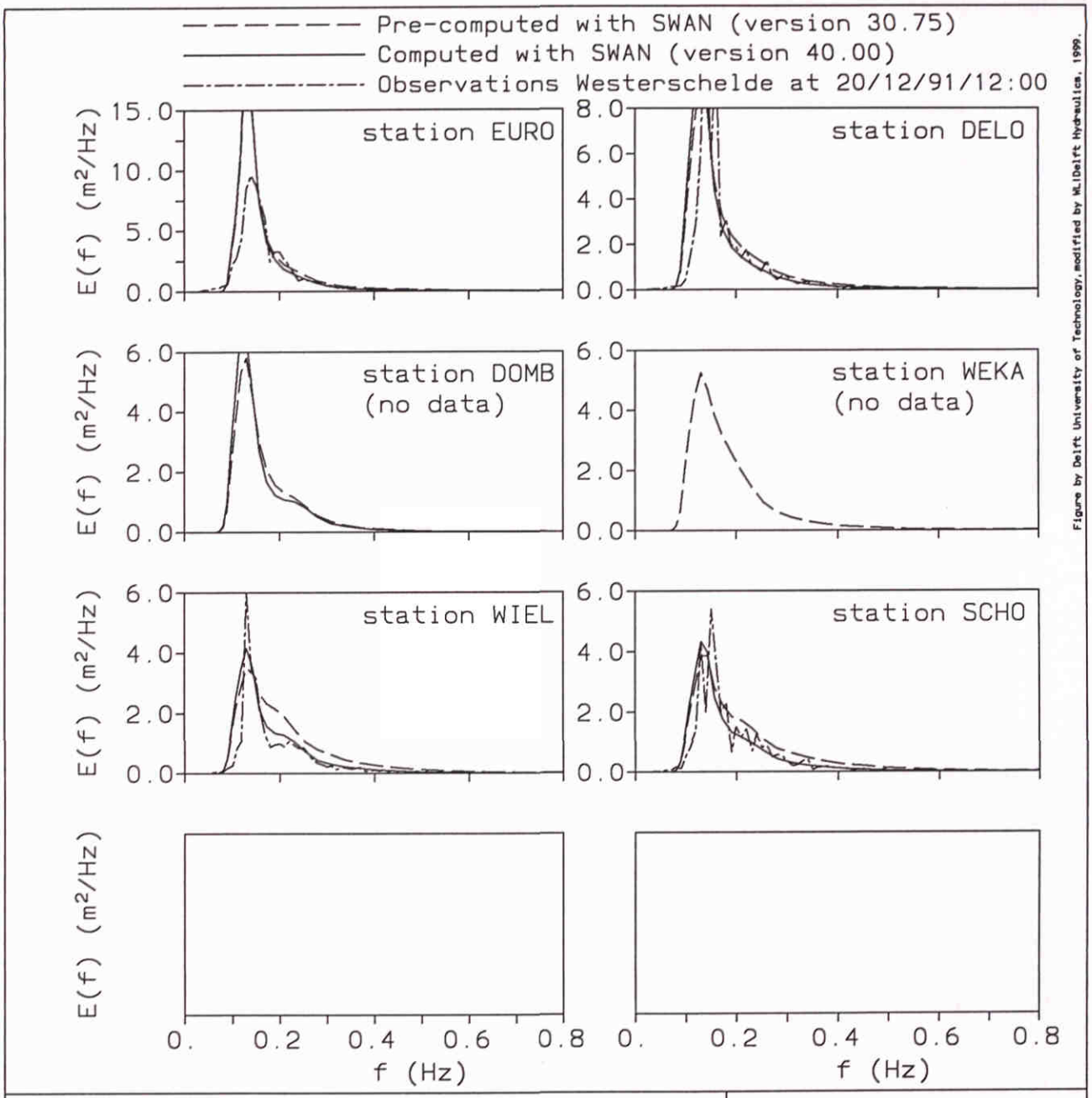


F61WesC1 F61a

Westerschelde Estuary

Westerschelde estuary

Extended Komen et al. (1984) expression with $\beta^{0.5}$

SWAN 40.00

WL | delft hydraulics

H3529

Fig. 7.11.a

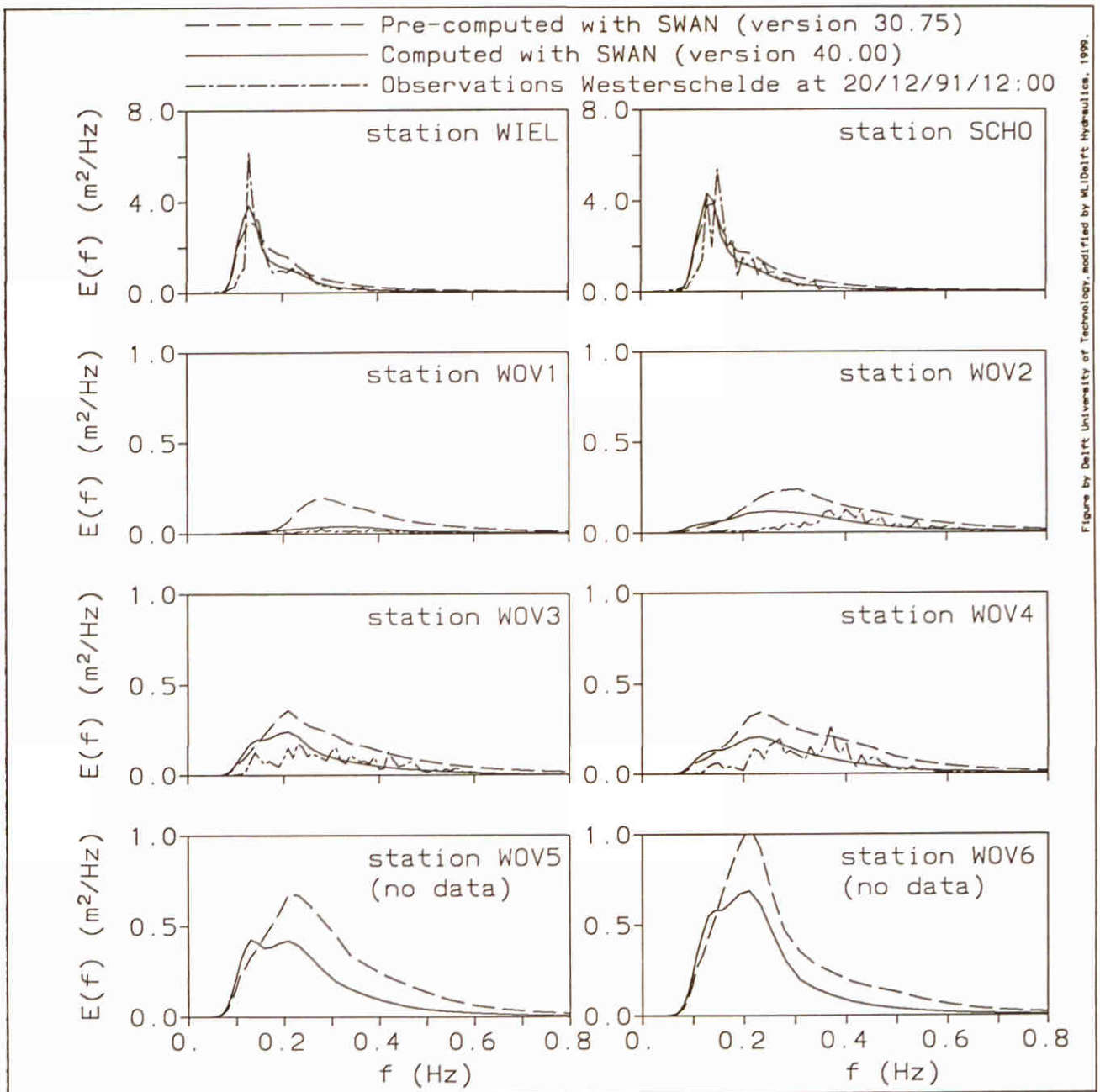


F61WesC1 F61b

Westerschelde Estuary

Westerschelde estuary

Extended Komen et al. (1984) expression with $\beta^{0.5}$

SWAN 40.00

WL | delft hydraulics

H3529

Fig. 7.11.b

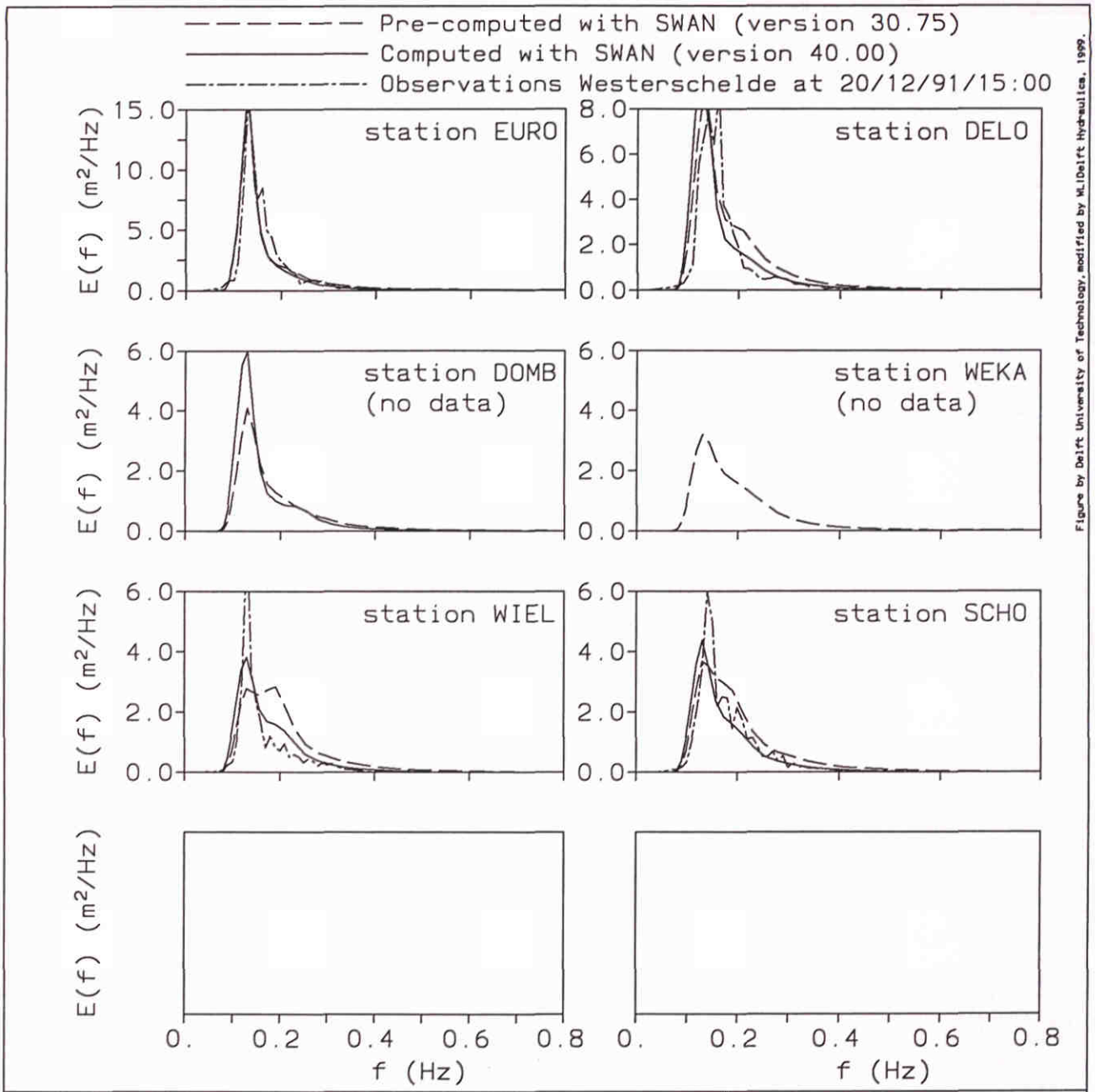


F61WesC2 F61c

Westerschelde Estuary

Westerschelde estuary

Extended Komen et al. (1984) expression with $\beta^{0.5}$

SWAN 40.00

WL | delft hydraulics

H3529

Fig. 7.11.c

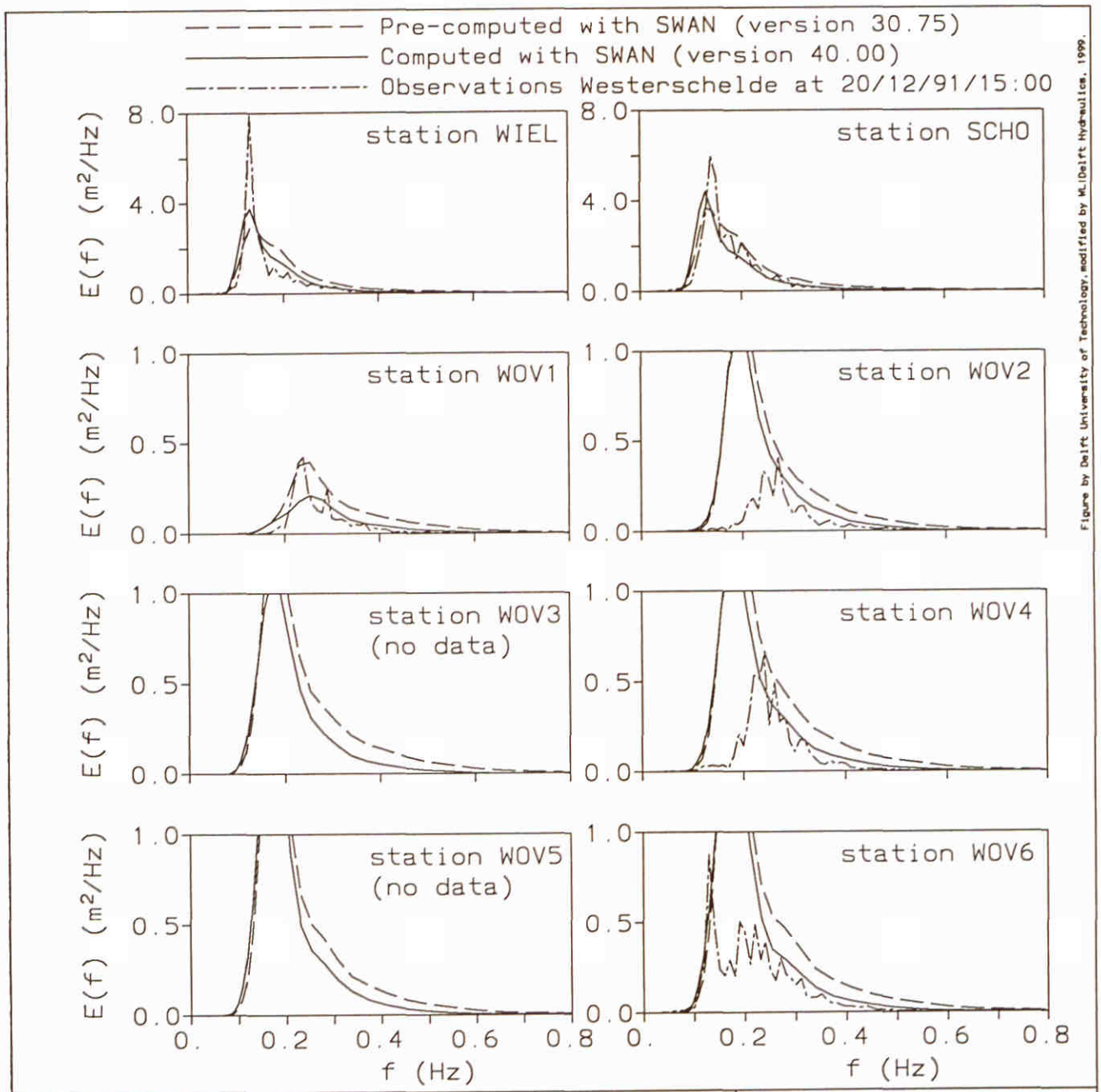


F61WesC2 F61d

Westerschelde Estuary

Westerschelde estuary

Extended Komen et al. (1984) expression with $\beta^{0.5}$

SWAN 40.00

WL | delft hydraulics

H3529

Fig. 7.11.d

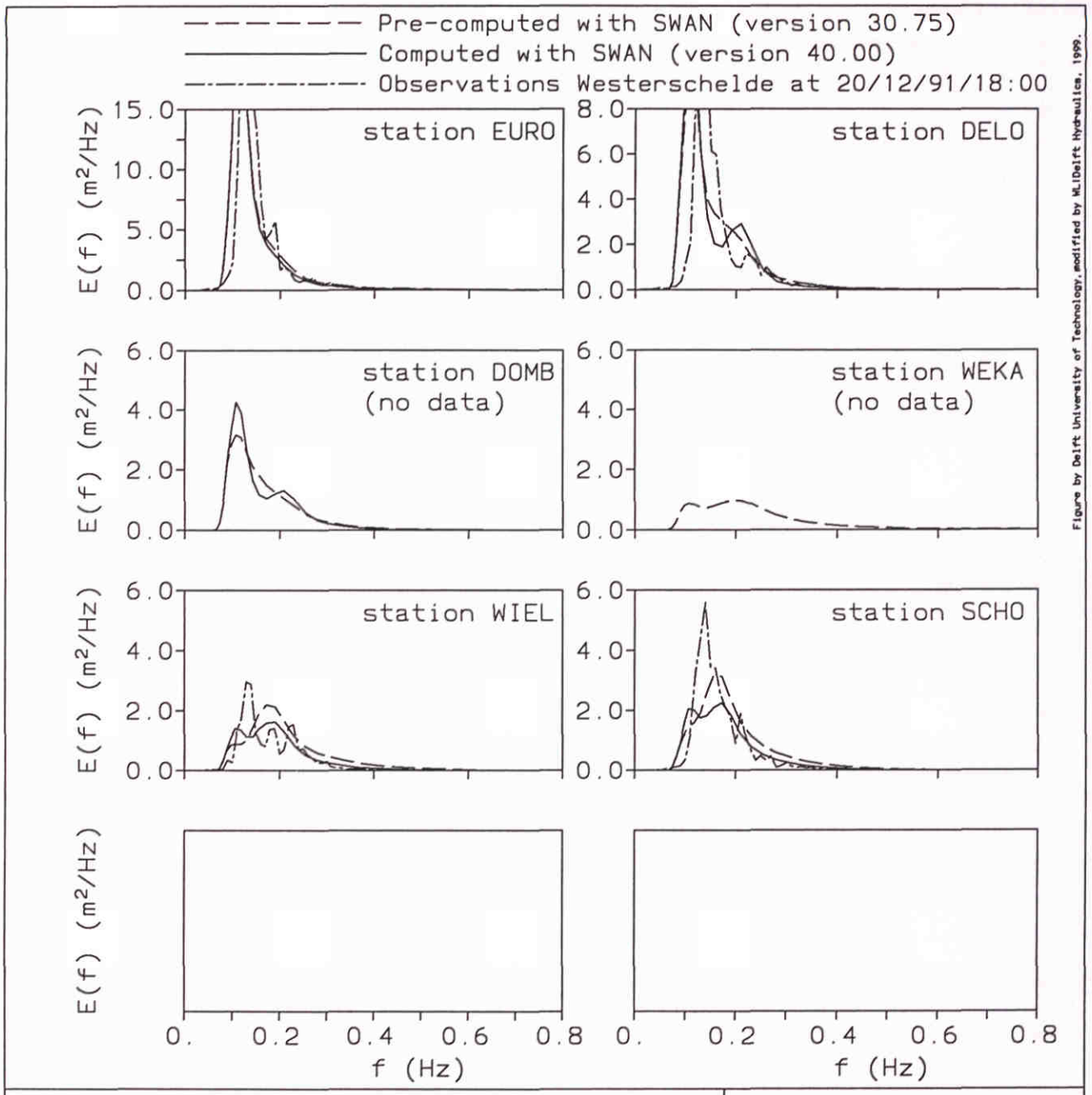


F61WesC3 F61e

Westerschelde Estuary

| | | |
|---|---|---|
| Westerschelde estuary<br>Extended Komen et al. (1984) expression with $\beta^{0.5}$ | SWAN 40.00 | |
| WL \| delft hydraulics | H3529 | Fig. 7.11.e |

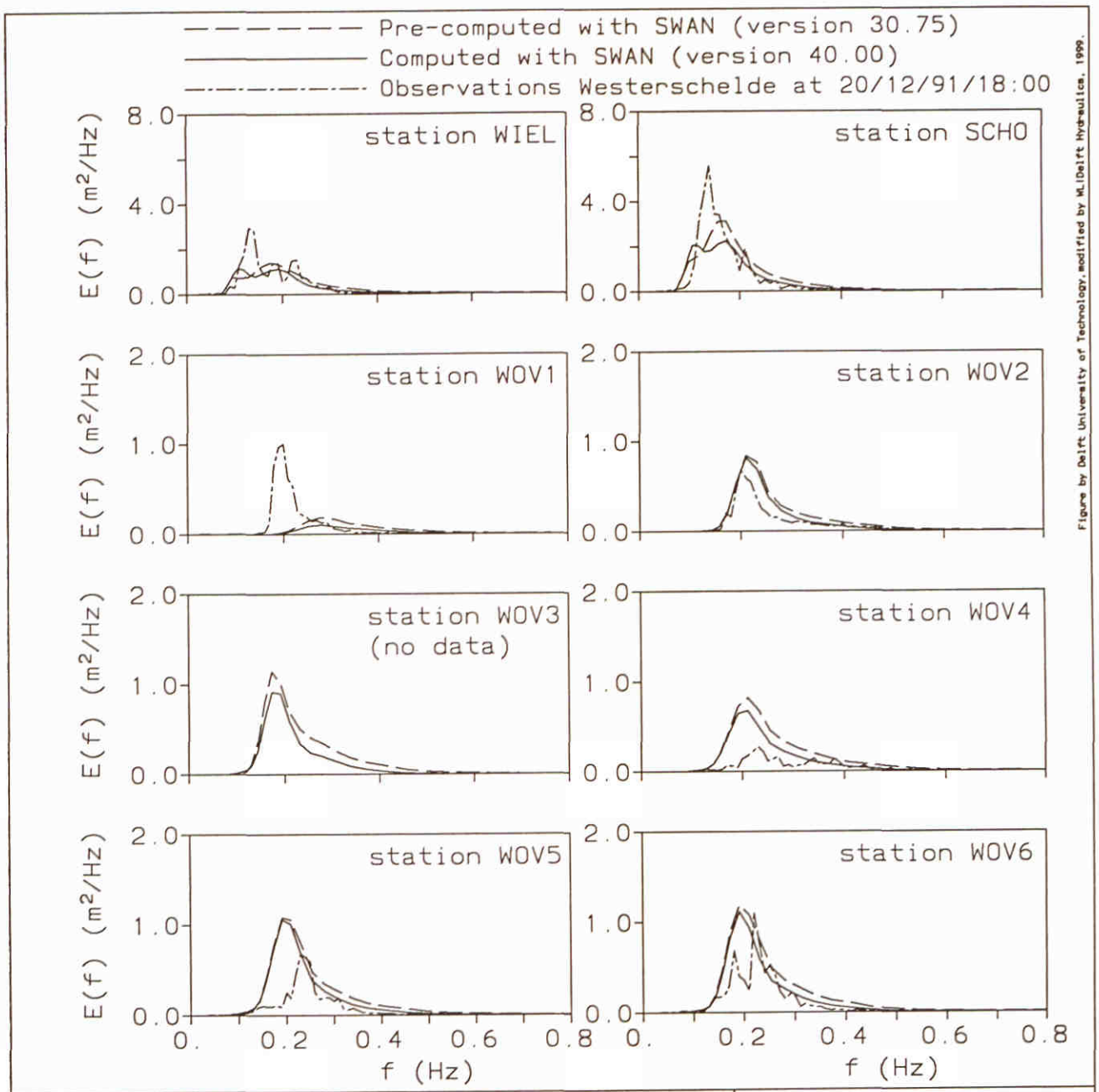


F61WesC2 F61f

Westerschelde Estuary

Westerschelde estuary

Extended Komen et al. (1984) expression with $\beta^{0.5}$

SWAN 40.00

WL | delft hydraulics

H3529

Fig. 7.11.f

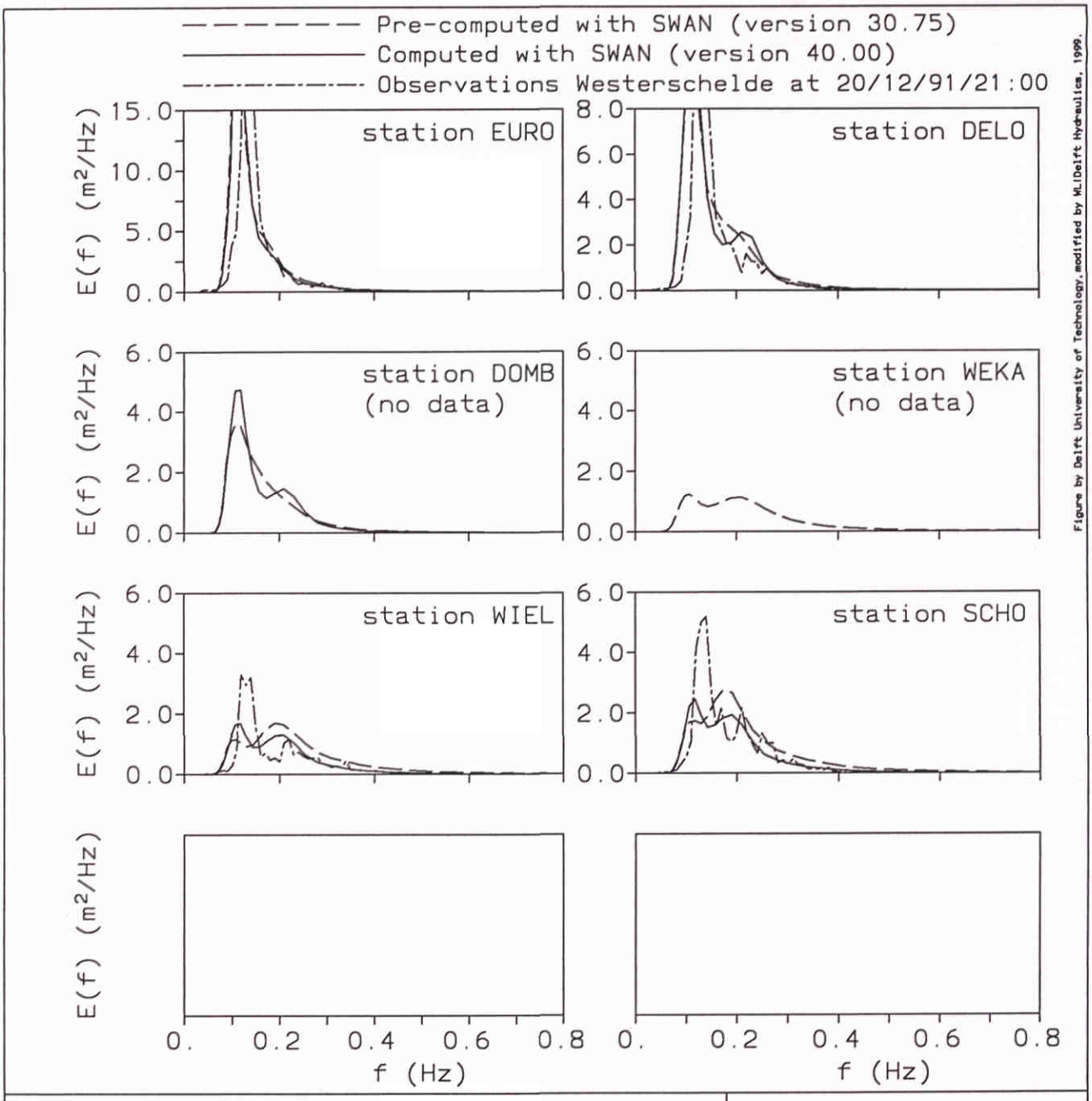


F61WesC4 F61g

Westerschelde Estuary

Westerschelde estuary

Extended Komen et al. (1984) expression with $\beta^{0.5}$

SWAN 40.00

WL | delft hydraulics

H3529

Fig. 7.11.g

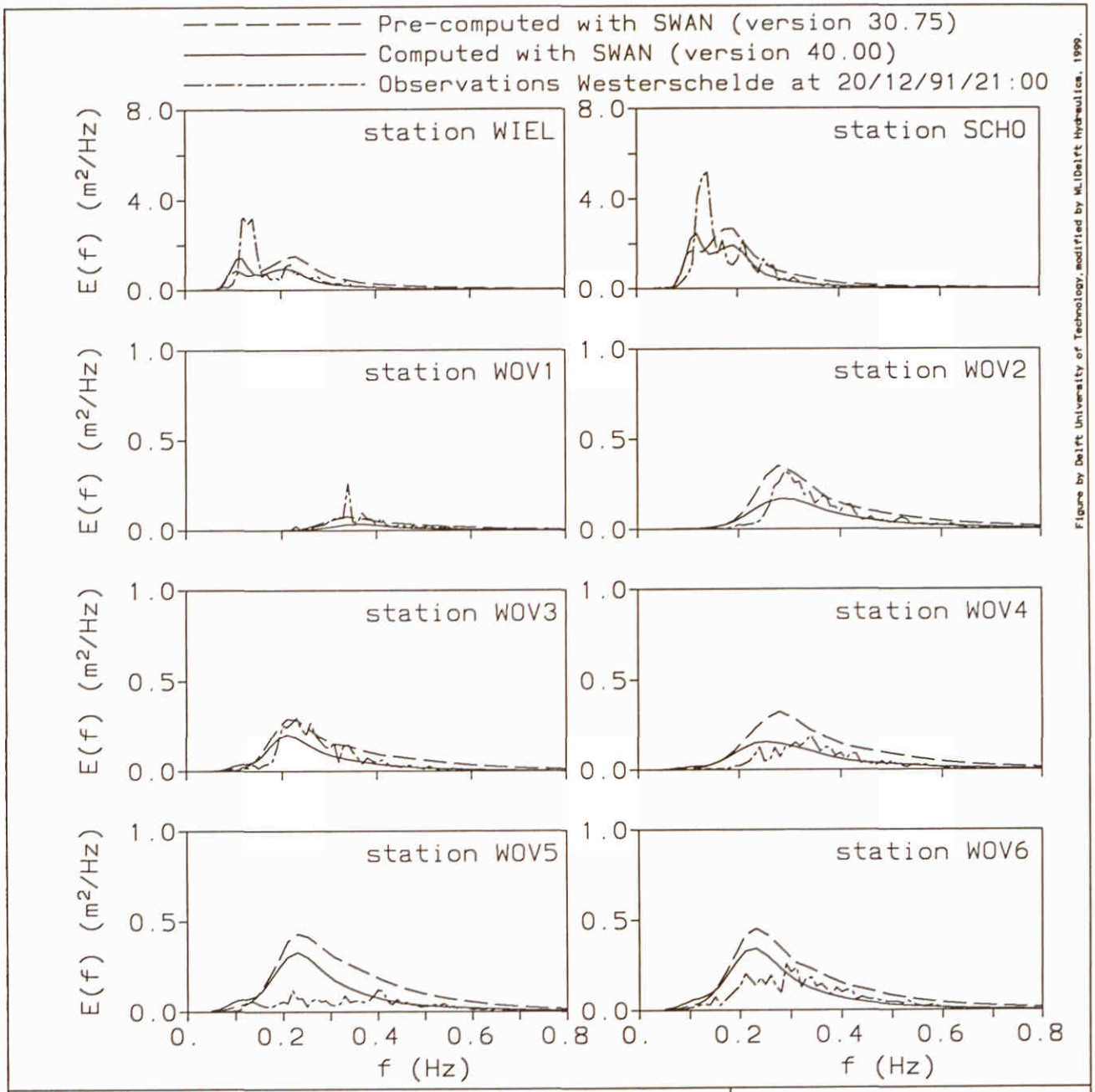


F61WesC4 F61h

Westerschelde Estuary

| | | |
|---|---|---|
| Westerschelde estuary<br>Extended Komen et al. (1984) expression with $\beta^{0.5}$ | SWAN 40.00 | |
| WL \| delft hydraulics | H3529 | Fig. 7.11.h |

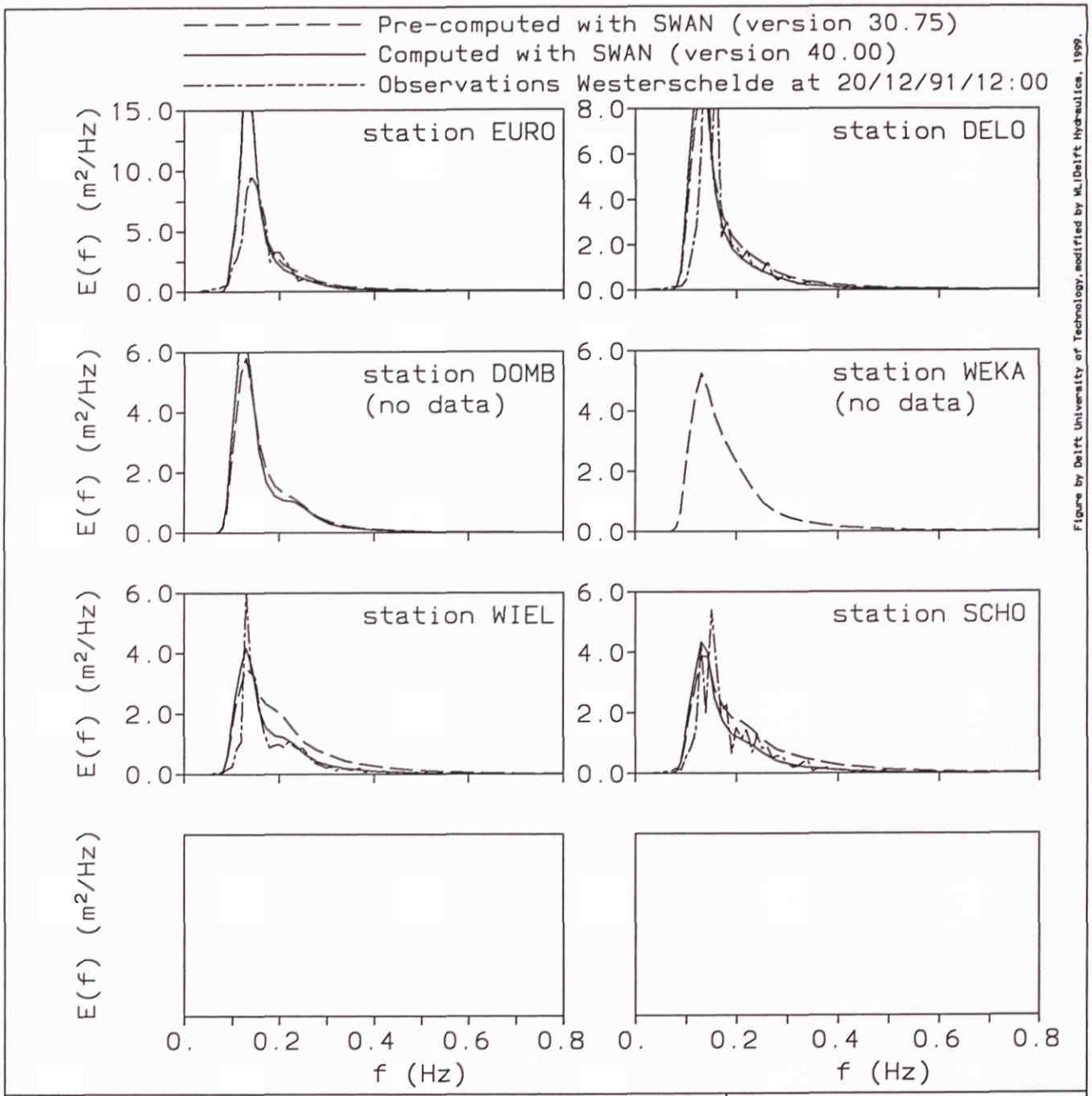


F61WesC1 F61a

Westerschelde Estuary

Westerschelde estuary

Extended Komen et al. (1984) expression with $\beta^1$

SWAN 40.00

WL | delft hydraulics

H3529

Fig. 7.12.a

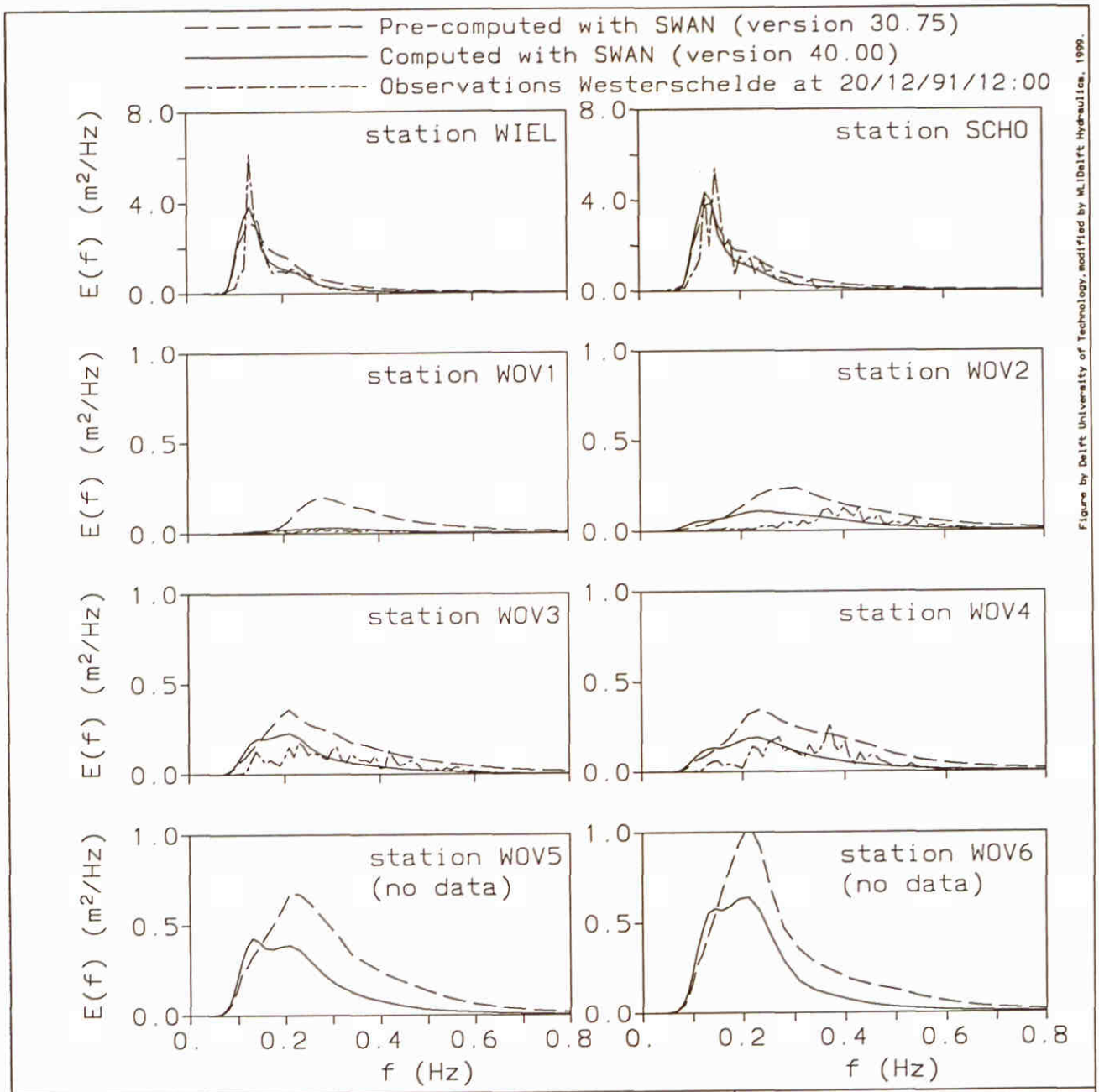


F61WesC1 F61b

Westerschelde Estuary

Westerschelde estuary

Extended Komen et al. (1984) expression with $\beta^1$

SWAN 40.00

WL | delft hydraulics

H3529

Fig. 7.12.b

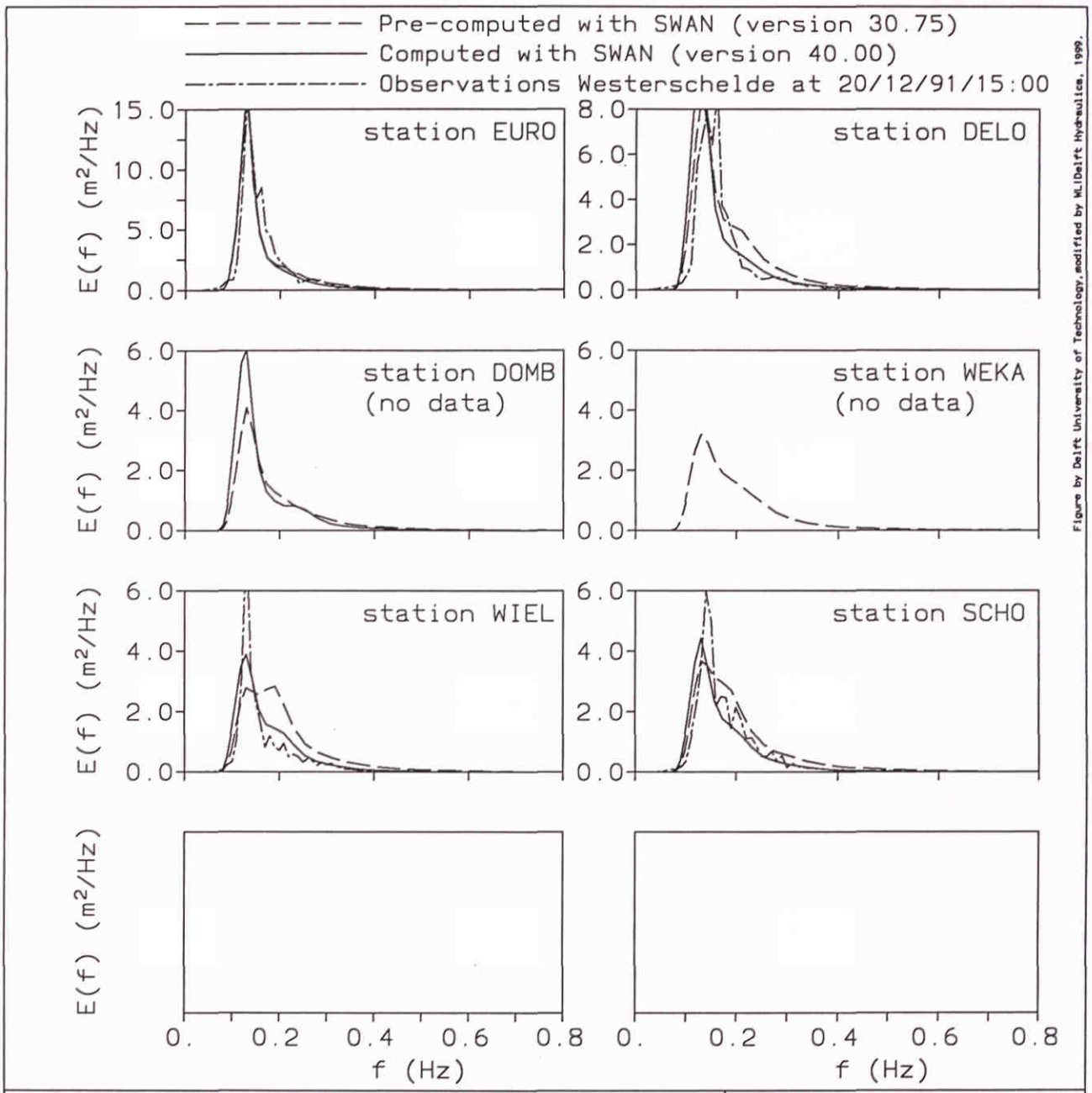


F61WesC2 F61c

Westerschelde Estuary

| | | |
|---|---|---|
| Westerschelde estuary<br>Extended Komen et al. (1984) expression with $\beta^1$ | SWAN 40.00 | |
| WL \| delft hydraulics | H3529 | Fig. 7.12.c |

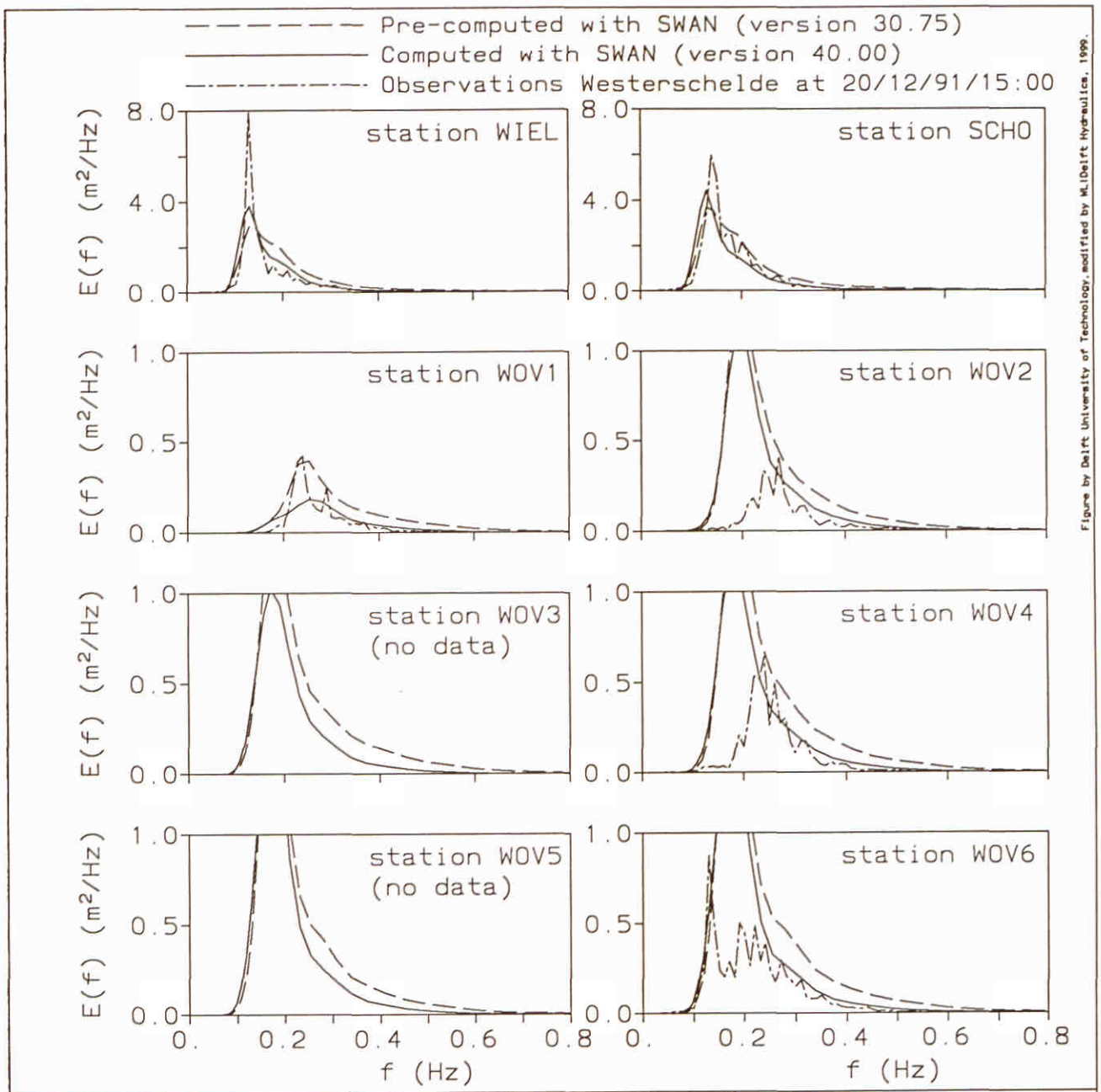


F61WesC2 F61d

Westerschelde Estuary

Westerschelde estuary

Extended Komen et al. (1984) expression with $\beta^1$

SWAN 40.00

WL | delft hydraulics

H3529

Fig. 7.12.d

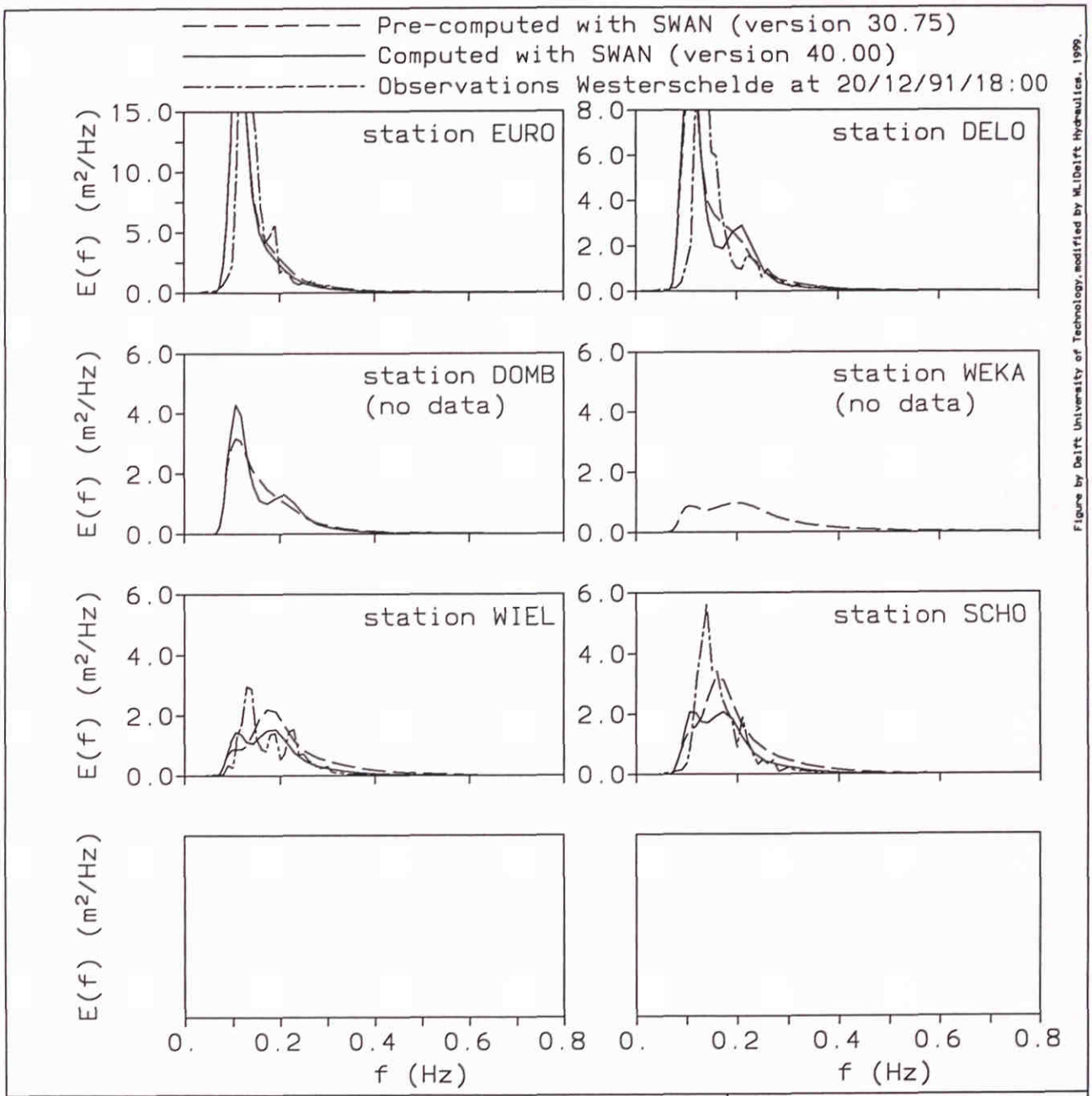


F61WesC3 F61e

Westerschelde Estuary

Westerschelde estuary

Extended Komen et al. (1984) expression with $\beta^1$

SWAN 40.00

WL | delft hydraulics

H3529

Fig. 7.12.e

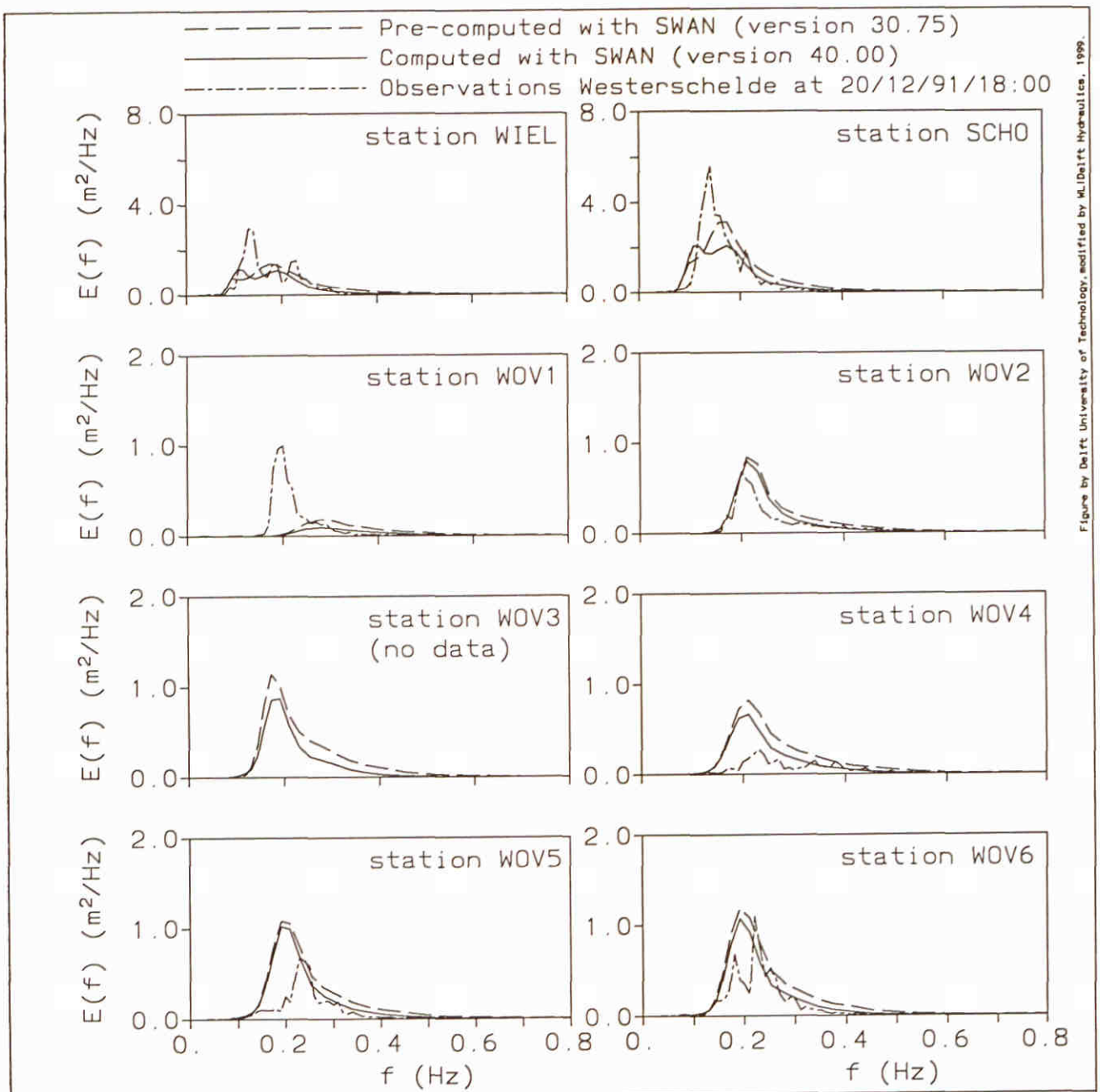


F61WesC2 F61f

Westerschelde Estuary

Westerschelde estuary

Extended Komen et al. (1984) expression with $\beta^1$

SWAN 40.00

WL | delft hydraulics

H3529

Fig. 7.12.f

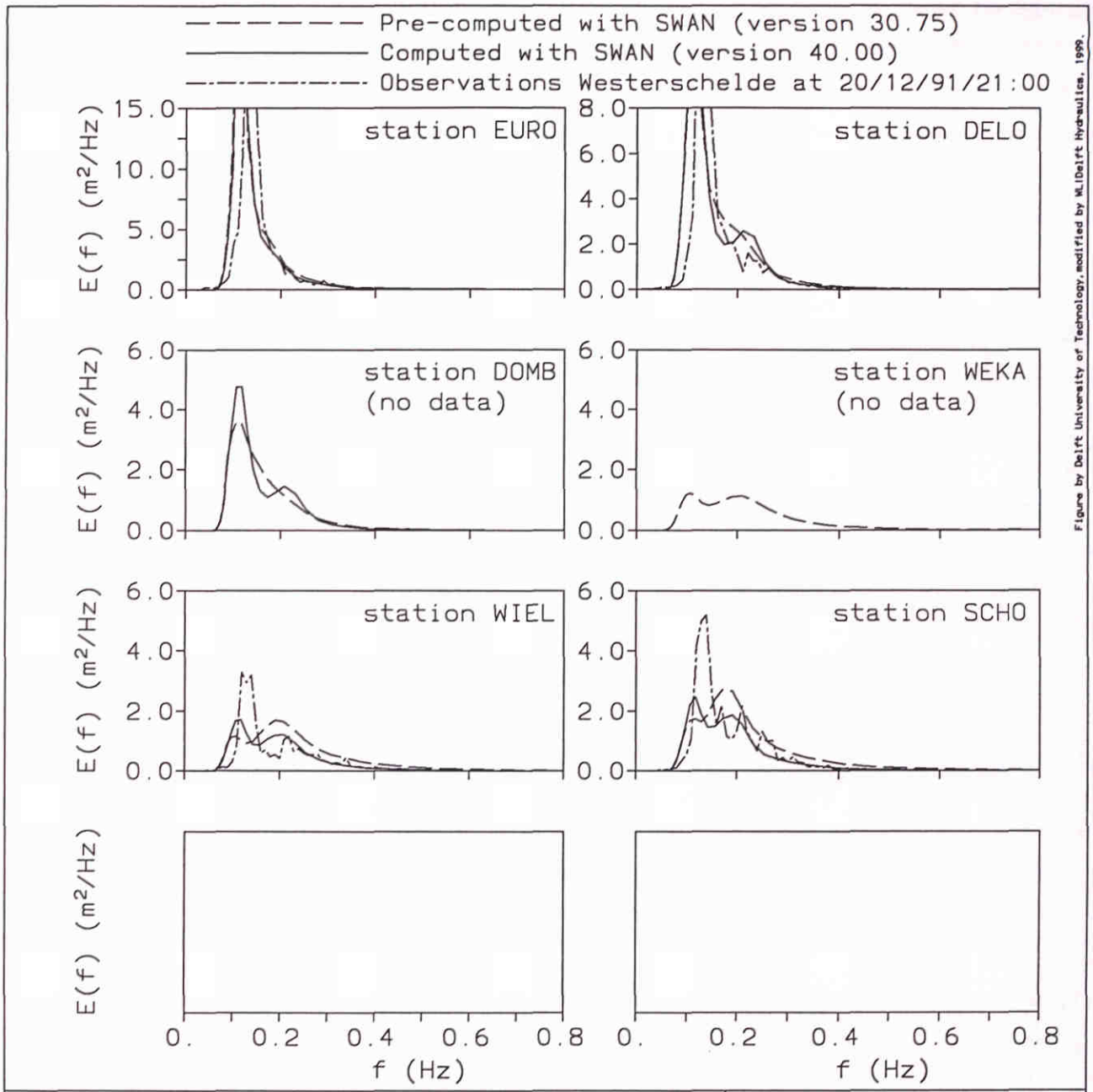


F61WesC4 F61g

Westerschelde Estuary

| | | |
|---|---|---|
| Westerschelde estuary<br>Extended Komen et al. (1984) expression with $\beta^1$ | SWAN 40.00 | |
| WL \| delft hydraulics | H3529 | Fig. 7.12.g |

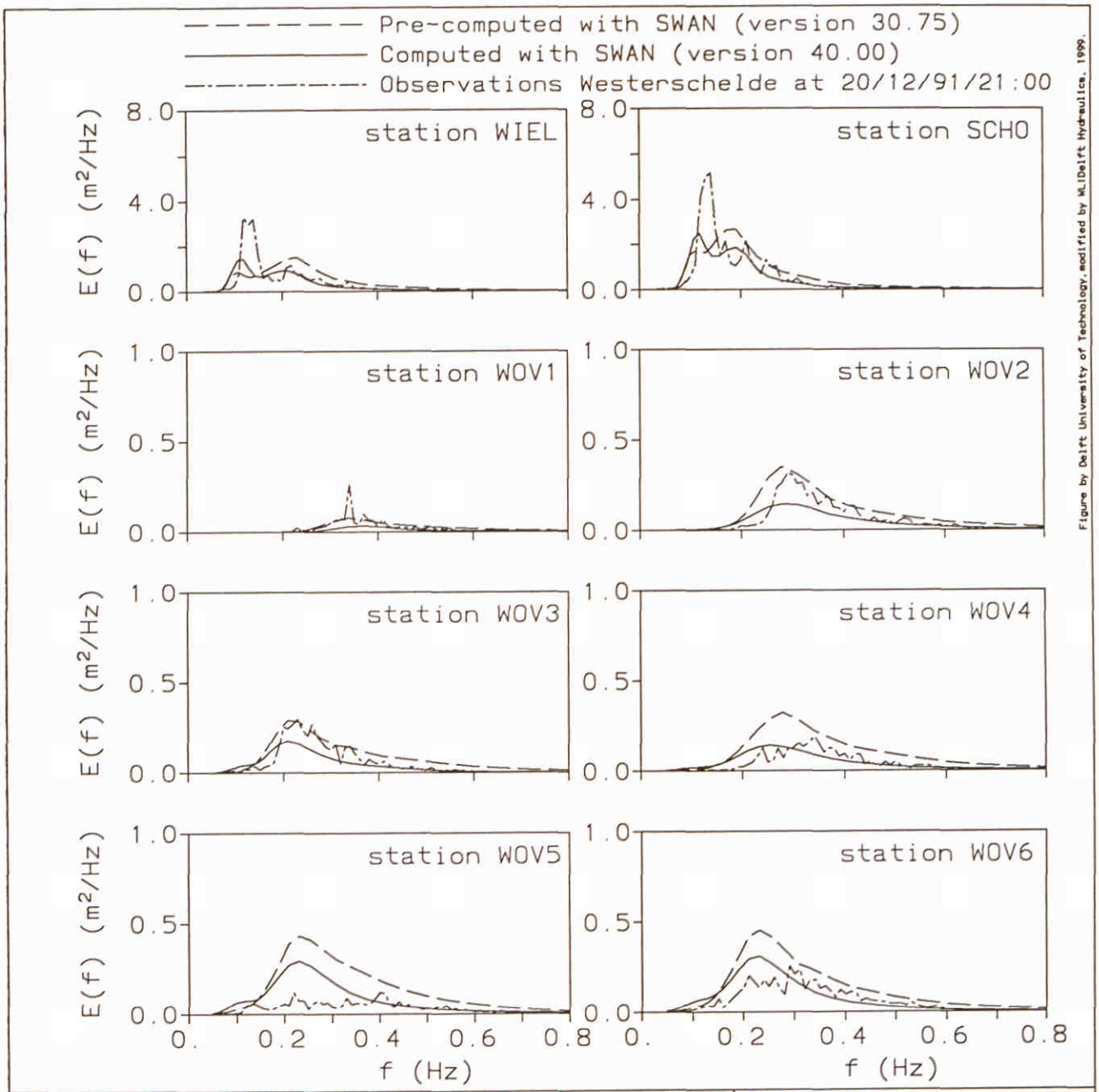


F61WesC4 F61h

Westerschelde Estuary

| | | |
|---|---|---|
| Westerschelde estuary<br>Extended Komen et al. (1984) expression with $\beta$[1] | SWAN 40.00 | |
| WL \| delft hydraulics | H3529 | Fig. 7.12.h |

# Appendices

# A Listing of new subroutine SWCAP7

In this appendix a listing of the source code of the new subroutine SWCAP7 is given.

```
C*************************************************************************
C
      SUBROUTINE SWCAP7 (MDC     ,MSC     ,MWCAP   ,ETOT    ,IMATDA  ,
     &                   KWAVE   ,ICMAX   ,PWCAP   ,KMESPC  ,SMESPC  ,
     &                   IDCMIN  ,IDCMAX  ,PLWCAP  ,ISSTOP  ,DISSC1  ,
     &                   AC2     ,KCGRD   ,MCGRD   ,SPCSIG  ,DDIR    ,
     &                   PWTAIL                                      )
C
C*************************************************************************
C
      INCLUDE 'swcomm4.inc'
      INCLUDE 'ocpcomm4.inc'
C
C
C       --|------------------------------------------------------|--
C         |                   1         1                2       2|
C         | Authors : R.C. Ris, E. Cecchi, L.H. Holthuijsen, N. Booij |
C         |                                                      |
C         | (1) WL | Delft Hydraulics                            |
C         |     Marine and Coastal Infrastructure department     |
C         |     P.O. Box 177, 2600 MH Delft, The Netherlands     |
C         |                                                      |
C         | (2) Delft University of Tecnology                    |
C         |     Faculty of Civil Engineering                     |
C         |     P.O. Box 5048, 2600 GA Delft, The Netherlands    |
C         |                                                      |
C       --|------------------------------------------------------|--
C
C
C     1. UPDATE
C
C        August 1999
C
C     2. PURPOSE
C
C        Compute the energy dissipation source term for whitecapping using an
C        alternative redefinition of integral (I) and local (L) wave steepness
C
C     3. METHOD
C
C        Compute the dissipation of energy due to whitecapping (third
C        generation white capping model ) :
C
C                                                 m
C        S_wc(s,d) = C s alphaL(s,d) * alphaI(s)  E(s,d)
C
C
C          Here :     C = pwcap(12) = 15
C
C                     m = pwcap(13) = 1
```

```
C
C                                  2
C                 alphaL(s,d) = k   s E(s,d)
C
C                                2  inf
C                                |  |          2
C                 alphaI(s) =    |  | f(s/so) k  E(s.d) dsdd
C                                0  0
C
C                              1
C                f = z / (z + - )      (filter function)
C                              z
C
C                               s
C                     n(1 -   -  )
C                z = e        so
C
C
C                n = 2                 (may vary between 0-10)
C
C
C     4. PARAMETERLIST
C
C        INTEGERS :
C        ----------
C        IS           Counter of relative frequency band
C        ID           Counter of directional distribution
C        ICMAX        Counter for the stencil
C        IDDUM
C        ISSTOP       Maxmum counter in freuqency space that is
C                     propagated within a sweep
C        MSC          Maximum counter of relative frequency
C        MDC          Maximum counter of directional distribution
C
C
C
C        REALS:
C        ----------
C        ETOT         Total wave energy
C        KMESPC       Mean wave number averaged over the energy spectrum
C
C        SCAPEO       White capping source term
C        SMESPC       Mean frequency averaged over the energy spectrum
C
C        one and more dimensional arrays:
C        --------------------------------
C        AC2      3D    Action density
C        ALPSTP   1D    Integral wave steepness parameter
C        ALPL     2D    Local wave steepness parameter
C        ESI      1D    Energy function of frequency
C        ESIDI    2D    Energy function of frequency and direction
C        IDCMIN   1D    Counter in directional space to indicate
C                       the minimum bin that is propagated in a sweep
C        IDCMAX         idem
C        IMATDA   2D    Coefficients of diagonal of matrix
C        KWAVE    2D    Wavenumber
C
C        PWCAP(12)  =   15  (Emperical coefficient)
C        PWCAP(13)  =   1   (Emperical coefficient)
C
C     5. SUBROUTINES CALLING
C
C        ---
C
C     6. SUBROUTINES USED
C
C        ---
```

```
C
C     7. ERROR MESSAGES
C
C        ---
C
C     8. REMARKS
C
C        ---
C
C     9. STRUCTURE
C
C   ------------------------------------------------------------
C   Compute the average steepness parameter
C   ------------------------------------------------------------
C   For every bin of the spectrum do
C       compute the dissipation of energy due to white capping
C   ------------------------------------------------------------
C
C     10. SOURCE
C
C*******************************************************************************
C
      INCLUDE 'swcomm4.inc'
      INCLUDE 'ocpcomm4.inc'
C
      INTEGER     MSMAX, MDMAX
      PARAMETER ( MSMAX = 200, MDMAX = 400 )
C
      INTEGER  IS    ,ID   ,MDC   ,MSC   , MWCAP,ICMAX ,IDDUM,ISSTOP,
     &         ICMAX ,MCGRD
C
      REAL     SCAPEO,KMESPC,SMESPC,ETOT ,TMP   ,COF1  ,COF2  ,STPSIG,
     &         DDIR  , ZETA1, ZETA2,EFFE1, EFFE2
C
      REAL     IMATDA(MDC,MSC)          ,
     &         KWAVE(MSC,ICMAX)         ,
     &         PWCAP(MWCAP)             ,
     &         PLWCAP(MDC,MSC,NPTST)    ,
     &         DISSC1(MDC,MSC)          ,
     &         AC2(MDC,MSC,MCGRD)       ,
     &         SPCSIG(MSC)              ,
     &         PWTAIL(*)
C
C
      INTEGER  IDCMIN(MSC)              ,
     &         IDCMAX(MSC)              ,
     &         KCGRD(ICMAX)
C
C     *** new additional arrays ***
C
      REAL     ESIDI(MDMAX,MSMAX)       ,
     &         ESI(MSMAX)               ,
     &         ALPSTP(MSMAX)            ,
     &         ALPL(MDMAX,MSMAX)
C
C
      SAVE IENT
      DATA IENT/0/
      IF (LTRACE) CALL STRACE (IENT,'SWCAP7')
C
C     *** initialize the arrays ***
C
```

```
      DO IS = 1, MSMAX
        ALPSTP(IS) = 0.0
        ESI(IS)    = 0.0
        DO ID = 1, MDC
          ESIDI(ID,IS) = 0.0
          ALPL (ID,IS) = 0.0
        ENDDO
      ENDDO
C
C     *** compute two and one dimensional energy spectrum E(s,d) and E(s)  ***
C
       DO IS = 1, MSC
         TMP = 0.
         DO ID = 1, MDC
           TMP = TMP + SPCSIG(IS) * AC2(ID,IS,KCGRD(1))
           ESIDI(ID,IS) = SPCSIG(IS) * AC2(ID,IS,KCGRD(1))
         ENDDO
         ESI(IS) = TMP * DDIR
       ENDDO
C
C      *** compute integral wave steepness ALPSTP(s) ****
C
       DO ISTMP = 2 , MSC
         STPSIG = 0.
         DO ISS = 2 , MSC
           ZETA1 = EXP ( 2. * (1. - SPCSIG(ISS)/SPCSIG(ISTMP)))
           EFFE1 = ZETA1 / (ZETA1 + 1./ZETA1)
           ZETA2 = EXP ( 2. * (1. - SPCSIG(ISS-1)/SPCSIG(ISTMP)))
           EFFE2 = ZETA2 / (ZETA2 + 1./ZETA2)
           DS    = SPCSIG(ISS) - SPCSIG(ISS-1)
           COF1  = EFFE1 * KWAVE(ISS,1  )**2 * ESI(ISS  )
           COF2  = EFFE2 * KWAVE(ISS-1,1)**2 * ESI(ISS-1)
           STPSIG = STPSIG + 0.5 * (COF1 + COF2) * DS
         ENDDO
         ALPSTP(ISTMP) = STPSIG
       ENDDO
       ALPSTP(1) = ALPSTP(2)
C
C      *** determine source term ***
C
       DO IS = 1,MSC
         DO IDDUM = IDCMIN(IS), IDCMAX(IS)
           ID = MOD ( IDDUM - 1 + MDC , MDC ) + 1
           ALPL(ID, IS) =  KWAVE(IS,1)**2 * SPCSIG(IS) * ESIDI(ID,IS)
           SCAPEO= PWCAP(12) * SPCSIG(IS) * ALPL(ID, IS) * ALPSTP(IS)**PWCAP(13)
           IMATDA(ID,IS) = IMATDA(ID,IS) + SCAPEO
           IF(TESTFL) PLWCAP(ID,IS,IPTST) = -1.* SCAPEO
         ENDDO
       ENDDO
C
C     *** test output ***
C
      IF ( TESTFL .AND. ITEST .GE. 1 ) THEN
        WRITE(PRINTF,6023) PWCAP(12), PWCAP(13), ISSTOP
 6023   FORMAT(' SWCAP6 : (12) (13) ISSTOP    : ',2E12.4,I4)
        WRITE(PRINTF,6033) KMESPC, SMESPC, ETOT
 6033   FORMAT(' SWCAP6 : KMESPC SMESPC ETOT: ',3E12.4)
        WRITE(PRINTF,6043) DDIR
 6043   FORMAT(' SWCAP6 : DDIR               : ',E12.4)
      END IF
C
C     end of subroutine SWCAP7
C
      RETURN
      END
```

# B Listing of new subroutine SWCAP6

In this appendix a listing of the source code of the new subroutine SWCAP6 is given.

```
C*******************************************************************
C
      SUBROUTINE SWCAP6 (MDC     ,MSC     ,MWCAP   ,ETOT    ,IMATDA  ,
     &                   KWAVE   ,ICMAX   ,PWCAP   ,KMESPC  ,SMESPC  ,
     &                   IDCMIN  ,IDCMAX  ,PLWCAP  ,ISSTOP  ,DISSC1  ,
     &                   AC2     ,KCGRD   ,MCGRD   ,SPCSIG  ,DDIR    ,
     &                   PWTAIL                                      )
C
C*******************************************************************
C
C       --|-----------------------------------------------------|--
C         |                   1         1                2      2|
C         | Authors : R.C. Ris, E. Cecchi, L.H. Holthuijsen, N. Booij |
C         |                                                     |
C         | (1) WL | Delft Hydraulics                           |
C         |     Marine and Coastal Infrastructure department    |
C         |     P.O. Box 177, 2600 MH Delft, The Netherlands    |
C         |                                                     |
C         | (2) Delft University of Tecnology                   |
C         |     Faculty of Civil Engineering                    |
C         |     P.O. Box 5048, 2600 GA Delft, The Netherlands   |
C         |                                                     |
C       --|-----------------------------------------------------|--
C
C     1. UPDATE
C
C        September 1999
C
C     2. PURPOSE
C
C        Compute the energy dissipation source term for whitecapping
C        using an extended formulation based on the formulation
C        according to Komen et al. (1984)
C
C     3. METHOD
C
C        Compute the dissipation of energy due to whitecapping (third
C        generation white capping model ) :
C
C                                        k                       ( k  ) [powk]
C        S_wc(s,d) = - Cds3  * Cds1  s^ -- ( (1-delta) + delta ( -- )       )
C                                        K^                      ( K^ )
C
C                                                  (     2           ) [pown]
C                         ( ALPHA(s) ) [powst]     ( K^(s) Et^(s)    )
C                      *  ( -------- )          * (-----------------)       * E(s,d)
C                         ( ALPHA_PM )             (     2           )
C                                                  (   K^ Etot       )
C
C                                          -5
C        Here:      Cds1 = pwcap(1) = 2.36x10
C                                         -3
C                   ALPHA_PM = pwcap(2) = 3.02x10
C
C                   powst = pwcap(9) = 2.
C
C                   delta = pwcap(10) = 1.
C
```

```
C                  pown  = pwcap(12) = 0.5
C
C                  cds3  = pwcap(13) = 1.
C
C                            inf
C                       2    ||
C        ALPHA(s)  = k^(s)    || E(s,d) dsdd
C                            s
C
C        with s^ and k^ equal (WAM 1989):
C
C                      ___   -1
C              s^ = ( 1/s )
C                                -2
C              k^ = ( 1/sqrt(k) )
C
C
C        and s^(s), k^(s) and Et(s) are identical to WAM but the integral
C        is taken from s to infinity (instead from 0 to infinity as in WAM).
C
C
C     4. PARAMETERLIST
C
C        INTEGERS :
C        ----------
C        IS           Counter of relative frequency band
C        ID           Counter of directional distribution
C        ICMAX        Counter for the stencil
C        ISSTOP       Maxmum counter in freuqency space
C        MSC          Maximum counter of relative frequency
C        MDC          Maximum counter of directional distribution
C
C        REALS:
C        ---------
C
C        ETOT         Total wave energy
C        KMESPC       Mean wave number averaged over the energy spectrum
C        SMESPC       Mean frequency averaged over the energy spectrum
C        SCAPEO       White capping source term
C        FACTOR       Straining parameter BETA
C
C        one and more dimensional arrays:
C        --------------------------------
C        AC2      3D    Action density
C        IMATDA   2D    Coefficients of diagonal of matrix
C        KWAVE    2D    Wavenumber
C        IDCMIN   1D    Counter in directional space to indicate
C                       the minimum bin that is propagated in a sweep
C        IDCMAX         idem
C        FRSME  1D      Mean frequency from s to infinity
C        FRKME  1D      Mean wave number from s to infinity
C        FRETOT 1D      Wave energy from s to infinity
C
C        PWCAP(1)  = ALFAWC   2.36e-5  (Emperical coefficient)
C        PWCAP(2)  = ALFAPM   3.02E-3  (Alpha of Pierson Moskowitz frequency)
C
C     5. SUBROUTINES CALLING
C
C        ---
C
C     6. SUBROUTINES USED
C
C        ---
C
C     7. ERROR MESSAGES
C
C        ---
```

```
C
C     8. REMARKS
C
C        ---
C
C     9. STRUCTURE
C
C   -------------------------------------------------------------
C   Compute the average steepness parameters and total energy
C   (in up frequency direction)
C   -------------------------------------------------------------
C   For every bin of the spectrum do
C       compute the dissipation of energy due to white capping
C   -------------------------------------------------------------
C
C     10. SOURCE
C
C*******************************************************************************

C
      INCLUDE 'swcomm4.inc'
      INCLUDE 'ocpcomm4.inc'
C
      INTEGER     MSMAX
      PARAMETER ( MSMAX = 500)
C
      INTEGER  IS    ,ID   ,MDC   ,MSC   ,MWCAP ,ICMAX ,IDDUM ,ISSTOP,
     &         MCGRD
C
      REAL     SCAPEO,KMESPC,SMESPC,ETOT  ,DDIR  ,SIG   ,SIG2  ,WAVEN ,
     &         ETOTD ,ATOTD ,AKREL ,TMPE  ,TMPA  ,TMPK  ,FACTOR,FRINTF,
     &         DISWCP,DISWC2
C
      REAL     IMATDA(MDC,MSC)          ,
     &         KWAVE(MSC,ICMAX)         ,
     &         PWCAP(MWCAP)             ,
     &         PLWCAP(MDC,MSC,NPTST)    ,
     &         AC2(MDC,MSC,MCGRD)       ,
     &         SPCSIG(MSC)              ,
     &         DISSC1(MDC,MSC)          ,
     &         PWTAIL(*)
C
      INTEGER  IDCMIN(MSC)              ,
     &         IDCMAX(MSC)              ,
     &         KCGRD(ICMAX)
C
C     ***  new additional arrays ***
C
      REAL     FRSME(MSMAX)             ,
     &         FRKME(MSMAX)             ,
     &         FRETOT(MSMAX)
C
      SAVE IENT
      DATA IENT/0/
      IF (LTRACE) CALL STRACE (IENT,'SWCAP6')
C
C     *** initialize arrays ***
C
      DO IS = 1, MSC
        FRSME(IS)  = 0.0
        FRKME(IS)  = 0.0
        FRETOT(IS) = 0.0
      ENDDO
C
C     *** integration constant for logaritmic distribution ***
C
      FRINTF = ALOG(SPCSIG(MSC) / SPCSIG(1) ) / FLOAT(MSC-1)
```

```
C
C     *** Compute the total energy denisty and contributions to integrals ***
C     *** per frequency looking in frequency upwind directions only       ***
C
      DO ISS = 1, MSC
        TMPE  = 0.
        TMPA  = 0.
        TMPK  = 0.
        DO IS = ISS, MSC
          SIG   = SPCSIG(IS)
          SIG2  = SPCSIG(IS) * SPCSIG(IS)
          WAVEN = KWAVE(IS,1)
          ETOTD = 0.
          ATOTD = 0.
          DO ID = 1, MDC
            ETOTD = ETOTD + SIG2 * AC2(ID,IS,KCGRD(1))
            ATOTD = ATOTD + SIG  * AC2(ID,IS,KCGRD(1))
          ENDDO
          TMPE = TMPE + FRINTF * DDIR * ETOTD
          TMPA = TMPA + FRINTF * DDIR * ATOTD
          TMPK = TMPK + FRINTF * DDIR * ATOTD * SIG / SQRT(WAVEN)
        ENDDO
C
C       *** add high frequency tail and store value in arrays ***
C
        TMPE = TMPE + PWTAIL(6) * DDIR * ETOTD
        TMPA = TMPA + PWTAIL(5) * DDIR * ATOTD
        TMPK = TMPK + PWTAIL(5) * DDIR * ATOTD * SIG / SQRT(WAVEN)
C
C       *** compute mean wave parameters per frequency ***
C
        IF ( TMPA .LE. 0. .OR. TMPE .LE. 0.) THEN
          FRSME(ISS)  = 10.
          FRKME(ISS)  = 10.
          FRETOT(ISS) = 0.
        ELSE
          FRSME(ISS)  = TMPE / TMPA
          FRKME(ISS)  = ( TMPE / TMPK )**2.
          FRETOT(ISS) = TMPE
        END IF
      ENDDO
C
C     *** compute whitecapping source term ***
C
      DO IS = 1, ISSTOP
C
        DISWCP = PWCAP(1) * SMESPC *
     &           (FRKME(IS)**2. * FRETOT(IS) / PWCAP(2))**PWCAP(9)
C
C       *** multipy with factor to enhance dissipation of local wind ***
C       *** sea in presence of low frequency waves                    ***
C
        IF ( PWCAP(12) .LT. 1.e-12 ) then
          FACTOR = 1.
        ELSE
          FACTOR= PWCAP(13) *
     &       ((FRKME(IS)**2.*FRETOT(IS)) /(KMESPC**2.*ETOT))**PWCAP(12)
        ENDIF
C
        DISWCP = DISWCP * FACTOR
C
        DISWC2 = DISWCP * PWCAP(10)
        DISWCP = DISWCP * (1. - PWCAP(10))
        AKREL  = KWAVE(IS,1)/KMESPC
        SCAPEO = AKREL * (DISWCP + DISWC2 * (AKREL ** PWCAP(11)))
C
C       *** store source term in matrix ***
```

```
C
        DO IDDUM = IDCMIN(IS), IDCMAX(IS)
          ID = MOD ( IDDUM - 1 + MDC , MDC ) + 1
          IMATDA(ID,IS) = IMATDA(ID,IS) + SCAPEO
          DISSC1(ID,IS) = DISSC1(ID,IS) + SCAPEO
          IF(TESTFL) PLWCAP(ID,IS,IPTST) = -1.* SCAPEO
        ENDDO
      ENDDO
C
C     *** test output ***
C
      IF ( ITEST .GE. 30 .and. TESTFL ) THEN
        WRITE(PRINTF,6023) PWCAP(12), PWCAP(13), ISSTOP, DDIR
 6023   FORMAT(' SWCAP6: (12) (13) ISSTOP DDIR: ',2E12.4,I4,F8.2)
        WRITE(PRINTF,5000) SMESPC, KMESPC, ETOT, 4. * SQRT(ETOT)
 5000   FORMAT(' SWCAP6: SMESPC KMESPC ETOT HS: ',4E12.4)
        IF ( ITEST .GE. 100 ) THEN
          DO IS = 1, MSC
            WRITE(PRINTF,5001) IS, FRSME(IS), FRKME(IS), FRETOT(IS),
     &              4. * SQRT(FRETOT(IS)),
     &             (FRKME(IS)**2. * FRETOT(IS)) / (KMESPC**2.*ETOT)
 5001       FORMAT(' SWCAP6: IS SM KM EM HSM FAC: ',I4,5E12.4)
          ENDDO
        ENDIF
      ENDIF
C
C     end of subroutine SWCAP6
      RETURN
      END
```

# C Wave flume experiment (Donelan, 1987): SWAN input file

In this appendix the listing of the standard SWAN input file for the wave flume experiment (Donelan, 1987) test cases is given.

```
$*************************************************
$
PROJ 'SWAN '    '001'
$
$************** MODEL INPUT ******************
$
MODE STA ONED
$
CGRID 0. 0. 0. 100. 0. 50 0 CIRCLE 360 0.35 2. 72
$
INPGRID BOTTOM 0. 0. 0. 1 0 100. 1.
READINP BOTTOM 1. 'deep.bot' 1 0 FREE
$
BOUN SIDE W CCW CON FILE 'swell.bnd' 1
$
WIND 27.5 0.
$
NUM ACCUR 1.e-5 1.e-5 1.e-5 97. 50
$
GEN3
$
$ WCAP EKOM 1. 1.
$
$************* OUTPUT REQUESTS **************************
$
POINTS 'spc1' 0. 0. 50. 0. 100. 0.
PLOT   'spc1' FILE 'flume.plt' SPEC
$
POINTS 'spc' 50. 0.
SPEC   'spc' SPEC1D 'flume.spc'
TABLE  'spc' HEAD XP DEP HS RTP DIR DSPR STEEP
$
CURVE 'LINE1' 0. 0. 500 100. 0.
TABLE 'LINE1' HEAD   'flume.tbl' DIST DEP HS TM01 DIR DSPR QB DISS
TABLE 'LINE1' NOHEAD 'flume.out' DIST DEP HS TM01 DIR DSPR QB DISS
$
POINT 'point' 0. 0. 50. 0. 100. 0.
SPEC  'point' SPEC1D ABS 'flume.sp1'
$
TEST POINTS 25 0 S1D 'flume.src'
POOL
COMPUTE
STOP
```

# D Lake George (Australia)

## Purpose

In this test, the performance of SWAN is studied in a nearly idealised depth-limited wave growth situation of Lake George, near Canberra, Australia.

## Situation

Lake George is a fairly shallow lake with a nearly flat bottom (depth about 2 m, see Young and Verhagen, 1996a, 1996b and 1996c). It is approximately 20 km long and 10 km wide (see Figure 1). The bottom is rather smooth (bottom ripples are practically absent) and the bottom material consists of fine clay. The water level varies with the season. Currents are absent. Wind conditions vary per test case. A series of eight wave gauges were situated along the north-south axis of the lake. At station 6, the wind velocity $U_{10}$ and the directional wave spectrum were measured. The wave measurements were carried out during the period from April 1992 till October 1993.

Conditions were considered to be nearly ideal, as the wind speed and direction were relatively constant during the 30 minutes sampling period and the wind direction stayed within 20° of the alignment of the wave gauge array (stations 1 to 6 only).

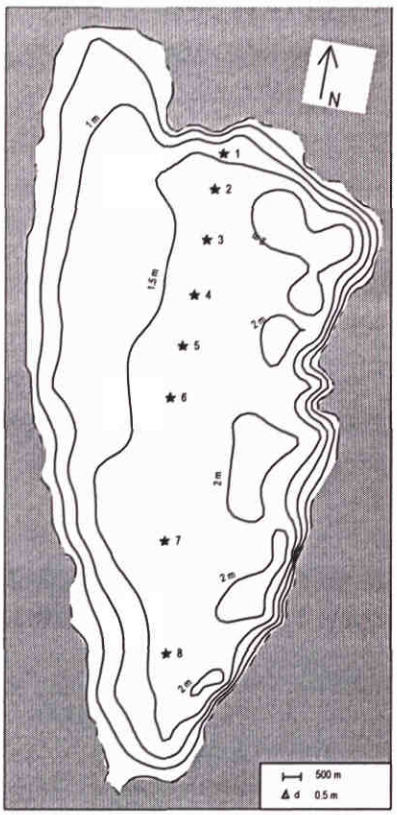


Figure 1 Bathymetry of Lake George (Australia) with the locations of the eight observation stations

## Test case description

To test the performance of the SWAN model, the 2-dimensional mode is used. From the extensive data set three typical examples, all with wind speeds from northerly directions, were selected for the computations:

1. case (a) 19-02-1993 / 22.00 hrs low wind speed of about $U_{10}$= 6.5 m/s;
2. case (b) 03-10-1993 / 17.00 hrs medium wind speed of about $U_{10}$= 11 m/s;
3. case (c) 11-11-1992 / 16.00 hrs high wind speed of about $U_{10}$= 15 m/s.

The incident wave field at the up-wave boundary is described by the observed frequency spectrum at station 1. To account for seasonal variations in the water level, for the test cases (a), (b) and (c), the water depth was increased with respectively +0.1 m, +0.3 m and +0.27 m over the entire lake. The physical processes of depth-induced wave breaking, bottom friction, triads, quadruplets and wind are activated in SWAN.

## Observations

The SWAN model results in terms of significant wave height $H_s$, peak period $T_p$ and spectral wave energy $E(f)$ are compared with the observations of Young and Verhagen (1996a, 1996b and 1996c).

## Model commands

| | **COMPUTATIONAL GRID** | | | | | | | |
|---|---|---|---|---|---|---|---|---|
| | 1D/2D | XPC | YPC | ALPC | XLENC | YLENC | | |
| | 2D | 1667 | 1667 | 0 | 11340 | 17907 | | |
| | ΔX | ΔY | DIR1 | DIR2 | Δθ | FLOW | FHIGH | MSC |
| a | 210 | 180 | 0° | 360° | 10° | 0.166 | 2.0 | 26 |
| b | 210 | 180 | 0° | 360° | 10° | 0.125 | 1.0 | 22 |
| c | 210 | 180 | 0° | 360° | 10° | 0.125 | 1.0 | 22 |

| | **PHYSICS** | | | | | | | | |
|---|---|---|---|---|---|---|---|---|---|
| | GEN | BREAK | FRIC | TRIADS | QUAD | WCAP | REFRAC | FSHIFT | SETUP |
| | 3 | on | on | on | on | on | on | off | off |

| | **BOUNDARY CONDITIONS** | | | | |
|---|---|---|---|---|---|
| | TYPE | BOU | C/V | P/R | NAME OF FILE |
| a | side | N | con | read boundary from file | 'f41lakc1.bnd' |
| b | side | N | con | read boundary from file | 'f41lakc2.bnd' |
| c | side | N | con | read boundary from file | 'f41lakc3.bnd' |

| | **BOTTOM:** | **WIND:** | **CURRENT:** | **WATER LEVEL:** |
|---|---|---|---|---|
| a | 'f41lakg.bot' | 'f41lakc1.wnd' | - | +0.10 m |
| b | 'f41lakg.bot' | 'f41lakc2.wnd' | - | +0.30 m |
| c | 'f41lakg.bot' | 'f41lakc3.wnd' | - | +0.27 m |

## Model results

In Figure F41a, the model results in terms of energy density spectra $E(f)$ and the observations for the different stations of Young and Verhagen in the low wind speed condition are shown (case a). For the same wind speed, the computed and observed values for $H_s$ and for $T_p$ are given in Figure F41b. For moderate wind speed (case b), the same information is shown in Figures F41c and F41d, respectively. Figures F41e and F41f respectively show energy density spectra and integral wave field parameters $H_s$ and $T_p$ for high wind speed (case c).

## References

Young, I.R. and L.A. Verhagen, 1996a: The growth of fetch limited waves in water of finite depth. Part I: Total energy and peak frequency, *Coastal Engineering*, 29, 47-78

Young, I.R. and L.A. Verhagen, 1996b: The growth of fetch limited waves in water of finite depth. Part II: Spectral Evolution, Coastal Engineering, 29, 79-99

Young, I.R. and L.A. Verhagen, 1996c: The growth of fetch limited waves in water of finite depth. Part III: Directional spectra, Coastal Engineering, 29, 101-121

Taylor, P.A. and R.J. Lee, 1984: Simple guidelines for estimating wind speed variations due to small-scale topographic features, *Climatol. Bull.*, 18, 3-32

## Acknowledgements

Data courtesy of I.R. Young, University of New South Wales, Canberra, Australia.

# E Haringvliet estuary (the Netherlands)

## Purpose

To test wave propagation and the formulations of the physical processes, in particular that of triads and the regeneration of waves by local wind effects, the SWAN model is applied in the complex field case of the Haringvliet Estuary (the Netherlands).

## Situation

The Haringvliet is a relatively shallow branch of the Rhine estuary in the south-west of the Netherlands, separated from this estuary by sluices (see Andorka Gal, 1995). The water depth is 4 to 6 m and the surface area is about 10 km × 10 km (see Figure 1). The bay is partly protected from the southern North Sea by a shoal (called 'Hinderplaat') extending half across the bay entrance. The waves approach the estuary from deep water and break over the shoal with a reduction of significant wave height. Deep inside the branch, the local wind regenerates the waves (which is evident as a high-frequency peak in the observed spectra). A constant wind speed $U_{10}$ is considered for each test case. Currents are assumed to be absent. The water level varies from +0.30 m in case (a) to +2.10 m in case (d).

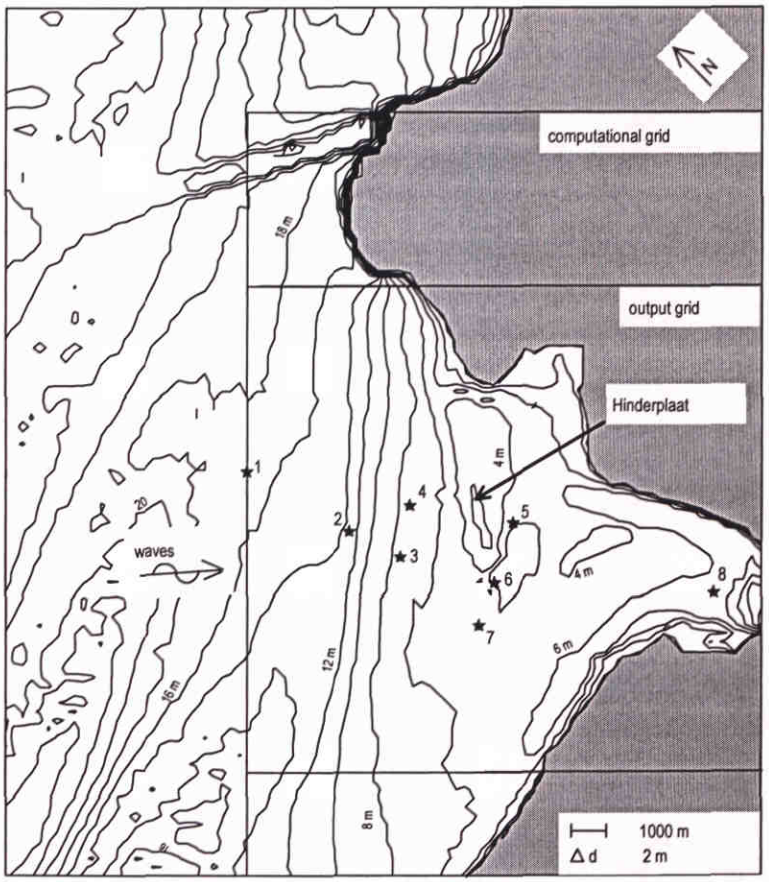


Figure 1 Bathymetry of the Haringvliet estuary (the Netherlands) with the locations of the eight observation stations.

## Test case description

In this test case, the 2D-mode of SWAN is activated. SWAN simulations have been performed for four different time levels, selected from the measurement data:

1. case (a) 14-10-1982 21.00 UTC $U_{10}$ = 12 m/s;
2. case (b) 14-10-1982 22.00 UTC $U_{10}$ = 17 m/s;
3. case (c) 14-10-1982 23.00 UTC $U_{10}$ = 14 m/s;
4. case (d) 14-10-1982 24.00 UTC $U_{10}$ = 15 m/s.

These time levels have been selected because (a) the wind speed and the wind direction were fairly constant, (b) the waves were fairly high (for the observation period of 13 weeks, (c) the water level was sufficiently low to see the generation of a significant secondary peak in the spectra near the shoal, but not so low that the shoal would be dry.

All physical processes are activated in SWAN.

## Observations

At 8 locations, wave observations are available (see Andorka Gal, 1995).

## Model commands

| | | | | | | | | | |
|---|---|---|---|---|---|---|---|---|---|
| | **COMPUTATIONAL GRID** | | | | | | | | |
| | 1D/2D | XPC | YPC | ALPC | XLENC | YLENC | | | |
| | 2D | 6960.2 | 0 | 0 | 14789.8 | 22000 | | | |
| | ΔX | ΔY | DIR1 | DIR2 | Δθ | FLOW | FHIGH | MSC | |
| | 150 | 250 | 0° | 360° | 10° | 0.0521 | 1.0 | 31 | |
| | **PHYSICS** | | | | | | | | |
| | GEN | BREAK | FRIC | TRIADS | QUAD | WCAP | REFRAC | FSHIFT | SETUP |
| | 3 | on | on | on | on | on | on | off | off |
| | **BOUNDARY CONDITIONS** | | | | | | | | |
| | TYPE | BOU | C/V | P/R | | NAME OF FILE | | | |
| a | side | W | con | read boundary from file | | 'f31harc1.bnd' | | | |
| b | side | W | con | read boundary from file | | 'f31harc2.bnd' | | | |
| c | side | W | con | read boundary from file | | 'f31harc3.bnd' | | | |
| d | side | W | con | read boundary from file | | 'f31harc4.bnd' | | | |
| | **BOTTOM:** | | | **WIND:** | | **CURRENT:** | | **WATER LEVEL:** | |
| a | 'f31harin.bot' | | | $U_{10}$: 12 m/s | $\theta_w$: 8.8° | - | | +0.30 m | |
| b | 'f31harin.bot' | | | $U_{10}$: 17 m/s | $\theta_w$: 8.8° | - | | +0.90 m | |
| c | 'f31harin.bot' | | | $U_{10}$: 14 m/s | $\theta_w$: 8.8° | - | | +1.70 m | |
| d | 'f31harin.bot' | | | $U_{10}$: 15 m/s | $\theta_w$: 8.8° | - | | +2.10 m | |

## Model results

In the Figures F31a, F32a, F33a, and F34a, the model results (in terms of energy density spectra $E(f)$) and the observations for eight stations of Andorka Gal (1995) are shown for the four time levels. The evolution of the energy density in time (case F31 to case F34) is shown in Figures F31p and F31c for the pre-computed and computed option, respectively. The model results in terms of integral wave parameters (the significant wave height $H_s$ and the mean wave period $T_{m01}$) for the different stations at 23.00 UTC, computed in case (c), are given in Figure F33b.

## References

Andorka Gal, J.H., 1995: Verification set Haringvliet -October 14, 1982- October 15, 1982-, Rep. - 95.112x, Ministry of Transport, Public Works and Water Management, Den Haag, The Netherlands

Dingemans, M.W., 1983: Verification of numerical wave propagation models with field measurements; CREDIZ verification Haringvliet, Rep. W488, Part 1b, Delft Hydraulics, Delft, The Netherlands

## Acknowledgements

Data courtesy of J.H. Andorka Gal and J.G. de Ronde of the Dutch Ministry of Public Works and Coastal Management (RIKZ), Den Haag, the Netherlands.

# F Norderneyer Seegat (tidal inlet in Germany)

## Purpose

In this test, the performance of SWAN is verified in the complex field situation of the Norderneyer Seegat (Germany).

## Situation

The Norderneyer Seegat is a tidal inlet situated between the barrier islands of Norderney and Juist (East-Frisian Islands in the north of Germany). The region behind the inlet is an inter-tidal area with shoals and channels over a distance of 7.5 km to the main land. The bathymetry for the 20 km x 25 km area is shown in Figure 1. The main channel (Norderneyer Riffgat, with a maximum depth of 16 m) penetrates deep around the head of Norderney to the east. Two smaller channels bifurcate from the Norderneyer Seegat to the south and south-west. North of the inlet lies a sandbank on which most waves coming from the North Sea break. Due to wind effects, in the inlet and behind the islands a local wind sea is generated.

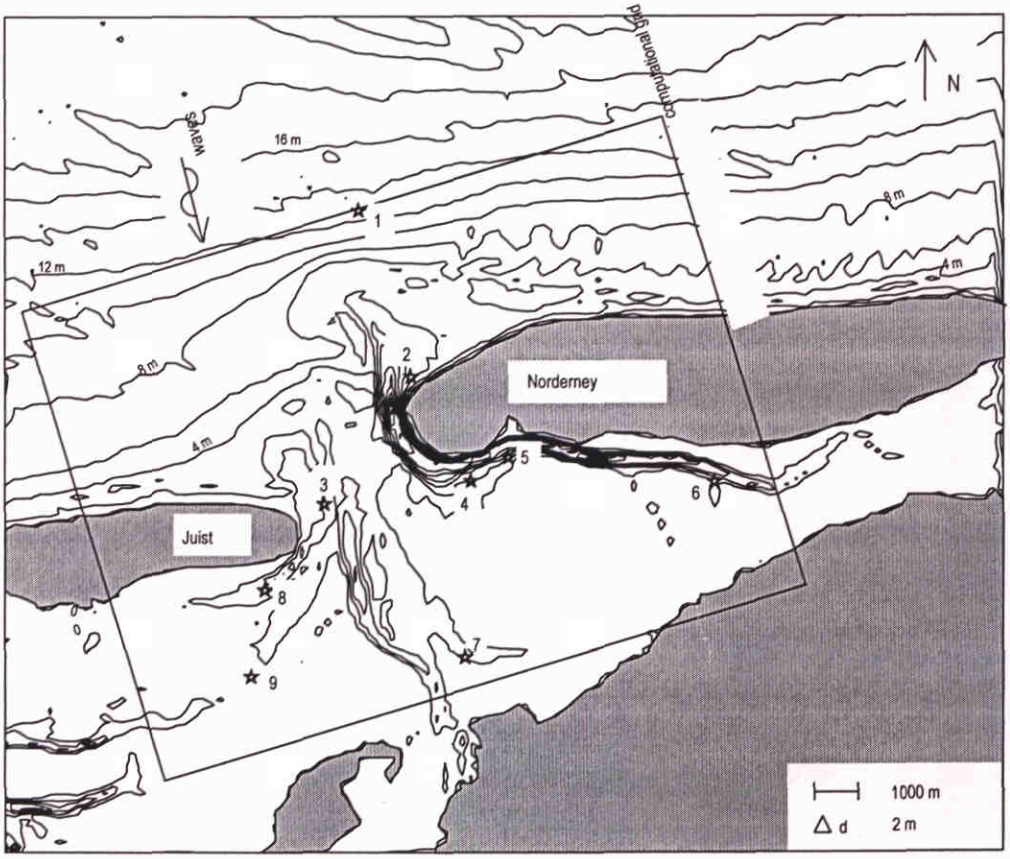


Figure 1 Bathymetry of the Norderneyer Seegat (Germany) with the locations of the nine observation stations

## Test case description

The geographical situation of the Norderneyer Seegat has been chosen, because detailed observations are available. For this verification, four typical situations have been selected from the extensive data set:

1. a high tide case (November 17, 1995, 3.58 UTC);
2. a low tide case (November 16, 1995, 21.58 UTC);
3. a high tide case (November 19, 1995, 7.59 UTC);
4. a high tide case (November 16 1995, 4.58 UTC).

These times have been chosen, because (a) at these times, all buoys were operating simultaneously (thus avoiding synchronisation problems); (b) the significant wave height was relatively high; (c) the frequency spectrum was uni-modal and (d) practically no currents were present, since it was turn of the tide. In the SWAN computation, all physical processes except wave-induced set-up have been taken into account.

## Model commands

| | **COMPUTATIONAL GRID** | | | | | | | |
|---|---|---|---|---|---|---|---|---|
| | 1D/2D | XPC | YPC | ALPC | XLENC | YLENC | | |
| | 2D | 66389 | 55613 | 287 | 11130 | 15200 | | |
| | ΔX | ΔY | DIR1 | DIR2 | Δθ | FLOW | FHIGH | MSC |
| | 100 | 100 | 0° | 360° | 10° | 0.04545 | 1.0 | 32 |
| | **PHYSICS** | | | | | | | |
| | GEN | BREAK | FRIC | TRIADS | QUAD | WCAP | REFRAC | FSHIFT | SETUP |
| | 3 | on | on | on | on | on | on | on | off |
| | **BOUNDARY CONDITIONS** | | | | | | | |
| | TYPE | BOU | C/V | P/R | NAME OF FILE | | | |
| a | side | N | con | read boundary from file | 'f81nord1.bnd' | | | |
| b | side | N | con | read boundary from file | 'f81nord2.bnd' | | | |
| c | side | N | con | read boundary from file | 'f81nord3.bnd' | | | |
| d | side | N | con | read boundary from file | 'f81nord4.bnd' | | | |
| | **BOTTOM:** | **WIND:** | | **CURRENT:** | **WATER LEVEL:** | | | |
| a | 'f81nord.bot' | $U_{10}$: 8 m/s | $\theta_w$: 292° | - | MSL +1.42 m | | | |
| b | 'f81nord.bot' | $U_{10}$: 13 m/s | $\theta_w$: 315° | - | MSL -0.07 m | | | |
| c | 'f81nord.bot' | $U_{10}$: 11.5 m/s | $\theta_w$: 290° | - | MSL +1.75 m | | | |
| d | 'f81nord.bot' | $U_{10}$: 5 m/s | $\theta_w$: 70° | - | MSL +1.11 m | | | |

## Model results

In Figure F81a, the SWAN model results in terms of energy density spectra *E(f)* and the observations for the different stations for the first case (high tide) are shown. For the same case, the computed and observed values for $H_s$ and for $T_{m01}$ are given in Figure F81b. For the second case (low tide), this information is shown in Figures F81c and F81d. Figures F81e and F81f respectively show energy density spectra and integral wave parameters for the third case (high tide), and F81g and F81h for the fourth (high tide).

## References

Niemeyer, H. D. and R. Kaiser, 1997: Variationen im lokalen Seegangsklimas infolge morphologischer Anderungen im Riffbogen. Berichte der Forschungsstelle Kuste, Band 41, 107-117, Norderney.

## Acknowledgements

Data courtesy of H. Niemeyer and R. Kaiser of the State Coastal Research Station at Norderney, Germany.

# G Westerschelde estuary (the Netherlands)

## Purpose

The goal of this case is to test the performance of SWAN in the complex field situation of the Westerschelde (the Netherlands), in the presence of currents and wind, using nested computational grids.

## Situation

The Westerschelde is an estuary of approximately 60 × 10 km$^2$ in the south-west of the Netherlands (see Andorka Gal and Roelse, 1997). The bathymetry varies significantly in two dimensions (see Figures 1 and 2). At its entrance, a multi-peaked wave spectrum is present, as swell is penetrating from deep water into the shallow part of the estuary and a local wind sea is generated in the inner area. Currents and wind are present. A storm event that occurred on December 20, 1991 is considered. The current velocities and water levels used in the computations have been obtained with the WAQUA circulation model (computations performed by the Dutch Ministry of Public Works and Coastal Management, RIKZ, 1999).

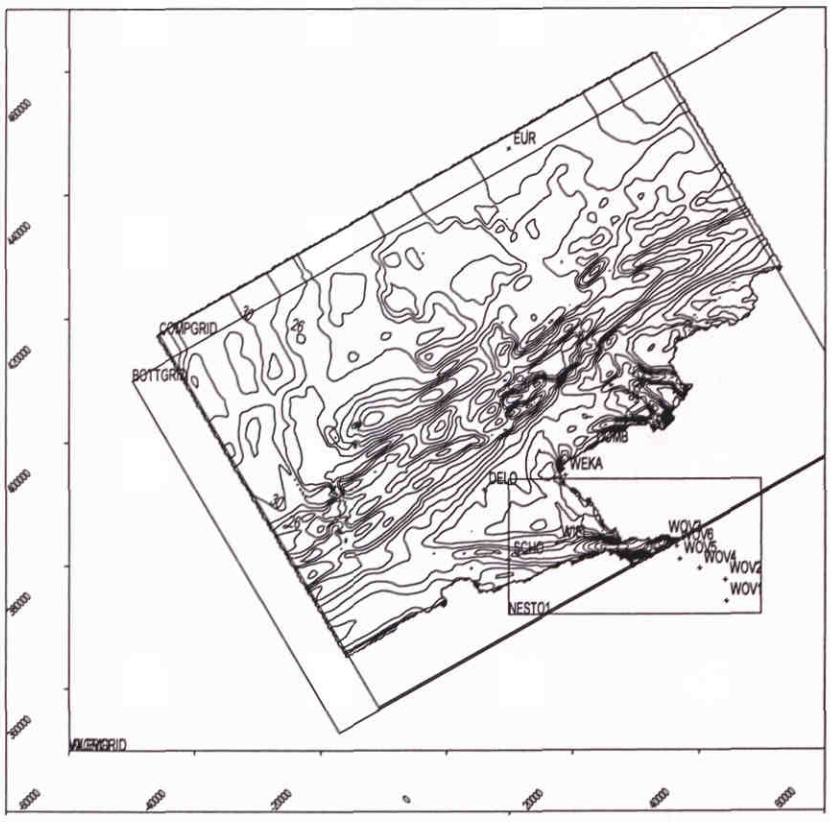


Figure 1 Bathymetry and computational grid of the outer region and the inner region of the Westerschelde (the Netherlands) with the locations of the observation stations

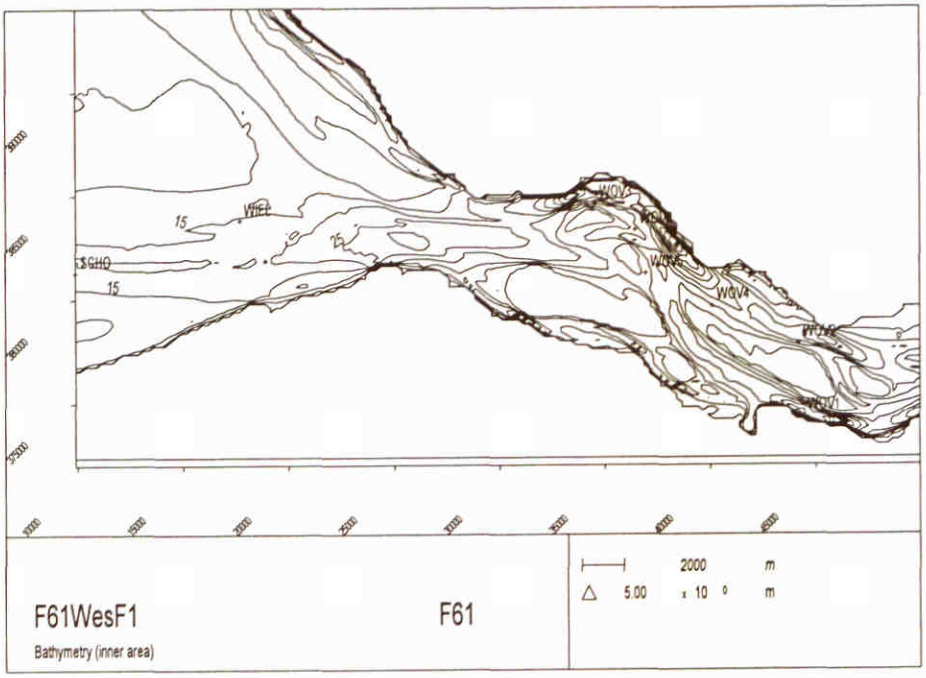


Figure 2 Bathymetry and computational grid of the inner region of the Westerschelde (the Netherlands) with the locations of the observation stations.

## Test case description

In this test case, the 2D-mode of SWAN is activated. The Westerschelde has been divided into an outer region (course computational grid) and an inner region (high-resolution grid) (see Figure 1). On the same nested grid, four computations have been made, using four different boundary conditions. From the available observations, the following four time levels have been selected:

| | | | |
|---|---|---|---|
| 1. | case (a) 20-12-1991 12.00 hrs | flood current | MWL = about 1.78 m +NAP; |
| 2. | case (b) 20-12-1991 15.00 hrs | ebb current | MWL = about 1.46 m +NAP; |
| 3. | case (c) 20-12-1991 18.00 hrs | ebb current | MWL = about 0.45 m +NAP; |
| 4. | case (d) 20-12-1991 21.00 hrs | flood current | MWL = about 0.63 m +NAP. |

All physical processes (except wave-induced setup) have been activated. In the computations, the wind velocity $U_{10}$ varies. Generally, in the outer region the wind speed is slightly higher than in the inner region (which is in agreement with the observations). The boundary for the computations on the nested grid are obtained from the results of the computations on the course grid. Output is generated at 12 different locations (see Figures 1 and 2).

## Observations

At a number of twelve locations, observations are available during the storm event (from the Dutch Ministry of Public Works and Coastal Management RIKZ, 1999).

## Model commands (outer region)

| | | | | | | | | | | | | |
|---|---|---|---|---|---|---|---|---|---|---|---|---|
| | **COMPUTATIONAL GRID** | | | | | | | | | | | |
| | SET | 1D/2D | XPC | YPC | ALPC | XLENC | YLENC | | | | | |
| | nautical | 2D | -45669 | 417500 | 300 | 70000 | 90000 | | | | | |
| | ΔX | ΔY | DIR1 | DIR2 | Δθ | FLOW | FHIGH | MSC | | | | |
| | 500 | 1000 | 0° | 360° | 15° | 0.05 | 0.8 | 29 | | | | |
| | **PHYSICS** | | | | | | | | | | | |
| | GEN | BREAK | FRIC | TRIADS | QUAD | WCAP | REFRAC | FSHIFT | SETUP | | | |
| | 3 | on | on | on | on | on | on | on | off | | | |
| | **BOUNDARY CONDITIONS** | | | | | | | | | | | |
| | TYPE | BOU | C/V | P/R | SHAPE | PE/ME | DSPR | LEN | HS | PER | DIR | DD |
| a | side | NW | con | par | Jonswap | peak | power | - | 4.15 | 7.7 | 277 | 2 |
| a | side | NE/SE | var | par | Jonswap | peak | power | 0 | 4.15 | 7.7 | 277 | 2 |
| a | | | | | | | | 58000 | 4.15 | 7.7 | 277 | 2 |
| b | side | NW | con | par | Jonswap | peak | power | - | 3.63 | 7.8 | 280 | 2 |
| b | side | NE/SE | var | par | Jonswap | peak | power | 0 | 3.63 | 7.8 | 280 | 2 |
| | | | | | | | | 58000 | 3.63 | 7.8 | 280 | 2 |
| c | side | NW | con | par | Jonswap | peak | power | - | 4.84 | 8.7 | 291 | 2 |
| c | side | NE/SE | var | par | Jonswap | peak | power | 0 | 4.84 | 8.7 | 291 | 2 |
| | | | | | | | | 58000 | 4.84 | 8.7 | 291 | 2 |
| d | side | NW | con | par | Jonswap | peak | power | - | 4.45 | 8.7 | 292 | 2 |
| d | side | NE/SE | var | par | Jonswap | peak | power | 0 | 4.45 | 8.7 | 292 | 2 |
| | | | | | | | | 58000 | 4.45 | 8.7 | 292 | 2 |

| | **BOTTOM:** | **WIND:** | | **CURRENT:** | **WATER LEVEL:** |
|---|---|---|---|---|---|
| a | 'f61wesc1.bot' | $U_{10}$: 17.5 m/s | $\theta_w$: 270° | 'f61wesc1.cur' | 'f61wesc1.lev' |
| b | 'f61wesc1.bot' | $U_{10}$: 16.5 m/s | $\theta_w$: 280° | 'f61wesc2.cur' | 'f61wesc2.lev' |
| c | 'f61wesc1.bot' | $U_{10}$: 18.5 m/s | $\theta_w$: 290° | 'f61wesc3.cur' | 'f61wesc3.lev' |
| d | 'f61wesc1.bot' | $U_{10}$: 18 m/s | $\theta_w$: 290° | 'f61wesc4.cur' | 'f61wesc4.lev' |

## Model commands (inner region)

| | | | | | | | | |
|---|---|---|---|---|---|---|---|---|
| | **COMPUTATIONAL GRID** | | | | | | | |
| | 1D/2D | XPC | YPC | ALPC | XLENC | YLENC | | |
| | 2D | 10000 | 372000 | 0 | 40000 | 22000 | | |
| | ΔX | ΔY | DIR1 | DIR2 | Δθ | FLOW | FHIGH | MSC |
| | 250 | 200 | 0° | 360° | 15° | 0.05 | 0.8 | 29 |
| | **PHYSICS** | | | | | | | |
| | GEN | BREAK | FRIC | TRIADS | QUAD | WCAP | REFRAC | FSHIFT | SETUP |
| | 3 | on | on | on | on | on | on | on | off |
| | **BOUNDARY CONDITIONS** | | | | | | | |
| a | 'f61wesf1.nst' | | | | | | | |
| b | 'f61wesf2.nst' | | | | | | | |
| c | 'f61wesf3.nst' | | | | | | | |
| d | 'f61wesf4.nst' | | | | | | | |

| | **BOTTOM:** | **WIND:** | | **CURRENT:** | **WATER LEVEL:** |
|---|---|---|---|---|---|
| a | 'f61wesf1.bot' | $U_{10}$: 14.5 m/s | $\theta_w$: 280° | 'f61wesc1.cur' | 'f61wesc1.lev' |
| b | 'f61wesf1.bot' | $U_{10}$: 16 m/s | $\theta_w$: 290° | 'f61wesc2.cur' | 'f61wesc2.lev' |
| c | 'f61wesf1.bot' | $U_{10}$: 14 m/s | $\theta_w$: 290° | 'f61wesc3.cur' | 'f61wesc3.lev' |
| d | 'f61wesf1.bot' | $U_{10}$: 13.5 m/s | $\theta_w$: 290° | 'f61wesc4.cur' | 'f61wesc4.lev' |

## Model results

Model results in terms of energy density spectra *E(f)* and observations for the different stations at 12.00h are shown in Figure F61a (outer region) and F61b (inner region). The same information for the time levels 15.00h, 18.00h and 21.00h is shown in Figures F61c and F61d, F61e and F61f, and F61g and F61h, respectively.

## References

Kamsteeg, A.T., J.H. Andorka Gal, J.G. de Ronde and J.C.M. de Jong, 1998:"Wave boundary conditions on the Westerschelde, given a 1/4000 wind velocity" (in Dutch: 'Golfrandvoorwaarden op de Westerschelde gegeven een 1/4000 windsnelheid'), RIKZ report no. 98.018, Ministry of Transport, Public Works and Water Management, Den Haag, The Netherlands

Andorka Gal, J.H. and P. Roelse, 1997: Wave modelling in the Westerschelde estuary and wave conditions along the sea defences (Westerschelde golfmodellering en golfrandvoorwaarden voor de dijkvakken, in Dutch), Rep. RIKZ/AB-96.868x, Ministry of Transport, Public Works and Water Management, Den Haag, The Netherlands

## Acknowledgements

Data courtesy of J.G. de Ronde and J.H. Andorka Gal of the Dutch Ministry of Public Works and Coastal Management (RIKZ), Den Haag, the Netherlands.


**WL | delft hydraulics**

Rotterdamseweg 185
postbus 177
2600 MH Delft
telefoon 015 285 85 85
telefax 015 285 85 82
e-mail info@wldelft.nl
internet www.wldelft.nl

Rotterdamseweg 185
p.o. box 177
2600 MH Delft
The Netherlands
telephone +31 15 285 85 85
telefax +31 15 285 85 82
e-mail info@wldelft.nl
internet www.wldelft.nl